TOMAS BATA UNIVERSITY IN ZLIN
FACULTY OF TECHNOLOGY
Department of Polymer Engineering

Jakub Kadlčák

FILLER DISPERSION AND RHEOLOGY OF POLYMERS

Disperze plniv a reologie polymerů

Doctoral Thesis

Programme:	P 2808 Chemistry and Materials Technology 2808V006
Course:	Technology of Macromolecular Compounds
Supervisor:	Assoc. prof. Ing. Roman Čermák, Ph.D.
Year:	2014

Study programme: P2808 Chemistry and Materials Technology

Study area: 2808V006 Technology of Macromolecular Compounds

Supervisor: Assoc. Prof. Ing. Roman Čermák Ph.D.

Published by Tomas Bata University in Zlín.

ABSTRACT

This monograph deals with the topic of carbon black behaviour in rubbers and aspects influencing this. The first part of the monograph is dedicated to the state of the art where theoretical background for the doctoral work is reviewed. At first, a brief introduction to rubber compounding is given and the most important ingredients in rubber compounds are described. One of the most important ingredients is carbon black thus its production, properties, its dispersion and general role in rubber compounds are described thoroughly. Methods for the evaluation of carbon black properties are introduced with the special focus on the carbon black structure evaluation. Furthermore, the topic of carbon black dispersion process is reviewed together with methods for the evaluation of filler dispersion quality. The filler dispersion quality is mainly given by the efficiency of mixing process. The mixing process and its stages are explained mentioning aspects influencing each stage. The special focus is given to post-mixing stages when dispersed filler due to ubiquitous physical forces tends to reagglomerate which can result in formation of filler network. This process has strong influence on the filler dispersion quality. Therefore, it is of high importance to monitor this process.

The state of the art is followed by the section devoted to the experimental work. The experimental work was divided into three main topics. The first one deals with the carbon black structure examined by mechanical compression. The second topic deals with the evaluation of quality of carbon black macrodispersion. The last topic which is the most extended area of this work is dedicated to the carbon black behaviour in rubbers and its interrelation to the processing and the material aspects.

Key words: *Reinforcement, Flocculation, Filler networking, Dispersion, Carbon black, Rubber, Dispergrader.*

ABSTRACT IN CZECH

Tato monografie pojednává o problematice chování sazí v kaučukových směsích a aspektech, které chování sazí ovlivňují. První část monografie je věnována teoretickému pozadí doktorské práce. Nejprve je zde poskytnut stručný úvod ke složení kaučukových směsí a jsou diskutovány nejdůležitější suroviny. Jednou z nich jsou saze. Potom je důkladně probrána výroba, vlastnosti sazí a jejich role a chování v kaučukové směsi. Mimoto jsou představeny metody pro hodnocení vlastností sazí a speciální pozornost je věnována hodnocení struktury sazí. Dále je zde řešena problematika disperze sazí stejně jako metody k jejímu hodnocení. Disperze je dána především účinností míchacího procesu. Jsou vysvětleny jednotlivé fáze míchacího procesu a aspekty, které je ovlivňují. Zvláštní pozornost je věnována fázi, která nastává po míchání, kdy distribuované plnivo má tendence působením fyzikálních sil znovu aglomerovat což může vést až k vytvoření plnivové sítě. Tento jev má silný vliv na kvalitu disperze a je proto důležité ho monitorovat.

Teoretické shrnutí následuje část věnována experimentální práci. Ta byla rozdělena na tři hlavní oblasti. První oblast pojednává o struktuře sazí a jejím vyhodnocování pomocí mechanického stlačování. Druhá oblast výzkumu řeší hodnocení kvality makrodisperze sazí. Poslední oblast výzkumu, která je nejrozsáhlejší, je věnována chování sazí v kaučukových směsích a procesním a materiálovým parametrům, které tento proces ovlivňují.

Klíčová slova: *Ztužení, Flokulace, Plnivo, Disperze, Saze, Kaučuk, Dispergrader*

ACKNOWLEDGEMENTS

I would like to express my sincere gratitude to my supervisor Assoc. prof. Roman Čermák, Ph.D. for giving me the opportunity to study Ph.D. at the Tomas Bata University in Zlín and his always helpful attitude and suggestions.

I am grateful for all the opportunities that I got at the Faculty of Technology and the Centre of Polymer Systems that have helped me grow into a better individual.

I would like to acknowledge Assoc. prof. Ing. et Ing. Ivo Kuřitka, Ph.D. et Ph.D. for our rich discussions and his innumerable advices which were always very inspirational and helpful not only at university but also in my life. I am grateful for his highly appreciated friendship.

Assoc. prof. RNDr. Petr Ponížil Ph.D. for his help and guidance through the amazing fields of mathematical statistics and physics.

Assoc. prof. Ing. Tomáš Sedláček Ph.D. for his guidance, the encouragement and sharing his knowledge in the machinery field. Also for his legendary parties and being a great friend.

Prof. Dr. Jorge Lacayo-Pineda for the opportunity to work with him, for sharing his knowledge with me, his guidance and advices not only during my internship in Continental Tire in Hannover but for the whole duration of my doctoral studies.

Dr. Du Bois, Dr. Láznička and Ing. Vilímek for giving me the opportunity to work in Continental labs in Hannover and Otrokovice and their help.

Queen Mary University of London where I got the opportunity to spent very productive and inspirational four months under the supervision of Prof. James Busfield. I would like to give my deepest thanks to James for this opportunity which positively affected my entire life.

Lorenzo, Lewis, Mario, Guangchang and Menglong and the whole rubber group at Queen Mary University of London for their helpful attitude, advices and warm welcome.

Hediyeh Zahabi for being my "خانم شاهزاده ی فارس" in London, her selflessness, her often exhausting help, her encouragement, fun time we had and her questions without which my life would have been miserable.

Klara Elsikova who was always my source of mental support, inspiration, power and always gave me various views on things around me. Everything you learned from us I learned.

My colleagues who became my good friends, namely Pavel U., Kuba, Pavel B., Tom P., Zuzka, Majkl and Ondra H. who made my journey fun and memorable.

My beloved Max, proud beagle who made my life much more rich and simply was the best dog. Rest in peace.

Music.

Above all, I would like to thank my family and especially my parents who gave me a huge portion of patience and even bigger portion of support during my entire studies from the first grade at the elementary school (which is actually 22 years ago) and I wish they could be proud of me always. They are my home, my stepping stone that I can stand on to reach my dreams.

Without my family and friends everything would be meaningless.

Time passes and the constants stay
James Blake

CONTENT

PREFACE

Carbon black is a very complex material widely used in rubber industries as a filler improving performance of rubbers. The magnitude of this improvement, generally called reinforcement depends on many aspects of both, carbon black and rubbers. Throughout literature, aspects influencing the rubber reinforcement are carbon black properties, filler-filler interactions, filler-polymer interactions, quality of carbon black dispersion and many others.

One of the most important carbon black characteristics influencing the behaviour of filled rubber compounds is carbon black structure. This is usually examined by oil absorption methods. Nowadays, an alternative method for the evaluation of carbon black structure via the mechanical compression of a dry sample is being also used. It is a renewed technique which is supposed to replace oil absorption techniques using aromatic or paraffinic oils which produce quantities of hazardous waste. Pilot studies were carried out on a device called Void Volume Tester, evaluating the carbon black structure via mechanical compression, in this research work.

Another very important aspect influencing the reinforcement is the quality of carbon black dispersion. The quality of filler dispersion is given especially by the efficiency of mixing process. During the mixing process, carbon black agglomerates incorporated into a rubber matrix are broken down to micro sized aggregates which are further distributed throughout the matrix. The quality of deagglomeration is usually referred as a macrodispersion and is evaluated by methods based on the optical microscopy. On the other hand, the distribution of aggregates is often described as microdispersion and is evaluated via methods such as transmission electron microscopy and image analysis.

In this work, the level of carbon black macrodispersion in rubbers has been investigated using a device called Dispergrader based on the optical microscopy in the reflection mode.

The quality of microdispersion, obtained after mixing, deteriorates during the stages of storage, extrusion or vulcanisation. This is a natural process caused by the Brownian motion or shear induced flow of carbon black aggregates leading to numerous collisions between them. Colliding aggregates due to attractive interactions stick together forming agglomerates which can at sufficiently long

time and thermal conditions evolve in a percolating filler cluster having a fractal like character. This process of reagglomeration is termed flocculation or alternatively filler networking. Because the term flocculation is more frequent in literature, it is used throughout this work also. Flocculation process must be considered during the dispersion process of any filler in rubbers. Many experiments were carried out in this field and different evaluation approaches of the flocculation process are described in several publications. The investigation of carbon black flocculation process was a next subject of investigation in this work when the influence of carbon black properties, rubber matrices' properties, processing conditions and testing conditions were examined.

CHAPTER I. STATE OF THE ART

Rubber compounding is a very important and comprehensive stage in the manufacturing of rubber products. The composition of rubber compounds influences processing as well as final properties of a product. Therefore, a lot of attention is devoted to this stage. By the selection of a rubber or a combination of rubbers, fillers and other ingredients the rubber compound properties can be adjusted in order to meet the required performance. Hence, the composition of rubber compounds is a very complex multidisciplinary science where the knowledge of material physics, organic, inorganic and macromolecular chemistry as well as chemical kinetics is necessary. Moreover, during the compounding, characteristics of each ingredient must be kept in mind as well as safety, environmental and economical aspects [1, 2].

Generally, rubber compounds contain five main ingredients:

- Rubber – natural rubber, synthetic rubbers
- Filler system – carbon black, silica, clays
- Vulcanisation system – sulphur, accelerator, activator, peroxides
- Stabiliser system – antioxidants, antiozonants
- Special materials – oils, pigments, resins, processing aids

The rubber compound thus is a dispersion system of components homogeneously dispersed or diluted in a rubber matrix or in a mixture of rubbers. The proportion of components is usually expressed in parts per hundred rubber – phr.

The rubber composition defined by the international standard ASTM D3192-09 is depicted in Table I-1.

Table I-1. A sample composition according to the ASTM D3192 [3].

Ingredients	Amount [phr]
Rubber	100.0
Antioxidant	1.5
Antiozonant	2.5
Stearic acid	3.0
Zinc oxide	5.0
MBTS	0.6
Sulphur	2.5
Carbon black	50.0

The most important ingredient is the rubber which provides the compound with specific physical and mechanical properties such as elasticity, reversible deformability and elongation. Rubber itself however does not provide all the properties to satisfy industrial needs. Strength and wear resistance as well as insolubility are gained after vulcanisation. Therefore, a vulcanising system is needed. The vulcanising system generally can be sulphur or peroxide based. The sulphur based vulcanising system contains sulphur, accelerators and activators. Sulphur during vulcanisation process creates crosslinks between macromolecules of rubber thus ensures required properties. Accelerators and activators assure the vulcanisation proceed more effectively and faster.

Very important component of every rubber compound is filler. Fillers can be active, semi-active or non-active. Active fillers act as a reinforcing agent enhancing performance of rubber compounds. The reinforcement of rubbers by carbon black is a very comprehensive topic and after many years of investigation still has not been fully explained [1, 2 and 4].

CARBON BLACK OVERVIEW

Carbon black is a complex, raw, nanomaterial which is specified by a range of quality parameters. Generally, it is the most widely used filler material and can have both filling and reinforcing effects [5]. Owing to its properties, about five million metric tons of carbon black is used in the tyre industry annually. Beside the tyre industry, reinforcing carbon blacks are used in many applications such as coatings, plastics, printing inks and variety of other applications [6].

The term carbon black is assigned to a group of industrial products involving thermal, furnace, channel and acetylene blacks obtained by the partial combustion or thermal decomposition of organic substances. Generally, carbon black is composed of elemental carbon in the form of quasi-spherical particles of colloidal size coalesced into particle aggregates. Aggregates usually agglomerate forming clusters, agglomerates [7].

CARBON BLACK PRODUCTION

Nowadays, due to precise control of the manufacturing processes industrial carbon blacks are provided with clearly defined properties. Therefore, these processes are different to where soot is released as a contaminated by-product. From a chemical point of view, there are two main categories of carbon black manufacturing processes, i.e. incomplete combustion and partial decomposition of hydrocarbons (solid, liquid or gaseous), depending on the presence or absence of oxygen. The process of partial decomposition also termed thermal oxidative decomposition is the most important one [7].

Several kinds of carbon black exist according to the manufacturing processes. Furnace black are made in furnace by partial decomposition of hydrocarbons (dehydrogenation). Channel blacks are manufactured by impingement of natural gas flames on channel irons (“U” profile iron). Thermal blacks are produced by thermal decomposition of natural gas, while acetylene black, a special type of thermal black, is made by exothermic decomposition of acetylene. Lampblack is made by burning hydrocarbons in open, shallow pans [8].

More than 90 % of the worldwide production constitutes the furnace black process.

The furnace blacks can be produced via an older gas furnace or a newer oil furnace process. The oil furnace process is the most modern and is based on the principle of thermal oxidative decomposition. It is a continuous process carried in a closed reactor into which a liquid feedstock (usually hydrocarbon oil) from the storage tank is injected. The flame in the reactor itself is produced by natural gas usually [9]. As simplified in Figure I-1, the reactor has four different sections which are as follows: the burner section, the furnace section, the quench section and the collection system. The fuel is admitted into the burner section together with air. The temperature reached in the flame is from 1200 to 1600 °C according to the carbon black type manufactured. The higher the temperature of the flame the finer the particles of carbon black. This is due to a higher combustion ratio which is the ratio of total air present to air needed for the complete combustion of all hydrocarbons present.

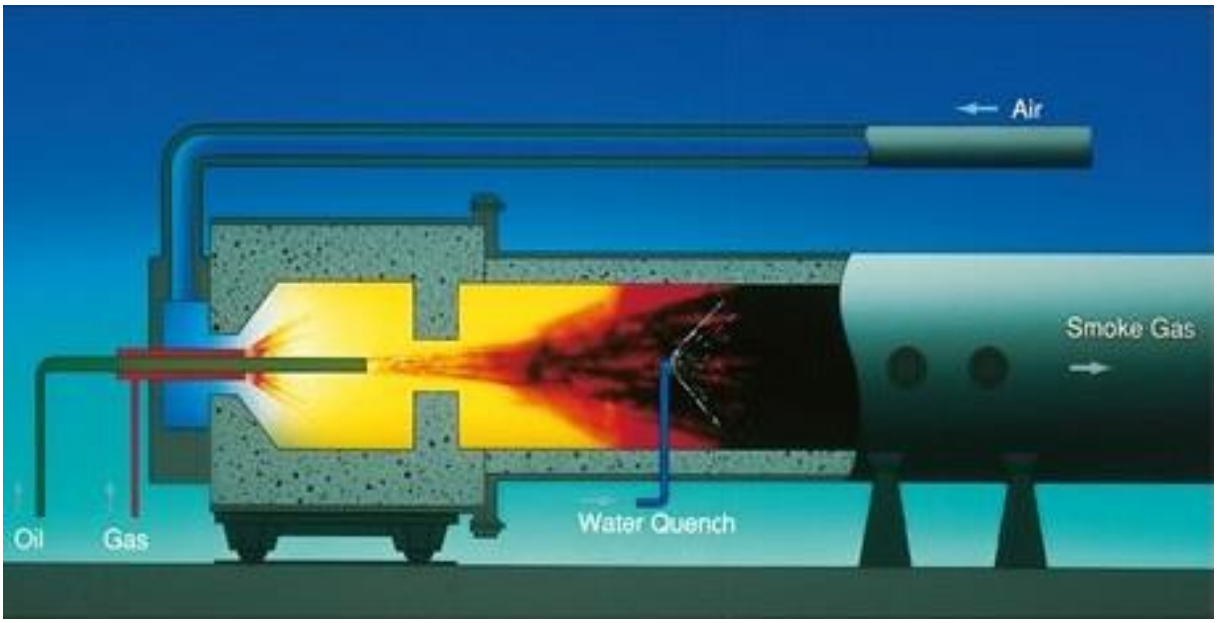

Figure I-1. The schema of the reactor for the production of the oil furnace carbon black [10].

When carbon black is formed in the flame region it goes through the furnace section at a high velocity with a residence time in milliseconds. This section determines the physical properties of carbon black such as specific surface area, particle size and structure complexity which are further discussed in the following section. In the next step, the reaction is cooled down by the injected

water to temperature around 650 °C in the quench zone. This also prevents any secondary reactions [11].

Horizontal as well as vertical furnaces lined with firebricks as insulation are in use, with either rectangular or cylindrical cross-section.

During the first stage of the formation of carbon black, highly viscous drops or solid particles with a quasi-spherical shape are formed. As these grow together, they coalesce and three dimensional branched structures evolve – i.e. aggregates. Aggregates usually form agglomerates bonded by Van der Waals forces. These are called fluffy. Fluffy carbon black which consists of secondary agglomerates is very difficult to handle. Therefore, fluffy carbon black is usually pelletized. Among pelletized carbon blacks a distinction is made between dry, wet and oil pelletizing process and final properties of pellets. In rubber industry, wet pelletized carbon black is offered mainly. However, carbon blacks are available in a powdery form also [5].

CARBON BLACK PROPERTIES

As described in the section above, there are many types of carbon black differing in the manufacturing processes and their properties. Therefore, there are many techniques and analytical methods monitoring the quality of carbon black production and properties. Carbon black manufactured with the intention of use in rubber industries is evaluated with consideration of its performance in rubbers [9].

Nowadays, it is known that carbon blacks are only rarely found as individual discrete spherical particles, but generally exist as aggregate of coalesced, fused elementary (primary) particles. Moreover, aggregates tend to agglomerate into larger units. An exception makes the thermal black composed mostly of single spherical particles [8]. Simplified schematic drawing of carbon black structural units is shown in Figure I-2. Each domain is described through literature as follows:

Carbon black particle is a small, para-crystalline spheroidal non-discrete component of a carbon black aggregate. Particle diameter can range from less than 20 nm in some furnace grades to a few hundred nanometres in

thermal blacks and can be separated from the aggregate by fracturing only [7, 12] The particles of a given carbon black do not all have the same diameters, but show a distribution curve characteristic of the particular sample [13].

Carbon black aggregate is a discrete, rigid, colloidal entity of extensively coalesced particles; the smallest dispersible unit of carbon black. Aggregate dimensions measured by the ferret diameter method can range from as small as 100 nm to a few micrometres [7, 12].

Carbon black agglomerate is a cluster of physically bond and entangled aggregates. Agglomerates can vary widely in size from less than a micrometre to a few millimetres in the form of pellet [7, 12].

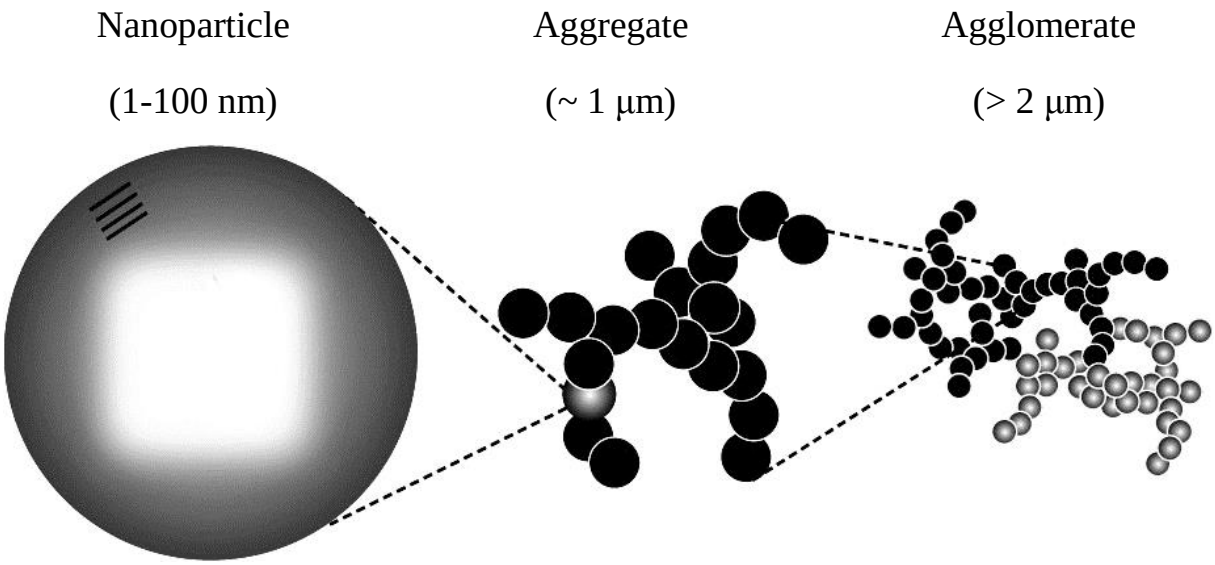

Figure I-2. Exemplification of carbon black structural units by Liu [13].

Primary particles size and its distribution are very important physical properties of carbon black in terms of end-use applications, even though particles usually do not exist as discrete entities. Methods for primary particle size evaluation can be direct or indirect such as electron microscope measurements, image analysis, colloidal techniques or tinting strength [7]. Table I-2 shows the overview of carbon black grades according to their primary particle size.

Table I-2. Overview of carbon black types according to their ASTM code and primary particle diameter [14].

ASTM numbers	Primary particle diameter [nm]	Previous nomenclature
900-999	201-500	MT: Medium Thermal
800-899	101-200	FT: Fine Thermal
700-799	61-100	SRF: Semi-Reinforcing Furnace
600-699	49-60	GPF: General Purpose Furnace
500-599	40-48	FEF: Fine Extrusion Furnace
400-499	31-39	FF: Fine Furnace
300-399	26-30	HAF: High Abrasive Furnace
200-299	20-25	ISAF: Intermediate Super Abrasive Furnace
100-199	11-19	SAF: Super Abrasive Furnace
000-099	1-10	-

For the industrial applications of carbon black, aggregates and agglomerates play the most important role [8] and considering the fact that carbon black aggregate is the primary unit of carbon black in rubber compounds, methods characterising aggregates are of the main importance. A brief review of the most widely used carbon black characteristics is given in Table I-3.

Table I-3. Common carbon black characteristics [12].

Test	**Measures**
Oil absorption number (DBP)	Structure
Oil absorption number of compressed sample (CDBP)	Structure after compression
Iodine adsorption number	Surface area
Nitrogen surface area (BET)	Total surface area
STSA	External surface area
CTAB surface area	External surface area
Tinting strength	Fineness/colour
Pellet hardness	Strength of pellets
Fines content	Dustiness level
Pour density	Bulk density
Ash content	Inorganics from water
Heating loss	Moisture
Sieve residue	Contaminants

The most important carbon black properties influencing its behaviour in filled rubbers are particle size or alternatively specific surface area, structure complexity and surface energy and chemistry. These factors are discussed in the following sections.

The specific surface area of carbon black

The specific surface area (SSA) is defined as the surface area accessible for interactions with polymer macromolecules in square metres per unit mass of carbon black in grams. The term accessible refers to micropores of some of carbon black grades which are included in surface area measurements but cannot be reached by polymer macromolecules [8]. Pores in carbon black can be open, referring to small pores on the surface in the order of nanometres and undefined shape, which may provide access to internal voids. On the other hand, internal voids which are not accessible to the surface are described as closed pores. For non-porous carbon black the measure of SSA shows inverse correlation with the particle size [7]. Methods for the evaluation of SSA are based on adsorption measurements [12].

Generally, the surface area of carbon black is calculated as follows:

$$S = \frac{W_m N_A A}{M} \qquad (1)$$

Where S refers to the surface area in squared metres, W_m is the weight of the adsorbate monolayer in grams, N_A is the Avogadro's number (6.022×10^{23} mol^{-1}), A is the cross-section area of adsorbate in squared metres and M is the molecular weight of the adsorbate in grams per mole [12].

Langmuir [7] assumed that the surface area for almost all solids can be determined from the volume or weight of molecules that are adsorbed as a monolayer on their surface. The surface of carbon black however is energetically heterogeneous which causes that molecule do not adsorp in a monolayer [12]. Brunauer, Emmett and Teller in 1938 defined a model which takes into account multilayer adsorption and still determines the number of molecules or atoms of the adsorbate that form a monolayer. This gave the basics

for the method known as the BET theory which was extensively reviewed elsewhere [7, 15].

Nowadays, the BET method is the most widely used for the determination of specific surface area of carbon black when the adsorption isotherm of N_2 molecules is measured mostly. Beside nitrogen, gases such as argon, krypton or xenon have been used for studying surface area as well. However, nitrogen adsorption gives the best results and therefore became an industrial standard.

The BET nitrogen adsorption gives information about total specific surface area since the molecule of nitrogen has shown a cross-sectional area of 16.2 Å thus ability to penetrate carbon black micropores [12]. The DeBoer model can be used to remove the influence of adsorption into micropores in order to calculate an external surface area. This calculation was derived empirically from experiments in which the N762 carbon black grade was tested and assumed to have no micropores. The theory based on the DeBoer method modified by McGee is known as the statistical thickness surface area (STSA). This method is supposed to give better information about the surface area accessible to rubber macromolecules than the BET method.

The STSA method has become a better alternative for the evaluation of external surface area than the adsorption of cetyltrimethyl ammonium bromide (CTAB). The CTAB method is based on the adsorption of large CTAB molecules which are not supposed to enter into micropores due to their size. Therefore, this method gives a measure of the external specific surface area.

There is a loose correlation between the SSA observed by BET theory and the so-called activity of filler [14].

BET < 10 $m^2.g^{-1}$:	inert filler
BET = 10-60 $m^2.g^{-1}$:	semi-active filler
BET > 60 $m^2.g^{-1}$:	active filler
BET > 100 $m^2.g^{-1}$:	very active filler

Another characteristic used for the SSA evaluation of carbon black is the adsorption of iodine. The iodine number is expressed in milligrams of iodine adsorbed per gram ($mg.g^{-1}$) of carbon black. It is not a true surface area but due to the adjustment of the iodine solution, the values are generally in a good agreement with the nitrogen surface area for non-porous and non-oxidized carbon black types. Iodine adsorption is influenced by microporosity but not as much as nitrogen adsorption due to the larger size of the iodine molecules.

The structure of carbon black

The term structure has been used in the carbon black industry for many years to describe one of the most important properties of carbon black that strongly affects properties of filled rubber compounds [16]. The term structure is defined by the international standard ASTM D3053 as the quality of irregularity and deviation from sphericity of the shape of a carbon black aggregate. Through the literature, primary and secondary structures of carbon black are differentiated usually.

The primary structure is an expression used to describe the irregularity and deviation from sphericity of individual aggregate. The primary structure undergoes only minor breakdown during mixing and dispersion, and requires a large energy to fracture [17].

The secondary or transient structure is a term used to describe an agglomeration of any number of aggregates, held together by attractive interactions such as Van der Waals forces or/and polymer bridges [12, 17]. Secondary structure is readily disrupted during processing and can be reversible [17]. The process of reversion of particles in a matrix is called flocculation and will be discussed later in this work.

Generally, there are two main approaches for the evaluation of carbon black structure – the determination of liquid absorption or specific volume at a given mechanical compression [7]. Both methods are based on the assessment of the amount of free air-filled voids between coalesced carbon black particles in the

aggregate. According to Donnet, the amount of free voids is referred as void volume [7]. The void volume can be calculated as follows:

$$VV = V_A - V_C \tag{2}$$

Where *VV* refers to the void volume in cubic centimetres per one hundred grams which is the difference between the volume of filler aggregates V_A and the equivalent volume of fully compacted solid body V_C.

The void volume in a given volume of carbon black is considered as a measure of carbon black structure, i.e. the degree of particles' aggregation [7]. The degree of particle aggregation determines the packing density of carbon black, i.e. the system of uniform spheres in tetrahedral packing has void volume of 36 %. However, the deviation from the sphericity of the shape of aggregates prevents a closer packing. Hundreds of megapascals are necessary to reach void volume corresponding to the packing of uniform spheres. In general, the larger the measured internal void volume, the more complex, open, and branched aggregates and the larger the structure [12].

The method of liquid absorption generally known as the oil absorption number (OAN) is based on filling up the voids in and between agglomerates and aggregates with an absorbent as simplified in Figure I-3. The oil absorption test is an automatic vehicle demand test where an absorbent, usually dibutyl phthalate (DBP) or paraffinic oil, is added dropwise into a small internal mixer where is mixed with a sample of carbon black by rotors. When enough oil is added to fill all the voids between aggregates there is a change in the mixture from a free-flowing powder to a semi-plastic compound, which raises a torque on the rotors to a preset torque endpoint, or alternatively the entire torque curve can be recorded and the endpoint is a certain percent (typically 70–80 %) of a maximal torque. Nowadays, paraffinic oil was approved by ASTM as a more suitable absorbent due to harmful impacts on environment and the carcinogenic character of DBP which is used the most widely [12].

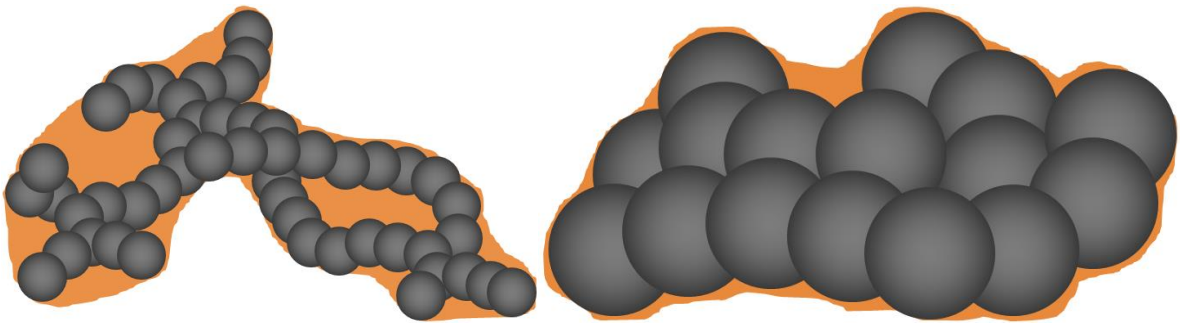

Figure I-3. The exemplification of the absorbent (surrounding contour) consumption according to the structure complexity of aggregates. High structured carbon black in the left hand side of the picture and low structured carbon black on the right.

There are some deficiencies cited with the oil absorption test however. Probably the most important is that OAN does not provide information about primary structure of carbon black and offers little insight into aggregate reduction, which is known to occur during the mixing or the dispersion cycle. Industries have been searching for a single experimental technique that could provide information on both the primary and secondary structure in a carbon black sample [16, 17]. Therefore, an improved structure test is the one that provides specific estimates of intra-aggregate void volume and correlates well to end-use applications including compound processability and reinforcement properties [16].

Thus an alternative method was developed and adopted for oil absorption wherein the sample is compressed at 24000 psi four times before the oil absorption is measured. Hence the alternative test referred as the oil absorption number of compressed sample (COAN) seeks to approximate the level of structure present in a carbon black that is mechanically mixed into rubber. Although the COAN has proved itself to be a useful tool, one is cautioned to consider that the breakdown of structure may vary considerably according to the parameters of the polymer into which the carbon black is mixed [12]. Nevertheless, COAN minimises the effects of secondary structure which provides a better relationship to in-rubber properties [16].

It was proposed many years ago that structure could be measured through volumetric measurements of compressed carbon black at specified compressions. Referred to as void volume it did not obtain favour over oil absorption methods during the time period of 1960’s as the equipment for this test did not provide values as precise as oil absorption techniques. This void

volume test was revisited in the 1990's when technology for load cells and other necessary equipment had improved significantly. These improvements in technology made it clear soon that void volume measurements by compression could be as accurate and precise as oil absorption methods [18]. In 1976 Donnet and Voet wrote an extensive review about the compressed void volume of carbon black describing a comprehensive investigation on the compressibility of carbon black and mentioning the superiority of the compression void volume method over the oil absorption approach [7]. Later on, Joyce et al. [16] and Wampler [18] validated that compressed void volume offers a significant improvement in carbon black structure measurement when compared to oil absorption methods.

In these days, a range of commercially available equipment for the assessment of compressed void volume exists, e.g. Void Volume Tester by Brabender (Figure I-4) or the Dynamic Void Volume Analyzer by Micromeretics.

Figure I-4. Void Volume Tester by Brabender.

The surface energy and chemistry of carbon black

The surface chemistry and energy of carbon black are other two important parameters of carbon black considering their influence on rubber reinforcement [14]. Schröder et al. [19] described energetic surface structure (sometimes also called microstructure) by the site energy distribution function *f(Q)*. This was determined by gas adsorption isotherms using ethene as the adsorbate. By deconvolution of the site energy distribution function of N220 to four Gaussian peaks (I-IV) it was shown that carbon black surface is energetically very heterogeneous and consists of at least four different energetic sites, as shown in Figure I-5.

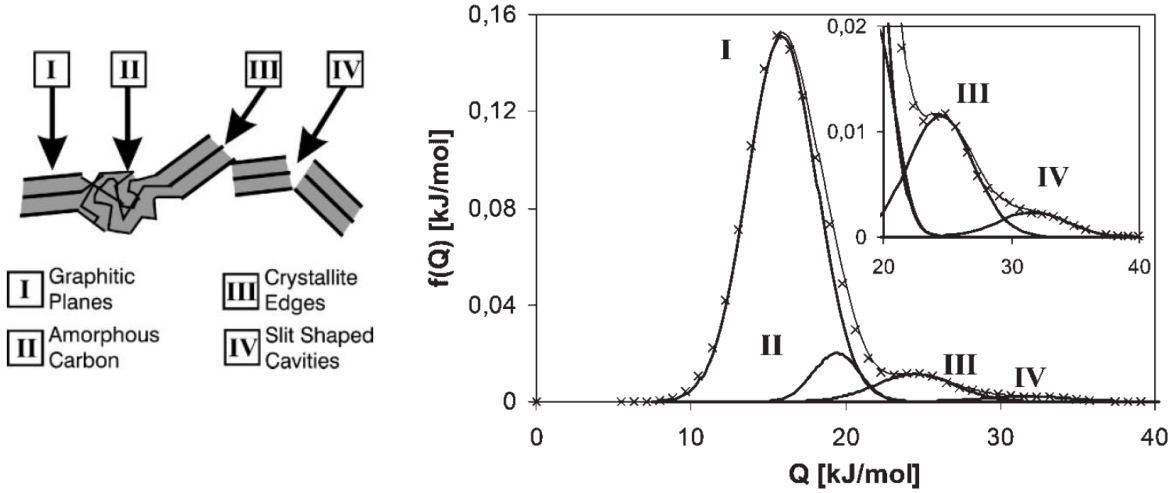

Figure I-5. Schematic picture of four different energy sites (left) as determined via gas adsorption isotherms [19].

These energy sites were found at the following Q values: I (Q ~ 16 kJ.mol^{-1}); II (Q ~ 20 kJ.mol^{-1}); III (Q ~ 25 kJ.mol^{-1}); IV (Q ~ 30 kJ.mol^{-1}). Graphitic regions were found to be the less energetic ones. The other three left domains correspond to amorphous carbon (with sp^3 hybridisation), microcrystallite edges or cavities between two crystallites. From lower to higher, energy sites described on the filler surface are: graphitic planes, amorphous carbon, crystallite edges and cavities.

The amorphous energetic sites vanish upon a graphitisation process. It is well known that graphitisation increases the degree of crystallisation of carbon black.

When virgin N220 and graphitised N220 are compared in Figure I-6 a significant difference in site energy distribution function is observed.

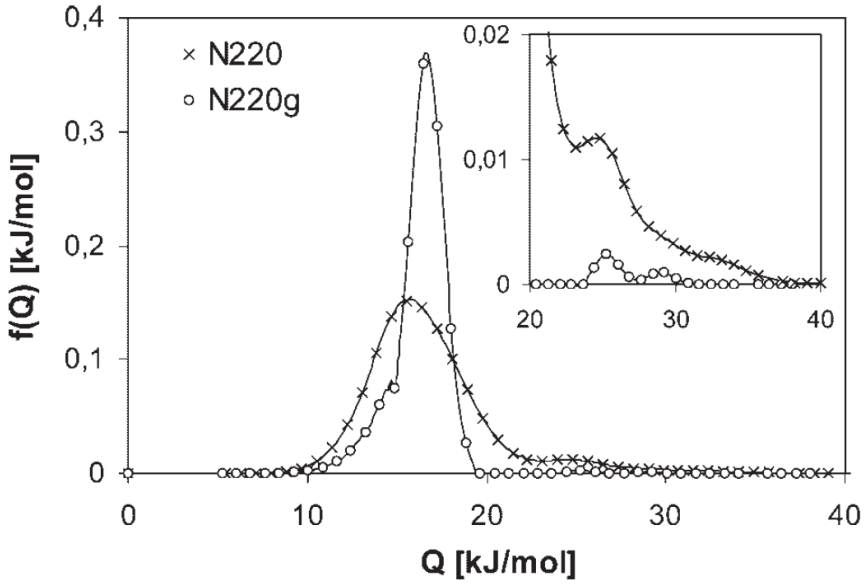

Figure I-6. The difference in energy distribution function for virgin and graphitised N220 [19].

Graphitised N220 is composed of more than 99 % of site I. Site II is missing completely because amorphous carbon is transformed to graphitic planes. III and IV sites related to crystallite edges and cavities are presented in traces only.

The presence of each site and mutual ratio depend on the production process and particle size of the carbon black grade, as shown in Table I-4.

Table I-4. Adsorption sites I-IV for ethene at the surface of various carbon black samples as determined by Schröder et al [19].

Energy sites	**N115 %**	**N220 %**	**N220g %**	**N550 %**	**N990 %**
I (Q ~ 16 kJ.mol^{-1})	69	84	99	93	96
II (Q ~ 20 kJ.mol^{-1})	13	7	-	6	-
III (Q ~ 25 kJ.mol^{-1})	15	7	<1	1	3
IV (Q ~ 30 kJ.mol^{-1})	3	2	<1	<1	1

Reinforcing effect of carbon black depends very closely on the amount of highly energetic sites. Furthermore, Schröder et al. [19] showed that with increasing particle size the amount of high energetic sites per gram of filler decreases dramatically showing very different surface activities to polymers. This means that the percentage of high energetic sites is not constant for the grades with different mean particle sizes, which leads to the conclusion that the value of specific surface area is not sufficient to describe the surface activity of the filler. Tunnicliffe et al. [20, 21] has carried out experiments where reinforcement potential and filler flocculation behaviour of graphitised carbon black was compared to a virgin carbon black. Fleck et al. [22] has carried out tests where carbon black surface was treated with an ionic liquid 1-allyl-3-methylimidazolium chloride (AMIC) which reacted with the highly energetic sites on its surface.

Both mentioned surface modifications, i.e. graphitisation and ‘coating’ as well as other methods [11], led to deactivation of the carbon black surface which is related to a decreasing amount of highly energetic sites. As the consequence, mechanical experiments show higher fragility of filler network of modified carbon black. Also the flocculation behaviour is changing significantly due to weaker polymer-filler interactions [11, 19-22].

It was shown that the surface morphology including surface crystallinity and roughness are key parameters on the final activity of carbon black which can be changed by surface modification such as plasma treatments or graphitisation. However, these presented parameters affect the dispersive component of the surface activity mainly which is the one governed by Van der Waals forces. Nevertheless, the chemical composition can play a very important role in the final activity of the filler also. The energy component affected by changing surface composition is named the specific component and is driven by polar interactions [11].

Because of its manufacturing process, carbon black surface includes some organic and mineral impurities. Organic impurities are mainly poly aromatic hydrocarbons. They correspond to partially unconverted feedstock that has adsorbed onto carbon black surface. Organic impurities are present at a very low content and it has been demonstrated that they have no significant effect on carbon black reinforcement [14].

Mineral impurities come from quench and pelletization in the carbon black production process. Even if this water is purified, the remaining mineral salts precipitate onto the carbon black surface and, because of the high temperature, they are reduced to basic salts. Mineral impurities do not seem to alter carbon black reinforcement properties but they have a significant effect on vulcanisation speed, which increases with the pH value of carbon black [14].

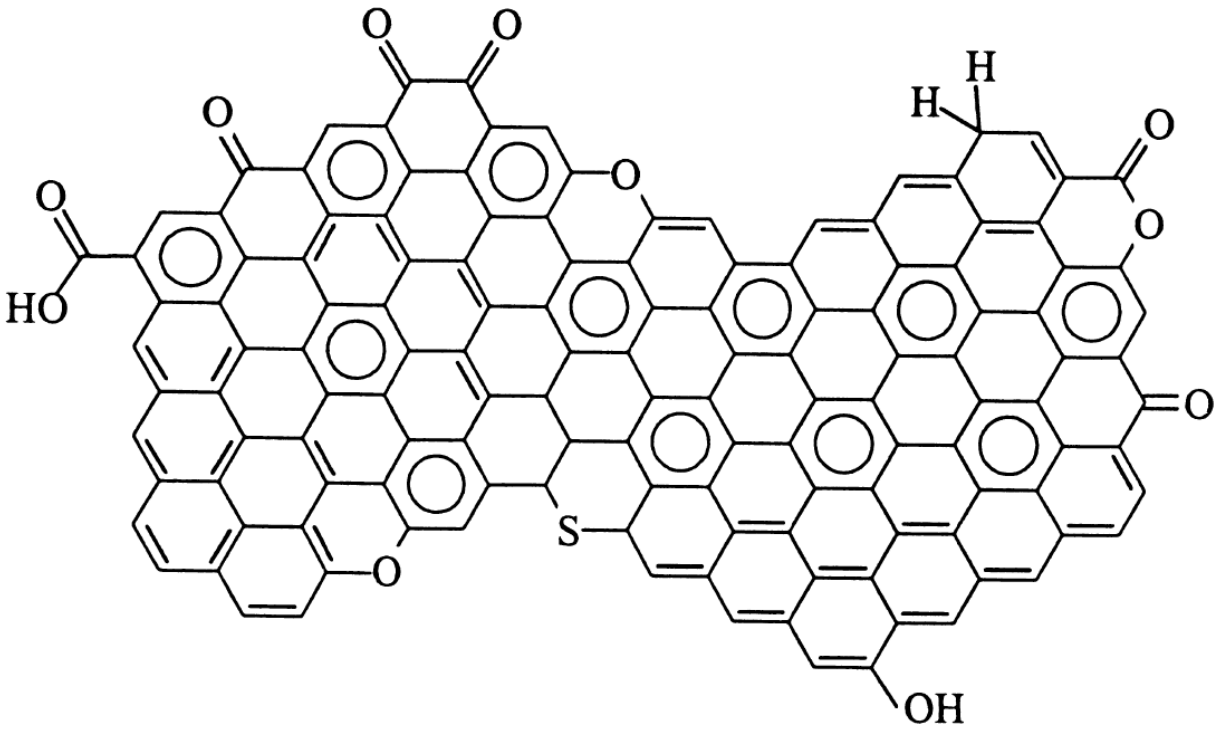

Figure I-7. Chemical functional groups on the surface of carbon black [14].

In Figure I-7 the wide accepted model of chemistry on carbon black surface made by Bueche is presented. In this model besides C some functional groups essentially composed of H and O such as carboxylates, lactones, phenols, aldehydes and quinones are present. When ratios of atoms are calculated the obtained values are 77.7 % for C, 9.8 % for O and 12.5 % for H [14]. However, Gerspacher et al. [23] shown that for furnace carbon black, the carbon content is between 95 and 99 %. Among the other components present on carbon black there is sulphur in between 1 and 1.5 %. Sulphur is carried into the carbon black through the feedstock. It is non-extractable and basically inert [11].

A large variety of oxygen containing functional groups, most in minute quantities, has been detected in carbon black. Donnet et al. emphasise that a

number of reported data have been obtained on lamp or gas blacks, which are sensitive to contamination by oxygen and other heteroatoms and it is well established today that carbon black surface chemistry plays a very minor role, if any, in the reinforcement of general purpose elastomers, i.e. essentially diene rubbers (NR, BR, SBR) and EPDM [7]. In contradiction seems to be a finding of a strong correlation between a hydrogen content of carbon black and their reinforcing ability [14].

However, it is important to note that the surface of carbon black cannot be considered as chemically inert and among surface area and structure complexity, the surface energy and chemistry of carbon black are important parameters related to the reinforcement of rubbers.

DISPERSION OF CARBON BLACK IN RUBBERS

There are many definitions of the term dispersion throughout the literature and authors use this term in different ways. According to Parfitt [24] the term dispersion is used to refer to the complete process of incorporating a powder into a medium such that the final product consists of fine particles distributed throughout the medium [24]. This definition suit to the concept of this work well.

Systems of particles in liquid are commonly encountered in a wide range of industrial processes. The size of dispersed particles can vary from fractions of a millimetre to few nanometres. Since carbon black is generally considered as nanomaterial, having at least one dimension with a size less than about one micrometre, carbon black systems are usually termed colloidal [25].

To reach homogeneous dispersion of particles in a medium, many methods exist which are usually based on more than one-step mixing.

In rubber industries, mixing of rubber compounds is a very sophisticated task [26]. This is due to the fact, that a common rubber compound is formed of at least ten different components which can be dosed in all the possible forms such as bales, powders, oils, pellets, chips, resins or pastes [26]. The form of each component together with various solubility parameters make the homogenisation

of all components very complicated. Therefore, the knowledge of physics, chemistry and chemical kinetics is required. Thermodynamically, the mixing is driven by the Gibbs free energy. The Gibbs free energy of the compound must be lower than the free energy of each ingredient generally. The Gibbs free energy ΔG is given by:

$$\Delta G = \Delta U + p.\Delta V - T\Delta S \qquad (3)$$

Where ΔU is the enthalpy of mixing, which is a measure of the change of internal energy in Joules; ΔS is the entropy change; p is the pressure in Pascal; T is the temperature in °C; and ΔV is the volume change during mixing in cubic metres. The mixing process is efficient when $\Delta G < 0$ [5].

For the homogenisation of these components into a free flowing form, discontinuous mixing in an internal mixer (kneader) or a two-roll mill or continuous mixing in continuous mixers can be used. The mixing via internal mixers is still the most versatile and economic solution [5].

It is important to adjust mixers correctly to reach the maximum mixing effect in a certain device because ingredients in rubber compounds are delivered in various forms as already mentioned. The efficiency of the mixing process can be influenced by the following factors:

- Mixing time
- Chamber temperature
- Torque
- Energy
- Absolute number of revolutions [5].

The mixing process can be accelerated by increasing the number of revolutions, shear or ram pressure [5]. However, after a certain time of mixing a constant dispersion level is reached which does not improve any further.

There are two basic types of internal mixers differing in the shape of rotors – tangential and intermeshing rotors.

Tangential rotors

Featured characteristic of the tangential rotors is that the movement pattern of the wing tips of each rotor does not pervade each other. Thus there is an existing gap between the wing tips of the two rotors. For some mixers, the gap is adjustable. This, together with the independent speed control of each rotor, provides the main advantage of this mixer type. Usually, one rotor runs 10 % faster than the other. Quite recently, so-called even speed mixing has been used where rotors run at the same speed and the adjustment of the radial distance between rotors is used to enhance the mixing efficiency. However, in tangential rotors the area with the highest mixing efficiency is between the rotor and the chamber wall.

Tangential rotors, as presented in Figure I-8, have several types and profiles. They can differ in the number of the wings, the shape of the wings, the position of the wings, the wing length and the angle to the central axis of the rotor. The variability of tangential rotors is much higher than for the intermeshing rotors. Subsequently, all the mentioned parameters affect the mixing efficiency and the energy they introduce into the compound.

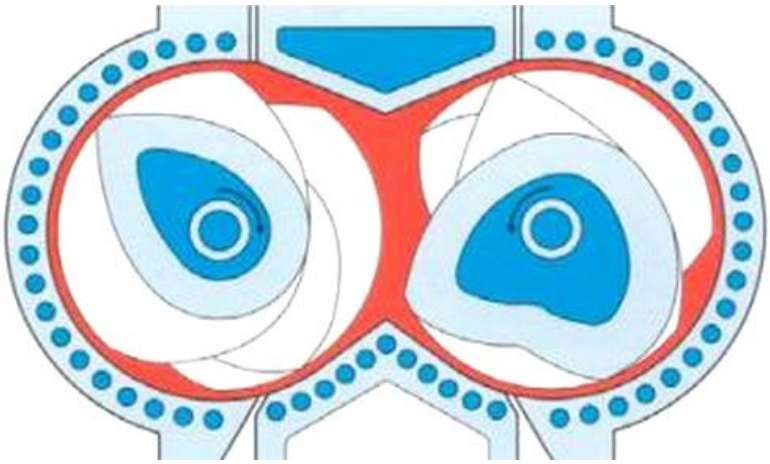

Figure I-8. Tangential rotors [27].

One limitation of internal mixers is that the mixing chamber cannot be filled completely in order to achieve high quality mixing. Compounds need free space in the chamber so that they can move around in an optimal manner. Filling is driven by the fill factor which is the ratio between the useful volume and the free volume. Usually, the optimal fill factor in case of tangential rotors is between 70 and 85 % and differs according to a particular compound composition and properties [5]. The tangential rotors are used when carbon black compounds are mixed due to the higher fill factor [2, 5].

Intermeshing rotors

The main difference to tangential rotors is that the paths described by intermeshing rotor tips do overlap each other as shown in Figure I-9. Therefore, the radial distance between the two rotors is fixed and the rotors speed is the same. The highest efficiency of mixing is in the common gap between the two rotors. A very high level of deagglomeration can be achieved using the intermeshing rotors. Intermeshing rotors occupy more space in the mixing chamber so the fill factor is approximately 5-10 % smaller than for the tangential system. Consequently, the intermeshing system offers a more efficient cooling system. The intermeshing rotors are used particularly when silica compounds are mixed.

The mixing efficiency is significantly increased compared to the tangential rotors [2, 5].

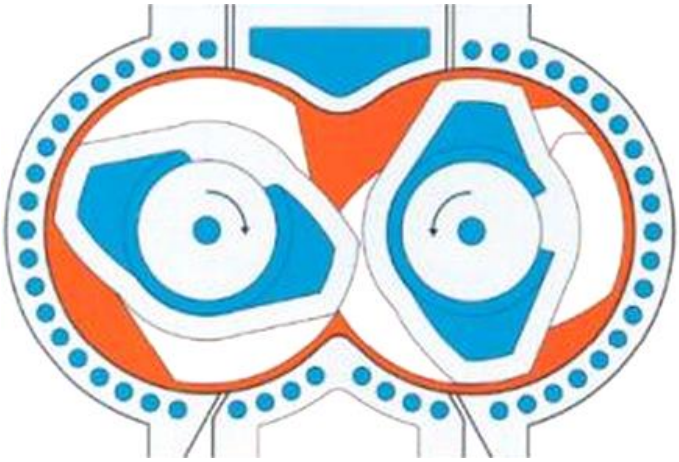

Figure I-9. Intermeshing rotors [27].

Solid fillers, i.e. carbon black or silica are usually delivered in pelletized form. Thus, the general purpose of the mixing process is to break up the pellets and ensure homogeneous distribution of filler aggregates in a shortest time possible [5]. Always, the filler dispersion has been known to be critical to the final characteristics of rubber compounds. With the development of high performance elastomers and the more efficient use of raw material in the last decade, this subject has gained even higher interest. Good filler dispersion improves tyre properties such as rolling resistance, wear resistance and traction [26].

The mixing process can be divided into two main stages. For the final properties and performance of rubber products both phases are very important [2, 26]:

1. Incorporation of carbon black
2. Distribution of carbon black aggregates

Incorporation of carbon black

The incorporation is the first stage of the mixing process when all the components of a rubber compound are mixed together and form a compact mixture. First, when a rubber is being fed into a mixing chamber the so-called mastication proceeds. Mastication is a process of lowering the viscosity of rubber when polymer macromolecules are deformed at high shear and tensile forces up to their breakage point.

Since carbon black is usually transported in form of pellets in the size range from less than a micrometre to a few millimetres, they must be fractured from its original size into pellet fragments and large agglomerates. These are further deagglomerated in the shear field of the mixing chamber to smaller entities when a so-called dispersive mixing takes a place. Pellets may require a considerable mechanical energy to break them down completely to the point when the surface of each aggregate is available to the wetting rubber. Presumably agglomerates which cohere by Van der Waals forces would

normally require less energy than aggregates where large pressures are necessary for fracture [2, 24].

As a result of dispersive mixing, the interface becomes larger and phase bonding is improved. Subsequently, wetting of the solid surface and encapsulation of the pellet fragments and agglomerates by polymer macromolecules proceeds. This leads to the further size reduction and finally the formation of filler aggregates [26]. For the rubber macromolecules it is necessary not only to wet the external surface of carbon black aggregates, they must also displace air from the internal voids in aggregates [24]. This is driven by the shear forces and pressure in the mixer when polymer macromolecules are squeezed into the voids replacing air [26]. Hence this aspect will involve knowledge of the wetting characteristics of the system and some assessment of the dimensions of the internal surfaces [24].

Shiga and Furuta [28] described the deagglomeration process by the “onion skinning” model where the small aggregates sheared from the agglomerates are distributed in the flow direction around the agglomerates. The model, shown in Figure I-10, explains that the number of aggregates increases exponentially during the dispersion phase. Due to the increasing particle number, inter particle distance lowers and approach a critical value at which a filler network formation starts [2, 5].

The quality of filler incorporation (deagglomeration) can be described by the parameter called filler macrodispersion. The filler macrodispersion is according to ASTM D7723-11 defined as the degree of distribution of filler into a compound, generally on a scale of less than 100 micrometres but greater than 2 micrometres.

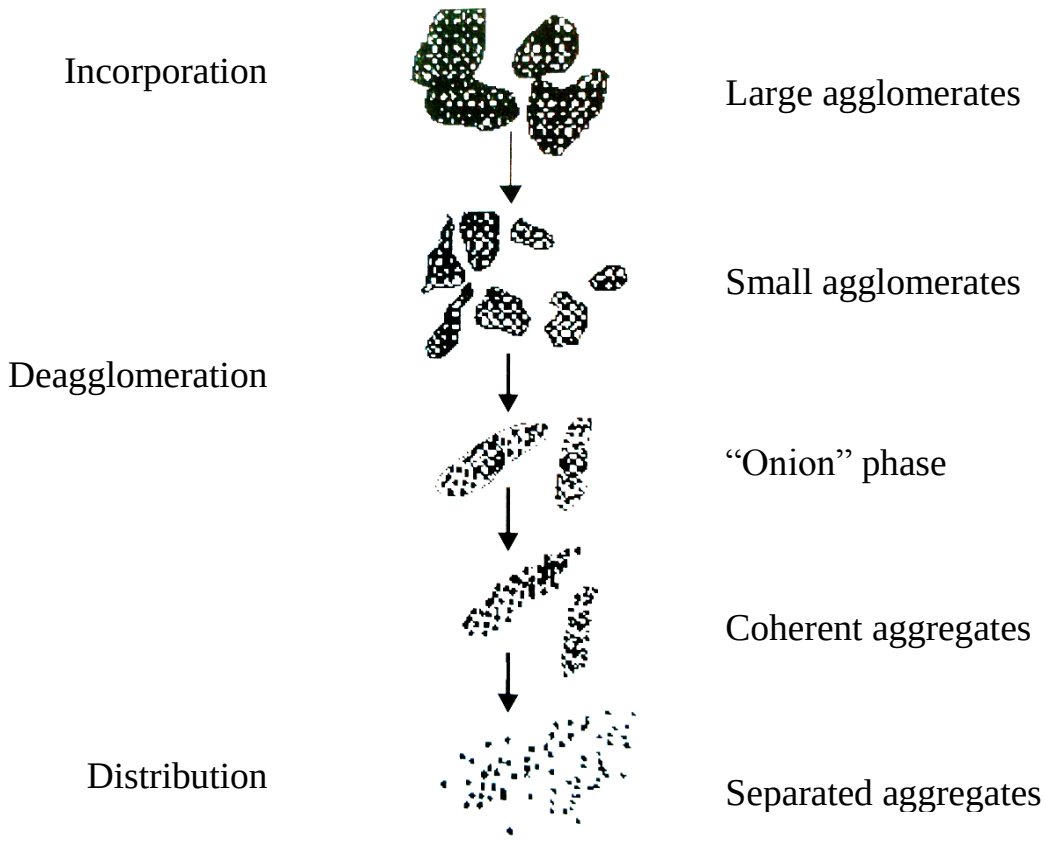

Figure I-10. The model of carbon black dispersion process proposed by Shiga and Furuta [26].

Distribution of carbon black aggregates

With distributive mixing a degree of uniformity throughout the mixture is supposed to be achieved. In an ideal distributive mixing process, there is no breakdown of agglomerates anymore and the interface per unit volume remains constant. The randomisation of the filler aggregates with a constant size is an important feature at this stage of mixing. The distributive mixing thus leads to a homogeneous distribution of the particles. The filler concentration fluctuations in small volume areas of the rubber matrix are decreased while the average particle size remains unchanged [26].

The distribution process can be enhanced by repeated shearing and folding of the rubber compound. By the randomisation and transportation, the aggregates are separated from mutual vicinity. Homogeneity of filler distribution inside the rubber compound increases asymptotically. Nevertheless, even after this stage a degree of concentration fluctuates and the agglomerates are still monitored in many cases. This is why the standard deviation of a real mix is always high [2].

The comparison of good and low deagglomeration and distribution is given in Figure I-11.

The quality of filler incorporation can be described by the level of macrodispersion. On the other hand, the quality of aggregates distribution throughout matrix can be described by the parameter called filler microdispersion. This is related to aggregates on a scale of less than 2 micrometres.

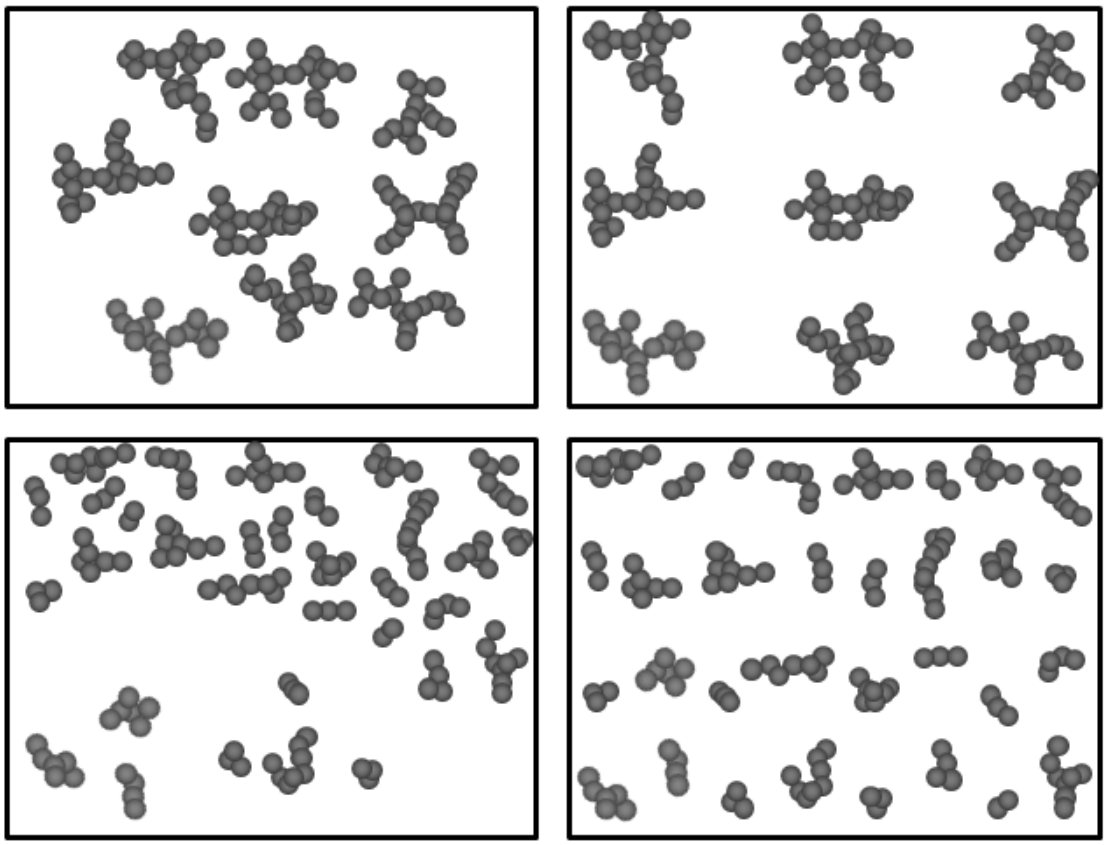

Figure I-11. The comparison of good and low deagglomeration and distribution. From upper left clockwise: 1. low deagglomeration, low distribution; 2. low deagglomeration, good distribution; 3. good deagglomeration, low distribution; 4. good deagglomeration, good distribution.

The incorporation of active fillers into a rubber or rubber blends generates unique improvements in dynamic-mechanical properties of elastomers generally termed reinforcement [6, 26]. The reinforcement of rubbers has become a primary purpose of carbon black since the invention of its positive influence on material properties of filled rubbers [7]. Since the third century B.C. until 1912, carbon black has been used primarily as a pigment in black inks. It was in England in 1912, when the great improvement in wear resistance after the incorporation of carbon black into natural rubber was invented.

Although the reinforcement of rubbers is not fully understood after many years yet and many mechanisms have been proposed the reinforcement is referred as the enhancement of tensile strength, modulus, abrasion and tear resistance obtained by the addition of a particulate material [1, 29]. It is generally recognised that the main parameters of fillers governing their reinforcing ability in rubbers are:

- The primary particle size or specific surface area which, together with loading, determines the effective contact area between the filler and polymer matrix. The influence of particle size on the reinforcement is shown in Table I-5.
- The structure or the degree of irregularity of the filler unit, which plays an essential role in the restrictive motion of elastomer chains under strain.
- The surface activity, which is the predominant factor with regards to filler-filler and filler-polymer interactions [30].

Table I-5. The potential of carbon black particle size for reinforcement of rubbers [8].

Particle size [nm]	**Strength**
1000-5000	Small reinforcement
<1000	Medium reinforcement
<100	Strongest reinforcement

The reinforcement phenomenon of carbon black has been studied by numerous researchers and many reviews were elaborated, e.g. by Kraus [31], Leblanc [32, 33] and Donnet and Custodero [8]. Principal mechanisms contributing to this phenomenon are assigned as follows: Van der Waals forces between filler and filler, Van der Waals forces between filler and polymer; chemical crosslinks or the chemisorption of polymer chains on the fillers' surface; the mechanical interlocking of polymer chains on to the filler surface and in the voids [8, 31-36].

The magnitude of reinforcement is usually evaluated at increasing dynamic shear strain. Under increasing strain amplitude, the dynamic properties of unfilled rubbers display only a little change while the dynamic modulus of filled rubbers decreases substantially as shown in Figure I-12, where the dependence of the dynamic moduli on the shear strain amplitude is plotted. Since the change in modulus of unfilled rubber is very small, the effect has been fully attributed to the filler related interactions. Hence, the addition of fillers to rubber compounds has a strong impact on the static and dynamic behaviour of rubber samples. In Figure I-12 Fröhlich et al. [30] summarised mechanisms influencing the reinforcement.

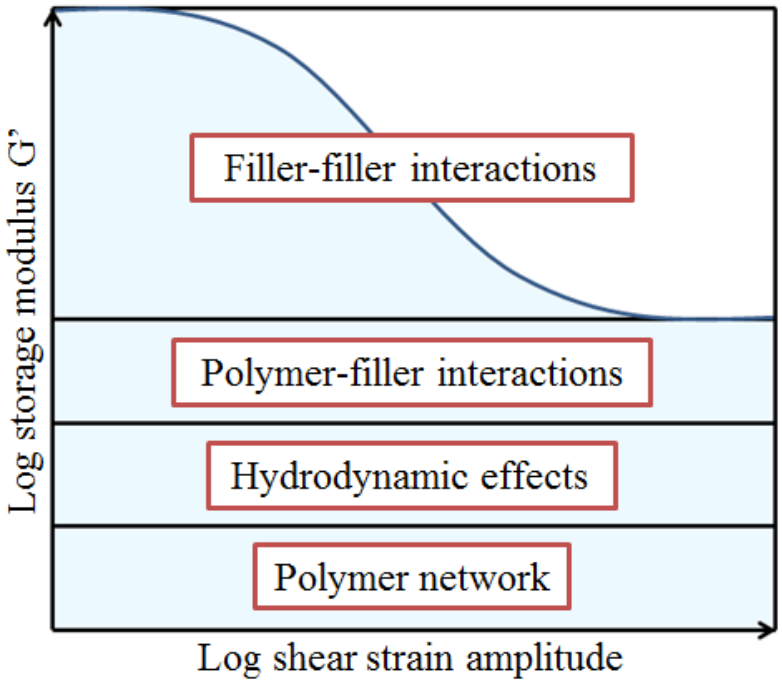

Figure I-12. Schematic diagram of the Payne effect.

The observation of behaviour of filled rubber compounds as presented in Figure I-12 was carried out using dynamic tests where cyclic strain is applied to the sample. Dynamic shear complex modulus *G** can be expressed simply as follows:

$$G^*(\gamma) = G'(\gamma) + iG''(\gamma) \quad (4)$$

Where *G'(γ)* is the storage, in-phase modulus and *G''(γ)* is the imaginary, out-of-phase modulus. The loss factor tan δ is given by the ratio of *G''(γ)* and *G'(γ)*.

In Figure I-12, the strain independent part of the modulus as a combination of the polymer network, the contribution from hydrodynamic effects and the modulus resulting from the in-rubber structure can be seen.

The polymer network contribution depends on the crosslink density of the matrix and the nature of the polymer.

The hydrodynamic effect is given by the effect of strain amplification, resulting from the fact that the filler is the rigid phase, which cannot be deformed. A theory of stiffening of rubber by a rigid filler is based on the Einstein's theory for the increase in viscosity of a suspension due to the presence of spherical colloidal particles:

$$\eta = \eta_0(1 + 2.5\Phi) \quad (5)$$

Where η is the viscosity of suspension, η_0 is the viscosity of incompressible fluid and Φ is the volume fraction of spherical particles.

Guth and Gold adapted the viscosity law to predict the small strain modulus of a rubber filled with rigid spherical particles and suggested

relationship between modulus and loading based on the hydrodynamic effect and mutual disturbance caused by sphere particles. They added an additional term to account for the interaction of fillers at large filler volume fractions [36-38]:

$$G' = G'_0(1 + 2.5\Phi + 14.1\Phi^2) \quad (6)$$

Where G' and G'_0 are shear moduli of the filled and the neat vulcanised rubbers and Φ is the so-called corrected volume fraction of spherical particles calculated from DBP parameter of carbon black [14].

However, the Equation 6 is limited to low concentrations of carbon black and assumes sphericity of the filler particles. Therefore, Guth introduced a shape factor *f* to take into account the asymmetry of the filler:

$$G' = G'_0(1 + 0.67f\Phi + 1.62f^2\Phi^2) \quad (7)$$

Where f is defined as the ratio of filler particles' longest length to its perpendicular breadth [30, 37]. The factor *f* accounts for all effects of filler properties on the modulus through effective loading and the structure which is very important. It was found that the experimental data of most fillers only fit this equation up to certain levels of loading which is defined as the critical loading Φ_{crit}. Above the critical loading, deviations are usually observed when experimental data are higher than predicted by this model.

The effect of polymer-filler interactions is attributed to the 'in-rubber structure', which can be understood as a combination of the structure of the filler in the in-rubber state and the extent of filler–polymer interaction. The in-rubber structure is the measure for the occluded rubber, which is shielded from deformation and therefore increases the effective filler content leading to a strain-independent contribution to the modulus. The filler-polymer interaction can be attributed to physical (van der Waals) as

well as to chemical linkages or a mixture of both. In the case of the silica-silane system this interaction is formed by chemical linkages.

Some authors [31, 39] suggested that the contribution of occluded rubber to reinforcement depends on the surface area of the filler when higher surface area would have greater amount of occluded rubber. In case of occluded rubber there is no reduction in the chain mobility of the rubber.

On the other hand, in the case of the bound rubber, there is a rubber layer in the vicinity of filler particle where molecular motion is restricted. Bound rubber is the amount of rubber which is not extracted when non-crosslinked filled rubber is subjected to solvent extraction. It is given by a combination of physical adsorption of polymer macromolecules, chemisorption and mechanical interlocking.

Fukahori [40] suggested three areas on a carbon black particle-rubber interface: GH (glassy hard) inner polymer layer where molecular motion is strictly constrained, i.e. the immobilised (bound) layer; SH (sticky hard), which is outer polymer layer where molecular motion is constrained compared to the bulk; and bulk polymer. This is shown in Figure I-13.

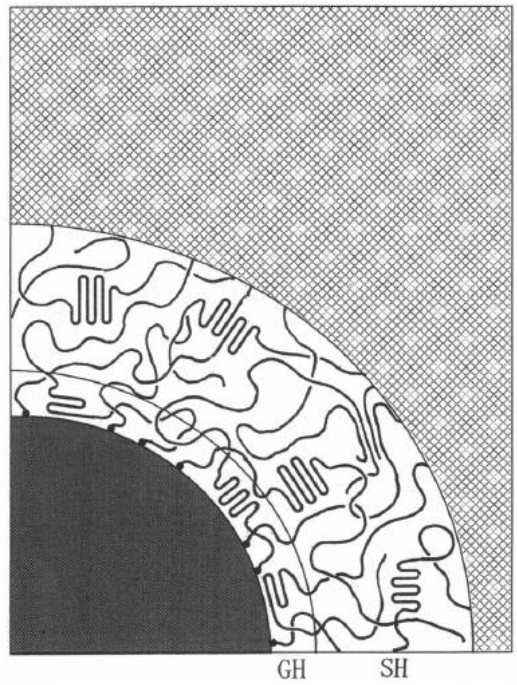

Figure I-13. Schematic picture of the interface model for carbon black particle-polymer matrix consisting of GH and SH layers and the bulk polymer [40].

On the other hand, Berriot et al. [41, 42] using H-NMR identified only two contributions – the immobilised interphase and the bulk, where the thickness of the immobilised layer is in the order of 1-2 nanometres and may increase or decrease under given external and internal conditions, e.g. temperature. He explained the presence of the immobilised layer by modified dynamic of polymer chains in the vicinity of a particle surface. Also a glass transition temperature gradient near a particle is discussed as shown in Figure I-14.

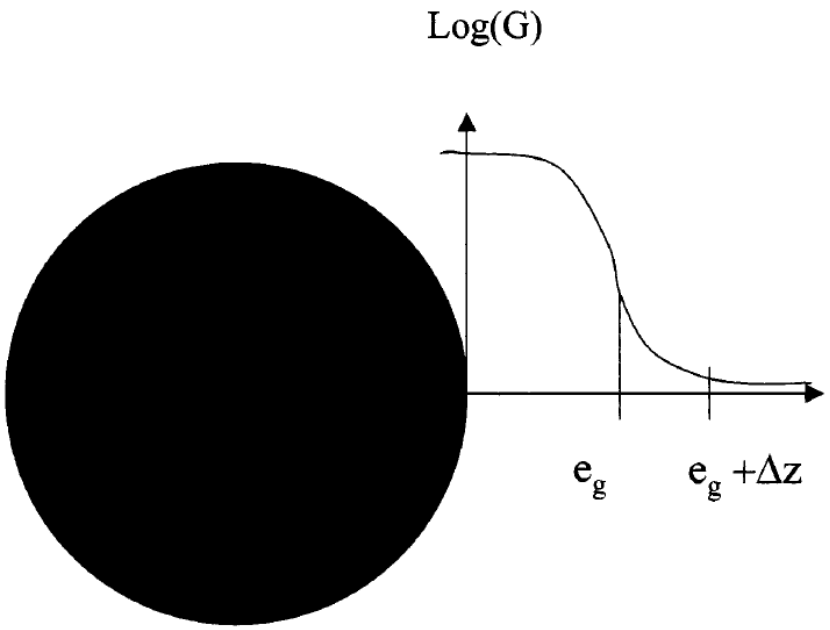

Figure I-14. Schematic diagram of the modulus variation in a vicinity of a particle (black) versus the distance from the particle surface. For $z < e_g$, the polymer is in a glassy state ($G = G_{glass}$). At $z > e_g + z$, $G = G_N$, where G_N is the plateau modulus of the rubber matrix.

Fukahori [40] and other authors [43, 44] proposed that the segmental immobilisation mechanism contributes to the overall composite reinforcement with the extent primarily affected by the size of inclusions. They stated that the nanoparticles, in contrast to microparticles, do not represent filler in the common sense but rather represent an agent able to modify the chain conformation structure and entropy as well as segmental dynamics.

The stress softening (filler-filler interactions). The non-linearity in behaviour at small strains is assigned to the gradual breakdown of inter-aggregate adhesion, i.e. filler network disintegration and this is generally known as the Payne effect [37, 45 and 46] which plays an important role in the understanding of reinforcement mechanism of filled rubber samples [47].

The strain-softening behaviour at medium to large deformations under quasi-static loading conditions is termed the Mullins effect and is attributed to the detachment of rubber macromolecules from the surface of filler particles [38]. Houwink [48] and later Dannenberg [7, 14, 35 and 49] explained that the detachment is caused by the slippage of rubber molecules over the filler surface as shown in Figure I-15. Regardless of the magnitude of applied strain amplitude, Wang [36] stated that the Payne effect can serve as a measure of filler networking which originates from filler-filler as well as filler-polymer interactions.

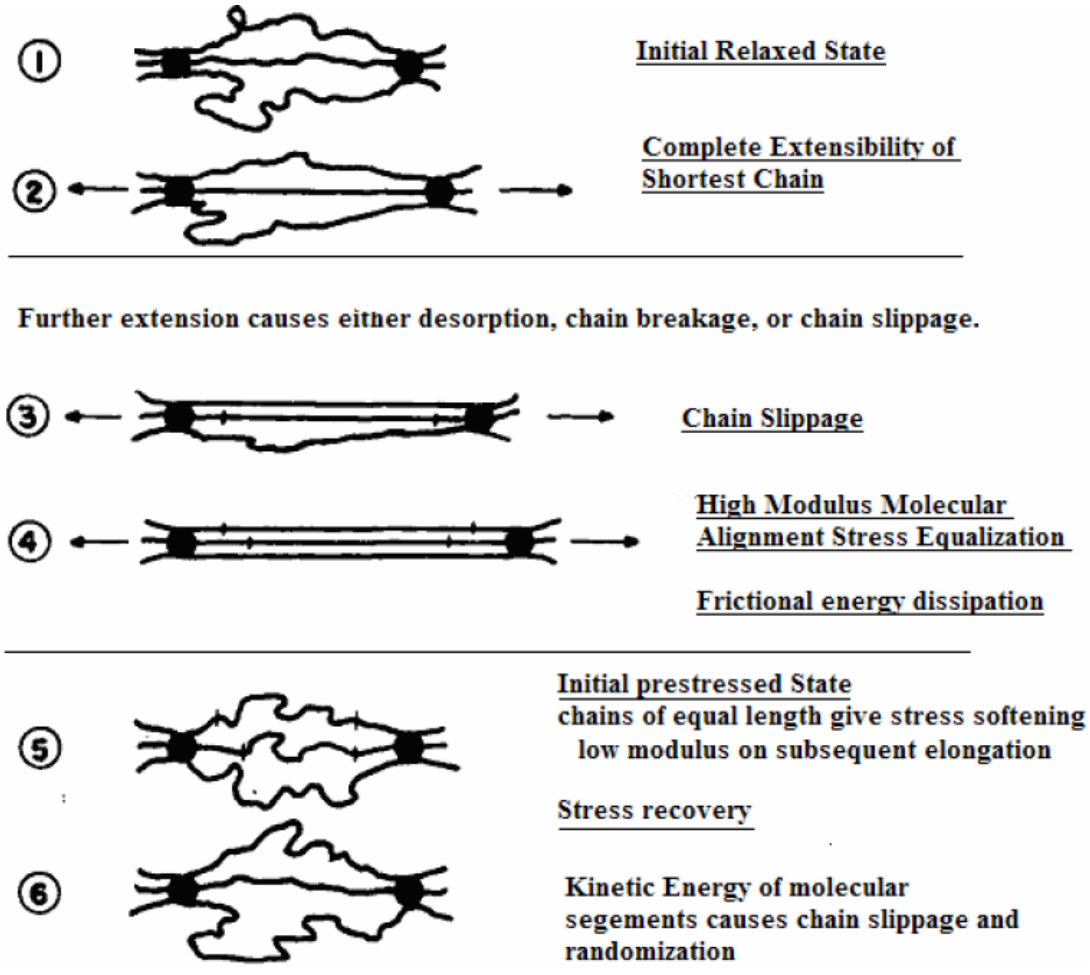

Figure I-15. The slippage mechanism proposed by Dannenberg [14, 35].

Kalfus [44] stated that the concept based on the assumption that the polymer matrix properties are modified by the filler surface corresponding to the immobilisation mechanism when during large strain amplitudes, the chain desorption, slippage and subsequent segmental mobilisation occur is the only concept able to bring a physically correct solution of the Payne effect and nanocomposites reinforcement above the T_g of a matrix.

CARBON BLACK FLOCCULATION IN RUBBERS

This chapter discuss carbon black behaviour in rubber compounds in post-mixing stages, when the process of carbon black dispersion is completed, i.e. the agglomerates are broken down and the aggregates are distributed throughout the matrix [24, 50 and 51].

The level of distribution is not stable in time since the aggregates tend to reagglomerate and reduce in number during post-mixing stages such as storage, extrusion and vulcanisation. Throughout literature, this process of agglomeration is described as flocculation or filler networking. Since, the term flocculation is used more frequently it is used in this work also. There are many definitions of the flocculation process [2, 15, 20, 36, 50, 52 and 53]. Schwartz et al. [53] described flocculation process as a reversible dynamic process during which aggregates that are dispersed in a matrix reagglomerate, forming larger objects called agglomerates connected to each other. Subsequently, these can be deagglomerated again by shear forces during mixing stage. Furthermore, Witten and Sander [54] and later Meakin [55] stated that at sufficiently long time and under favourable thermal conditions the growth of agglomerates can lead to the formation of a percolating filler cluster having a fractal like character.

Flocculation is a natural process caused by attractive interactions between the aggregates. These come into play when the mean spacing of the dispersed particles falls below a critical value due to the Brownian movement or a shear initiated movement caused by strain. Essentially, the flocculation behaviour of carbon black in rubber melts depends on two distinct influences [24, 25]:

- Collision mechanisms
- Interactions

Collision mechanisms

Particles must move in such a way that collisions occur. This may be achieved either by Brownian motion, fluid motion or sedimentation. Thus, there are three main collision mechanisms:

Perikinetic collision mechanism

Small particles in suspension can be seen to undergo continuous random movements of the Brownian motion [25], as depicted in Figure I-16. If a sufficiently long time is given to a particle undergoing the Brownian motion it will zig-zag back and forth, eventually visiting every point within the space confining the particle. This ergodicity of Brownian particles is the underlying reason for the spontaneous equalisation of particle concentration, a phenomenon generally known as diffusion. It should be pointed out that the equal probability for a Brownian particle to move back and forth at any one time does not conflict with the tendency of a Brownian particle to move away from its initial position over a period of time. The reference point, implied by the statement that a Brownian particle has an equal probability of moving back and forth, changes its position with time, but the initial position, from which the particle has a tendency to move away, is fixed over the period of time [25].

Brownian motion is the direct result of collisions between the particles and the fluid molecules surrounding them. In other words, it is a response to the thermal fluctuations of the surrounding fluid [25].

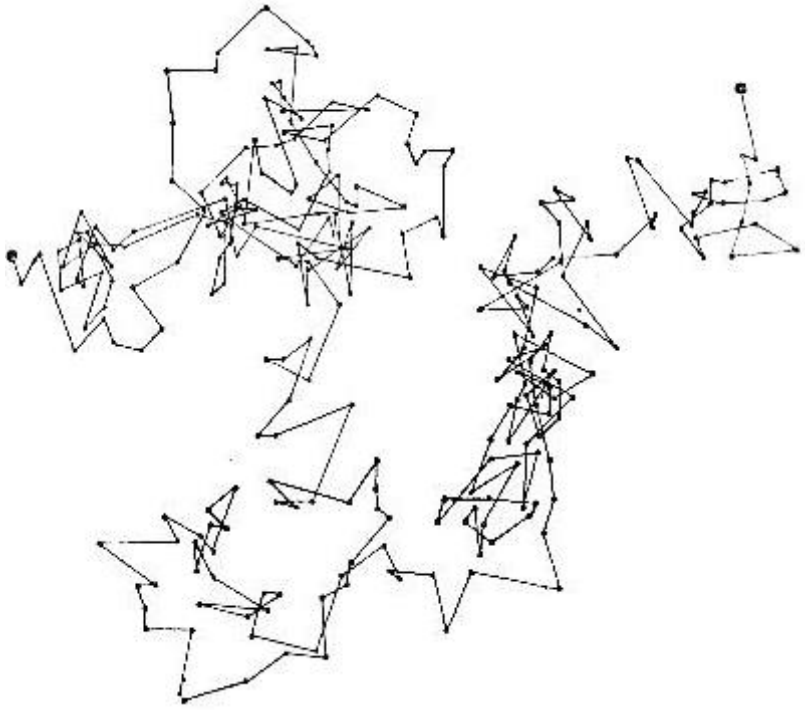

Figure I-16. Simplification of Brownian motion as observed by Perrin [56].

The Brownian motion of a particle is usually described by the mean square displacement. It is because the Brownian trajectory is not a mathematically smooth curve and the apparent velocity of a Brownian particle derived from it does not represent the true physically well-defined velocity of the particle. By tracking the movements of a colloidal particle at the usual experimental timescale intervals it was found its trajectory is of the self-similar nature. This ergodicity of Brownian particles is the essential reason for the spontaneous balancing of particle concentration, i.e. diffusion.

By treating Brownian motion as a series of random walks, Einstein showed that the mean squared displacement of Brownian particle is a one-dimensional projection, averaged over a long period of time *t* and can be expressed as:

$$< x^2 >= 2D_0 t \qquad (8)$$

Where x is the distance of the particle from the origin at time t, and D_0 is the diffusion coefficient.

Due to its entropic nature, the mean squared displacement of Brownian motion in three dimensions is as follows:

$$< r^2 >=< x^2 + y^2 + z^2 >= 3 < x^2 >= 6D_0 t \quad (9)$$

The diffusion coefficient is a constant for a single particle in an unbounded fluid, and is related to the friction coefficient ξ by the Stokes-Einstein relation:

$$D_0 = \frac{\mathrm{k}T}{\xi} \quad (10)$$

Where

$$\xi = 6\pi a_i \eta \quad (11)$$

Where k is the Boltzmann constant, T stands for the absolute temperature, a_i is the radius of a spherical particle and η is the viscosity of the suspending fluid [25, 57].

Orthokinetic collision mechanism

Fundamentally, flocculation processes are nearly always carried out under conditions where the suspension is subjected to some form of shear in practice. Either it is stirring or flow. Particle transport brought by fluid motion can give an enormous increase in the rate of interparticle collisions. This type of mechanism is known as orthokinetic.

It has been observed that aggregation of otherwise stable colloids can sometimes be achieved by the application of sufficiently high shear. The phenomenon of shear flocculation is probably an example of such an effect.

Collision efficiency for orthokinetic collisions cannot be adequately discussed without reference to hydrodynamic interaction. In fact, hydrodynamic or viscous effects can have a great effect on aggregation rates. As particles approach very close, it becomes increasingly difficult for the liquid between them to drain out of the gap and this tends to slow the aggregation process.

Although it needs to be considered, the hydrodynamic effect does not have a dramatic effect on the perikinetic aggregation, slowing the rate by a factor of no more than about 2. In the case of orthokinetic aggregation, viscous interaction can be much more significant.

In reality, universal van der Waals forces counteract the hydrodynamic resistance at close approach and particle contact can be achieved. In the absence of hydrodynamic interaction, van der Waals attraction has little effect on the stability ration over the usual range of values. This is because dispersion forces operate over a rather limited range, much less than the particle radius, and so give only a minor increase in the effective collision radius (less than 10 nm) [25, 57].

The Smoluchowski treatment of orthokinetic collision rate assumes that particles in a uniform shear field move along straight streamlines until they collide with another particle. In reality, stream lines curve around obstacles such as other particles which make collision less likely. The conventional ‘no slip’ assumption implies that in the absence of any other effect, particles could not come into contact as a result of fluid motion, because the last layer of liquid between them could not be removed by viscous flow. Brownian motion and the presence of attractive interparticle forces allow aggregation to occur however [57]

Differential sedimentation

Differential sedimentation is a very important collision mechanism arising whenever particles of different sizes or densities are settling from a suspension due to gravitational forces. These lead to a reduction in number of particles with time. This is important mainly for larger particles or the ones of a higher density, which will sediment faster than small ones or those of lower density and capture the latter as they fall. The thermal agitation is normally sufficient to keep small colloidal particles dispersed [25, 57].

The effect of sedimentation is however less important for the aggregation promotion when particles have diameter in nanoscale or low density. However, even for an initially uniform suspension of equal particles, aggregates of different size will be formed which settle at different rates. This occurs in the later stages of flocculation often [25].

Interactions

Many of the important properties of colloidal systems are determined directly or indirectly by interaction forces between particles. These colloidal forces consist of several components and are greatly dependent on the surface properties of particles.

Interactions between colliding particles must be permanent. Particles which repel each other are said to be stable since they do not form clusters. Colloidal interactions are of a very short range. Usually much less than the particle size, so that particles have to approach very close to each other before any significant interaction is reached [25].

The two most familiar colloidal interactions are Van der Waals attraction and electric double layer repulsion. Electrical interaction between colloidal particles is one of the most important influences on a particle flocculation, stability and deposition. When two dissimilar phases are in contact, it is likely that there will be separation of charges and a difference in electrical potential between them [57].

Van der Waals attraction

Van der Waals forces or induced-dipole interactions (or Keesom forces or charge-fluctuation interactions, London interactions or dispersion forces) exist between all atoms and molecules and do not depend on whether the species are electrically charged [57].

These forces are based on spontaneous electric and magnetic polarisations of dipoles within the particles [24, 25]. These may be the permanent dipoles of polar particles or the dipoles that may be induced in non-polar particles which are nevertheless polarisable. The interaction between the dipoles is

electromagnetic in character, and it can readily be shown that this force is always attractive [24].

There are two theoretical approaches to the evaluation of Van der Waals attraction, i.e. the classical approach by London (microscopic) and the alternative (macroscopic). In the classical approach, Hamaker [58] has shown that the interaction between two macroscopic bodies is obtained by the pairwise summation of all the relevant intermolecular interactions. However, the assumption of complete additivity is a rather serious deficiency and resulting expressions always overestimate the interaction.

The additivity assumption is overcome through use of the alternative, macroscopic approach suggested by Lifshitz [59]. The interaction is derived entirely from considerations of the macroscopic electromagnetic properties of the medium. Extensive application of this theory has been hampered because the appropriate data are available for only a very limited number of materials. The London theory is used for estimating usually.

Electric double layer repulsion

The absence of forces opposing to the forces attractive could eventually lead to the aggregation of colloidal particles into sufficiently large clusters that may sediment or cream out of suspension. Colloid stabilisation then requires one or more mechanisms to provide repulsive forces to counteract attractive interactions. The most often repulsion interaction is that of the electric double layer.

Since in a medium containing ions a charged particle with its electric double layer is electrically neutral, no net coulombic force exists between charged particles at large distances from each other. As the particles approach, the diffusive parts of the double layers interpenetrate giving rise to a repulsive force which increases in magnitude as the distance between the particles decreases [24, 57].

This effect can be generally imagined as an elastic effect when some kind of deformable bumper is attached to the particles. The bumper distorts as two particles approach one another. This deformation results in an elastic restoring force, tending to keep the particles apart [57].

Total interaction energy

Van der Waals attraction and electric double layer repulsion forms the well-known DLVO theory developed independently by Derjaguin and Landau (1941) and Verwey and Overbeek (1948). This theory explains a considerable amount of experimental data. Based on the DLVO theory, the total interaction energy between a particle and a collector surface is usually described by the potential energy calculated as the sum of Van der Waals and electrical double layer interactions:

$$V_T = V_A + V_R \tag{12}$$

Where V_T is referred as total potential energy which is the sum of the attractive energy V_A and the repulsive energy V_R. This is graphically demonstrated in Figure I-17.

Depending on conditions, particles may be stable or may aggregate into primary or secondary minima. It is possible that a suspension may be stable over a certain range of shear rates, but aggregate at higher and lower values. For aggregation into secondary minimum, high shear rates would tend to pull aggregated particles apart. However, high shear rates can increase the chance of colliding particles overcoming potential energy barrier and being captured in a primary minimum [34, 44].

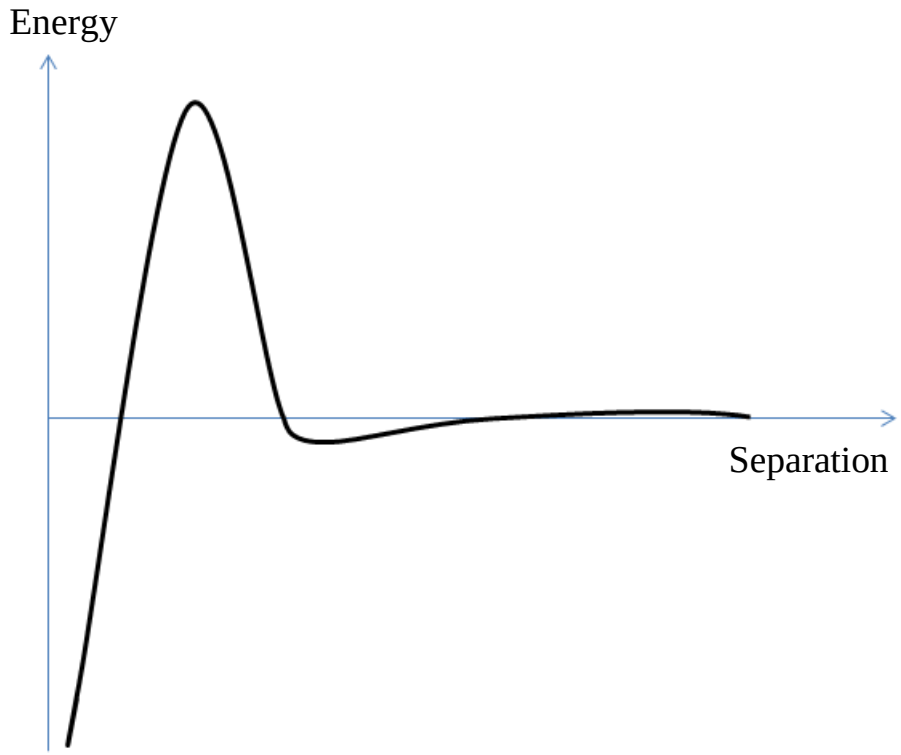

Figure I-17. Sketch of the potential energy versus interparticle separation taking into account repulsive forces and Van der Waals attraction. The absolute minimum is at contact between particles and a secondary minimum is at larger separations.

However, there are situations where other types of interaction have to be invoked because the combination of the two principal forces does not give satisfactory agreement with experimental data. In such cases, additional short-range forces may have to be included.

Structural force is the term associated with the forces that are developed as particles with adsorbed fluid interact. Structural force describes the interactions arising specifically from the adsorption of solvent, surfactant or macromolecules at the interface [25]:

$$V_T = V_A + V_B + V_R \tag{13}$$

Where the term V_B represents other short-ranged interactions here.

Polymer macromolecules can play a very important role in flocculation phenomena according to the adsorbed amount of polymer on surface of the filler particles. There are three mechanisms possible:

- Lack of polymer adsorption

Polymers which do not adhere to surfaces immersed in a solution induce attractive forces between them. This interaction arises from the depletion of polymers in the channel between the colloidal particles as shown in Figure I-18 [24].

Depletion attractions between colloids are specific example of the Perturbation-Attraction Theorem described elsewhere [57]. Depletion attraction occurs when large colloidal particles are in solvent containing smaller particles that cannot penetrate the colloidal particles. The theorem says that attractive interaction is expected when the separation between the surfaces is small enough to sense the structure of the solvent – the diameter of the small particle.

Consider the case where two surfaces are immersed in a suspension of smaller colloidal particles. When the particles are not excluded from the region between two large spheres, the pressures on each surface are balanced. However, when the particles are excluded by their size from entering the channel between the large particles, the osmotic pressure (Π) on the outer surfaces which is associated with the suspended particles is not counterbalanced, leading to an effective attractive force per unit area between the plates of magnitude Π. The range of this interaction is approximately the solvent/colloidal particle diameter [57].

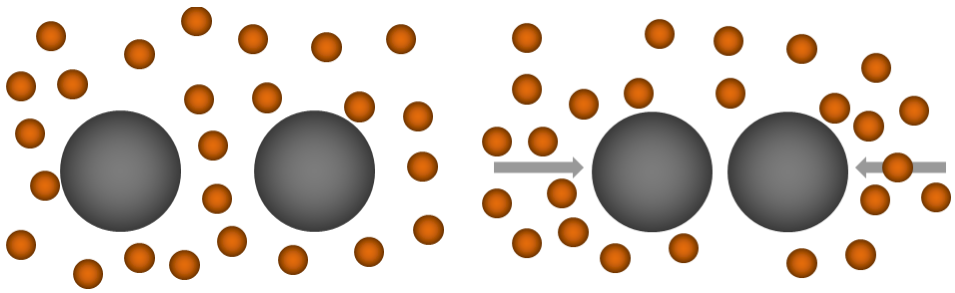

Figure I-18. Schematic interaction of two particles due to depletion forces.

- Small amount of adsorbed polymer

In some cases a small amount of adsorbed polymer can promote flocculation by a bridging mechanism when segments of a single polymer chain are adsorbed on more than one particle. This phenomenon is called bridging flocculation [53] and is simplified in Figure I-19.

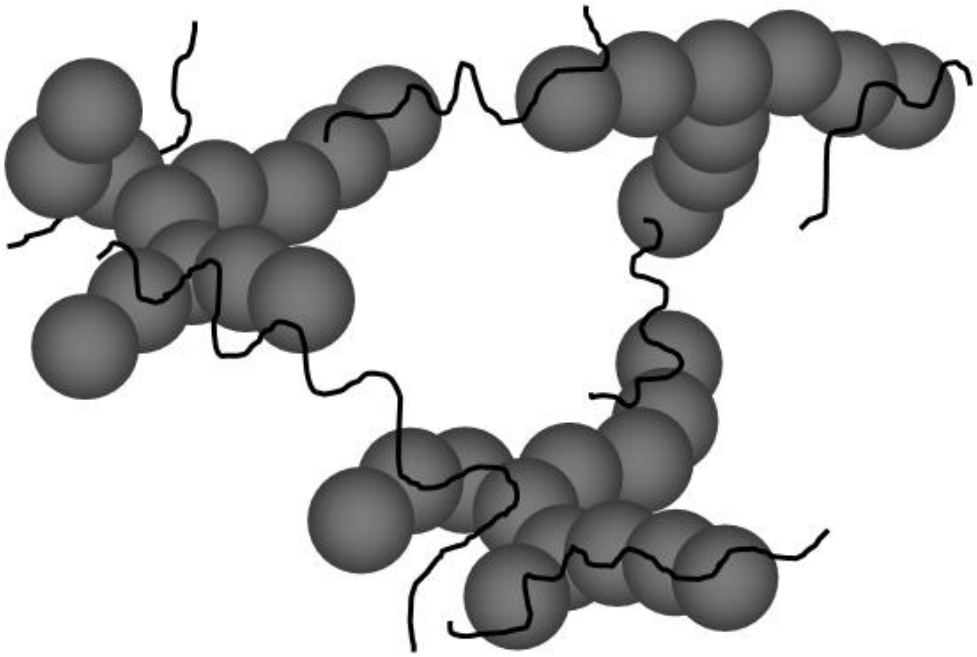

Figure I-19. Schematic drawing of the bridging flocculation.

When two particles are within a distance that can be spanned by one coil, a given chain can adsorb on both surfaces to form a bridge. Such bridging will contribute a negative term to the polymer free energy and thus an attractive component to the force between surfaces [57].

At equilibrium, an adsorbed polymer chain adopts a conformation consisting of bridges, trains, loops and tails (as demonstrated in Figure I-20), and a great deal of effort has been expended in both theoretical and experimental determinations of the segment density distribution as a function of distance from the adsorbing surface. It was stated that bridges and loop are essential for the reinforcing effect [25].

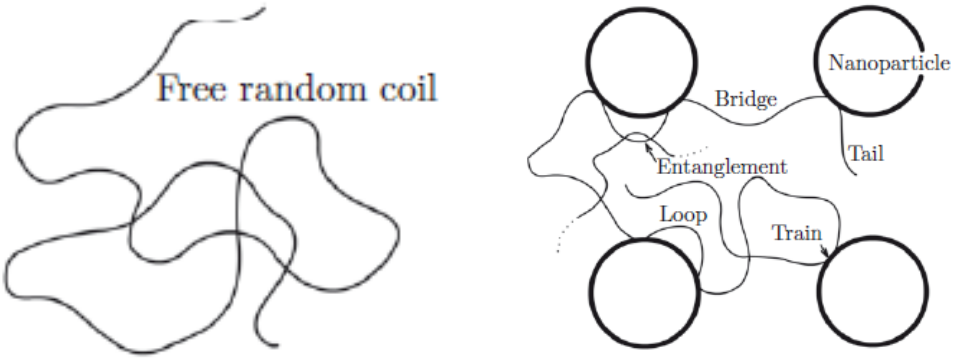

Figure I-20. Free random coil and conformations of polymer chains adsorbed on a surface of colloidal particles [44].

- Large amount of adsorbed polymer

In the case of colloidal dispersions with larger adsorbed amounts, the polymer can give an enhanced stability by an effect which is usually known as steric stabilisation (hairy particles) [25]. Thus, an effective stabilisation requires well-coated surfaces.

The attachment of the polymers to the surface may proceed by e.g. formation of covalent chemical bonds between an end monomer and the particle surface (hairy particles are created as shown in Figure I-21). Such bonds are generally sufficiently strong to prevent the polymers from leaving the surface except under the harshest treatments [57].

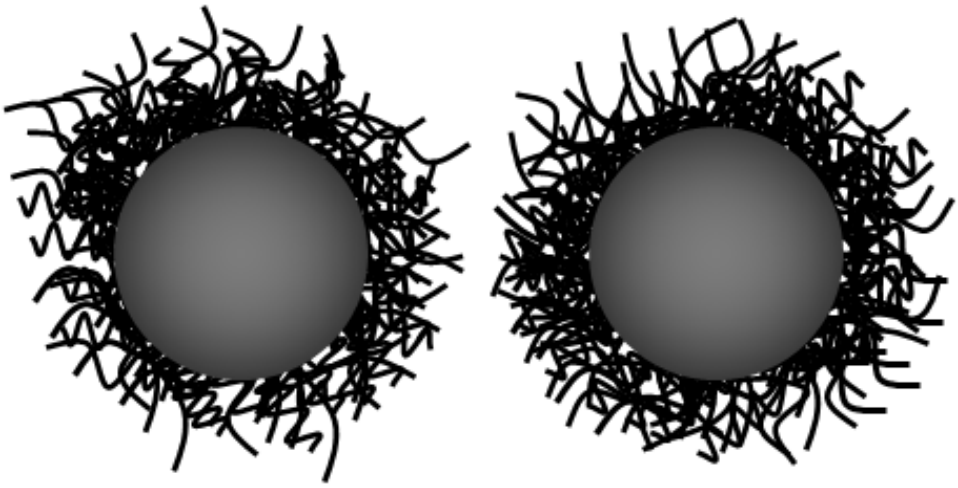

Figure I-21. Steric stabilisation proceeds by an adsorption of polymer chains on the surface.

FLOCCULATED STRUCTURES

As the result of flocculation, solid particles may adopt many different forms as simplified in Figure I-22. The simplest case of equal spheres is a shape of doublets in the form of a dumbbell. The third particle can attach in several different ways however. With higher number of particles the number of possible structures increases rapidly. Hence aggregates contain hundreds and thousands of primary particles [25].

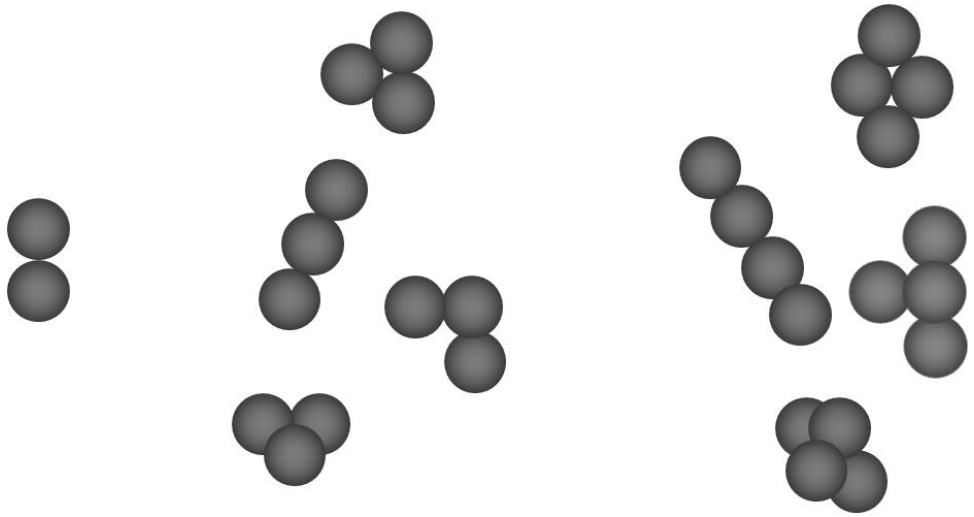

Figure I-22. Showing various forms of aggregates of equal spheres; in the left hand side of the picture are doublets, in the middle triplets and in the right side quadruplets are shown.

If the mutual attraction is strong enough to bring two aggregates together, usually it is strong enough to bring larger groups together also. The process of coming together feeds on itself, i.e. colloidal attraction grows in strength with the object size. It is important to note that reagglomerated structures in the rubber are different from those undispersed. Reagglomerated objects during reagglomeration lock rubber macromolecules into the voids between aggregates. Hence, reagglomerated objects contain trapped rubber while no macromolecules can penetrate undispersed agglomerates [26].

Flocculating carbon black aggregates have a strong tendency to agglomerate into large clusters which may shape into compact or tenuous structures under the influence of ubiquitous attractive forces [26, 57]. Witten and Sander stated that the growth of clusters can lead to a formation of a fractal like structures [54].

Reagglomerated carbon black structures can be considered as fractal like objects [25, 54-57, 60-64] hence fractals became an important tool for description of carbon black profile in the world of science.

The parameter generally used for the description of fractals is called mass fractal dimension (d_f) (or fractal dimension) which is observed from the plot of the mass against aggregate size (usually is taken as the radius of gyration of the aggregate). The plot may be linear but with a non-integer slope. The lower the fractal dimension, the more open or loose the aggregate's structure. For regular tree-dimensional objects, the value of the slope for plots is three. The relationship between aggregate mass (M) and size (L) is:

$$M \propto L^{d_f} \tag{14}$$

The size L can be defined in various ways and is often taken as the radius of gyration of the aggregate. Due to the fractal self-similar nature of aggregates their density decreases significantly as the size increases.

Computer modelling of aggregation has given very useful insights into the process of fractal formation. Early studies were based on the random addition of single particles to growing clusters. This describes the simplest aggregation model called the Sutherland's ghost model by Ball [65]. In this model, initially single particles combine to form dimers. Then all the dimers combine to form tetramers, and then all these combine to form octomers and so forth, as exemplified in Figure I-23. When two n-clusters combine, they stick together as randomly as possible. In general, combined clusters are not self-avoiding thus their particles intersect. Hence the name "ghost" is used [57].

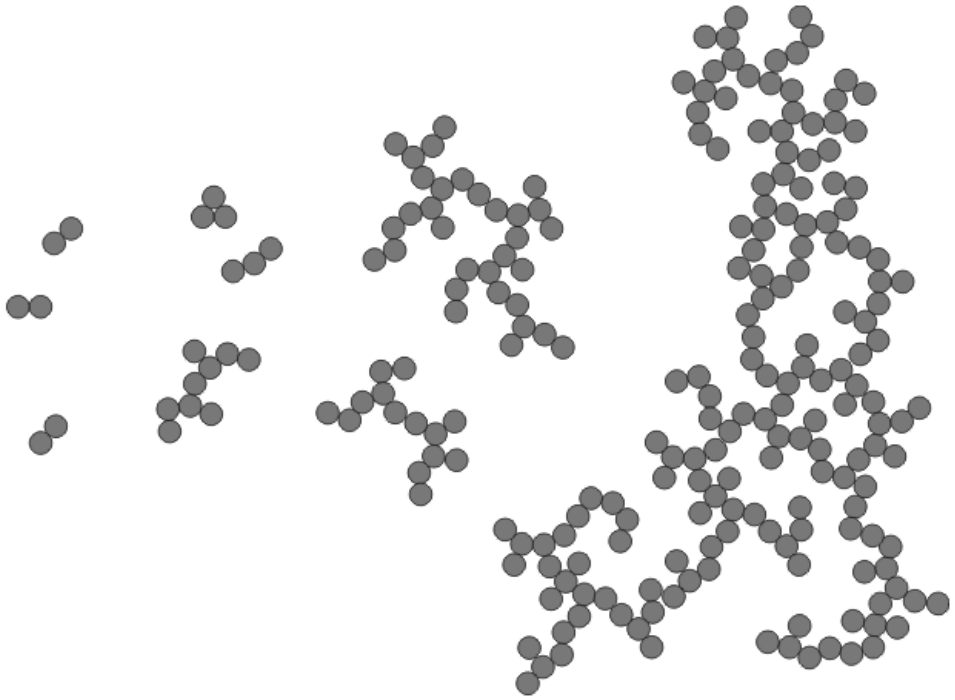

Figure I-23. The Sutherland's ghost model [66].

Later simulations of diffusion controlled aggregation, with single-particle addition (diffusion-limited aggregation) gave fairly good structures with d_f of around 2.5. The single-particle addition is not a realistic model in most of the cases since the aggregate's growth occurs as cluster-cluster encounters. In this case, built fractal like structures are much more open with a fractal dimension about 1.8 [35, 57, 60-62].

Nowadays, the diffusion-limited and reaction-limited regimes are recognised to be the most important mechanisms of fractal growth seen in colloidal systems. The universality of these two mechanisms was proven by Weitz et al. [67] when fractal growth of gold, silica and polystyrene colloidal particles was monitored.

Diffusion-limited aggregation (DLA) is called process when clusters move by Brownian motion and stick on contact. Repulsive forces between particles are negligible. It is a fast process limited only by the rate of Brownian diffusion of clusters. Fractal aggregates formed via DLA have the fractal dimension about 1.7 [25, 57]. Meakin [55] described the diffusion-limited cluster-cluster aggregation (DLCA) as the most realistic mechanism of fractal like structure formation in colloidal systems.

Sometimes diffusion is not the rate-limiting aspect of the aggregation process. Generally, when an aggregation process is inhibited by a repulsive barrier between two clusters, the so-called reaction-limited aggregation (RLA) proceeds. Indeed, this is the case for stabilised colloidal particles when two particles approaching each other have to overcome the repulsive barrier by thermal activation. RLA forms more compact structures as shown in the comparison in Figure I-24, since the collision efficiency is low and clusters need to collide many times before they actually stick. This gives more opportunity to explore other configurations and to achieve some degree of interpenetration. The fractal dimension of RLA aggregates is usually about 2.1 [25, 57].

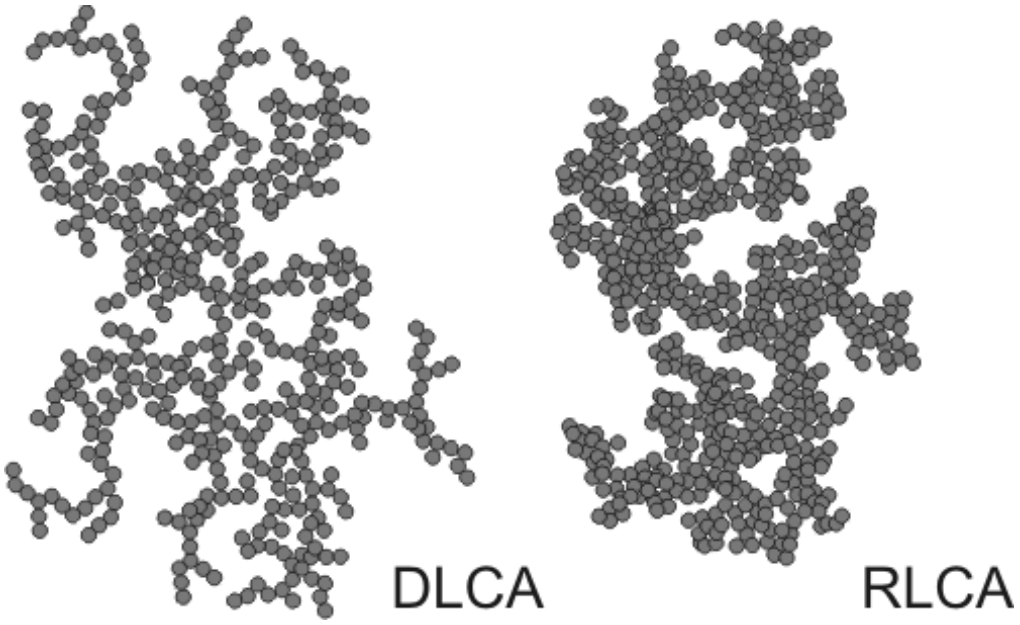

Figure I-24. The flocculated fractal structures formed via DLCA and RLCA mechanisms [66].

Other types of motion are also of interest such as ballistic aggregation, when the joining of clusters follows straight-line paths instead of random walks. One form of ballistic aggregation is sedimentation aggregation, in which the joining clusters are drifting downwards in a gravitational field. They join when a heavier cluster overtakes a lighter one [25, 57].

There are many techniques used for the simulation of aggregating colloidal systems. In literature, three groups are classified according to:

- their composition, for example solute particles in solvent (latex particles in solvent), polymer chains in colloidal systems, etc.
- concentration of substance
- presence or absence of external force which can be for example gravitational force, shear flow, etc.

In aggregating systems a rich variety of phenomena is observed. Competition between the physical mechanisms of interparticle attraction, intensity of external shear flow, and thermal energy determines whether a system will evolve reversibly or irreversibly. Different regimes are observed by varying the strength of interparticle interaction U related to thermal energy k_BT. When interparticle interaction is weak relative to the thermal energy and is less than some critical value, then the formation of only small aggregates is observed. As interparticle interaction becomes stronger, larger aggregates are formed [68].

Currently, the following simulation approaches for aggregation are commonly used according to the scale of the system [54, 69-72]:

- Molecular Dynamics (MD), usually used in microscales.
- Mesoscale methods, such as Langevin Dynamics (LD) and Brownian Dynamics (BD), Stochastic Rotational Dynamics (SRD) [69] and Dissipative Particle Dynamics (DPD) [71, 73].
- Monte Carlo methods, such as Lattice Monte Carlo (LMC) method and Off-Lattice Monte Carlo (OLMC) method [74].

Ideally the model which is chosen to predict any colloidal nanoparticle aggregation should accurately describe physical and chemical interactions of relatively large physical systems, and at the same time, simulate at a low

computational cost. In reality this is hard to achieve. Nevertheless, a computational model should maintain the balance between the level of accuracy and computational efficiency [68].

Nowadays, Molecular Dynamics (MD) simulation is established technique that can be used to simulate colloidal nanoparticle aggregation in the scale of 1 to 100 nanometres [70].

The MD method was first introduced by Alder and Wainwright in the late 1950's [75-77] to study the interactions of hard spheres. Molecular dynamics gained popularity in materials science and since the 1970s also in biochemistry and biophysics. Molecular dynamics is frequently used to refine three-dimensional structures of proteins and other macromolecules based on experimental constraints from X-ray crystallography or NMR spectroscopy. In physics, molecular dynamics is used to examine the dynamics of atomic-level phenomena that cannot be observed directly. It is also used to examine the physical properties of nanotechnological devices that have not or cannot yet be created.

In the MD approach, solute and solvent particles interact through a modeled, intermolecular potential, and the positions and velocities of these particles evolve in time according to Newton's equations of motion:

$$F_i = m_i \cdot a_i \tag{15}$$

Where F is the force exerted on the particle i, m is its mass and a is its acceleration. Then, the force can be expressed as the gradient ∇_i of the potential energy:

$$F_i = -\nabla_i \cdot V \tag{16}$$

The combination of the two equations gives:

$$-\frac{dV}{dr_i} = m_i \cdot \frac{d^2 r_i}{dt^2} \quad (17)$$

Where *V* is the potential energy of the system. Newton's equation of motion can relate the derivative of the potential energy to the changes in position as a function of time [78].

By knowing the force on each atom, it is possible to determine the acceleration of each atom in the system. Integration of the equations of motion then yields a trajectory that describes the positions, velocities and accelerations of the particles as they vary with time. From this trajectory, the average values of properties can be determined. The method is deterministic, i.e. once the positions and velocities of each atom are known, the state of the system can be predicted at any time in the future or the past. One disadvantage of Molecular Dynamics simulations is that it can be time consuming and computationally expensive. One alternative is to use Monte Carlo approaches for nanoparticle aggregation [78]

Bossis and Brady in 1984 [79] have developed an elegant method, called Stokesian Dynamics, for numerically simulating the dynamics of interacting particles on Stokes flow. In its original form, Stokesian Dynamics uses a MD-like approach to follow the time evolution of particles. Since then Brownian motion has also been incorporated [80], the resulting algorithm provides a general and versatile framework, capable of predicting both microstructural and macroscopic properties of colloidal dispersions, and encompassing both high (Stokesian limit) and low (Brownian limit) *Pe* number limits as special cases with no change in the approach or procedure.

Using Stokesian Dynamics with Brownian motion, Bossis and Brady (1987) [79, 80] have carried out simulations of a monolayer of identical Brownian hard spheres in a simple shear flow, and predicted the pair distribution function and self-diffusivity of the monolayer dispersion as a function of the Peclet number.

Foss and Brady [81] examined the rheology of hard-spheres suspensions in simple shear flow in the absence of hydrodynamic interactions by Brownian Dynamics.

Pranami et al. [82] used Molecular Dynamics simulation for diffusion of fractal aggregates formed via method developed by Thouy and Jullien which can be find elsewhere [83].

Heyes et al. [84] defined self-diffusion coefficient and shear viscosity of model nanocolloidal dispersion using Molecular Dynamics simulation. In another his work, he used Molecular Dynamics to study translational and rotational diffusion of model nanocolloidal dispersion.

Merkatsuya [68] used Brownian Dynamics simulation for evaluation of colloidal aggregation process and Langevin Dynamics simulation to calculate the effect of shear on colloidal aggregation of a model system.

Starr et al. [85, 86] has studied a model nanoparticle embedded in a dense melt of unentangled polymers via Molecular Dynamics simulation. They found that changes in the melt structure caused by the nanoparticle are largely insensitive to the interactions between the nanoparticle and the polymer.

Smith et al. [87] used Molecular Dynamics to study the viscoelastic properties of model polymer-nanoparticle composites, i.e. to evaluate the influence of the nanoparticle-polymer interface.

Liu et al. [88] studied nanoparticle dispersion and aggregation in polymer nanocomposites by Molecular Dynamics.

REFERENCES

1. B. Rodgers, W. Waddell. The Science of Rubber Compounding. J.E. Mark, B. Erman, F.R. Eirich. Science and Technology of Rubber. Elsevier Academic Press 2005; 9: p. 401-454. ISBN 0-12-464786-3.
2. P.S. Johnson. Rubber Processing. Mnichov : Hanser Gardner Publications 2001; 145p. ISBN 3-446-21578-6.
3. ASTM D3192-09. Standard Test Methods for Carbon Black Evaluation in NR (Natural Rubber). ASTM International. 2009. ICS 83.040.20.
4. A.N. Gent. Engineering with Rubber: How to Design Rubber Components. 3rd Ed. Munich: Hanser Publishers 2012; 433p. ISBN 978-3-446-42764-8.
5. H. Keuter. Effect of Process Parameters on Product Properties. A. Limper. Mixing of rubber compounds. Munich: Hanser Publishers 2012; p. 107-171. ISBN 978-3-446-41743-4.
6. R.N. Rothon. Particulate Filled Polymer Composites. 2nd Ed., Rapra Technology Limited 2003; 556p. ISBN 1-85957-382-7.
7. J.B. Donnet, R.Ch. Bansal, M.J. Wang. Carbon Black - Science and Technology. Marcel Dekker Inc. 1993; 461p. ISBN 0-8247-8975-X.
8. J.B. Donnet, A. Voet. Carbon Black: Physics, Chemistry, and Elastomer Reinforcement. New York: Marcel Dekker 1976; 351p. ISBN 0-8247-6345-9.
9. B. Rodgers. Rubber Compounding: Chemistry and Applications. New York: Marcel Dekker 2004; 645p. ISBN 0-8247-4871-9.
10. Carbon Black Manufacturing [online]. [viewed 2014-05-01]. Available from: www.orioncarbons.com/technologies.
11. N.T. Rosell. Plasma Modification of Carbon Black Surface: From Reactor Design to Final Applications. Doctoral Thesis. Universitat Ramon Llull 2007.
12. W.A. Wampler, T.F. Carlson, W.R. Jones. Carbon Black. B. Rodgers. Rubber Compounding: Chemistry and Applications. New York: Marcel Dekker 2004; 6: p. 239-284. ISBN 0-8247-4871-9.
13. M. Liu. Coating Technology of Nuclear Fuel Kernels: A Multiscale View. M. Aliofkhazraei. Modern Surface Engineering Treatments. InTech Rijeka 2013; p. 159-185. ISBN 978-953-51-1149-8.
14. J.B. Donnet, E. Custodero, Reinforcement of Elastomers by Particulate Fillers. J.E. Mark, B. Erman, F.R. Eirich, Science and Technology of

Rubber. Elsevier Academic Press 2005; 8: p. 367-400. ISBN 0-12-464786-3.

15. T. Allen. Particle Size Measurement: Surface Area and Pore Size Determination. 5th Ed., Chapman and Hall London 1997; p. 39-103. ISBN 0-412-75330-8.
16. G.A. Joyce, W.M. Henry, R.W. Magee. Advances in Structure Measurements of Carbon Black. Technical Meeting of the Rubber Division of the American Chemical Society 2008; 23p.
17. G.A. Joyce, W.M. Henry. Modelling the Equilibrium Compressed Void Volume of Carbon Black. Rubb Chem Technol 2006; 79(5): p. 735-764.
18. W. Wampler. Improved Test for Determination of Carbon Black Structure. Carbon Black World 2004; 26p.
19. A. Schröder, M. Klüppel, R.H. Schuster. Characterisation of Surface Activity of Carbon Black and Its Relation to Polymer-Filler Interaction. Macromol Mater Eng 2007; 292(8): p. 885-916.
20. L.B. Tunnicliffe, J. Kadlcak, Y. Shi, et al. Flocculation and Viscoelastic Behaviour in Carbon Black-Filled Natural Rubber. Macromol Mater Eng 2014; DOI: 10.1002/mame.201400117.
21. L.B. Tunnicliffe, A.G. Thomas, J.J.C. Busfield. Mechanisms of Particulate Reinforcement of Elastomers at Small Strains. RubberCon 2014, Manchester 2014; p. 1-8. ISBN 1-86125-176-9.
22. F. Fleck, M.M. Möwes, M. Klüppel. Effect of Ionic Liquids on Mechanical and Rheo-Dielectric Properties of Carbon Black filled Elastomers. RubberCon 2014, Manchester 2014; p. 1-5. ISBN 1-86125-176-9.
23. M. Gerspacher, C.P. O'Farrell. Energy at the Interface. Tire Technology International Conference 1999.
24. G. Parfitt. Dispersion of Powders in Liquids: With Special Reference to Pigments. 2nd Ed. London: Applied Science Publ. 1973; 418p. ISBN 0-85334-533-3.
25. M. Elimelech, J. Gregory, X. Jia, et al. Particle Deposition and Aggregation – Measurement, Modelling and Simulation. Butterwort-Heinemann 1995; 441p. ISBN 0-7506-7024-X.
26. R.H. Schuster. Dispersion and Distribution of Fillers. A. Limper. Mixing of rubber compounds. Munich: Hanser Publishers 2012; p. 173-236. ISBN 978-3-446-41743-4.

27. D. Berkemeier. Internal Mixer – Configuration and Design. A. Limper. Mixing of rubber compounds. Munich: Hanser Publishers 2012; p. 1-46. ISBN 978-3-446-41743-4.
28. S. Shiga, M. Furuta. Processability of Electron-Paramagnetic-res in an Internal Mixer. 2. Morphological-Changes of Carbon-Black Agglomerates During Mixing. Rubb Chem Technol 1985; 58(1): p. 1-22.
29. F.W. Barlow. Rubber Compounding: Principles, Materials, and Techniques. 2nd Ed. New York: Marcel Dekker 1993; 294p. ISBN 0-8247-8968-7.
30. J. Fröhlich, W. Niedermeier, H.D. Luginsland. The Effect of Filler-Filler and Filler-Elastomer Interactions on Rubber Reinforcement. Compos Part A-Appl S 2005; 36(4): p. 449-460.
31. G. Kraus. Reinforcement of Elastomers by Carbon Black. Rubb Chem Technol 1978; 51(2): p. 297-321.
32. J.L. Leblanc. Rubber-Filler Interactions and Rheological Properties in Filled Compounds. Prog Polym Sci 2002; 27(4): p. 627-687.
33. J.L. Leblanc. Filled Polymer – Science and Industrial Application. CRC Press 2010; 3-4: p. 15-184. ISBN 978-1-4398-0042-3.
34. J.J. Brennan, T.E. Jermyn. Correlation of Vulcanizate Properties with Polymer and Black Interaction. J Appl Polym Sci 1965; 9(8): p. 2749-2762.
35. E.M. Dannenberg. Bound Rubber and Carbon Black Reinforcement. Rubb Chem Technol 1986; 59(3): p. 512-524.
36. M.J. Wang. Effect of Polymer-Filler and Filler-Filler Interactions on Dynamic Properties of Filled Vulcanizates. Rubb Chem Technol 1998; 71(3): p. 520-589.
37. J. Vineetkumar. Carbon Black Filler Reinforcement of Elastomers. Doctoral thesis. Queen Mary University of London 2008.
38. L. Mullins. Softening of Rubber by Deformation. Rubb Chem Technol 1969; 42(1): p. 339-362.
39. A.I. Medalia. Morphology of Aggregates .6. Effective Volume of Aggregates of Carbon Black from Electron Microscopy . Application to Vehicle Absorption and to Die Swell of Filled Rubber. J Colloid Interf Sci 1970; 32(1): p. 115-&.

40. Y. Fukahori. Generalized Concept of the Reinforcement of Elastomers. Part 1: Carbon Black Reinforcement of Rubbers. Rubb Chem Technol 2007; 80(4): p. 701-725.
41. J. Berriot, F. Lequeux, L. Monneire, et al. Filler–Elastomer Interaction in Model Filled Rubbers, a H NMR Study. J Non-Cryst Solids 2002; 307: p. 719-724.
42. J. Berriot, H. Montes, F. Lequeux, et al. Evidence for the Shift of the Glass Transition Near the Particles in Silica-Filled Elastomers. Macromolecules 2002; 35(26): p. 9756-9762.
43. J. Jančář. Interphase phenomena in Polymer Micro- and Nanocomposites. J. Karger-Kocsis, S. Fakirov. Nano- and Micro- Mechanics of Polymer Blends and Composites. Hanser 2009; 7: p. 241-266. ISBN 978-3-446-43012-9.
44. J. Kalfus. Viscoelasticity of Amorphous Polymer Nanocomposites with Individual Nanoparticles. J. Karger-Kocsis, S. Fakirov. Nano- and Micro-Mechanics of Polymer Blends and Composites. Hanser 2009; 6: p. 207-240. ISBN 978-3-446-43012-9.
45. A.R. Payne. The Dynamic Properties of Carbon Black-Loaded Natural Rubber Vulcanizates. Part I. J Appl Polym Sci 1962; 6(19): p. 57-63.
46. J. Kadlcak, L.B. Tunnicliffe, J. Lacayo, et al. Rapid Payne Effect Test – A Novel Method for Study of Strain-Softening Behavior of Rubbers Filled with Various Carbon Blacks. – Manuscript number POTE-D-14-00258 (Polymer Testing).
47. A.I. Medalia. Effect of Carbon-Black on Dynamic Properties of Rubber Vulcanizates. Rubber Chem Technol 1978; 51(3): p. 437-523.
48. R. Houwink. Slipping of Molecules during the Deformation of Reinforced Rubber. Rubb Chem Technol 1956; 29(3): p. 888-893.
49. Ch. Nah, J.Y. Lim, B.H. Cho, et al. Reinforcing Rubber with Carbon Nanotubes. J Appl Polym Sci 2010; 118(3): p. 1574-1581.
50. E. Kissa. Dispersions – Characterization, Testing and Measurement. Marcel Dekker, Inc. 1999; 708p. ISBN 0-8247-1994-8.
51. E. Allen, J. Henshaw, P.A. Smith, Review of Particle Agglomeration. AEAT/R/PSEG/0398; AEA Technology Engineering Services, Inc.: Harwell, 2001.
52. G.G.A. Böhm, M.N. Nguyen. Flocculation of Carbon Black in Filled Rubber Compounds. I. Flocculation Occurring in Unvulcanized

Compounds during Annealing at Elevated Temperatures. J Appl Polym Sci 1995; 55(7): p. 1041-1050.

53. G.A. Schwartz, S. Cerveny, A.J. Marzocca, et al. Thermal Ageing of Carbon Black Filled Rubber Compounds. I. Experimental Evidence for Bridging Flocculation. Polymer 2003; 44(23): p. 7229-7240.
54. T.A. Witten, L.M. Sanders. Diffusion-Limited Aggregation, a Kinetic Critical Phenomenon. Phys Rev Lett 1981; 47 (19): p. 1400-1403.
55. P. Meakin. Formation of Fractal Clusters and Network by Irreversible Diffusion-Limited Aggregation. Phys Rev Lett 1983; 51(13): p. 1119-1122.
56. Y. Han, A.M. Alsayed, M. Nobili, et al. Brownian Motion of an Ellipsoid. Science 27 [online]. October 2006; p 626-630. [viewed 2014-04-20]. Available from: http://www.2physics.com/2006/10/brownian-motion-of-ellipsoidal.html.
57. T.A. Witten, P.A. Pincus. Structured Fluids – Polymers, Colloids, Surfactants. Oxford University Press. New York 2004; 216p. ISBN 978-0-19-958382-9.
58. H.C. Hamaker. The London-Van der Waals Attraction between Spherical Particles. Physica 1937; 4: p. 1058-1072.
59. E.M. Lifshitz. Theory of Molecular Attractive Forces. Soviet Phys JETP 1956; 2: p. 73-83.
60. B.B. Mandelbrot. The Fractal Geometry of Nature. 1st Ed., W. H. Freeman and Company 1982; 468p. ISBN 0-7167-1186-9.
61. T. Vicsek. Fractal Growth Phenomena. 2nd Ed., World Scientific Pub Co Inc 1992; 488p. ISBN 9810206682.
62. B.H. Kaye. A Random Walk Through Fractal Dimensions. 2nd Ed., VCH Publishers New York 1994; 443p. ISBN 1-56081-818-2.
63. A.I. Medalia, F.A. Heckman. Morphology of Aggregates .2. Size and Shape Factors of Carbon Black Aggregates from Electron Microscopy. Carbon 1969; 7(5): p. 567-&.
64. G. Heinrich, M. Klüppel, T.A. Vilgis. Reinforcement of Elastomers. Curr Opin Solid St M 2002; 6(3): p. 195-203.
65. R.C. Ball, T.A. Witten. Particle Aggregation Versus Cluster Aggregation in High Dimensions. J Stat Phys 1984; 36(5-6): p. 873-879.
66. Particle Aggregation [online]. [viewed 2014-05-01]. Available from: http://en.wikipedia.org/wiki/Particle_aggregation.

67. M.Y. Lin, H.M. Lindsay, D.A. Weitz, et al. Universality in Colloid Aggregation. Nature 1989; 339: p. 360-362.
68. S. Merkatsuya. Modeling and Simulation of Nanoparticle Aggregation in Colloidal Systems. Doctoral Thesis. Iowa State University 2010.
69. A. Malevanets, R. Kapral. Mesoscopic Model for Solvent Dynamics. J Chem Phys 1999; 110(17): p. 8605-8613.
70. D.E. Ulberg, N.V. Churaev, V.V. Ilyin, et al. Molecular-Dynamics Simulation of the Aggregation of Colloidal Particles. Colloid Surface A 1993; 80(2-3): p. 93-102.
71. P.J. Hoogerbrugge, J.M.V.A. Koelman. Simulating Microscopic Hydrodynamic Phenomena with Dissipative Particle Dynamics. Europhys Lett 1992; 19(3): p. 155-160.
72. D.L. Ermak. Computer-Simulation of Charged-Particles in Solution .1. Technique and Equilibrium Properties. J Chem Phys 1975; 62(10): p. 4189-4196.
73. P. Espanol, P.B. Warren. Statistical Mechanics of Dissipative Particle Dynamics. Europhys Lett 1995; 30(4): p. 191-196.
74. R. Salazar, L.D. Gelb. Off-Lattice Dynamic Monte Carlo Simulations of Aggregation in One Dimension. Physica A 2005; 356(1): p. 190–195.
75. B.J. Alder, T.E. Wainwright. Phase Transition for a Hard Sphere System. J Chem Phys 1957; 27(5): p. 1208-1209.
76. B.J. Alder, T.E. Wainwright. Studies in Molecular Dynamics .1. General Method. J Chem Phys 1959; 31(2): p. 459-466.
77. B.J. Alder, T.E. Wainwright. Studies in Molecular Dynamics .2. Behavior of a Small Number of Elastic Spheres. J Chem Phys 1960; 33(5): p. 1439-1451.
78. Theory of Molecular Dynamics Simulations. [online]. [viewed 2014-05-29]. Available from: http://www.ch.embnet.org/MD_tutorial/pages/MD .Part1.html.
79. G. Bossis, J.F. Brady. Dynamic simulation of sheared suspensions. I. General method. J Chem Phys 1984; 80(10): p. 5141-5154.
80. J.F. Brady, G. Bossis. Stokesian Dynamics. Ann Rev Fluid Mech 1988; 20: p. 111-157.
81. D.R. Foss, J.F. Brady. Brownian Dynamics simulation of hard-sphere colloidal dispersions. J Rheol 2000; 44(3): p. 629-651.

82. G. Pranami, M.H. Lamm, R.D. Vigil. Molecular Dynamics Simulation of Fractal Aggregate Diffusion. Phys Rev E 2010; 82(5): 051402.
83. R. Thouy, R. Jullien. A Cluster-Cluster Aggregation Model with Tunable Fractal Dimension, J Phys A: Math Gen 1994; 27(9): p. 2953-2963.
84. M.J. Nuevo, J.J. Morales, D.M. Heyes. Self-Diffusion Coefficients and Shear Viscosity of Model Nanocolloidal Dispersions by Molecular Dynamics Simulation. Phys Rev E 1998; 58(5): p. 5845-5854.
85. F.W. Starr, T.B. Schroder, S.C. Glotzer. Molecular Dynamics Simulation of a Polymer Melt With a Nanoscopic Particle. Macromolecules 2002; 35(11): p. 4481-4492
86. F.W. Starr, T.B. Schroder, S.C. Glotzer. Effects of a Nanoscopic Filler on the Structure and Dynamics of a Simulated Polymer Melt and the Relationship to Ultrathin Films. Phys Rev E 2001; 64(2): 021802.
87. G.D. Smith, D. Bedrov, L. Li, et al. A Molecular Dynamics Simulation Study of the Viscoelastic Properties of Polymer Nanocomposites. J Chem Phys 2002; 117(20): p. 9478-9489.
88. J. Liu, Y. Gao, D. Cao, et al. Nanoparticle Dispersion and Aggregation in Polymer Nanocomposites: Insights from Molecular Dynamics Simulation. Langmuir 2011; 27: p. 7926-7933.

CHAPTER II. AIMS OF DOCTORAL STUDY

The work which has been carried out within this doctoral thesis entitled "Filler Dispersion and Rheology of Polymers" can be summarised in the following points:

- Carbon black structure – Evaluation by mechanical compression
- Macrodispersion evaluation – Reference object for topography of materials
- Evaluation of carbon black behaviour in rubber compounds

CARBON BLACK STRUCTURE – EVALUATION BY MECHANICAL COMPRESSION

A novel approach using mechanical compression has been used for the investigation of carbon black structure. The aim was to verify this new method by measuring several carbon black grades at various test conditions in order to define optimal conditions for testing. Subsequently, characteristics observed at the optimal conditions were examined to find correlations and interconnections to results of commonly used oil absorption techniques as well as in-rubber properties of carbon black.

MACRODISPERSION EVALUATION – REFERENCE OBJECT FOR TOPOGRAPHY OF MATERIALS

For the macrodispersion evaluation of carbon black in rubber compounds the device of Alpha Technologies called Dispergrader was used. During measurements however, it was found that the precision of results obtained by Dispergrader is relatively low. Therefore, optical microscopy was used as the alternative method for the evaluation of macrodispersion. Comparing the results of the optical microscopy and those from Dispergrader, distinct differences were observed. Moreover, the international standard ASTM D7723 – 11 called "Standard Test Method for Rubber Property – Macro-Dispersion of Fillers in Compounds" does not contain any precision statement. The aim of the work altered into designing of a calibration tool which could be used as a precision

statement in the ASTM standard possibly – hence the reference object for topography of materials was designed.

EVALUATION OF CARBON BLACK BEHAVIOUR IN RUBBER COMPOUNDS

Phenomena of reinforcement and flocculation of any particulates in a dispersive phase is a big issue for any industrial application. One of the aims of the doctoral studies was to design a flocculation test and subsequently monitor the flocculation behaviour of carbon black relating to its properties, dispersion quality, properties of a rubber matrix and various test conditions such as temperature.

CHAPTER III. CARBON BLACK STRUCTURE – EVALUATION BY MECHANICAL COMPRESSION

Mechanical compressed void volume measured by Void Volume Tester is a novel approach for the evaluation of carbon black structure. In this chapter, a broad range of furnace carbon blacks varying in structure complexity were examined for compressed void volume and compared to the results observed by liquid absorption techniques, i.e. oil absorption number and oil absorption number of compressed sample. Subsequently, results of these characteristics were compared to in-rubber characteristics, i.e. vulcanisation characteristics and the Payne effect. Compressed void volume was investigated at standardised conditions and the geometrical mean void volume was used for the purpose of evaluation. Throughout the experiment, it was found that the compressed void volume gives generally a better insight on the behaviour of carbon black in rubber compounds than the oil absorption methods.

THEORETICAL BACKGROUND OF CHAPTER III

The term structure has been used in the carbon black industry for many years to describe one of the most important properties of carbon black that strongly affects the properties of filled rubber compounds including processability and reinforcement [1]. Generally, there are two main approaches for the evaluation of carbon black structure – the determination of liquid absorption and specific volume at a given mechanical compression [2]. Both methods are based on the assessment of the amount of free air-filled voids between coalesced carbon black particles in the aggregate. According to Donnet, the amount of free voids is referred as void volume [2].

Void volume in a given volume of carbon black is considered as a measure of carbon black structure [2]. In general, the larger the measured internal void volume, the more complex, open, and branched aggregates and the larger the structure [3].

The method of liquid absorption generally known as the oil absorption number (OAN) is based on filling up the voids in and between agglomerates and aggregates with an absorbent (usually DBP or paraffinic oils) [3]. However,

there are some deficiencies cited with the oil absorption test where the most important is that OAN does not provide information about primary structure of carbon black and offers little insight into aggregate reduction, which is known to occur during the mixing or the dispersion cycle. Thus an alternative method providing information on both the primary and secondary structure in a carbon black sample was developed and adopted for oil absorption wherein the sample is compressed at 24000 psi four times before the oil absorption is measured [1, 4]. The alternative test referred as the oil absorption number of compressed sample (COAN) seeks to approximate the level of structure present in a carbon black that is mechanically mixed into rubber. Although the COAN has proved itself to be a useful tool, it is important to consider that the breakdown of structure may vary considerably according to the parameters of the polymer into which the carbon black is mixed [3]. Nevertheless, COAN minimises the effects of secondary structure which provides a better relationship to in-rubber properties [1].

It was proposed many years ago that structure could be measured through volumetric measurements of compressed carbon black at specified compressions. Referred to as compressed void volume it did not obtain favour over oil absorption methods during the time period of 1960's as the equipment for this test did not provide values as precise as oil absorption techniques. This void volume test was revisited in the 1990's when technology for load cells and other necessary equipment had improved significantly. These improvements in technology made it clear soon that compressed void volume measurement of a carbon black sample could be as accurate and precise as oil absorption methods [5]. In 1976 Donnet and Voet wrote an extensive review about the compression void volume of carbon black describing a comprehensive investigation on the compressibility of carbon black and mentioning the superiority of the compression void volume method over the oil absorption approach [2]. Later on, Joyce et al. [1] and Wampler [5] validated that compressed void volume offers a significant improvement in carbon black structure measurement when compared to oil absorption methods.

In these days, a range of commercially available equipment for the assessment of compression void volume exists, e.g. Void Volume Tester (VVT) by Brabender or the Dynamic Void Volume Analyzer (DVVA) by Micromeretics.

Tien et al. [6] defined the geometrical mean (*GM*) pressure, as a friction-independent measure suitable for void volume assessment. The applied force

was observed to be equivalent to the sum of the force transmitted through the sample and radial force loss due to the friction. The level of applied pressure, die wall friction coefficient and the aspect ratio are some of the key parameters describing radial force losses. There are other approaches that separate the effects caused by friction and these are reported elsewhere [6-10]. Nevertheless, Joyce et al. [11] during his extended work on DVVA stated that in a cylinder where the applied pressure transmission decays exponentially, a geometrical mean pressure (P_{GM}) should provide the best approximation of the central tendency. Later on, Joyce et al. [11] in their work using DVVA confirmed the independence of void volume with sample mass and aspect ratio when using geometric mean pressure average and void volume scans at geometrical mean pressures have been found to provide compression data isolated from the effects of the sample-wall friction [11]. Moreover, Joyce et al. [4, 11] demonstrated that friction coefficients are not constant, but vary with applied pressure and apparent density of the compact.

One of the aims of this work was to verify the functionality of Void Volume Tester of Brabender. Furthermore, the purpose was to extend the knowledge about the void volume of carbon black as examined by mechanical compression and find out relations between obtained results and in-rubber properties. Also, the comparison of results measured by Void Volume Tester and the results obtained by oil absorption methods is provided.

METHODOLOGY OF CHAPTER III

CARBON BLACK CHARACTERISATION

Ten carbon black samples used in this work were produced by CS Cabot, Valasske Mezirici, Czech Republic and Columbian Tiszai Carbon Ltd., Tiszaujvaros, Hungary. They vary in specific surface area (SSA) and structure. Properties of carbon black samples are listed in Table III-1.

Table III-1. Properties of used carbon black.

Producer	Carbon black grade*	Iodine adsorption [mg/g]	STSA [m^2/g]	BET [m^2/g]	OAN [cm^3/100 g]	COAN [cm^3/100 g]
Columbian	N121	121.0	107.1	144.8	135.7	116.3
CS Cabot	N220	121.6	105.0		114.5	98.0
CS Cabot	N234	120.4	113.0	120.0	125.7	102.0
CS Cabot	N326	82.2	78.0	78.0	72.0	68.0
CS Cabot	N330	82.4	75.0		102.0	88.0
Columbian	N339	90.0	86.6	88.3	120.1	97.6
CS Cabot	N550	43.2	40.0		122.0	84.0
Columbian	N660	34.5	34.8	39.2	91.4	74.0
CS Cabot	N772	30.3	31.0	31.0	65.0	58.0
CS Cabot	N-**	27.5	27.0		121.0	80.0

* Nomenclature according to the international standard ASTM D1765–13.

**N- stands for a high structured carbon black grade known as SPHERON 5000A. This grade has not got any nomenclature according to the ASTM standard up to date when the work was carried out.

Traditional methods

Firstly, characterisation of carbon black was carried out using traditional methods widely used in carbon black industry. For the surface area investigation – Iodine adsorption, STSA and BET methods were used. For the structure complexity evaluation, oil absorption techniques were used. This examination has been carried out in the material lab of CS Cabot in Valasske Mezirici.

Void volume via mechanical compression

In the second stage, an additional characterisation of carbon black structure using Void Volume Tester (Brabender, Duisburg) was carried out. The principle is based on the uniaxial mechanical compression, when weighed dry carbon black sample in a cylindrical chamber of a specific diameter (Figure III-1) is compressed under set conditions (time and pressure).

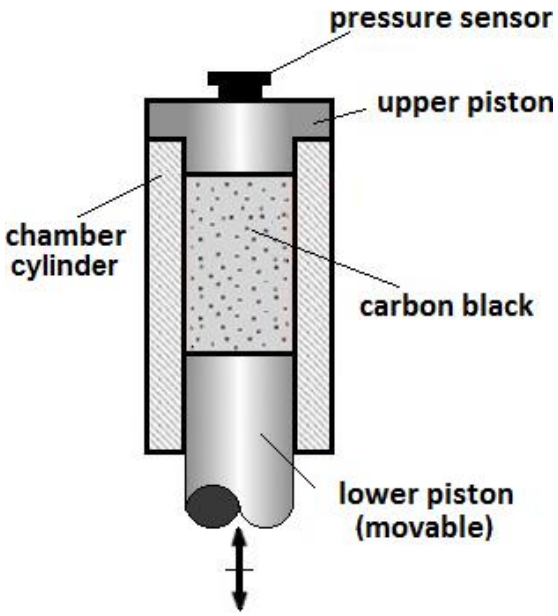

Figure III-1. The schematic representation of the testing chamber in Void Volume Tester.

As a result, the dependence of the sample volume on the pressure is plotted. This is exemplified in Figure III-2 for N234 grade. Void Volume Tester examines the void volume of a sample by its mechanical compression while the oil absorption methods evaluates void volume by filling up the voids with aromatic or paraffinic oil (primarily dibutylphtalate – DBP is used).

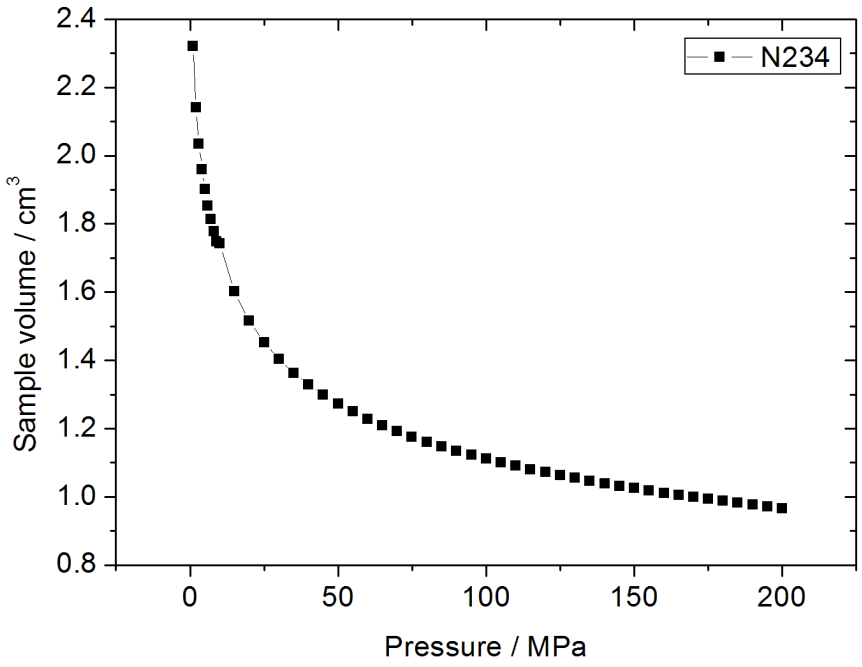

Figure III-2. The dependence of the sample volume on the pressure applied on the sample.

Recently, according to Tien et al [6] the geometric mean pressure (P_{GM}) at a specific void volume was proposed to be used for the purpose of carbon black structure characterisation via Void Volume Tester:

$$P_{GM} = (P_A \cdot P_T)^{0.5} \tag{18}$$

Where P_A stands for the applied pressure exerted on a sample mass by a movable piston and P_T is the transmitted pressure read at the upper sensor. This is defined by the applied pressure and radial pressure losses resulting from a transmission of pressure through a sample into the wall of chamber.

The geometrical mean void volume (*VV*) is expressed as the difference between the experimental volume and the theoretical compressed volume:

$$V_C = \frac{D^2}{4} \cdot \pi \cdot h \tag{19}$$

$$V_{CB} = \frac{m}{\rho} \tag{20}$$

$$VV = \frac{V_C - V_{CB}}{100\ g} \tag{21}$$

V_c is the experimental (cylinder) volume that is occupied by a compressed carbon black bed. V_{CB} is the theoretical volume of carbon black which is the volume of a compact sample without voids. The difference is normalised to 100 grams of a sample then.

RUBBER MATRIX CHARACTERISATION

The molecular structure of the natural rubber – SMR 10 was investigated using a gel permeation chromatography (PL-GPC 220, CPS) at temperature 160 °C and trichlorbenzene (TCB) as the solution was used. The tested SMR 10 shows molecular weights M_n = 132000, M_w = 329000 and polydispersity index 2.5.

CARBON BLACK COMPOUNDING

Certain carbon black samples from Table III-1 were chosen and incorporated into the rubber compounds using a laboratory mixer (Everplast Machinery, Taiwan) in order to investigate in-rubber characteristics. All compounds were mixed according to the international standard ASTM D3192 recipe shown in Table III-2.

Table III-2. Rubber compounds were mixed according to the ASTM D3192 recipe.

Ingredients	Rubber compound [phr]
Rubber matrix (SMR 10)	100.0
Carbon black*	50.0**
Stearic acid	3.0
Zinc oxide	5.0
Benzothiazyl disulfide (MBTS)	0.6
Sulfur	2.5

*Various carbon black samples were incorporated.

**No carbon black used in a neat rubber sample.

IN-RUBBER PROPERTIES

Vulcanisation characteristics and viscoelastic properties were measured for filled rubber compounds in order to find the influence of carbon black on the behaviour of rubber compounds. The properties of filled rubber compounds were examined using the oscillating die rheometer called Rubber Process Analyzer 2000 (RPA, Alpha Technologies).

Vulcanisation characteristics

Vulcanisation tests were measured at the temperature of 160 °C, the frequency of 1.67 Hz and the strain amplitude of 6.97 %. Four main characteristics can be obtained from a vulcanisation curve: M_L – minimal torque which is equal to the viscosity of a rubber compound; M_H – maximal torque suggests the maximal strength of a rubber compound after the vulcanisation (in neat rubber matrix depends on the density of crosslinking); t_s2 – scorch time which indicates the time when the torque increase begins; *t90* – the so-called optimum of vulcanisation which is specified by the time where there is 90 % difference between maximal and minimal torque (M_H-M_L).

Another value usually used for the characterisation of vulcanisation kinetics is the vulcanisation rate – *u*:

$$u = \frac{1}{t90 - t_s2} \tag{22}$$

This indicates the real vulcanisation rate of a rubber compound in s^{-1}.

Viscoelastic properties

In-rubber characteristics of carbon black were measured with the focus on their reinforcing effect in the rubber. The characteristic called Payne effect representing the filler-filler and the filler-polymer interaction was measured.

The non-linearity in behavior of filled rubber compounds at applied shear strains is well known. To name the most significant contributions, work of Houwink [12], Payne [13], Mullins [14, 15], Kraus [16], Dannenberg [17], Wang [18], Donnet [19] and Leblanc [20, 21] should be mentioned. The non-linearity is assigned to the gradual breakdown of inter-aggregate adhesion, i.e. filler network disintegration and this is generally known as the Payne effect [13]. Wang et al. [18] stated that regardless to the magnitude of applied shear strain the Payne effect is a term for the typical non-linear behavior of filled

rubber compounds and can serve as a measure of filler network complexity originating from filler-filler as well as filler-polymer interactions.

Within the framework of the Payne effect test a sample is exposed to the strain sweep from 0.3 to 140.0 % at frequency 1.67 Hz and temperature 70 °C.

Based on the results, the Payne softening (*PS*) is calculated as follows:

$$PS = G'_{0.3\,\%} - G'_{140\,\%} \tag{23}$$

Where *PS* stands for Payne softening which describes the magnitude of the rubber reinforcement by carbon black; $G'_{0.3\%}$ is the storage modulus measured at the low shear strain and $G'_{140\%}$ is the modulus measured at the high shear strain.

RESULTS AND DISCUSSION OF CHAPTER III

THE INVESTIGATION OF CARBON BLACK STRUCTURE VIA VOID VOLUME TESTER

Pilot measurements of compressed void volume

In the first stage of the experimental work, carbon black samples presented in Table III-1 were examined using Void Volume Tester.

A range of test conditions was tested using a one specific type of carbon black, namely N326 provided by CS Cabot, Valasske Mezirici, see Table III-3 below.

Table III-3. Various conditions of the measurement.

Maximal pressure [MPa]	Testing time [s]	Sample weight [g]	Compression speed [MPa/s]
400	1000	1	0.8
350	350	1	2
350	175	1	4
350	175	2	4
350	35	1	20
200	800	1	0.5
200	200	1	2
200	80	1	5
200	20	1	20

In the above table, you can see all the conditions applied during the investigation. Three representatives were chosen for the purpose of additional experimental study work. These conditions were providing varied compression speeds from 2 to 20 $MPa.s^{-1}$, when the maximal pressure was fixed to 200 MPa and testing time was varied from 20 to 200 s.

One of the important findings observed in this part of the experimental work was the influence of hydraulic oil temperature on the results. During measurements it was found that the temperature of the hydraulic system of Void Volume Tester has a large influence on the obtained characteristics. Thus most of the test conditions seem to be inconvenient due to the overheating of the hydraulic system during the test. The oil temperature increases more rapidly for slow compression speeds. The compression speed 2 $MPa.s^{-1}$ is recommended to be the lower limit speed considering the overheating issue. Generally, to ensure slower increase of the oil temperature, the use of a combination of high compression speed and short testing time is recommended.

In Figure III-3, the results of the investigation of the influence of oil temperature on the void volume characteristics, namely the geometrical mean energy consumed for sample compression is represented. The test was carried out using N550 grade at the fixed conditions 200 MPa and 200 seconds providing the compression speed 2 $MPa.s^{-1}$.

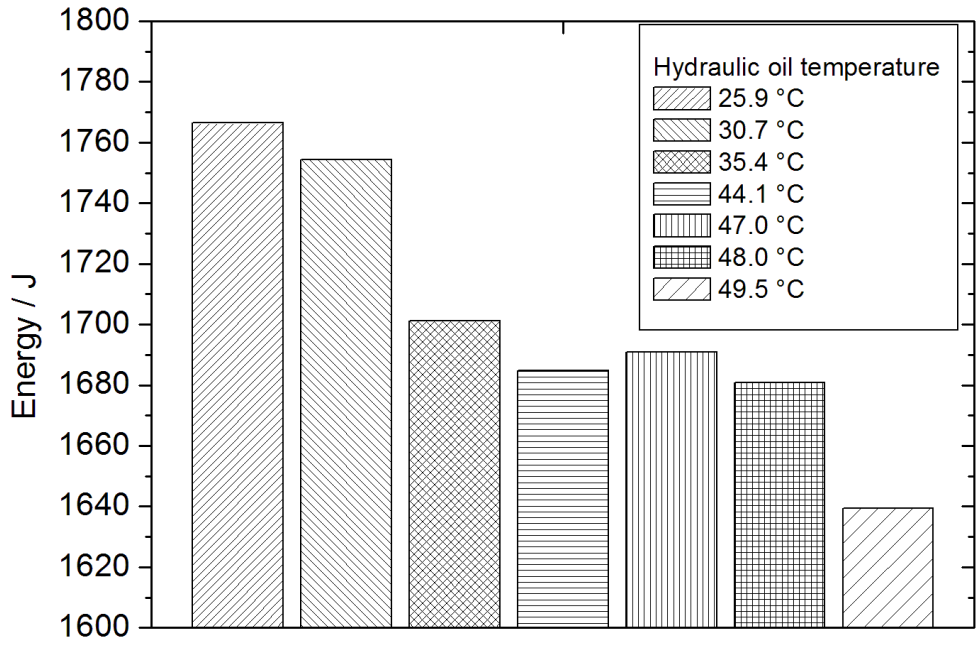

Figure III-3. The dependence of energy on the hydraulic oil temperature measured for SSO.

It was observed that the energy depends on the hydraulic oil temperature significantly. According to the increasing temperature of the oil, the energy decreases and the difference between the highest and the lowest measured values is approximately 120 Joules. Considering the tested sample of carbon black is the same, this difference is rather significant.

Moreover, at both high and low temperatures, Void Volume Tester was not able to meet the set compression speeds. It was found that the compression speed at oil temperature 25.9 °C is higher than the set speed 2 $MPa.s^{-1}$. On the other hand, at higher temperatures such as 49.5 °C the compression speed is lower.

It is proposed to use one specific set temperature of hydraulic oil during the test to ensure the stability thus repeatability and reproducibility of the results. This temperature should be around 30±1 °C according to the investigation since the set conditions of compression are met perfectly at this temperature. However, this is impossible without having an oil temperature regulator. Therefore, the recommendation for the producer of Void Volume Tester is to provide the device with an oil temperature control system.

The influence of compression speed on void volume

Seven carbon black samples were used in order to investigate the influence of the compression speed on void volume characteristics. The comparison of observed results for N234 is given in Figure III-4.

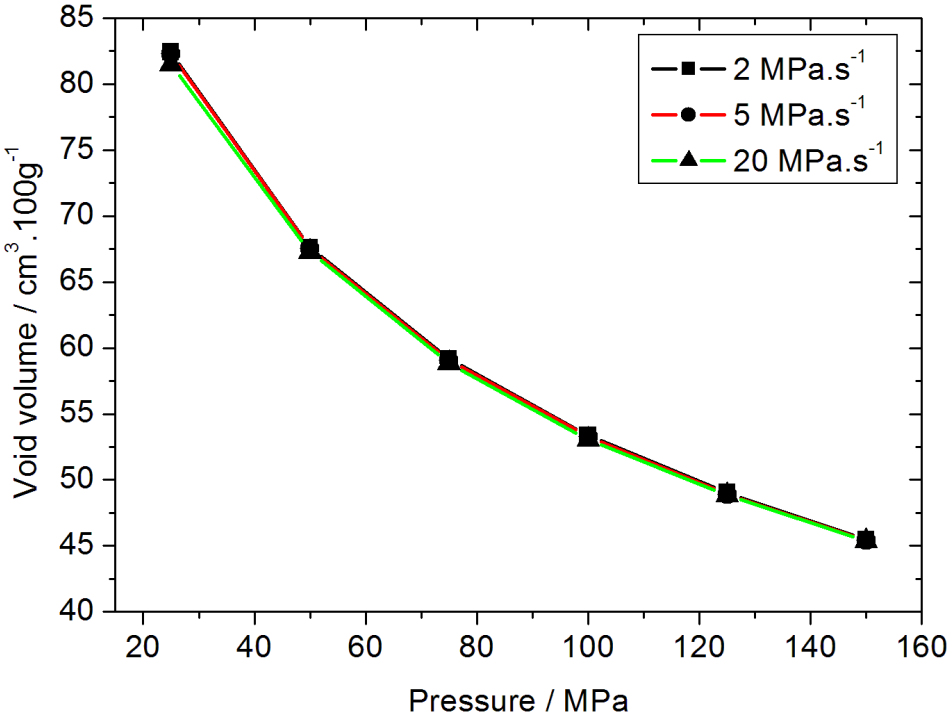

Figure III-4. The dependence of void volume on the pressure for N234 measured at various compression speeds.

From Figure III-4, it is clear immediately that the difference in void volume of the specific sample measured at varied compression speeds is rather insignificant.

For the further evaluation of the observed data, the correlation matrix for void volume results and oil absorption techniques is presented in Table III-4. To examine the correlation of the results the Pearson's correlation coefficient R was calculated. Geometrical mean of void volume observed at 25, 50, 75, 100, 125 and 150 MPa pressures for samples N220, N234, N326, N330, N550 and N772 was used for the purpose of the correlation.

Table III-4. Correlations between carbon black structure results measured via void volume where void volume characteristics were read at various pressures and results observed from oil absorption techniques (all being expressed in $cm^3.100\ g^{-1}$).

Void Volume	25 MPa	50 MPa	75 MPa	100 MPa	125 MPa	150 MPa
2 MPa.s^{-1}						
OAN	0.870	0.858	0.840	0.823	0.806	0.792
COAN	0.985	0.987	0.985	0.983	0.980	0.977
5 MPa.s^{-1}						
OAN	0.878	0.872	0.856	0.841	0.828	0.817
COAN	0.985	0.988	0.988	0.988	0.987	0.985
20 MPa.s^{-1}						
OAN	0.883	0.874	0.862	0.846	0.834	0.818
COAN	0.985	0.987	0.987	0.987	0.986	0.984

As shown in Table III-4, higher correlations were observed for void volume and COAN in general. In the case of compression speed 2 MPa.s^{-1}, the highest correlation was observed at 50 MPa, while at the two other compression speeds, the highest correlations were observed at compression speeds of 50 to 100 MPa. However, the correlation coefficients observed at all the measured pressures are very high.

In this part of the experiment, it was found that trends observed for the compression speed of 2 MPa.s^{-1} also persist for the other two compression speeds. Since the ASTM standard set the standardised compression speed between 1 and 2 MPa.s^{-1}, the latter is used primarily for further examinations.

The comparison of compressed void volume for various samples

At this stage, various carbon black grades are examined using Void Volume Tester. Results are plotted in Figure III-5.

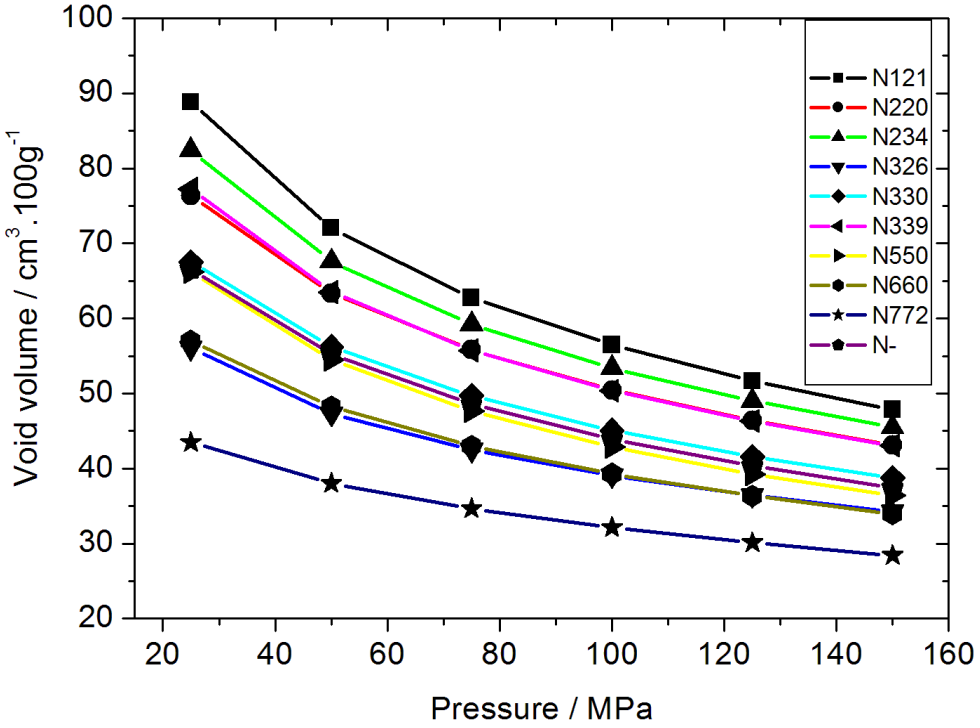

Figure III-5. The dependence of the geometrical mean void volume on the geometrical mean pressure for various carbon black samples.

It was found that void volume decreases towards higher compressions. This is given by the fracturing of carbon black and air release from voids in the secondary structure at low pressures as well as primary structure at higher pressures. Joyce et al. [4, 11] described that the steep decrease in volume in the first part of the curve corresponds to easily disrupt secondary or transient structure of agglomerates and subsequent gradual decrease correlates to aggregates, i.e. the primary structure.

The greater the void volume the greater the carbon black aggregate irregularity and non-sphericity. In Figure III-6, it is shown that the highest void volume at specified conditions was obtained for N121 grade.

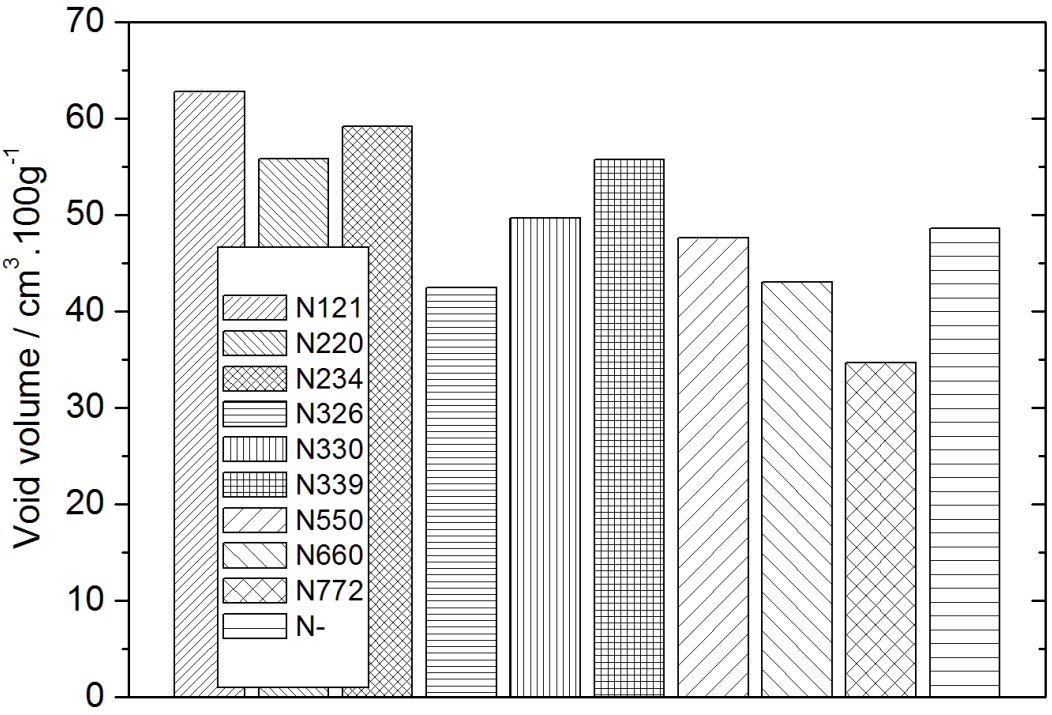

Figure III-6. Void volume data obtained at the standardised conditions 75 MPa and 2 MPa.s^{-1}.

In the following Table III-5 it can be seen that the results of void volume have a linear dependence on the results measured by oil absorption methods. The Pearson's correlation coefficient was used in order to find out the correlation between void volume measured at pressures 50, 75 and 100 MPa and results observed by oil absorption methods.

Table III-5. Pearson's correlation coefficient for void volume parameters obtained at compression speed 2 MPa.s^{-1} and oil absorption numbers.

	OAN	**COAN**	**VV 50**	**VV 75**	**VV 100**
OAN	1	0.876	0.887	0.875	0.863
COAN	0.876	1	0.991	0.990	0.989
VV 50	0.887	0.991	1	0.999	0.999
VV 75	0.875	0.990	0.999	1	0.999
VV 100	0.863	0.989	0.999	0.999	1

As shown in Table III-5, generally high correlations were observed between void volume measured by mechanical compression and oil absorption. The Pearson's correlation coefficient between void volume and COAN characteristics demonstrates a perfect correlation giving R approximately 0.99 at all the specified pressures. The highest Pearson's correlation coefficient was found between COAN and void volume read at 50 MPa then. On the other hand, the correlation between void volume and OAN results shows only a moderate Pearson's correlation coefficient.

According to the obtained results and limited statistics presented, it can be stated that COAN and compressed void volume could be considered as qualitatively equal methods, although additional statistic evaluation is needed and more various samples need to be measured to give more statistically relevant conclusions.

THE INVESTIGATION OF IN-RUBBER PROPERTIES OF CARBON BLACK

Sample preparation

Six varied carbon black grades presented in Table III-6 were incorporated into SMR 10 in order to examine their in-rubber properties with a special focus on carbon black structure. Moreover, a rubber compound composed of a neat rubber and chemicals without carbon black content was prepared as a reference sample.

Table III-6. Carbon black grades selected for the investigation of in-rubber properties.

Carbon black grade	**Iodine adsorption [mg/g]**	**STSA [m^2/g]**	**BET [m^2/g]**	**OAN [cm^3/100 g]**	**COAN [cm^3/100 g]**	**VV_75 MPa [cm^3/100 g]**
N220	121.6	105.0		114.5	98.0	60.6
N234	120.4	113.0	120.0	125.7	102.0	64.6
N326	82.2	78.0	78.0	72.0	68.0	45.1
N330	82.4	75.0		102.0	88.0	53.2
N550	43.2	40.0		122.0	84.0	51.1
N772	30.3	31.0	31.0	65.0	58.0	36.1

In Figure III-7, the dispersion process of carbon black using a laboratory mixer with tangential rotors is recorded.

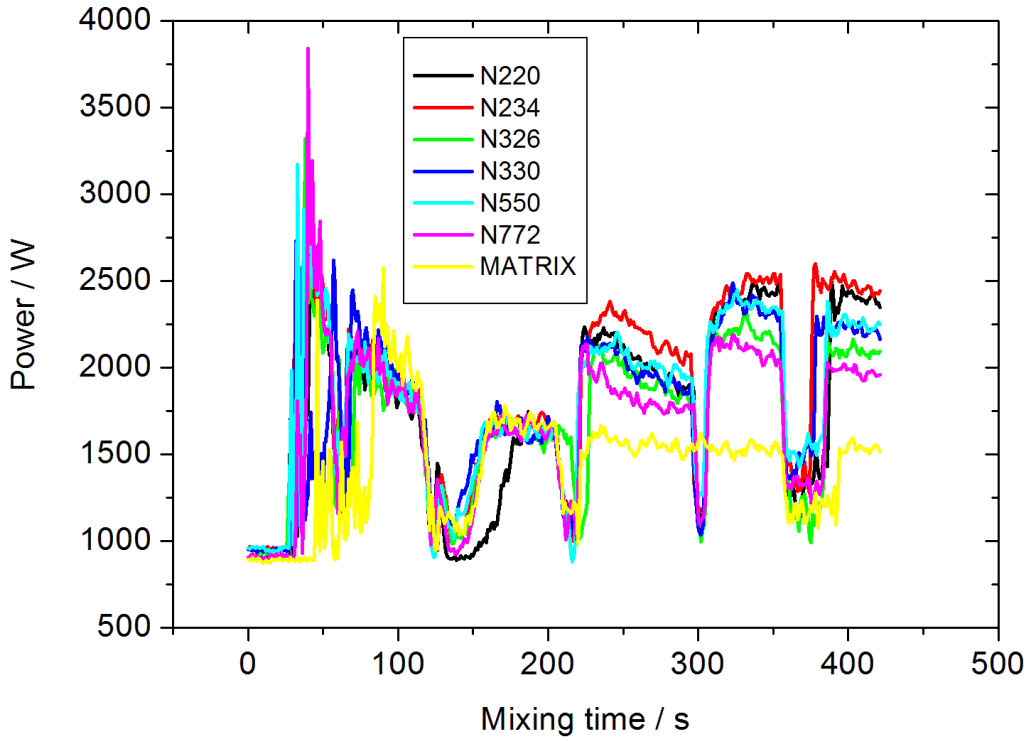

Figure III-7. Mixing process, the evolution of the power with the addition of single ingredients in time.

The dependence of power on the time changes according to the added chemicals. In the mixing time 210 s, when the first half of carbon black was added, a steep increase in power can be monitored. At 300 s, when the second half of carbon black was added, another significant increase in power was observed. The steep increase of power and its subsequent gradual decrease is defined by the process of carbon black mixing itself. In the first stage carbon black incorporation takes place when agglomerates are added into the mixer and a compact mixture is created. The compound viscosity increases rapidly at this stage. Then, as the agglomerates are being deagglomerated due to shear forces the viscosity tends to gradually decrease again. During this phase aggregates are formed. Subsequently, the distribution of formed aggregates throughout a matrix is ensured due to shear forces and material flow [22]. The time necessary for the mixing of carbon black where a compound viscosity increases and subsequently decreases and stabilizes is widely known as the black incorporation time (BIT) [3].

In Table III-7, the power read at the end of the mixing process when all the components were added is shown.

Table III-7. Power consumption for mixing of rubber compounds.

Carbon black grade	**N220**	**N234**	**N326**	**N330**	**N550**	**N772**	**Matrix**
Power at 400 s	2438	2462	2103	2245	2249	1994	1555

It was observed that the power varies according to the properties of incorporated carbon black. For the incorporation of carbon black grades with higher structure complexity and SSA, the higher power was necessary. The carbon black grade N234 having the highest structure and SSA shows the highest power consumption. The power consumption for mixing compounds is connected to the viscosity of compounds which is higher for high structured carbon black types [19, 21]. This is further discussed in the rheological section.

The role of carbon black in vulcanisation process

Vulcanisation curves and derived characteristics M_L, M_H and u are presented in order to describe the influence of carbon black properties on vulcanising process.

In Figure III-8, vulcanisation curves are shown.

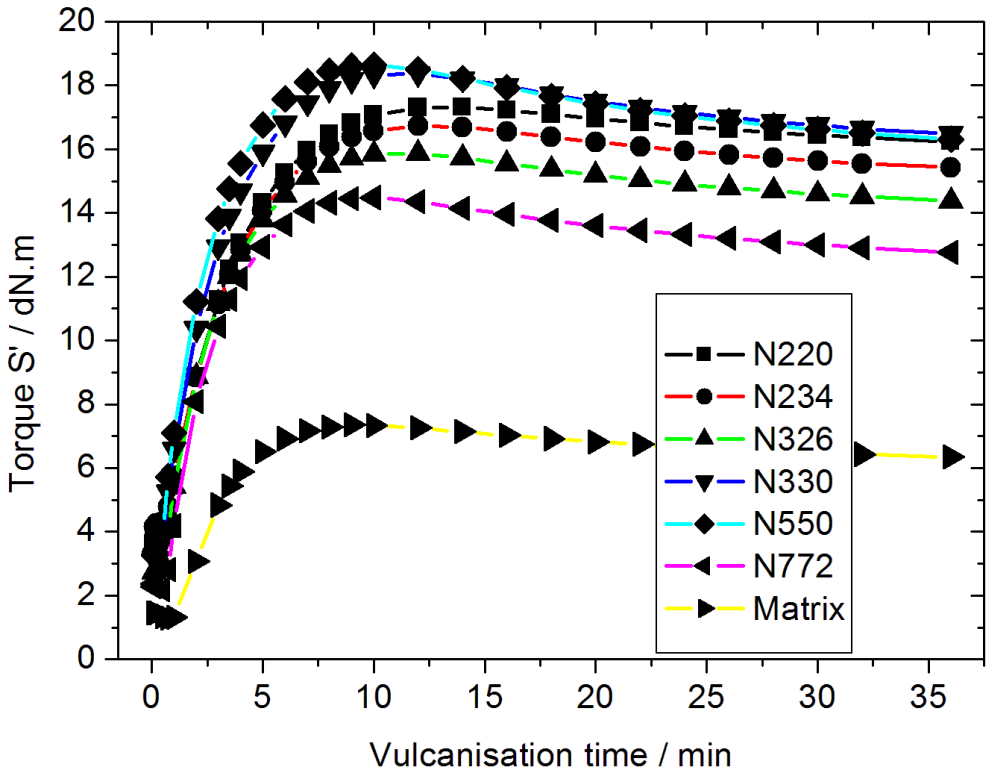

Figure III-8. Vulcanisation curves obtained for specific carbon black grades.

It is shown that the maximal torque *S'* obtained for filled compounds rise up twice the value of the neat rubber compound. For all the compounds, a significant reversion was obtained. This behaviour is rather normal for natural rubbers and should not be assigned to the influence of carbon black. According to Coran et al. [23] the reversion is caused by crosslinks disappearance. However, when the reversion time, defined as the time at which torque *S'* decrease about two percent from M_H, was quantified, the longest time was found for the compound containing N234. Generally, the reversion was found to be more significant for carbon black having lower SSA or larger particle size respectively.

One of the parameters read from the vulcanisation curve is M_L. The comparison of measured M_L values is shown in Figure III-9.

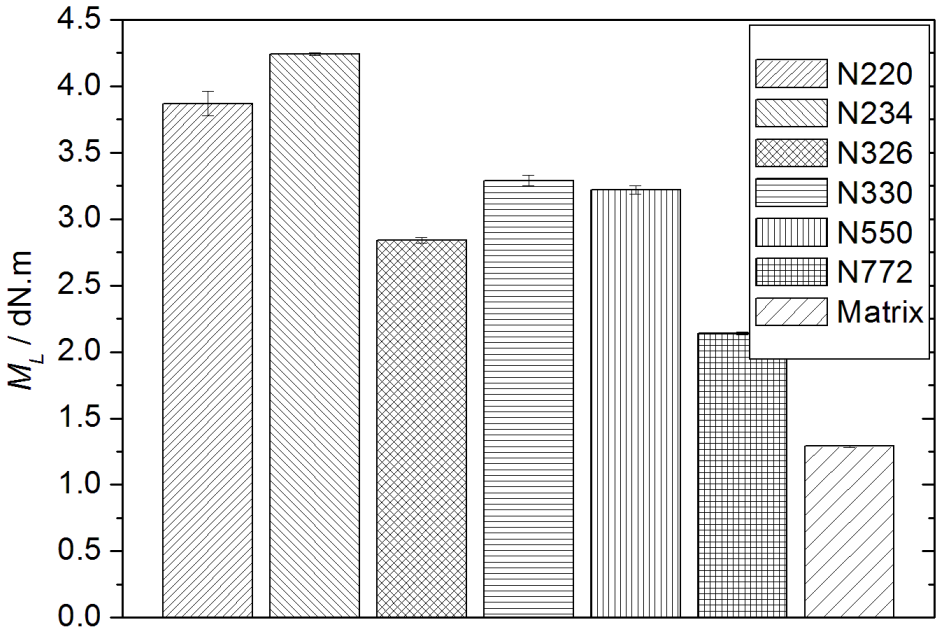

Figure III-9. The M_L characteristics observed for the specified carbon black grades.

Since the M_L is a parameter describing rubber compound viscosity, a strong dependence on carbon black structure can be found as discussed in the sample preparation section already. In Table III-8, the Pearson's correlation coefficient calculated for the M_L results, oil absorption methods and void volume is shown.

Table III-8. Pearson's correlation coefficient for M_L and COAN and void volume.

	OAN	**COAN**	**50 MPa**	**75 MPa**	**100 MPa**	$\boldsymbol{M_L}$
OAN	1	0.916	0.895	0.879	0.866	0.872
COAN	0.916	1	0.992	0.990	0.986	0.978
50 MPa	0.895	0.992	1	0.999	0.998	0.996
75 MPa	0.879	0.990	0.999	1	1.000	0.997
100 MPa	0.866	0.986	0.998	1.000	1	0.997
$\boldsymbol{M_L}$	0.872	0.978	0.996	0.997	0.997	1

In Table III-8, higher Pearson's correlation coefficient was obtained between void volume and M_L rather than for COAN and M_L. The highest correlation parameter was obtained for the void volume measured at compression 100 MPa. The value measured by OAN technique correlates with the M_L the least.

Investigation of the carbon black influence on M_H is plotted in Figure III-10.

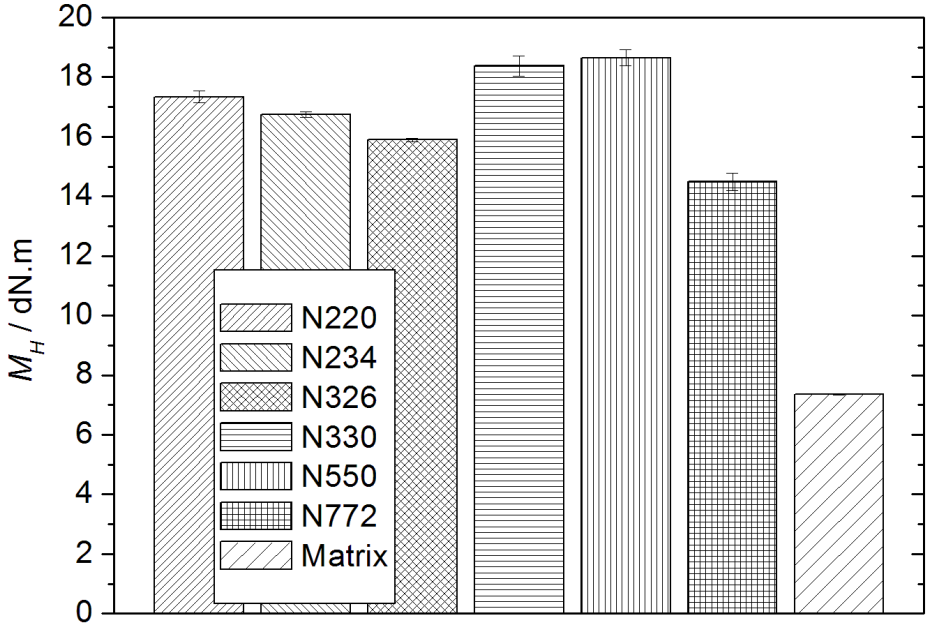

Figure III-10. The M_H characteristic observed for the specified carbon black grades.

The influence of M_L was obvious from Figure III-9, however this is not the case for the parameter M_H (Figure III-10), as no clear trend was monitored and the dependence of M_H on carbon black properties is rather random. This could be caused by the simultaneous creation of sulphur crosslinks and filler-polymer interactions which might have impeding effect on each other.

Another monitored parameter was the vulcanisation rate – u. Results of vulcanisation rates are presented in Figure III-11.

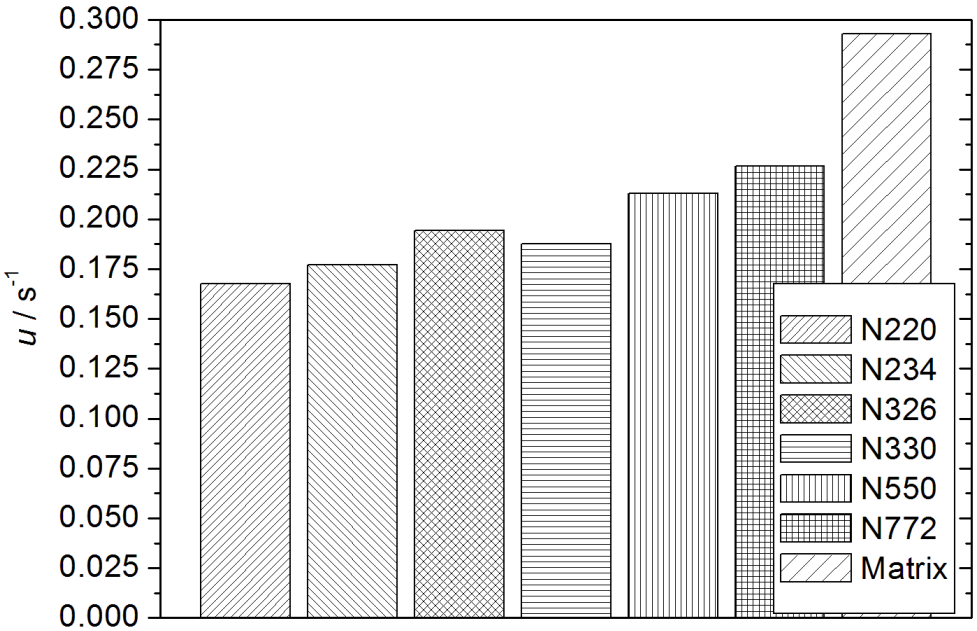

Figure III-11. The vulcanisation rate u observed for the specified carbon black grades.

It was found that all the carbon black grades have negative influence on the rate of vulcanisation process when compared to the neat rubber compound although generally the influence of carbon black is rather negligible. The rate for the neat rubber compound was 0.293 s^{-1} while between the filled rubber compounds the highest vulcanisation rate obtained was 0.227 s^{-1}. Thus, the vulcanisation rate for all the filled compounds is generally lower. It was found that the vulcanisation rate decreases disproportionally to an increasing SSA up to 0.168 s^{-1}, measured for the N220 having the largest SSA.

The role of carbon black properties in filler networking

For the purpose of evaluation of interactions between carbon black and rubber the well-known Payne effect test was employed and Payne softening was calculated according to Equation 23. Results are presented in Figure III-12.

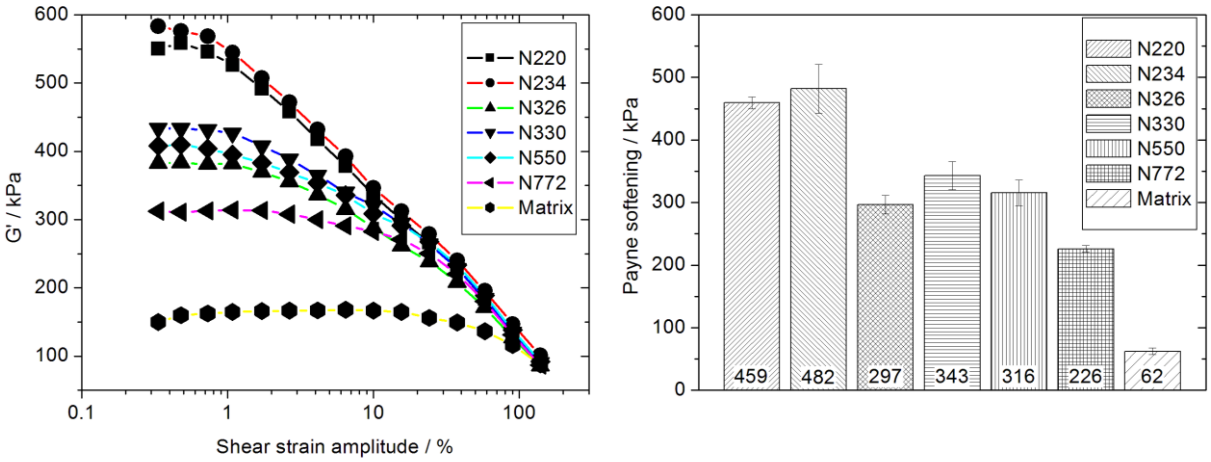

Figure III-12. Payne effect (left hand side) and Payne softening calculated for rubber compounds filled with various carbon black grades.

Results presented in Figure III-12 show the Payne softening data where strong dependence on carbon black properties, primarily on the structure can be seen. The highest Payne softening was observed for the rubber compound containing N234 having the highest structure and SSA. Standard deviations represented by error bars are caused by rubber compounds' heterogeneity as statistically described in detail elsewhere [24]. In the case of neat matrix, the measure of rubber mastication is shown rather than strain softening.

In order to find out correlations between measured structure characteristics and Payne softening, Pearson's correlation coefficients were calculated and is summarised in Table III-9.

Table III-9. Pearson's correlation coefficients for structure parameters.

	25 MPa	**50 MPa**	**75 MPa**	**100 MPa**	**125 MPa**	**150 MPa**	**OAN**	**COAN**
2 MPa.s^{-1}								
Payne softening	0.957	0.965	0.972	0.976	0.979	0.981	0.784	0.945
5 MPa.s^{-1}								
Payne softening	0.952	0.958	0.964	0.969	0.972	0.975	0.784	0.945
20 MPa.s^{-1}								
Payne softening	0.949	0.956	0.962	0.968	0.971	0.974	0.784	0.945

The Pearson's correlation coefficient between compressed void volume, measured at various compression speeds and read at various pressures, oil absorption characteristics and Payne softening is shown. Higher correlation coefficients were observed between compressed void volume and Payne softening compared to results of oil absorption techniques and Payne softening. Furthermore, the precision of the Pearson's correlation coefficient was found to be dependent on compression at which void volume was read. At higher compressions, higher correlation coefficients could be observed possibly. Moreover, the precision of correlation coefficients increases according to lower compression speeds.

Based on the correlation coefficients it can be concluded that the compressed void volume gives more relevant characteristic to the process of deagglomeration of carbon black during mixing than COAN. In other words, compressed void volume might be possibly used to predict behaviour of carbon black in rubber compounds.

CONCLUSIONS OF CHAPTER III

Several experiments were carried out and many correlation parameters were calculated in this work.

Based on the results, several conclusions can be made:

- During the void volume investigation, significant problems caused by the temperature of oil in a hydraulic system were found. An oil temperature control system was suggested to be implemented to Void Volume Tester to minimise the influence of oil temperature on the results.
- Trends observed for speed 2 $MPa.s^{-1}$ also persist for the other two examined compression speeds.
- Regarding vulcanisation process, it was found that the vulcanisation rate of filled rubber compounds decreases disproportionally to an increasing SSA.
- Compressed void volume relate to the M_L characteristic with a higher correlation coefficient than COAN thus provides a parameter which gives better insight to carbon black behaviour in filled rubber compounds compared to COAN.
- Considering Payne softening, higher correlation coefficients were observed between compressed void volume and Payne softening than between oil absorption methods and Payne softening. Apart from the M_L, Payne softening is another parameter describing in-rubber behaviour of carbon black where compressed void volume gives higher correlation than COAN.

Based on the observed data, it can be concluded that Void Volume Tester evaluating carbon black structure complexity gives more reasonable results than oil absorption techniques considering the in-rubber properties hence compressed void volume could be used for prediction of behaviour of carbon black in rubber compounds.

ACKNOWLEDGEMENTS

This work was carried out with the financial support of Internal Grant Agency of Tomas Bata University in Zlín (reg. number: IGA/FT/2013/012) funded from the resource of specific university research. This work was done with the support of Operational Program Research and Development for Innovations co-funded by the European Regional Development Fund (ERDF) and the national budget of Czech Republic, within the framework of project Centre of Polymer Systems (reg. number: CZ.1.05/2.1.00/03.0111). Authors are grateful to the Tomas Bata University in Zlín which made this research possible and to companies Continental Barum, Otrokovice and CS Cabot, Valasske Mezirici for

the material and machinery support. Some of the authors would like to thank to Dr. André de Bois, Dr. Jan Sumfleth and Dr. Patrick Lamprecht for their help and suggestions.

REFERENCES

1. G.A. Joyce, W.M. Henry, R.W. Magee. Advances in Structure Measurements of Carbon Black. Presented at the Fall 164th Technical Meeting of the Rubber Division of the American Chemical Society, Inc. 2008; 23p.
2. J.B. Donnet, R.Ch. Bansal, M.J. Wang. Carbon Black - Science and Technology. Marcel Dekker Inc. 1993; 461p. ISBN 0-8247-8975-X.
3. W.A. Wampler, T.F. Carlson, W.R. Jones. Carbon Black. B. Rodgers. Rubber Compounding: Chemistry and Applications. New York: Marcel Dekker 2004; 6: p. 239-284. ISBN 0-8247-4871-9.
4. G.A. Joyce, W.M. Henry. Modelling the Equilibrium Compressed Void Volume of Carbon Black. Rubb Chem Technol 2006; 79(5): p. 735-764.
5. W. Wampler. Improved Test for Determination of Carbon Black Structure. Carbon Black World 2004; 26p.
6. Y.M. Tien, P.L. Wu, C.A. Chu, et al. The Friction-Free Compressibility. Phys Chem Earth 2007; 32(8-14): P. 809-819.
7. B.J. Briscoe, S.L. Rough, The Effects of Wall Friction in Powder Compaction. Colloid Surface A 1998; 137(1-3): p. 103-116.
8. I.M. Cameron, D.T. Gethin. Exploration of die wall friction for powder compaction using a discrete finite element modelling technique. Model Simul Mater Sc 2001; 9(4): p. 289-307.
9. C.Y. Wu, O.M. Ruddy, A.C. Bentham, et al. Modelling the mechanical behaviour of pharmaceutical powders during compaction. Powder Technol 2005; 152(1-3): p. 107-117.
10. I.C. Sinka, J.C. Cunningham, A. Zavaliangos. The effect of wall friction in the compaction of pharmaceutical tablets with curved faces: a validation study of the Drucker-Prager Cap model. Powder Technol 2003; 133(1-3): p. 33-43.
11. G.A. Joyce, W.M. Henry. Carbon Black Intra-Aggregate Void Volume from Dynamic Compression Measurements. Rubber World 2011; 244(6): p. 12.
12. R. Houwink. Slipping of Molecules during the Deformation of Reinforced Rubber. Rubb Chem Technol 1956; 29(3): p. 888–893.

13. A.R. Payne. The Dynamic Properties of Carbon Black-Loaded Natural Rubber Vulcanizates. Part I. J Appl Polym Sci 1962; 6(19): p. 57–63.
14. L. Mullins, N.R. Tobin. Stress Softening in Rubber Vulcanizates .I. Use of a Strain Amplification Factor to Describe Elastic Behavior of Filler-Reinforced Vulcanized Rubber. J Appl Polym Sci 1965; 9(9): p. 2993-3009.
15. L. Mullins. Softening of Rubber by Deformation. RubbChemTechnol1969; 42(1): p. 339–362.
16. G. Kraus. Reinforcement of Elastomers by Carbon Black. Rubber Chemistry and Technology 1978; 51(2): p. 297–321.
17. E.M. Dannenberg. Bound Rubber and Carbon Black Reinforcement. RubbChemTechnol1986; 59(3): p. 512–524.
18. M.J. Wang. Effect of Polymer-Filler and Filler-Filler Interactions on Dynamic Properties of Filled Vulcanizates. Rubb Chem Technol 1998, 71(3): p. 520–589.
19. J. B. Donnet, E. Custodero. Reinforcement of Elastomers by Particulate Fillers. J.E. Mark, B. Erman, F.R. Eirich. Science and Technology of Rubber. Elsevier Academic Press 2005; 8: p. 367–400. ISBN: 0-12-464786-3.
20. J.L. Leblanc. Rubber-Filler Interactions and Rheological Properties in Filled Compounds. Prog Polym Sci 2002; 27(4): p. 627–687.
21. J.L. Leblanc. Filled Polymer – Science and Industrial Application. CRC Press 2010; 3–4: p. 15–184. ISBN: 978-1-4398-0042-3.
22. P.S. Johnson. Rubber Processing. Mnichov : Hanser Gardner Publications, 2001. 145 p. ISBN 3-446-21578-6
23. A.Y. Coran. Vulcanisation. J.E. Mark, B. Erman, F.R. Eirich. Science and Technology of Rubber. Elsevier Academic Press 2005; 7: p. 321–366. ISBN: 0-12-464786-3.
24. J. Kadlcak, L.B. Tunnicliffe, J. Lacayo, et al. Rapid Payne Effect Test – A Novel Method for Study of Strain-Softening Behavior of Rubbers Filled with Various Carbon Blacks. – Manuscript number POTE-D-14-00258 (Polymer Testing).

CHAPTER IV. MACRODISPERSION EVALUATION – REFERENCE OBJECT FOR TOPOGRAPHY OF MATERIALS

In real compounds, the heterogeneous particles are present in agglomerates of filler (carbon black, silica, chalk, clay and others). During the mixing of a compound, the agglomerates change the diameter and are incorporated to the matrix on microdispersion level. The final distribution of macro particles is broad and not well-defined. The calibration of devices for the evaluation of macrodispersion cannot be performed on a real compound. As a consequence, the ASTM D7723-11 does not have a precision statement. Mentioned disadvantages and deficiency can considerably be solved by the reference object for topography of materials intended for the calibration of a device evaluating the quality of filler macrodispersion. The procedure of the preparation of the reference object for topography of materials is described in this work. This object provides a simple tool valid for the calibration of devices measuring the quality of macrodispersion of fillers in a rubber matrix by quantifying the surface roughness of a freshly cut specimen using an optical microscope in the reflection mode. The reference object for topography of materials is made from a two-phase composite material based on a continuous phase and a discrete phase which is composed of inert globular particles having narrow size distribution with a variation coefficient up to 1.

THEORETICAL BACKGROUND OF CHAPTER IV

Since the quality of filler dispersion influences the performance of final products such as tires significantly, many methods for the monitoring of quality of the filler incorporation into the rubber matrix are in use across rubber industries nowadays. The quality of filler incorporation is described as the quality of filler macrodispersion, which is the degree of distribution of filler into a compound, generally on a scale of less than 100 micrometres but greater than 2 micrometres representing micro range agglomeration [1]. One of the most broadly used methods measuring the quality of macrodispersion of reinforcing fillers such as silica and carbon black, as well as inert fillers such as chalk, clay and other solids is an optical microscope in the reflection mode evaluating the surface roughness of a freshly cut specimen, which is due to its rapidity and

relative simplicity. This method is described in the international standard ASTM D7723-11 “Standard Test Method for Rubber Property – Macro-Dispersion of Fillers in Compounds” [1]. This standardised method uses mathematical algorithms to quantify the surface roughness of freshly cut rubber specimens as measured by a reflected light optical method when the specimen is cut and large agglomerates are pushed to one side or the other leaving a contoured surface where contours are referred as nodges. The sample preparation from uncured compound is described in document US 6,795,172 called “Method for preparing a cut surface in uncured rubber samples for measuring filler dispersion” [2]. The light microscope is equipped with a Charged Coupled Device (CCD) or Complementary Metal Oxide Semiconductor (CMOS) sensor capturing surface images. The apparatus works in the dark field mode when an aperture is lit at a 30° angle for analysis. The sensor picks up the reflection of bumps on the surface where nodges represent undispersed filler whilst flat areas disperse the light out of sensor thus appear dark in the sensor. The scan of the surface is digitalised and is analysed as a binary image by the image processing software. The procedure of analysis is described in the international standard ISO 11345 called “Rubber – Assessment of Carbon Black and Carbon Black/Silica Dispersion – Rapid Comparative Methods” [3]. From a binary image, the ratio of the white area represented by nodges to the total area of the image can be calculated according to the ASTM D7723-11 [1] providing the quality of filler macrodispersion in percentage.

Tests on rubber compounds in rubber industry are conducted in order to determine properties and behaviour of materials [4-6]. Obtained characteristics can serve as manufacturing and processing supervision and for the quality control of raw, semi and final products. Rubber materials are known for their high molecular weight and very complex viscoelastic behaviour, e.g. reversible deformation up to 1000 % at low compressibility [7, 8]. Because of their complex behaviour, their processing is complicated. Behaviour of these materials differs depending on their composition and type of each component in a compound [9-11]. Then, single tests and conditions is necessarily to be chosen according to the variability of the rubber compounds, because viscoelastic response will differ with test temperature, stress, frequency, the magnitude of imposed strain and many other parameters [12-18]. The process of a sample preparation is very important, because the precision of a preparation can influence test results significantly. Moreover, sample history, e.g. ageing or storage are also important [15, 19-23]. In general, testing should be carried at

very similar (nearly the same) conditions as the intended application of a product [5].

METHODOLOGY OF CHAPTER IV

MATERIALS

The reference object for topography of materials is a two-phase product where the continuous phase is a silicone rubber (Sylgard® 184, Dow Corning GmbH) and as the discrete phase are fractions of glass spheres having, according to producer, narrow particle size distribution from 0.5 to 25 micrometres and of 25 to 32 micrometres respectively.

Glass spheres characterisation

Glass spheres were characterised via optical microscopy first and subsequent image analysis was done for the characterisation of the particle size distribution evaluation.

Sample preparation

The reference object for topography of material was composed by 100 phr of silicone rubber, 10 phr of crosslinking agent and 1 phr of glass spheres. Silicone rubber in a liquid phase was measured into a beaker, where was mixed with a crosslinking agent. Subsequently, a specific amount of glass spheres were added. This compound has been mixed by an electrical stirrer for five minutes at velocity 300 revs/min at room temperature. This suspension was transformed into a small container having dimensions required by an application. The minimal area of the sample necessary for the macrodispersion investigation according to ASTM D7723 is 5 by 5 millimetres however. Subsequently the suspension was inserted into a vacuum oven for half an hour for the deaeration process. After the deaeration process the suspension was heated up to 80±5 °C for at least 1.5 hour, until the crosslinking process is complete. The process of sample preparation is schematically shown in Figure IV-1.

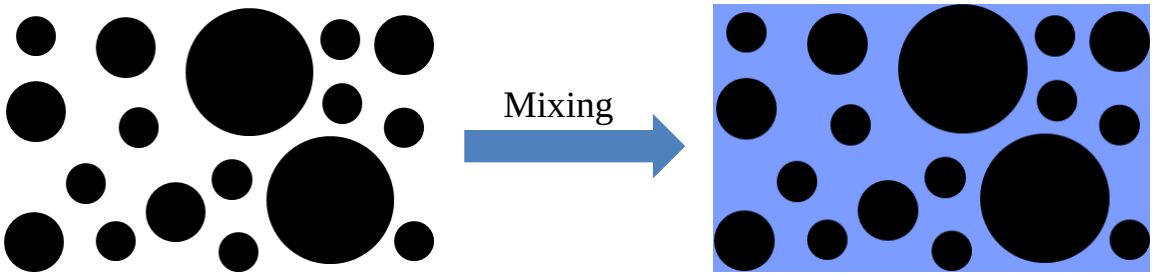

Figure IV-1. Schematic representation of the sample preparation, where the black dots represent filler particles and coloured neighbours represent the matrix.

Sample characterisation

Prepared samples were characterised via Dispergrader (Alpha Technologies) and via optical microscopy, when microtome cuts were investigated.

Dispergrader works in the dark field mode when an aperture is lit at a 30° angle as schematically shown in Figure IV-2. The sensor picks up the reflection of bumps on the surface where nodges represent undispersed filler whilst flat areas disperse the light out of sensor thus appear dark in the sensor. The scan of the surface is digitalised as a binary image and it is analysed by the image processing software. From a binary image, the ratio of the white area, represented by nodges, to the total area of the image is calculated according to Equation 24 and the quality of filler macrodispersion is evaluated:

$$Macrodispersion\ index = \frac{V_{filler,undispersed}}{V_{filler,total}} \tag{24}$$

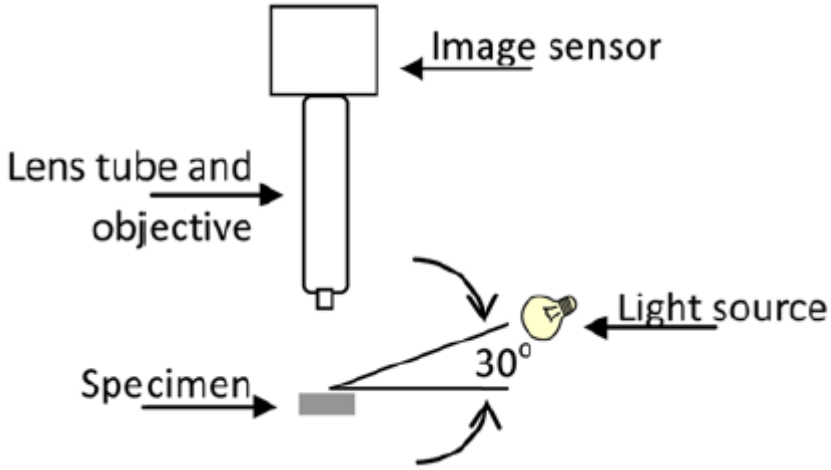

Figure IV-2. The principle of Dispergrader.

RESULTS AND DISCUSSION OF CHAPTER IV

MACRODISPERSION OF GLASS SPHERE SIZE EVALUATED VIA OPTICAL MICROSCOPY

The Figure IV-3 shows an example of the scan obtained by the optical microscope for fraction of 25 to 32 micrometres.

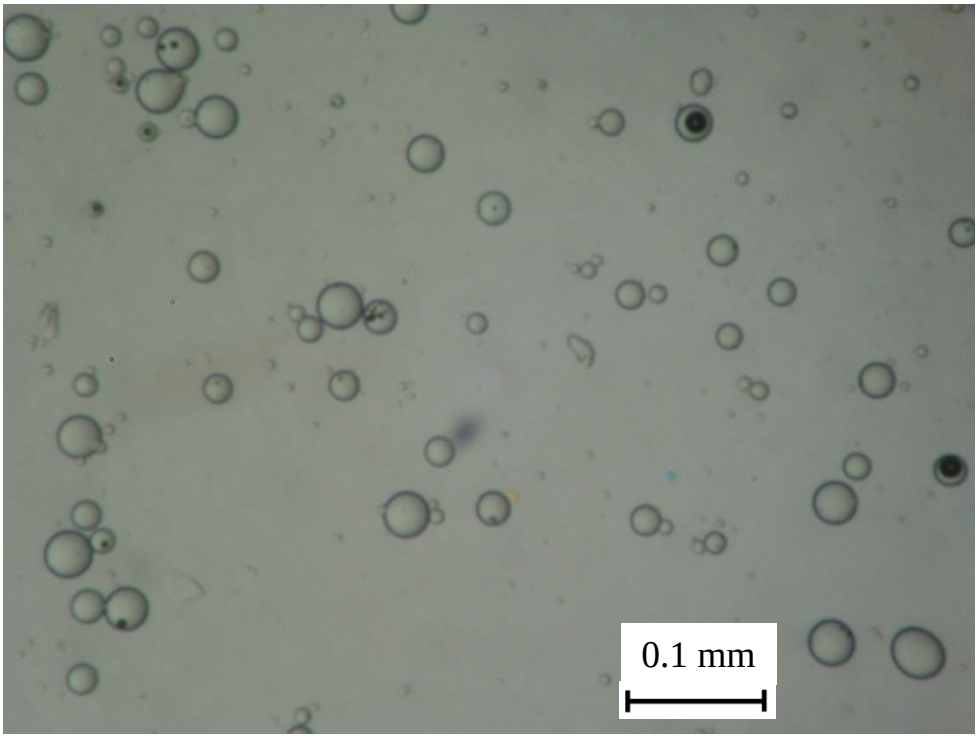

Figure IV-3. An exemplified microscopy scan of glass spheres with a diameter between 25 and 32 micrometres.

Images obtained via optical microscopy were analysed and the glass sphere size distribution was evaluated using the image processing software. All the presented histograms are based on at least 250 spheres. Thus, the histograms are normalised for the same number of particles. In Figure IV-4, the frequency against glass spheres' size for glass sphere fraction 0.5-25 micrometres is plotted.

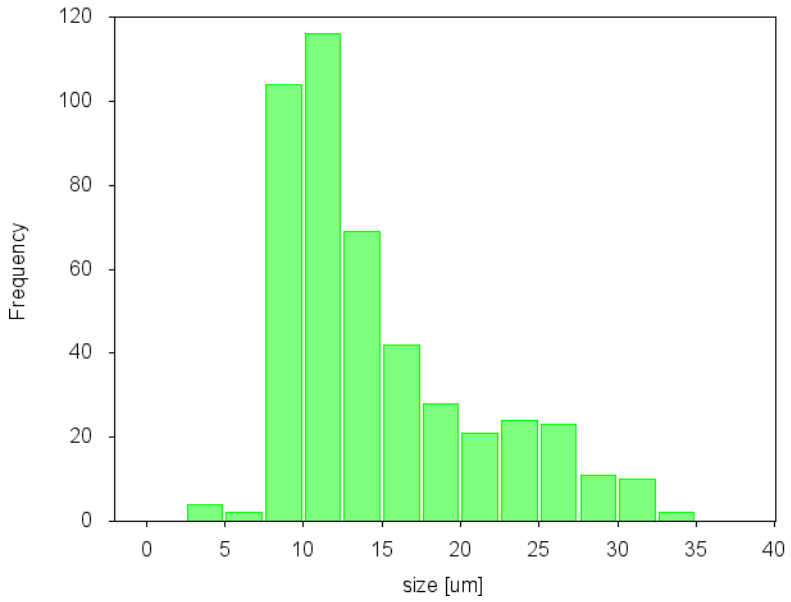

Figure IV-4. Particle size distribution obtained via optical microscopy.

It can be seen that the size distribution is in range of approximately 3 to 32 micrometres which is slightly different than the information of producer. The coefficient of variation of incorporated glass spheres was 0.55.

The distribution curve presented in Figure IV-5 was obtained for samples filled with fraction 0.5-25 micrometres prepared by a microtome.

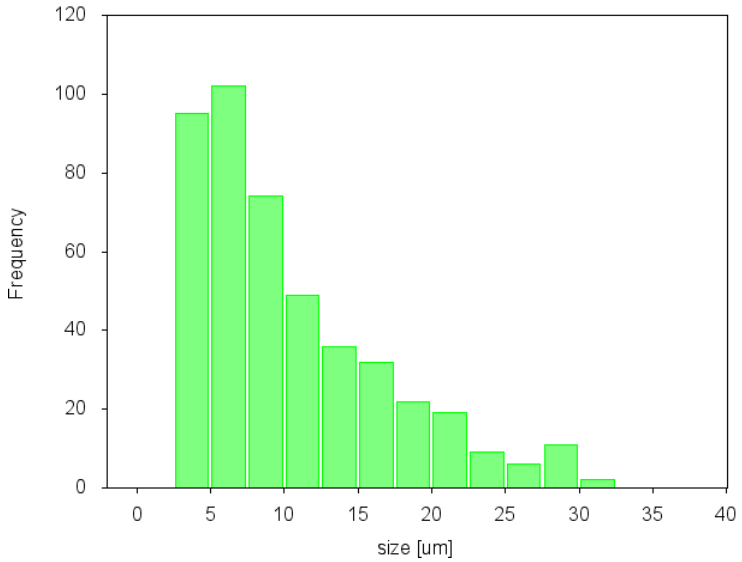

Figure IV-5. Particle size distribution obtained via optical microscopy of microtome cuts.

As you can see, the shape of size distribution curve is very similar to the results measured for the reference sample. The size distribution is in range of 3 to 30 micrometres. From the observed data it seemed that glass spheres in paraffinic oil, which was used to separate single spheres (Figure IV-4), are systematically larger compared to the result of microtome which could be caused due to the layer of oil formed on the surface of spheres. Therefore, presented results of glass spheres dispersed in the paraffinic oil were diminished about 5 micrometres and the comparison between the two distributions is done in Figure IV-6.

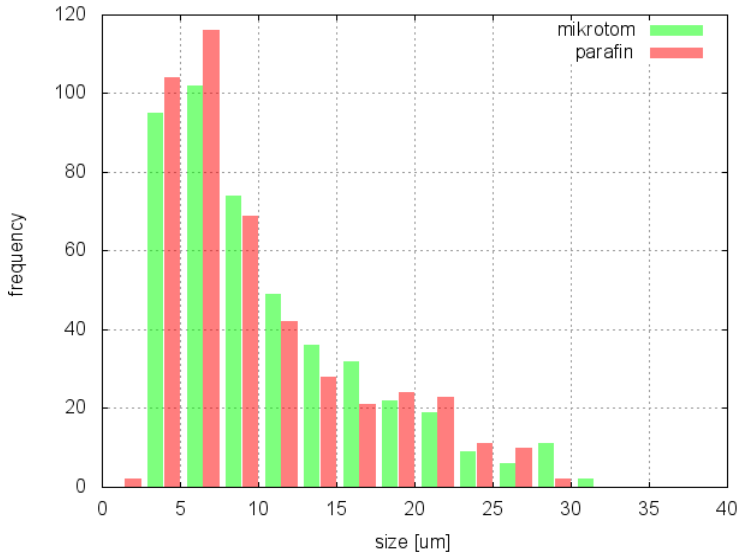

Figure IV-6. The comparison of particle size distribution for spheres in paraffinic oil and microtome cuts.

From the comparison in Figure IV-6, it was found no significant difference between the two distributions.

MACRODISPERSION OF GLASS SPHERE SIZE EVALUATED VIA DISPERGRADER

Figure IV-7 shows the results of the distribution of the glass spheres fraction 0.5-25 micrometres in silicone rubber investigated by Dispergrader.

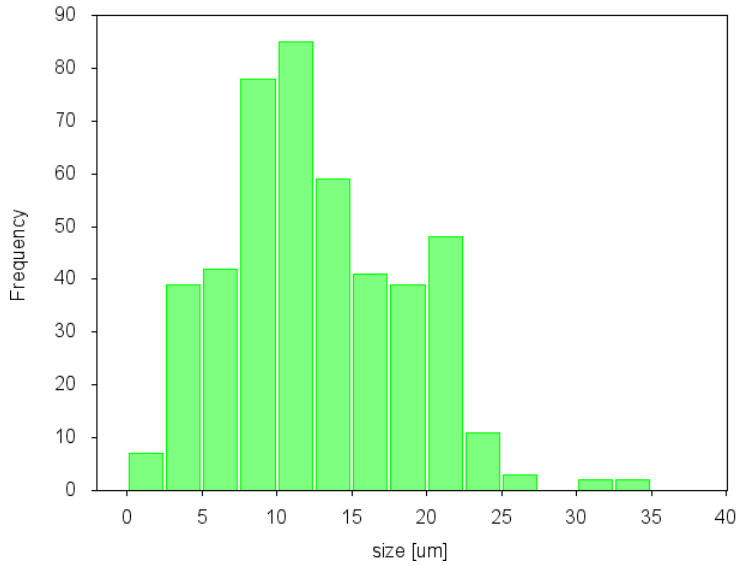

Figure IV-7. The particle size distribution obtained via Dispergrader.

The shape of the distribution curve measured by Dispergrader shows a significant difference compared to the other two distribution curves obtained via optical microscopy. Even the size distribution is in the same range.

In the Figure IV-8, all the obtained results are compared. It can be seen that results observed by optical microscopy (paraffinic oil and microtome) are identical. On the other hand, the data from Dispergrader show a different trend and do not match with the optical microscopy results. It can be concluded that results provided by Dispergrader are distinct.

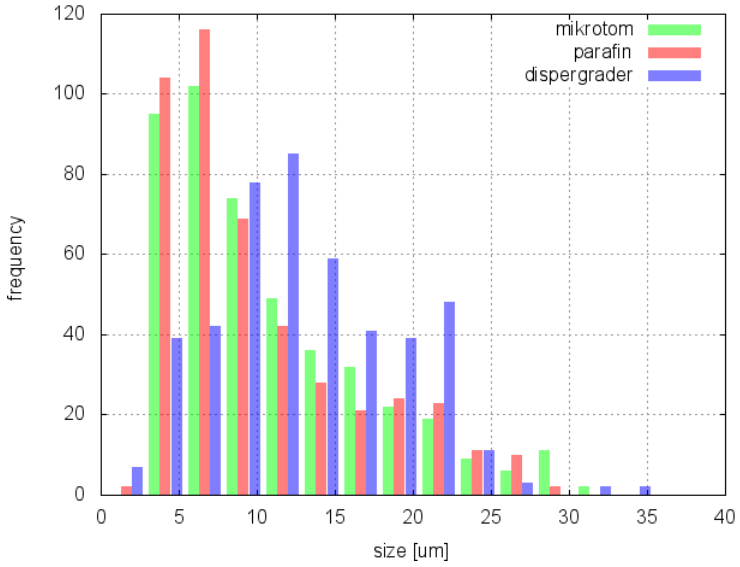

Figure IV-8. The comparison of all the data observed using different evaluation methods.

Moreover, Table IV-1 shows parameters measured by Dispergrader for different reference objects prepared for different levels of macrodispersion. Moreover, corrected standard deviations (CSD) show on the narrow distribution size of glass spheres in prepared reference objects for topography of materials which in results points at the beneficial use of glass spheres as a model filler.

Table IV-1. Characteristics of the various reference objects for topography of materials observed via Dispergrader.

Glass spheres fraction [µm]	**Amount [%wt]**	**White Area [%]**	***Z* [%]**	**CSD**	**Variation coefficient [%]**
0-25	0.10	0.08	**99**	0.040	0.04
0-25	3.00	0.68	**98**	0.075	0.08
0-25	10.00	0.97	**97**	0.186	0.19
25-32	10.00	1.48	**96**	0.079	0.08
25-32	20.00	1.73	**95**	0.187	0.20

Where the White area represents the amount of undispersed filler, Z stands for the value of macrodispersion, CSD is corrected standard deviation which together with the Variation coefficient shows on the narrow distribution of glass spheres' sizes.

CONCLUSIONS OF CHAPTER IV

The two-phase reference object for topography of material composed of silicone rubber and glass spheres with a narrow size distribution from 3 to 32 micrometres with the coefficient of variation 0.55 was prepared and inspected by Dispergrader. An optical microscopy was used for the subsequent evaluation of particle size distribution in paraffinic oil and microtome cuts. The data from the optical microscopy were used for the verification of results observed by Dispergrader. Based on the results it was concluded that Dispergrader provides significantly different results of glass spheres size distribution compared to the results obtained via the optical microscope, even the particle size is in the same range. Therefore, based on the results, it was concluded that the technique for the calibration of Dispergrader is needed. For this purpose, the reference object for topography of material was prepared which offers an efficient and simple way of calibration.

A range of reference objects providing various levels of macrodispersion can be prepared according to the presented procedure as shown in Table IV-1and Dispergrader can be calibrated according to these.

The reference object can contain any inert particles of globular shapes having diameters in the range of 0.5 to 500 micrometers and narrow size distribution with the coefficient of variation up to 1. Preferred diameter of the inert globular particles is in the range of approximately 3 to 30 micrometers and its content is approximately 1 %wt in 100 %wt of the continuous phase. The continuous phase can be formed by any polymer matrix based on an elastomer, preferably a silicone rubber, any polymer matrix based on a thermoplastic or a thermoset. Alternatively, as the continuous phase, a low-molecular weight organic material as wax, paraffinic oil or glue can be used. Inert globular particles are preferably glass spheres, but also particles of organic nature, e.g. carbon black, ceramic spheres or metal spheres can be used.

The reference object for topography of materials according to this work improves the process of evaluation of macrodispersion quality based on the surface roughness of a freshly cut sample.

The patent application of this work has been submitted in the Czech Republic and the original Czech patent is enclosed in Appendix A. Moreover, the international PCT (Patent Cooperation Treaty) application has been submitted under the International application No. PCT/CZ2014/000043.

ACKNOWLEDGEMENTS

This work was carried out with the financial support of Internal Grant Agency of Tomas Bata University in Zlín (reg. number: IGA/FT/2013/012) funded from the resource of specific university research. This work was written with the support of Operational Program Research and Development for Innovations co-funded by the European Regional Development Fund (ERDF) and the national budget of Czech Republic, within the framework of project Centre of Polymer Systems (reg. number: CZ.1.05/2.1.00/03.0111). Authors are grateful to Continental Reifen Deutschland GmbH and Tomas Bata University in Zlín which made this research possible. Some authors would like to thank to Pavol Priekala from Alpha Technologies.

REFERENCES

1. ASTM D7723-11. Standard Test Method for Rubber Property – Macro-Dispersion of Fillers in Compounds. ASTM International. 2011. ICS 87.060.10.
2. J.B. Putman, M.C. Putman, J.B. Bulman. Method for preparing a cut surface in uncured rubber samples for measuring filler dispersion. United States Patent US 6,795,172 B2. 2004.
3. ISO 11345. Rubber – Assessment of Carbon Black and Carbon Black/Silica Dispersion – Rapid Comparative Methods. International Standard 2006. Ref. no. ISO 11345:2006(E).
4. R. Brown. Physical Testing of Rubber. 4th ed. New York, NY: Springer, 2006, viii, 387 s. ISBN 0-3872-8286-6.
5. J.S. Dick. Basic Rubber Testing: Selecting Methods for a Rubber Test Program. West Conshohocken, PA: ASTM, c2003, xviii, 236 s. ISBN 0-8031-3358-8.
6. A.N. Gent. Rubber Elasticity: Basic Concepts and Behavior. J.E. Mark, B. Erman, F.R. Eirich, Science and Technology of Rubber. Elsevier Academic Press 2005; 1: p. 1-28. ISBN 0-12-464786-3.
7. B. Rodgers, W. Waddell. The Science of Rubber Compounding. J.E. Mark, B. Erman, F.R. Eirich, Science and Technology of Rubber. Elsevier Academic Press 2005; 9: p. 401-454. ISBN 0-12-464786-3.
8. P.S. Johnson. Rubber Processing. Mnichov : Hanser Gardner Publications 2001; 145p. ISBN 3-446-21578-6.
9. B. Rodgers. Rubber Compounding: Chemistry and Applications. New York: Marcel Dekker 2004; 645p. ISBN 0-8247-4871-9.
10. F.W. Barlow. Rubber Compounding: Principles, Materials, and Techniques. 2nd Ed. New York: Marcel Dekker 1993; 294p. ISBN 0-8247-8968-7.
11. W.A. Wampler, T.F. Carlson, W.R. Jones. Carbon Black. B. Rodgers. Rubber Compounding: Chemistry and Applications. New York: Marcel Dekker 2004; 6: p. 239-284. ISBN 0-8247-4871-9.
12. A.N. Gent. Engineering with Rubber: How to Design Rubber Components. 3rd Ed. Munich: Hanser Publishers 2012; 433p. ISBN 978-3-446-42764-8.

13. K.L. Ngai. The Viscoelastic Behavior of Rubber. J.E. Mark, B. Erman, F.R. Eirich, Science and Technology of Rubber. Elsevier Academic Press 2005; 5: p. 183-236. ISBN 0-12-464786-3.

14. J.L. White. Rheological Behavior and Processing of Unvulcanized Rubber. J.E. Mark, B. Erman, F.R. Eirich, Science and Technology of Rubber. Elsevier Academic Press 2005; 6: p. 237-321. ISBN 0-12-464786-3.

15. L.B. Tunnicliffe, J. Kadlcak, Y. Shi, et al. Flocculation and Viscoelastic Behaviour in Carbon Black-Filled Natural Rubber. Macromol Mater Eng 2014; DOI: 10.1002/mame.201400117.

16. G. Kraus. Reinforcement of Elastomers by Carbon Black. Rubb Chem Technol 1978; 51(2): p. 297-321.

17. A.R. Payne. The Dynamic Properties of Carbon Black-Loaded Natural Rubber Vulcanizates. Part I. J Appl Polym Sci 1962; 6(19): p. 57-63.

18. M.J. Wang. Effect of Polymer-Filler and Filler-Filler Interactions on Dynamic Properties of Filled Vulcanizates. Rubb Chem Technol 1998; 71(3): p. 520-589.

19. J.W. Mani, J.G Meier, M. Klüppel. Study of Flocculation Dynamics of Carbon Black in Rubber Melts under Shear by Dielectric Spectroscopy. KGK 2006; 59(12): p. 648-652.

20. G.A. Schwartz, S. Cerveny, A.J. Marzocca, et al. Thermal Ageing of Carbon Black Filled Rubber Compounds. I. Experimental Evidence for Bridging Flocculation. Polymer 2003; 44(23): p. 7229-7240.

21. J. Kadlcak, L.B. Tunnicliffe, J.J.C. Busfield, et al. Evaluation of Carbon Black Flocculation in Natural Rubber Melts. RubberCon 2014, Manchester 2014; p. 1-9. ISBN 1-86125-176-9.

22. J. Kadlcak, J. Lacayo, R. Cermak, et al. The Influence of Mixing on the Flocculation Time of Carbon Black Aggregates in Rubber Compounds. Plastko Conference 2012. Tomas Bata University in Zlín 2012; p. 294-295. ISBN 978-80-7454-137-7.

23. J. Kadlcak, L.B. Tunnicliffe, J.J.C. Busfield, et al. Evaluation of Carbon Black Flocculation in Rubber Melts. Plastko Conference 2014, Tomas Bat University in Zlín 2014; p. 428-438. ISBN 978-80-7454-335-7.

CHAPTER V. EVALUATION OF CARBON BLACK BEHAVIOUR IN RUBBER COMPOUNDS

1. RUBBER REINFORCEMENT BY CARBON BLACK – A NOVEL METHOD FOR STUDY OF STRAIN-SOFTENING BEHAVIOUR OF RUBBERS FILLED WITH VARIOUS CARBON BLACKS

In this section, the strain-softening process in rubber compounds filled with carbon black is the subject of investigation. First people to observe this process were Fletcher and Gent in 1954. Later, Payne did extensive investigation thus the test is generally known as Payne effect test. Based on the test results, so-called Payne softening can be calculated. The Payne softening is broadly considered as the measure of the strain-softening. In order to obtain strain-softening properties of a rubber compound usually up to twelve strain amplitudes are imposed during a Payne effect test. In this work, a rapid version of the test containing only two strain amplitudes is introduced and subsequently verified. It was proven that the measure of carbon black filler network disintegration by the application only the large deformation is the same for the rapid test as for the standard one. Moreover, the total test time is within thirty percent of the original test and result reliability is proved. The new method is exemplified for a study of three different rubbers filled with various carbon blacks.

THEORETICAL BACKGROUND OF CHAPTER V-1

Dynamic-mechanical properties of rubbers are crucial for most rubber industry applications. Rubbers are usually filled with high loadings of fillers; i.e. carbon black or silica. Incorporation of active fillers into a rubber compound significantly influences the dynamic-mechanical properties of the rubber compound such as strength and stiffness in general applications and rolling resistance, dry, wet and snow traction, tread wear and other mechanical properties in tire applications especially. The reinforcement effect of used fillers is considered to be the main reason for obtaining the required functional

properties of the particular compound [1]. The reinforcement phenomenon of carbon black has been studied by numerous researchers and many reviews were elaborated, e.g. by Kraus [2], Leblanc [3, 4] and Donnet and Custodero [5]. Principal physical mechanisms contributing to this phenomenon are assigned as follows: van der Waals forces among carbon black particles, van der Waals forces between carbon black particles and a polymer; chemical crosslinks or the chemisorption of a polymer chain on the fillers' surface; the mechanical interlocking of a polymer chain on to the filler surface [1–7].

The monitoring of the evolution of dynamic modulus over a certain range of strain amplitudes is of major importance for most rubber applications, such as the tire tread [5]. Under increasing strain amplitude, the dynamic properties of unfilled rubbers display only a little change while the dynamic modulus of filled rubbers decreases substantially. Since the changes of modulus of unfilled rubbers are very small, the effect has been fully attributed to the filler related interactions. The non-linearity in behaviour at small strains is assigned to the gradual breakdown of inter-aggregate adhesion, i.e. filler network disintegration and this is generally known as the Payne effect [8, 9].The strain-softening behaviour at medium to large deformations under quasi-static loading conditions is termed the Mullins effect and is attributed to the detachment of rubber macromolecules from the surface of filler particles [10]. Houwink [11] and later Dannenberg [5, 12] explained that the detachment is caused by the slippage of rubber molecules over the filler surface. Regardless to the magnitude of applied strain amplitude, Wang et al. [9] stated that the Payne effect can serve as a measure of filler networking which originates from filler-filler as well as filler-polymer interactions. Generally, the Payne effect test is based on the monitoring of dynamic moduli during increasing strain amplitude applied to the rubber sample. There is not one exclusively correct standard version of the test and the magnitude of applied strain amplitudes and frequency is not strictly defined; they are rather empirical and arbitrary. The basic concept is to design test simulating the conditions within a mixing chamber, i.e. by the right combination of the magnitude of strain amplitudes and frequency to meet the shear rate of mixing process at which carbon black agglomerates deagglomerate thus ensuring both the breakage of filler-filler and filler-polymer interactions. In his work Payne [8] applied strain amplitudes from very low 0.001 to 10 % at the frequency 0.1 Hz to rubber compounds, on the other hand Böhm and Nguyen [13] used amplitudes from 0.2 to 14 % at frequency 1 Hz and Wang et al. [9] worked with strain amplitudes from 0.1 up to 100 % and frequency 10 Hz.

Understanding of such a complex phenomenon as well as development and improvement of suitable test methods remain an open challenge for research. Here we present a rapid (shortened) version of the Payne effect test of our own design exemplified on the study of a set of model carbon black filled rubber compounds. This investigation was performed in order to prove or disapprove the interchangeability of commonly accepted current test methods and our originally developed shortened version and if possible to introduce the rapid test method to the scientific community and demonstrate a viable substitute to the more time demanding old version of the Payne effect test. Moreover, the influence of the carbon black grade and rubber matrix choice on the properties of resulting compounds is investigated.

METHODOLOGY OF CHAPTER V-1

MATERIALS

Carbon black

Six different carbon black grades (Orion Engineered Carbons GmbH, Germany) were used. General characteristics of specific surface area (SSA), i.e. iodine number, statistical thickness surface area (STSA) and nitrogen adsorption (NSA) as well as the oil absorption techniques describing the complexity of structure are presented in Table V-1.

Table V-1. Properties of incorporated carbon blacks as given by the provider.

Carbon black type	**Iodine adsorption [mg/g]**	**STSA [m^2/g]**	**NSA [m^2/g]**	**OAN [cm^3/100 g]**	**COAN [cm^3/100 g]**	**VV[a] [cm^3/100 g]**
N121	121	114	122	132	111	62.8
N220	121	106	114	114	98	55.3
N326	82	77	78	72	68	40.2
N339	90	88	91	120	99	55.7
N550	43	39	40	121	85	49.3
N660	36	34.8	35	91.4	74	43

[a]VV – void volume parameter characterising carbon black structure complexity measured at mechanical compression speed 2 MPa.s^{-1} and read at 75 MPa.

Rubbers

Three various polymer matrices, i.e. natural rubber (NR), styrene-butadiene rubber (SBR) and ethylene propylene diene rubber (EPDM) were used. Their chemical formulas are shown in Figure V-1.

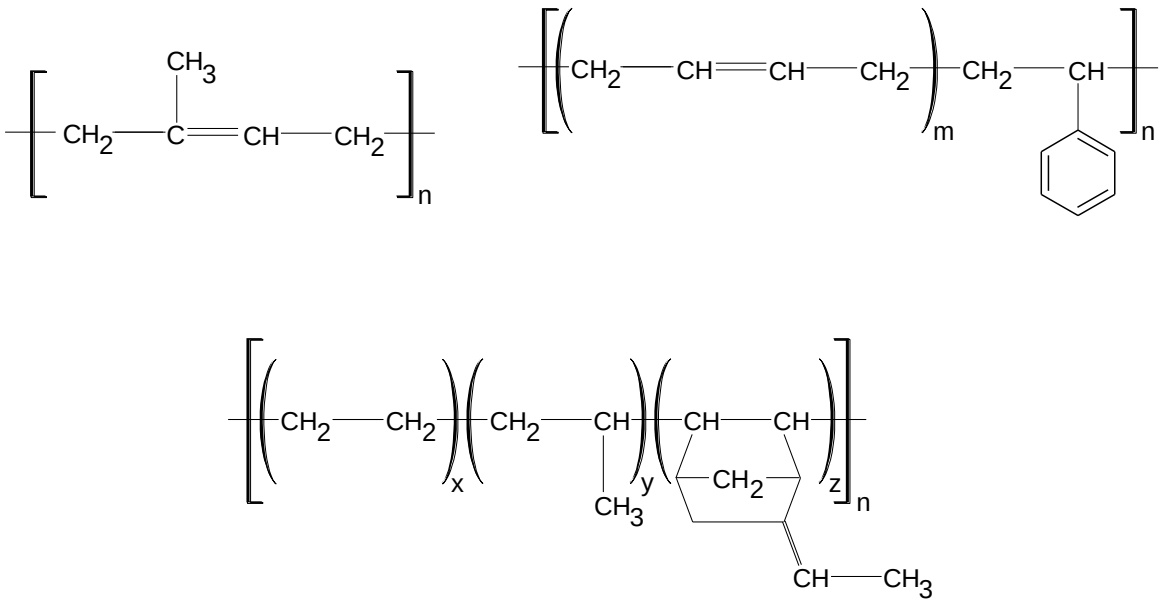

Figure V-1. Chemical formulas of rubbers. From upper left, clockwise: NR, SBR and EPDM.

For the characterisation of neat polymers a gel permeation chromatography (PL-GPC 220, Agilent Technologies) was used. Tests were carried at temperature 160°C and trichlorbenzene was used as the solution. Observed data are listed in Table V-2.

Table V-2. Molar mass ditribution characteristics of used rubbers.

Matrix	**M_n**	**M_w**	**M_z**	**M_{z+1}**	**M_p**	**Polydispersity**
NR	132000	329000	2210000	12348000	295000	2.5
EPDM	144000	777000	2859000	11964000	413000	5.7
SBR	70000	532000	2581000	5529000	141000	7.6

RUBBER COMPOUNDS

In the experiment 21 varied compounds were mixed. Composition and mixing of these compounds were carried out according to the international standard ASTM D3192. Compounds do not contain a complete vulcanising system but there is the addition of anti-ageing agents as shown in Table V-3. Standardised mixing process was executed using the Laboratory mixer (Everplast Machinery, Taiwan).

Table V-3. Compounds were mixed according to ASTM D3192 recipe.

Ingredients	**Rubber compound [phr]**
Matrix (NR or EPDM or SBR)	100
Carbon black (N121, N220, N326, N339, N550, N660)	50*
6PPD**	1.5
Ozone wax	2.5
Stearic acid	3
ZnO	5

*No addition of carbon black was used in the case of a neat matrix sample compounding.
**6PPD denotes N-(1,3-dimethylbutyl)-N´-phenyl-1,4-Benzenediamine, available under the trade name Kumanox 13.

Overall, 18 filled rubber compounds and 3 neat matrices composed from rubber and chemicals without the addition of carbon black were prepared.

SAMPLE CHARACTERISATION

Firstly, the dynamic viscosity of three neat matrices containing no carbon black was measured. In the second phase of the experiment, the Standard Payne Softening Test (SPST) and the shortened Rapid Payne Softening Test (RPST) were carried out on prepared uncured compounds. All rheological tests were done in triplicate. For the characterisation of prepared compounds the rotorless shear rheometer RPA 2000 (Alpha Technologies) was used and all tests were carried out at a constant temperature of 70 °C.

Dynamic viscosity

Using the Cox-Merz rule (Equation 25), which describes the relation between the apparent viscosity $\eta_{app}(\dot{\gamma})$measured via capillary rheometer and the complex dynamic viscosity η*(ω) measured using an oscillatory rheometer, it was established that the real dynamic viscosity η' corresponds to the corrected viscosity measured using the capillary rheometer. Hence, the real part of the dynamic viscosity η' was used for the characterisation of tested matrices. Samples of matrices were exposed to the frequency sweep from 33.000 to 0.005 Hz at the strain amplitude 7 % selected from the area of linear elasticity [14].

$$\eta_{app}(\dot{\gamma}) = \eta^*(\omega) \tag{25}$$

Shear thinning is used for the characterisation of non-Newtonian fluids such as rubber compounds. It is described as the decrease in viscosity with increasing shear rate of the sinusoidal strain when the rapidity of the decrease is also important [14].

Standard Payne Softening Test

The Standard Payne Softening Test (SPST), considered here is based on the pattern of the Payne effect test as described in 1962 [8]. This test is composed of a sequence of twelve strain amplitudes in the range from 1 to 140 %. The test lasts 4.5 minutes and the strain frequency is 1.667 Hz.

The dependence of complex dynamic moduli on dynamic shear strain observed for NR based compounds is illustrated in Figure V-2 as an example. This viscoelastic behaviour of filled rubber compounds is widely known and published. To name the most significant contributions, work of Houwink [11], Payne [8], Mullins [10], Kraus [2], Dannenberg [7], Wang [9], Donnet [5] and Leblanc [3, 4] should be mentioned.

The Payne softening (*PS*) is calculated as the subtraction of the modulus measured at the highest strain from the initial modulus observed at the small strain amplitude ($PS = G^*_{1\%} - G^*_{140\%}$).

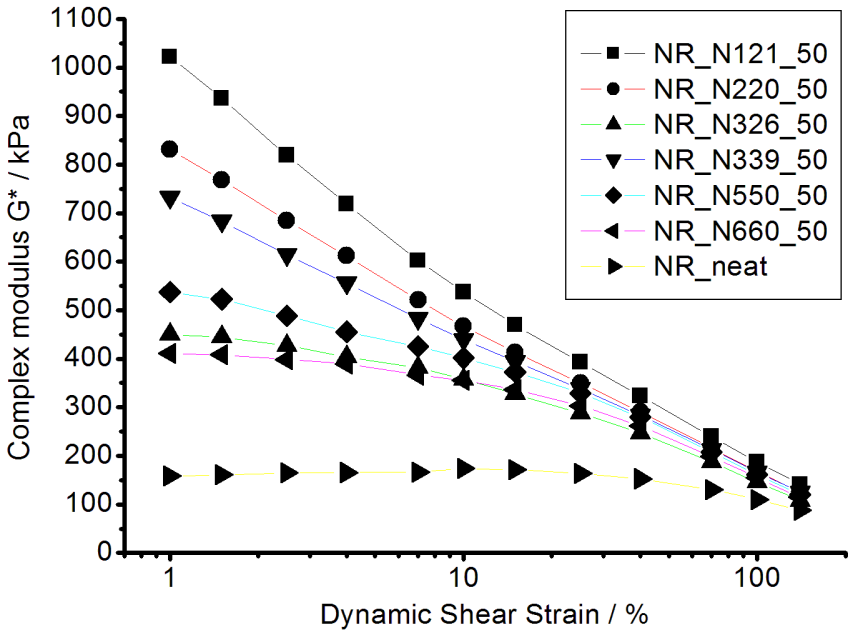

FigureV-2. Evolution of the complex modulus of NR compounds with increasing dynamic shear strain for the Standard Payne Softening Test.

Rapid Payne Softening Test

Comparing with the SPST, the shortened Rapid Payne Softening Test (RPST) is defined by two strain amplitudes only. At the start of the test, the modulus is measured at 1% strain amplitude and then at 140% strain amplitude immediately. This test lasts 1.5 minutes. The calculation of the Payne softening follows the same procedure as described in the above section related to SPST.

REPEATABILITY AND TWO METHODS AGREEMENT ASSESSMENT METHODOLOGY

Initially, the average (x_i) and it's standard deviation (SD_i) were calculated for each sample of *i*-th compound, obtained by the two Payne softening test versions in order to present a general overview of experimental data in Figure V-4:

$$x_i = \frac{\sum_{j=1}^{k} x_{ij}}{k} \tag{26}$$

$$SD_i = \sqrt{\frac{\sum_{j=1}^{k}\left(x_{ij} - x_i\right)^2}{k-1}} \tag{27}$$

Where j indexes specimens within the triplicate measurement and k is the number of specimens measured for each compound (i.e. $k = 3$).

During the experiment, repeatability of measurements of the Payne softening of carbon black containing compounds was evaluated for both standard and rapid (shortened) testing methods. Next, the two methods were compared and tested for agreement. Both investigations were performed according to Bland-Altman's statistical method [15, 16]. The repeatability of any Payne softening test method is influenced considerably by the rubber compounds' dispersion inhomogeneity in filler due to an imperfect mixing process. The variability between specimens taken from one compound is of significance in rubber research and industry, therefore the estimation of a mean value and its standard deviation obtained from triplicate measurements is usually practiced [14].

According to [15-17], the coefficient of repeatability (*CR*) expresses the 95 % probability limits for two subsequent readings by the same method to be within ±*CR* interval. The narrower the interval the better the repeatability and hence the value of *CR* can be used for a quantitative comparison between different methods used for measurements of the same quantity. The following equation defines the *CR* with the use of one-way analysis assuming the normal distribution of the differences between replicates:

$$CR = t \cdot \sqrt{2} \cdot sw \tag{28}$$

Where t is the value of the *t*-criterion for the sample size n (in our case 21 compounds), *sw* is the within subject standard deviation calculated as the square root from within sample variance (sw^2):

$$sw^2 = \frac{\sum_{i=1}^{n}\sum_{j=1}^{k}\left(x_{ij} - x_i\right)^2}{DoF \cdot n} \tag{29}$$

Where *DoF* is the degree of freedom within the sample, i.e. *DoF* = *k*– 1, where *k* is the number of replicates (in our case of triplicates k = 3), x_{ij} is the Payne softening value measured for *j*-th specimen of *i*-th sample and x_i is the average Payne softening value calculated for each data triplet obtained for *i*-th compound.

The agreement between the two methods can be assessed by the use of the Agreement limit (*AL*) which is based on the differences between the values obtained by measurements of the same set of samples by both methods. The mean difference is the measure of the consistent tendency for one method to exceed the other, which is called bias. The variation about this mean is estimated by the standard deviation (*SD*) of the differences. Both the bias and the variability are assumed to be uniform throughout the measurement which is checked graphically in the respective figures. If the differences are normally distributed, 95 % are expected to be found within an interval above and below the mean called ±*AL* which is actually the definition of the *AL* [15-17]. Following equation defines the *AL* with the use of *SD*:

$$AL = t \cdot SD \tag{30}$$

Where the *t* is the value of the *t*-criterion for the sample size *n* (in our case 21 compounds), *SD* is the standard deviation of the differences between average SPST and average RPST obtained for each sample, calculated as:

$$SD = \sqrt{\frac{\sum_{i=1}^{n}\left(x_{i\,SPST} - x_{i\,RPST}\right)^2}{n-1}} \tag{31}$$

Where the variables have the same meaning as in the equations above, just indexed with SPST or RPST to point towards the used version of the Payne softening test.

It was mentioned above that the repeatability coefficient and the agreement limit approaches to the treatment of the differences both assume the normal distribution of the foresaid differences. If a relationship is manifest between the difference and magnitude of the measured variable, logarithmic transformation of the data is extremely useful as it can be simply performed prior to data analysis and the obtained *CR*s and *ALs* can be back-transformed and interpreted in direct relation to the original data [15-17]. The repeatability coefficients and limits of agreement obtained from log transformed data as intervals ±*CR log* or ±*AL log* give backward limits for the ratio of the actual values as the coefficients multiplying the actual value – antilog of *CR log* or *AL log* which is higher than 1 for the upper limit and reciprocal value of the antilog of *CR log* or *AL log* which is lower than 1 for the lower limit because the antilog of addition and subtractions results into multiplication or division respectively.

The Spearman's rank correlation coefficient (ρ) was used for evaluation of the statistical dependence of the data. As the independent quantity, any of the physical characteristic of carbon blacks in Table V-1 was chosen (c_i) and the related quantity was the value of PS (x_i). The ρ value was calculated six times for each characteristic, i.e. three sets of samples according to the used type of matrix using values obtained by SPST and RPST. Seven pairs of each of raw scores c_i , x_i were converted to ranks C_i and X_i and the Spearman's ρ was calculated according to:

$$\rho = \frac{\sum_i (C_i - \bar{C}_i)(X_i - \bar{X}_i)}{\sqrt{\sum_i (C_i - \bar{C}_i)^2 \sum_i (X_i - \bar{X}_i)^2}} \qquad (32)$$

Where *i* ranges from 1 to 7, 8 to 14 or 15 to 21 for the respective type of matrix, and $\bar{C}_i$ and $\bar{X}_i$ are average rank values. To assess the significance of the test, the *P*-values were estimated. Due to small number of observations the *P*-values were taken from critical tables [18].

DYNAMIC VISCOSITY OF NEAT MATRICES

The results of dynamic viscosity measurements of the used rubber matrices are presented in Figure V-3.

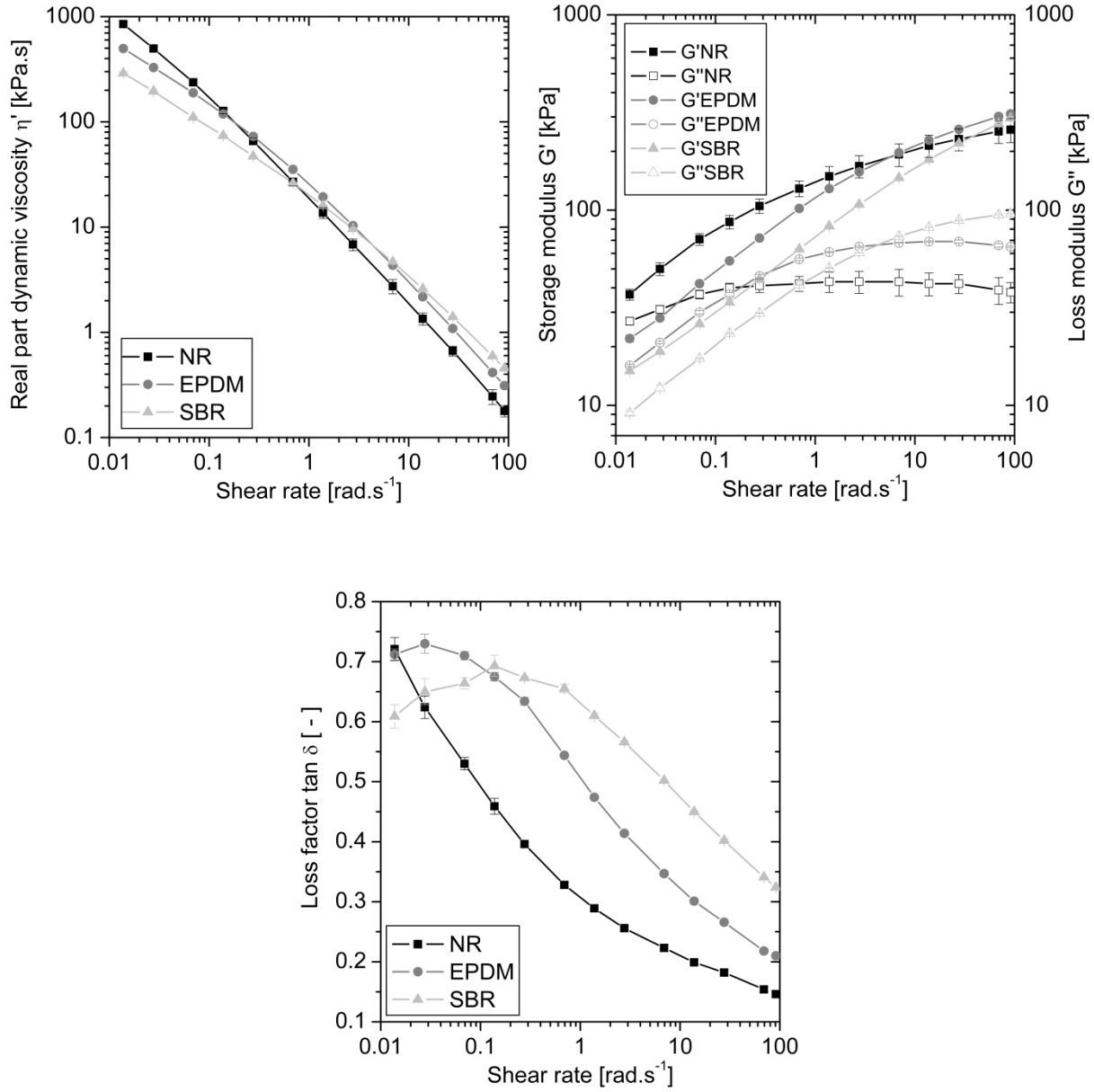

Figure V-3. Viscosity characteristics. Arranged clockwise from the upper left: A) Real part of the dynamic viscosity plotted against the shear rate, B) The dependence of the two parts of dynamic complex modulus on the shear rate, C) Loss factor tan δ plotted against the shear rate.

Figure V-3A shows a log-log plot of the real part dynamic viscosity against shear rate (frequency in radians per second). The most pronounced shear thinning was observed for NR matrix, where the viscosity drop with increasing strain rate is the most rapid among tested matrices. To the contrary, the SBR matrix showed only a gradual decrease of the modulus. This suggests greater macromolecular entanglement of the SBR matrix, since the disturbation of molecular structure occurs at the highest strain rate. The SBR matrix proved the highest viscosity in the mixing area which is generally defined in the range between 10 and 100 rad.s^{-1} (e.g. at the shear rate 27.7 rad-s^{-1} following viscosities were observed: NR = 666 Pa.s^{-1}, EPDM = 1090 Pa.s^{-1}, SBR = 1404 Pa.s^{-1}). The shear forces in the mixer generated due to the highest viscosity of the SBR matrix are supposed to ensure the highest levels of carbon black macro- and microdispersion (deagglomeration and distribution). Besides the highest viscosity the SBR matrix proves the highest loss dynamic modulus (G'') in the area of mixing which further contributes to the mixing efficiency due to material flow (see Figure V-3B).

The development of the ratio between viscous and elastic parts of the dynamic moduli, generally known as the loss factor (tan δ), is shown in Figure V-3C where tan δ is plotted against shear rate. The significant part of real dynamic modulus of NR and EPDM matrices ensures a deformation of macromolecules under the shear but not necessarily a flow.

Moreover, Beelen [19] described the shape of the tan δ plotted against strain rate may be indicative of the polymer's molecular weight distribution (MWD) and chain branching. Using this approach, the maximum tan δ of NR is out of the scale and its shape proves the linear character of macromolecules with a narrow MWD. On the contrary, SBR and EPDM show reduced strain dependence at low strain rates. The maximum tan δ for EPDM was observed at shear rate 0.03 rad.s^{-1} while the maximum tan δ for SBR was observed at shear rate even higher, i.e. 0.2 rad.s^{-1}. In comparison to the NR a more branched macromolecular structure and wider MWD are suggested for these two matrices. For the SBR matrix, the effect of branching and MWD is even more significant which is supported by the GPC analysis summarised in Table V-2. SBR has the highest polydispersity coefficient which fully corresponds to the conclusion based on the tan δ characteristic. The same trend persists for EPDM and NR, showing moderate and lowest polydispersity coefficients respectively.

Figure V-4 presents a general overview of the results obtained for all the samples to compare the two methods for assessing the Payne softening. The average results of the RPST for each compound ($x_{i\,RPST}$) were plotted against average results of the SPST ($x_{i\,SPST}$). The error bars show standard deviation of each data triplet (SD_i) in x and y axes directions for SPST and RPST method respectively. The graph also shows the line of equality with the slope 1 and there is no apparent bias between the data sets obtained by the two different methods. Next, an increase in variability of differences between actual sample values and their triplet average obtained by either of the two methods can be seen as the magnitude of softening increases. This suggests the type of measurement with constant relative error rather than a measurement with constant error indicating dependence between the differences and magnitude invoking a more sophisticated analysis of repeatability. All these preliminary assessments were studied in more detail and simultaneous estimation of repeatability and agreement was performed by analysis of collected replicated data.

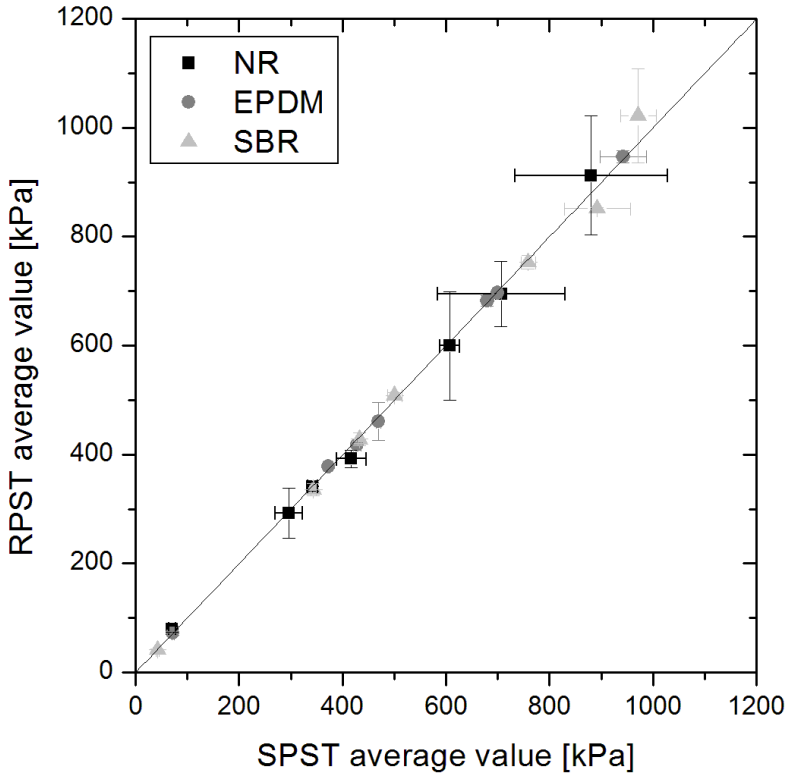

Figure V-4. Payne softening measured on RPA by SPST and RPST methods with the line of equality.

Repeatability of both methods

The repeatability of each of the two experimental methods can be analysed with the aid of the graphs in Figure V-4, where the differences of replicates' values from mean values are plotted against the average values for SPST (Figure V-5A) and in Figure V-5B for RPST respectively. The mean difference between replicates is zero and is plotted by a full line for better clarity. The differences are shown as full circles and it can clearly be seen that in both cases the scatter of the differences increases as the average value of the Payne softening increases. Therefore, a logarithmic transformation of both measurements was performed before further analysis.

The difference versus mean plots for log transformed data are shown in Figure V-6 again as full circles for SPST (Figure V-6A) and in Figure V-6B for RPST respectively. Two log transformed readings by the same method will be within the interval between lines ±CR log with 95 % probability. The within subject standard deviations (sw_{log}) are 0.0297 and 0.0296 for SPST and RPST respectively. It can be seen that the transformation was successful in producing data differences unrelated to the average. Back-transformed limits for the ratio of the actual measurement were obtained as antilog of CR for the upper limit and (antilog of CR)$^{-1}$ for the lower limit and they are plotted by dash and dot lines respectively in both graphs in Figure V-5. A perfect agreement of the back transformed limits with scattered data resembling an open fan in shape is obvious. One has to keep in mind different scales for y and x axes during intuitive interpretation of the graphs. Repeatability of the two methods can be compared by the use of obtained antilog CRs and the values of 1.225 and 0.816 for SPST and 1.224 and 0.817 for RPST can be considered as identical. One source of the fully comparable repeatability in this case is that both methods employ the same apparatus and, indeed, there is no reason for manifestation of any difference resulting from the used machine. The second and more important source of the observed perfect match of repeatability is that the shortened test version is physically relevant as the standard version and that it is still sufficient from the point of the collected data quality although it is three times faster than the standard one (both at the frequency 1.667 Hz).

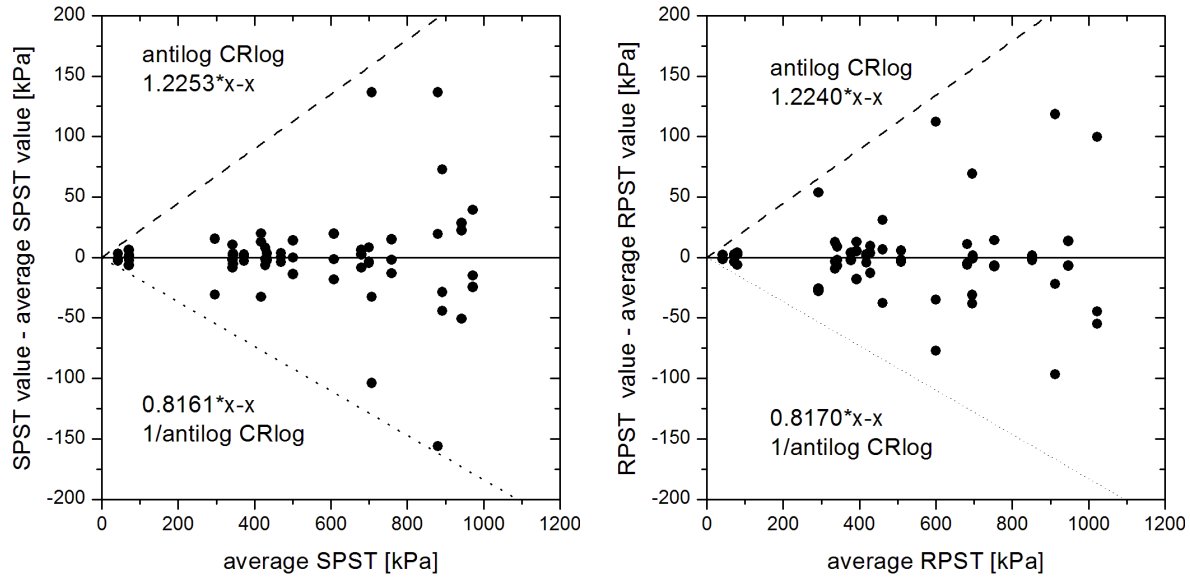

Figure V-5. The repeatability of the two experimental methods; in the left hand side is the repeatability of SPST and on the right the repeatability of RPST.

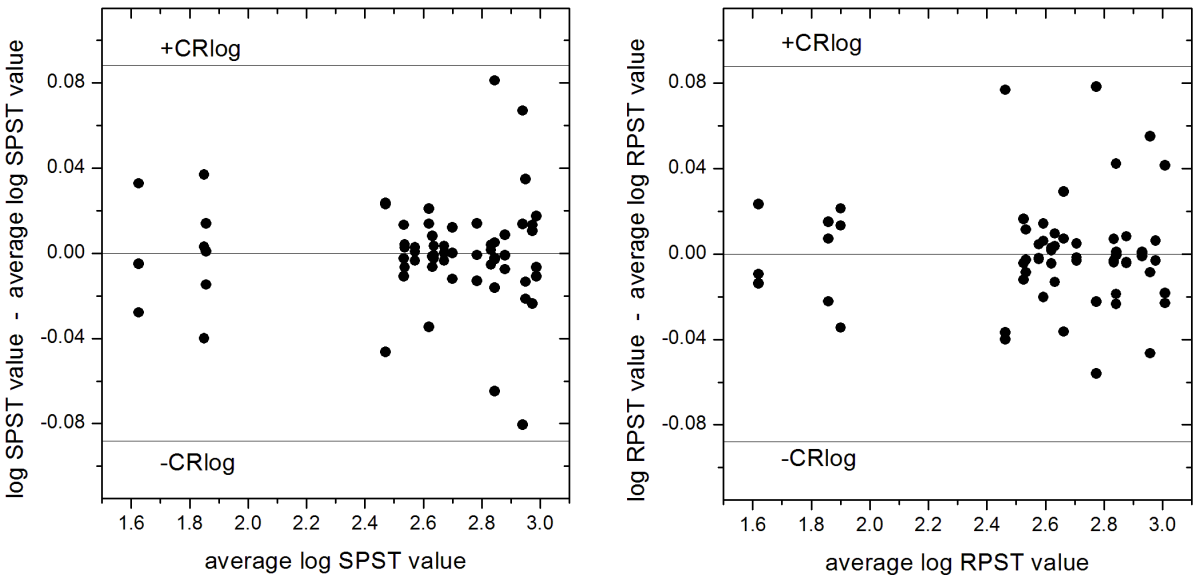

Figure V-6. The difference versus mean plots for log transformed data of both methods bounded by the lines of coefficient of repeatability; SPST on the left and RPST on the right side.

Two methods agreement analysis

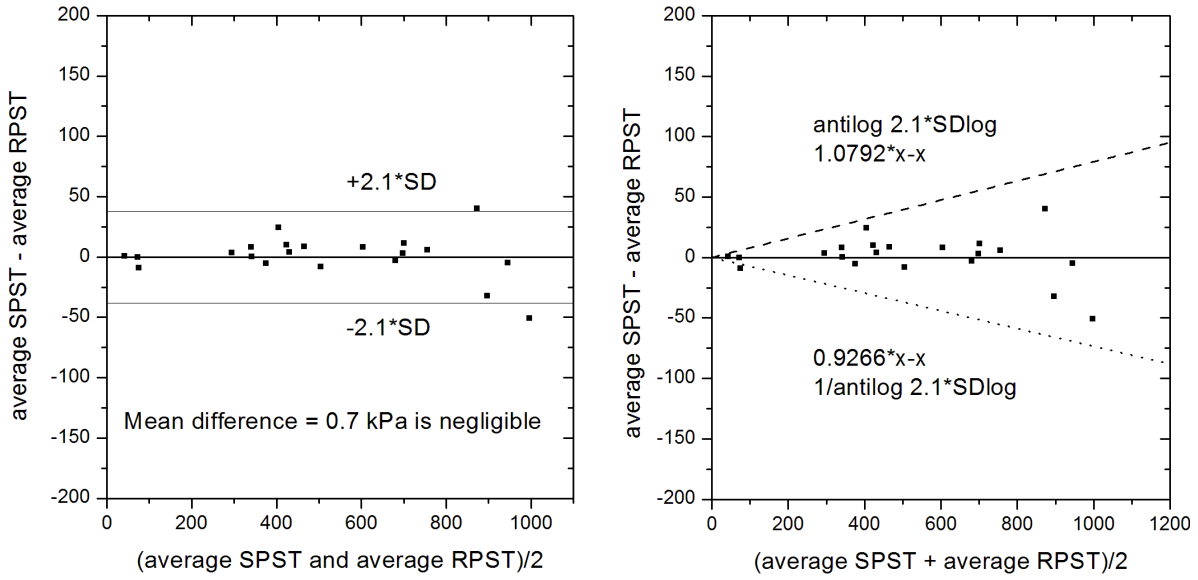

Figure V-7. The Bland-Altman plot showing differences between the two methods of ±38 kPa.

The repeatability investigated in the above section dealt with two single readings by each method. To suppress the variability of the results for each subject, an average of the replicate measurements was calculated. Three measurements on samples from each tested compound were introduced already by Payne in his pioneering version of the softening effect test. The same number of replicas was also used in our rapid version. Averaging removes some of the measurement errors and improves the precision of obtained results. We assume that although single measurements can be performed, the customary use of average of the three measurements together with the identical repeatability of the two methods justifies their comparing on the base of average results obtained on triplicates only. Figure V-7A shows the Bland-Altman plot with 95 % limits of agreement based on the assumption that the differences are normally distributed. The *t* value is 2.1 for sample size of 21 compounds and the standard deviation is 19 kPa, therefore the width of the interval is $\pm AL$ = 2.1*19, i.e. 38. The mean of differences 0.7 kPa is negligible with respect to the width of the interval and no bias between the data obtained by the two methods is manifested. There is no tendency of the differences to one or other direction in dependence on the mean value of the average SPST and average RPST. Therefore, the agreement between the two methods can be considered as very

good if the triplicate measurement is used and the average value is calculated in both tests for each examined compound.

Although the differences looked uniform at the first sight, a slight increase in their scatter with increased measured value can be observed. This becomes more visible after plotting the agreement limit bands in Figure V-7B. It seems that averaging cannot fully suppress the deterioration of repeatability with increasing value of softening. Therefore, the data were log transformed and back transformed similarly as in the repeatability study. The log transformation safely removed the slight relationship between the variability of the differences and the average value of the Payne softening measured by the two methods. Quite narrow relative limits 1.079 and 0.927 were obtained as antilog of 2.1**SD* for the upper limit and (antilog of 2.1**SD*)$^{-1}$ for the lower limit after back transformation and they are plotted by dash and dot lines respectively in the graph in Figure 6B. This method seems to be more appropriate to the observed increasing variability of results with an increase in the measured value for each test method which is obviously manifested in their comparison. With regard to this, agreement of the two methods can be assessed as excellent and the 95 % limit of agreement is more reliable even for small measured values of Payne softening where the former approach overestimates largely the uncertainty. It can be seen, that the agreement of the two methods is excellent as the measurements by the two methods agreed very closely on average with negligible bias. Another advantage of this data treatment as opposed to the one using raw data without transformation is that it produces data which can be compared to the *CRs* obtained in the repeatability study where the transformation was perceived as more urgent. The width of the *AL* suggests how good the agreement between the methods for individuals is. The *AL* can be compared with *CRs*. It is more than 2.5 narrower limits than the repeatability for two single readings by each of the methods which is due to their reinforcing by triplication and because of presence of no other factor lowering the agreement between methods.

To summarise, both methods can be used for Payne softening investigation giving statistically the same results in terms of both, the value and its variability (standard deviation). Furthermore, both methods are fully comparable, have the same level of precision and they can be used interchangeably.

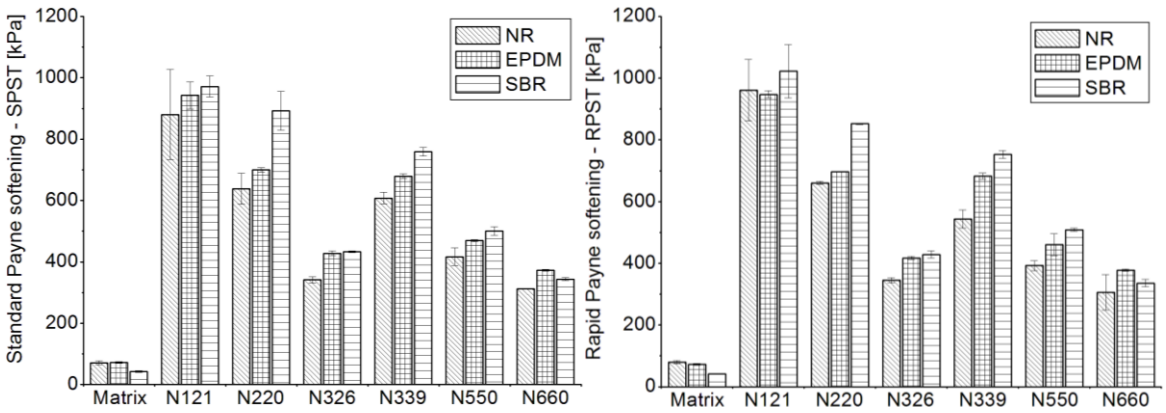

Figure V-8. Payne softening characteristics observed by the two experimental methods; SPST on the left and RPST on the right side.

Based on the previous section, the discussion of observed PS phenomena with respect to the carbon black grades and used matrix type persists for the results obtained by both methods without any loss of relevance. Considering the fact that results are measured using twelve strain amplitudes in the case of the standard test and using one large amplitude in the rapid test, these results are rather surprising and show on the fragility of the filler network which carbon black forms in rubber melts. Graphical representation of PS values obtained for all uncured compounds by the SPST and RPST are shown in Figure V-8A and V-8B respectively. Even here, the interchangeability of the two test methods can be followed. In case of neat rubber matrices, the measure of rubber mastication is shown rather than the softening.

The influence of the two key parameters on the PS can be evaluated in the framework of the experiment, i.e. influences of a rubber macromolecular structure and carbon black grades respectively. Referring to the appearance of the bar graphs in Figure V-8, there are two effects differing in magnitude and significance. First, the PS value strongly depends on the used carbon black. The differences between compounds with the same matrix and different fillers are much larger than standard deviations of the compared values. Next, there is an observable, relatively weak and less clear but still pronounced dependence of the PS value on the nature of the polymer matrix. The PS value increases with the change of the matrix from NR through EPDM to SBR for fillers N220, N339

and N550, while such effect is unconvincing for N121 as it is buried in the scatter of measured values. On the other hand, neat matrix compounds have nearly opposite behaviour. The materials with N326 and N660 might show possibly transient behaviour between these two trends. It is evident, that the matrix does not contribute linearly to the observed effect. Therefore, the multiple regression analysis is not suitable for the analysis, or if used, it would show very high error for the parameter bound with the matrix properties. However, the low number of used matrices and large standard deviations limit the possibility of evaluation of these effects by any other quantitative method.

Considering the strong influence of carbon black grade, the highest PS was observed for compounds containing N121 grade. N121 has the highest structure as presented by oil absorption techniques and the highest SSA also. Observed values of PS were tested with the use of the Spearman's rank correlation coefficient and the correlation between characteristics of carbon black types is indicated in Table V-1. The use of this relatively robust and non-parametric test is based on the assumption, that the PS value measured for each compound depends monotonously on the properties of the used carbon black filler but the dependence function is not known (most likely non-linear). The level of correlation between different parameters and the PS value can be compared simply by comparison of the coefficient's value. The relationship is better as its value approaches unity. The test was always performed for all compounds and strong correlation of the PS to all carbon black type characteristics was found but there was no difference between the three matrices observed. Furthermore no difference between results obtained from SPST or RPST was obtained. The physical characteristics can be divided into three groups ranked according to the ρ value. All three SSA characteristics employed as independent variables gave the same ρ value about 0.96 with P-value in the range of $0.01>P>0.001$ indicating almost perfect correlation. The next characteristic was COAN with $\rho=$ 0.93 and P-value in the range of $0.01>P>0.001$, which is almost as good as the SSA. The worst score was found for OAN with ρ = 0.82 with P-value in the range of $0.025>P>0.01$.

The excellent correlation of PS with SSA characteristics of carbon blacks can be explained as the manifestation of the microphysical reinforcing effect related to the specific surface size well known for nanocomposites. The larger the surface area available for polymer-filler interaction, the greater the reinforcement effect. This fact was proved for example in the work of Wang [9] where the increasing amount of a specific carbon black grade resulted in the

enhanced reinforcement effect of a rubber compound. Kraus [2] carried out experiments on bound rubber, investigating interactions between filler and polymer and came to similar conclusions. Detailed discussion of reinforcement by carbon black can be found in the references [4, 5 and 20]. The accessibility of the carbon black surface to polymer matrix macromolecules is dependent on the carbon black deagglomeration achieved during mixing which is theoretically best characterised by COAN. This parameter, by the ASTM D3493-13 definition, describes carbon black structure obtained after the compression at 24000 psi four times (24M4) simulating the deagglomeration during mixing. On the other hand, OAN characteristic which describes carbon black structure before (without) mixing, shows lower correlation with the in-rubber property.

The shape of tan δ curves revealed that the polymer matrices differ in their molecular weight distribution and branching. GPC supported this fact by results of the polydispersity parameter. The highest level of polydispersity was found for SBR = 7.6 and the lowest for NR = 2.5 while the moderate value belongs to EPDM = 5.7. The molar mass distribution as the leading microphysical parameter (Mn, Mw, etc. and polydispersity) correlates well with results of the dynamic viscosity test. The higher the polymer viscosity, the more power is required to mix the compound and higher shear forces are generated during mixing process. For neat matrices it is obvious that the largest PS is observed for the material with the lowest viscosity, ceteris paribus. Payne effect was measured at the frequency 1.667 Hz which corresponds to the shear rate of approximately 4.5 $rad.s^{-1}$. In Figure V-3B, the moduli of NR and SBR are both higher in this shear rate area than the modulus of SBR which predominates towards the higher shear rates. From the dependence of tan δ in Figure V-3C, it can be observed that the NR shows the highest storage modulus at the given frequency which ensures the most enhanced Payne softening. Whilst for the SBR showing the lowest storage modulus the smallest Payne softening was observed. The lower the tan δ at a given frequency, the higher the elastic part of the dynamic modulus. Tan δ equal to zero would mean the material is completely elastic [14].

Then, the situation changes in case of filled compounds. Shear forces directly affect the quality of carbon black incorporation into the compound. Gerspacher et al. [21] stated that during the carbon black incorporation, agglomerates are deagglomerated to aggregates by shear forces and the subsequent mixing ensures the distribution of liberated aggregates through the polymer matrix. It also means that the compound with the most viscous matrix should have the best

dispersion and distribution of carbon black s and should show the highest reinforcing effect. This effect can be expected to be stronger for carbon black s with higher structure rather than for those of lower structure. Mutual action of these two material predispositions (high matrix viscosity and high filler structure) results in a complimentary effect. On the other hand, it means that the same compound with the highest reinforcement should be the most sensitive to the strain applied during the PS test as it has the strongest tendency to disrupt any network of the carbon black already developed within the material volume. The incorporation of carbon black in SBR should be the most efficient according to viscosity results and, indeed, the PS was the most pronounced for SBR matched with high-structured carbon black in our material selection. The highest reinforcing effect was measured for the compound constituted by the SBR matrix and N121 carbon black grade filler.

CONCLUSIONS OF CHAPTER V-1

In this work the Rapid Payne Softening Test (RPST) was introduced and successfully established. It was found that this shortened approach can replace the Standard Payne Softening Test (SPST). The rapid test shows the same measure of filler network disintegration calculated by Payne softening (PS) as shows the standard version of the test. Since the same results were observed using only one large strain amplitude instead of twelve strain amplitudes, the time of the rapid test is shortened to thirty percent of the standard test which is another benefit of the test. The interchangeability of the test methods was demonstrated on 21 different uncured rubber compounds. Repeatability of the two methods was tested using triplicate repeats and was found to be identical. Also, there is no bias between the two methods, so they give principally the same values on average and, the agreement limits are quite narrow due to the use of averages obtained from the triplicates. However, the full acceptation of the yet developed RPST by the scientific and professional community will require more extensive studies to confirm its reproducibility and applicability to the large spectrum of possible carbon black-rubber matrix combinations.

Furthermore, based on the results of strain-softening tests, it can be concluded that compounds containing carbon black with high SSA and high structure, so-called hard carbon black, showed high Payne softening. On the contrary, compounds containing soft carbon black (with low SSA, low structure) showed

systematically lower Payne softening. The correlation between SSA or COAN and Payne softening was found to be highly significant. With respect to that, the influence of the rubber matrix seems to be a less significant contribution, however, a synergy between the structure of carbon black and matrix microphysical parameters through their mutual interaction during mixing was demonstrated.

ACKNOWLEDGEMENTS

This section has been written with the financial support of Internal Grant Agency of Tomas Bata University in Zlín (reg. number: IGA/FT/2013/012) funded from the resource of specific university research. This work has been carried out with the support of Operational Program Research and Development for Innovations co-funded by the European Regional Development Fund (ERDF) and the national budget of Czech Republic, within the project 'Centre of Polymer Systems' (reg. number: CZ.1.05/2.1.00/03.0111) and the project 'Advanced Theoretical and Experimental Studies of Polymer Systems' (reg. number: CZ.1.07/2.3.00/20.0104). Authors are grateful to companies Continental Barum, Otrokovice and Trelleborg, Skalná for the material support.

REFERENCES

1. J. Fröhlich, W. Niedermeier, H.D. Luginsland. The Effect of Filler-Filler and Filler-Elastomer Interactions on Rubber Reinforcement. Composites Part A 2005; 36(4): p. 449–460.
2. G. Kraus. Reinforcement of Elastomers by Carbon Black. Rubber Chemistry and Technology 1978; 51(2): p. 297–321.
3. J.L. Leblanc. Rubber-Filler Interactions and Rheological Properties in Filled Compounds. Prog Polym Sci 2002; 27(4): p. 627–687.
4. J.L. Leblanc. Filled Polymer – Science and Industrial Application. CRC Press 2010; 3–4: p. 15–184. ISBN: 978-1-4398-0042-3.
5. J. B. Donnet, E. Custodero. Reinforcement of Elastomers by Particulate Fillers. J.E. Mark, B. Erman, F.R. Eirich. Science and Technology of Rubber. Elsevier Academic Press 2005; 8: p. 367–400. ISBN: 0-12-464786-3.
6. J.J. Brennan, T.E. Jermyn. Correlation of vulcanizate properties with polymer and black interaction. J Appl Polym Sci 1965; 9(8): p. 2749–2762.
7. E.M. Dannenberg. Bound Rubber and Carbon Black Reinforcement. RubbChemTechnol1986; 59(3): p. 512–524.
8. A.R. Payne. The Dynamic Properties of Carbon Black-Loaded Natural Rubber Vulcanizates. Part I. J Appl Polym Sci 1962; 6(19): p. 57–63.
9. M.J. Wang. Effect of Polymer-Filler and Filler-Filler Interactions on Dynamic Properties of Filled Vulcanizates. Rubb Chem Technol 1998, 71(3): p. 520–589.
10. L. Mullins. Softening of Rubber by Deformation. RubbChemTechnol 1969; 42(1): p. 339–362.
11. R. Houwink. Slipping of Molecules during the Deformation of Reinforced Rubber. Rubb Chem Technol 1956; 29(3): p. 888–893.
12. Ch. Nah, J.Y. Lim, B.H. Cho, et al. Reinforcing Rubber with Carbon Nanotubes. J Appl Polym Sci 2010; 118(3): p. 1574–1581.
13. G.G.A. Böhm, M.N. Nguyen. Flocculation of Carbon Black in Filled Rubber Compounds. I. Flocculation Occurring in Unvulcanized Compounds during Annealing at Elevated Temperatures. J Appl Polym Sci 1995; 55(7): p. 1041–1050.

14. J.S. Dick. Rubber technology: compounding and testing for performance. 2nd ed. Munich: Hanser Publishers 2009; p. 567. ISBN: 978-1-56990-465-7.
15. J.M. Bland, D.G. Altman. Measuring agreement in method comparison studies. Stat Methods Med Res 1999; 8(2): p. 135–160.
16. J.M. Bland, D.G. Altman. Statistical methods for assessing agreement between two methods of clinical measurement. Int J Nurs Stud 2010; 47(8): p. 931–936.
17. B. Carstensen, J. Simpson, L.C. Gurrin. Statistical Models for Assessing Agreement in Method Comparison Studies with Replicate Measurements. Int J Biostat 2008; 4(1): p. 1–26.
18. J.H. McDonald. Handbook of Biological Statistics (2nd ed.). Baltimore, Maryland: Sparky House Publishing 2009; p. 221-223.
19. H.J.H. Beelen. High performance EPDM polymers based on a new technology of controlled long chain branching. Paper at IRC'97, Nurnberg.
20. J.B. Donnet, R.Ch. Bansal, M.J. Wang. Carbon Black - Science and Technology. Marcel Dekker Inc. 1993; 461 p.. ISBN: 0-8247-8975-X.
21. M. Gerspacher, L. Nikiel, H.H. Yang, et al. Flocculation in Carbon Black Filled Rubber Compounds. KGK 2002; 55(11): p. 596–604.

2. CARBON BLACK FLOCCULATION IN RUBBERS

The flocculation process of carbon black in rubber compounds is the subject of investigation in this section. This process arises during post-mixing stages when aggregates tend to recreate the thermodynamic stability agitated after milling. In order to monitor this process, a new approach for the flocculation assessment is introduced here, which is derived from the method of Coran and Donnet published in 1992. This new approach combines Payne effect test and the technique for the flocculation behaviour determination. Therefore, the filler macrodispersion and microdispersion effects in rubber compounds can be evaluated. Effects of carbon black properties, its volume fraction, the properties of matrices and temperature on carbon black behaviour in rubber compound melts and crosslinked samples were investigated using the proposed test.

THEORETICAL BACKGROUND OF CHAPTER V-2

The formation of filler networks in rubber matrices depends on the filler properties, the quality of filler distribution, polymer-filler and notably filler-filler interactions [1]. In the case of carbon black filled rubber matrices, a filler network evolves when carbon black is incorporated into a rubber. During the incorporation, where the intensive mixing takes place, carbon black agglomerates are broken down to aggregates by shear forces in a significant extent. However, certain amount of agglomerates remains unbroken usually. This amount is described as the level of carbon black macrodispersion where the better the macrodispersion the lower the amount of undispersed filler. Subsequent extensive mixing ensures the distribution of aggregates throughout the matrix. The level of aggregates distribution is described as the level of carbon black microdispersion. Gerspacher et al. [2] stated that it is one of the main factors influencing the performance of rubber products. Later on, Lin et al. [3] and Donnet et al. [4] found that the level of filler microdispersion greatly affects rolling resistance, dry, wet and snow traction, tread wear and other mechanical properties of pneumatic tyres.

However, the level of aggregate dispersion at micro scales obtained after the mixing stage deteriorates during the stages of storage, extrusion or vulcanisation. This process, where aggregates microdispersed in a matrix

gradually reagglomerate forming larger macro objects which are connected to each other is known as filler flocculation. This yields in the thermodynamic equilibrium within the matrix [5-7]. Witten and Sander stated that at favourable conditions (temperature and time) carbon black aggregates can form a complex three dimensional percolating cluster. This is often described as a fractal like structure [8, 9].

The filler flocculation is influenced by many factors and mechanisms. These are reported as follows: differences in surface energies between filler and a polymer matrix as described by Wang et al. [10, 11]; the Brownian movement and diffusion process published by Gerspacher [2], Böhm and Nguyen [12] and Allen et al. [13]; or Van der Waals forces and other non–DLVO interactions between carbon black particles [2, 12, 14]. Many researchers have considered flocculation of carbon blacks and other particulate fillers in the polymer melt in terms of Brownian motion and particulate mobility via the particle diffusion coefficient given by the Stokes-Einstein equation (33), where D_0 is the diffusion coefficient, k is the Boltzman constant, T is the temperature, η is the viscosity of the matrix and r is the particle radius [10, 11].

$$D_0 = \frac{kT}{\eta 6\pi r} \tag{33}$$

Many experiments have been performed in this field and different evaluation approaches of the flocculation process are described in several publications [1, 3, 5, 12, 15-22].

The method for carbon black dispersion evaluation used here is based on the method introduced by Coran and Donnet [15]. They established a test for the evaluation of carbon black dispersion quality, which is based on the application of strain amplitude to rubber compounds and the subsequent monitoring of a recovery of the modulus.

It is proposed to consider filler dispersion at different length scales. The Payne effect is often taken as a measure of overall dispersion without distinguishing the differences in the multi scale nature of dispersion (macro and microdispersion). The Payne effect describes the level of filler macrodispersion determined by the quality of carbon black deagglomeration during its

incorporation into a rubber compound. On the other hand, the flocculation test describes the level of carbon black microdispersion which is a measure of the quality of aggregates' distribution in the matrix [20]. Whereas the Payne effect deals with the strain-softening, i.e. modulus lowering, the flocculation is considered as modulus recovery, i.e. stiffening.

Many different definitions of flocculation are employed to describe this process in literature [12-14, 17-22]. According to the generally accepted theory, Schwartz et al. describe flocculation process as a reversible dynamic process during which aggregates dispersed in a matrix reagglomerate forming larger objects called agglomerates connected to each other [22]. These can be deagglomerated again by shear forces during mixing stage [22].

This work in four separated sections (A-D), each composed of methodology, results and discussion and conclusions, examines the effect of filler volume fraction, filler dispersion, particle size, particle morphology and matrix type, on the flocculation behaviour of carbon black in the rubber melts as well as in crosslinked samples and attempts to relate the observed phenomena to the underlying physical mechanisms.

A. THE INFLUENCE OF CARBON BLACK DISPERSION, VOLUME FRACTION AND PROPERTIES ON FILLER FLOCCULATION IN NATURAL RUBBER MELTS

METHODOLOGY OF SECTION A

Sample preparation

In the experiment, five varied carbon black types (Orion Engineered Carbons GmbH, Germany) whose properties are presented in Table V-4 were incorporated in to the natural rubber type SMR 10 (SMR – Standard Malaysian rubber) having the index of polydispersity 2.5, M_n = 132000 and M_w = 329000 as measured using gel permeation chromatography (PL–GPC 220, Agilent Technologies). GPC tests were carried out at 160°C and trichlorobenzene was used as the solution.

Table V-4. Properties of used carbon black grades given by the manufacturer.

Carbon black type	Iodine adsorption [mg/g]	STSA* [m^2/g]	NSA* [m^2/g]	OAN* [cm^3/100 g]	COAN* [cm^3/100 g]
N121	121	114	122	132	111
N220	121	106	114	114	98
N326	82	77	78	72	68
N339	90	88	91	120	99
N550	43	39	40	121	85

*STSA – statistical thickness surface area; NSA – nitrogen surface area (based on the B.E.T. theory); OAN – oil absorption number; COAN – oil absorption number of compressed sample.

All compounds were mixed according to the international standard ASTM D3192 with the addition of anti-ageing agents as shown in recipe in Table V-5. Standardised mixing process was executed using a Laboratory mixer (Everplast Machinery, Taiwan).

Table V-5. Sample recipe according to the ASTM D3192.

Ingredients	Rubber compound [phr]
Natural rubber (RSS)	100
Carbon black	40 – 50 – 60
Antioxidant	1.5
Antiozonant	2.5
Stearic acid	3
ZnO	5

Besides the ASTM standard compounds, some of the compounds were re-milled twice (referred as well mixed) in the internal mixer to ensure significantly different levels of carbon black macro and microdispersion between batches. In the two following tables (Table V-6 and Table V-7), two sets of prepared samples are summarised.

Table V-6. Samples varying in the number of re-mills and the carbon black content.

Carbon black grade	Mixing	Carbon black loading [phr]
N121	good	40
N121	poor	40
N121	good	50
N121	poor	50
N121	good	60
N121	poor	60

Table V-7. Samples varying in the carbon black grade.

Carbon black grade	Mixing	Carbon black loading [phr]
N121	good	50
N220	good	50
N326	good	50
N339	good	50
N550	good	50

Sample characterisation

For the characterisation of prepared samples the rotorless shear rheometer RPA 2000 (Alpha Technologies) was used. All rheological tests were carried out at a constant temperature of 70 °C and frequency 1.667 Hz (100 cpm).

Firstly, the Payne effect was measured using a dynamic shear strain sweep from 0.3 to 140.0 %. After the disintegration of the filler network by the Payne test, a series of single small strains (1 %) was applied to the sample immediately in order to monitor the storage modulus recovery. Small strain was imposed every 2^n minute (where n = 1, 2, 3, …8). All rheological tests were done on uncured samples in triplicate.

The quality of carbon black macrodispersion in a rubber matrix was evaluated using Dispergrader (Alpha Technologies). Dispergrader is a device evaluating the quality of macrodispersion by quantifying the surface roughness of a freshly cut specimen using an optical microscope in the reflection mode.

The influence of carbon black dispersion, volume fraction and properties on the flocculation behaviour in natural rubber melts was monitored and evaluated. In Figure V-9, the Payne effect and flocculation data of prepared samples are presented. The ordinate scales are equivalent for ease of comparison.

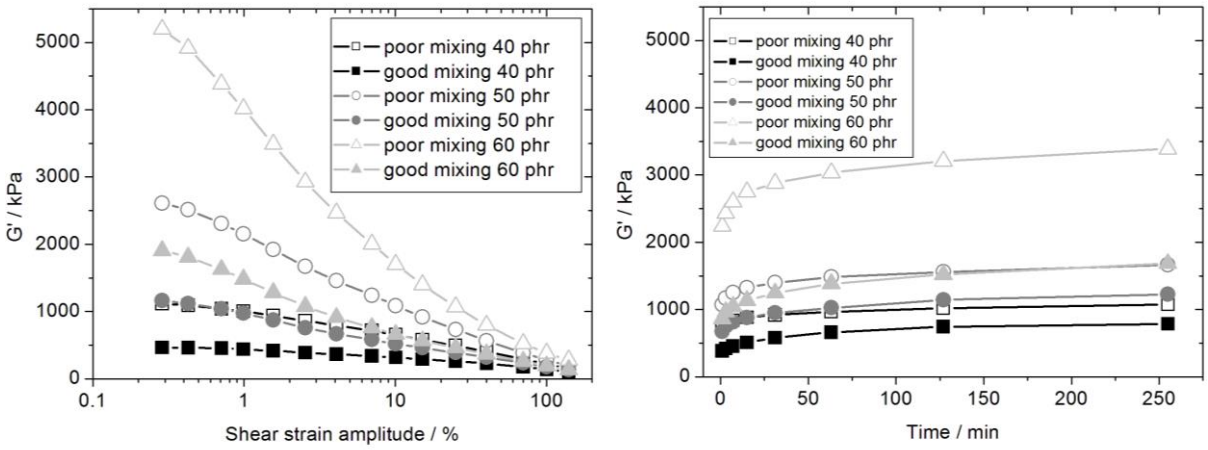

Figure V-9. Rheological data observed for rubber compounds varying in the carbon black volume fraction and the quality of carbon black dispersion. On the left, the Payne effect and on the right, the flocculation test results are shown.

From observed results it is evident that the carbon black loading and the quality of carbon black dispersion both have a significant influence on the rheological properties of filled rubbers. The observed non-linear dependence of a storage modulus on strain sweep, plotted on the left hand side of Figure V-9, is well-known as the Payne effect. Usually this is assigned either to the gradual breakdown of inter-aggregate adhesion, i.e. filler network disintegration or to the detachment of rubber macromolecules from the surface of filler particles depending on the magnitude of strain imposed to a sample [23-27]. Wang [11] however stated that regardless of the magnitude of applied strain the Payne effect can serve as a measure of filler networking which originates from filler-filler as well as filler-polymer interactions.

It was found that samples with poor filler macrodispersion show higher modulus at small strains than samples containing better macrodispersed carbon black. The steep decrease of the storage modulus at large strains is observed for samples containing poor macrodispersed carbon black which is due to the

additional breakdown of carbon black agglomerates that is not the case for better macrodispersed samples where carbon black was effectively deagglomerated during mixing. The moduli of both, poor and well macrodispersed samples decrease to approximately the same level at large strains. At this point the carbon black network is broken down and primarily the hydrodynamic reinforcing effect of disintegrated particulates is observed.

Generally, higher moduli were observed for higher carbon black filled samples. Similar behaviour was monitored by Wang [11] during his experiments and he stated that the larger the surface area available for the polymer-filler interaction, the greater the reinforcement effect.

Besides, a quantitative evaluation of carbon black macrodispersion quality has been performed using Dispergrader. Figure V-10 shows two pictures of freshly cut surfaces of uncured samples. In the left picture a smooth surface of well mixed N121 sample with a good macrodispersion of carbon black is shown. On the right side, a rough surface of poor mixed N121 sample containing large agglomerates of poorly dispersed carbon black is presented respectively. In this picture, areas with assemblies related to the poor carbon black distribution can be seen also. The average size of carbon black agglomerates examined by Dispergrader was 6.76 micrometres in the well macrodispersed sample while in the second case it was 13.19 micrometres. The white area representing the area of undispersed filler was 1.05 % for the sample with high macrodispersion and 9.62 % for the sample containing poor macrodispersed carbon black. One representative example is reproduced here however the same trends were observed for all the samples in this study. Clear differences in macrodispersion between well mixed compounds and compounds with no re-mill can be seen.

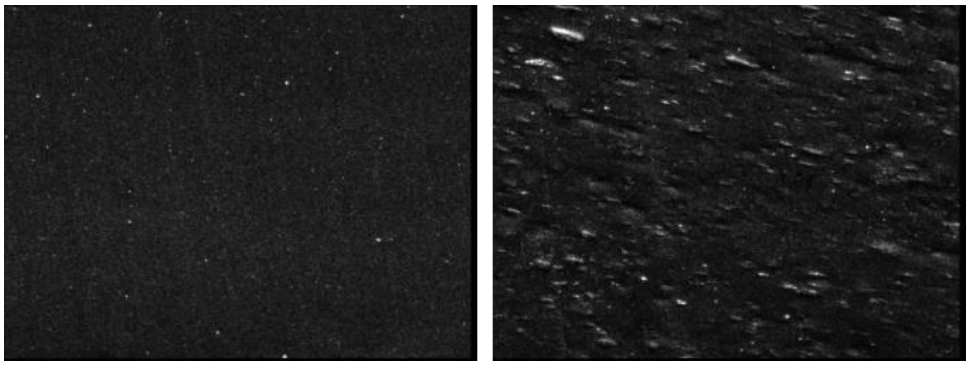

Figure V-10. Binary pictures of well (left) and poor (right) macrodispersed carbon black examined by Dispergrader.

After the release of the large strain, a substantial recovery of the storage modulus is monitored immediately. This is presented in the right hand side of Figure V-9. It is structural relaxation phenomena that provides information about cluster-cluster aggregation kinetics generally termed as a flocculation process. The flocculation process is monitored as the development of the storage modulus in time. It can be seen that the increase in storage modulus is more significant for the samples with poor carbon black macrodispersion. Moreover, the significance of the flocculation process increases towards the higher carbon black loadings.

Based on the macrodispersion evaluation, smaller aggregates are presented in well macrodispersed samples compared to compounds with no re-mill. Keeping the same loading, there is a higher number of aggregates in re-milled compounds and a higher level of their distribution connected to higher microdispersion quality can be reached. This is connected to longer distances and weaker attractive interactions between aggregates. Therefore, flocculation in these samples is less significant. Attractive interactions are of very short range, usually less than the particle size so that particles have to approach very close to each other before any significant interaction is reached [28]. The interaction phenomenon is well described by the DLVO theory [28, 29]. Furthermore, Witten and Pincus [29] stated that the attraction increases with particle size. Samples with poor macrodispersion contain larger aggregates compared to well dispersed samples and this could contribute to the more significant flocculation extent.

Generally, it has been noted that a flocculation curve is composed of at least two different flocculation rates. In first moments of the process a rapid recovery of the filler network is observed. At longer timescales the recovery process is rather gradual and gives only a small contribution to the total filler network recovery. Meier and Klüppel [21] observed similar behaviour during thermal annealing of non-crosslinked filled S-SBR samples. They stated that flocculation is a two-stage process where the fast process may be associated with the formation of clusters on smaller length scales. This stiffens the polymer matrix, indicating that the increase of the modulus results from the flocculation of primary aggregates. The slow process may be linked with the cluster growth process on large length scales where secondary structures develop the percolating carbon black network. The process can be parameterised by the bi-exponential fitting model (34):

$$G' = y_0 + G'_1\left(1 - e^{\frac{-t}{k_{fast}}}\right) + G'_2\left(1 - e^{\frac{-t}{k_{slow}}}\right) \quad (34)$$

Where t is the experimental time, k_{fast} is the time constant corresponding to the initial rapid contribution and k_{slow} is the time constant for the slower contribution. An example is shown in Figure V-11, where flocculation kinetics of the NR/N339 compound at 160 °C is analysed. Time constants from bi-exponential fit model are shown in Table V-8 then.

Table V-8. Time constants from bi-exponential fitting for samples differing in mixing conditions and carbon black loading.

Carbon black grade	**Mixing**	**Carbon black loading [phr]**	k_{fast} **[min]**	k_{slow} **[min]**
N121	good	40	**0.58**	**73.49**
N121	poor	40	**0.48**	**59.82**
N121	good	50	**0.53**	**70.10**
N121	poor	50	**0.47**	**56.69**
N121	good	60	**0.50**	**65.20**
N121	poor	60	**0.44**	**54.30**

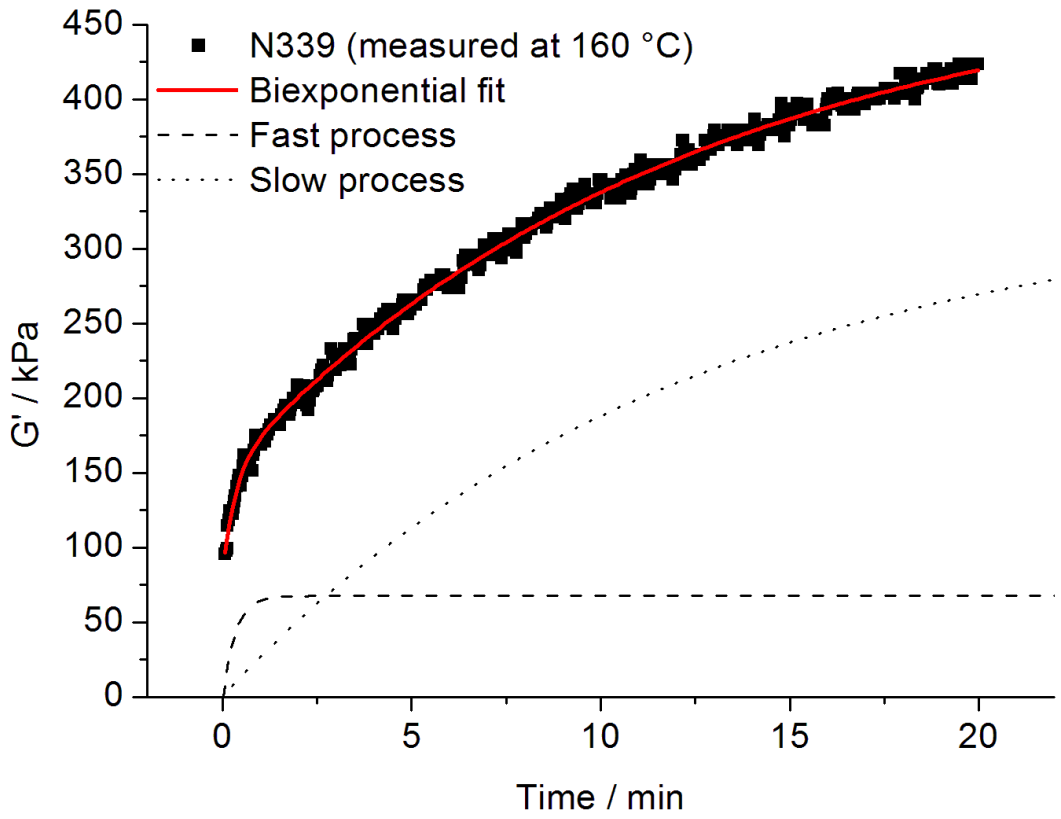

Figure V-11. Bi-exponential fitting of flocculation data. The solid line represents the sum of two exponential functions according to the Equation 34. The two exponential functions are depicted separately also.

In Figure V-12, the flocculation tests for samples with different carbon black grades are shown.

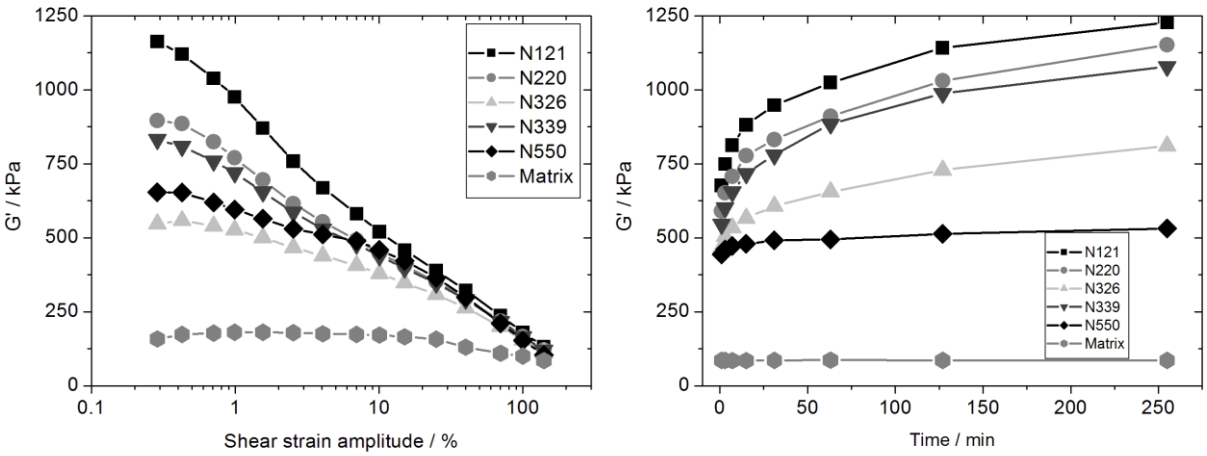

Figure V-12. Rheological data observed for samples with different carbon black grades. On the left, the Payne effect test and on the right, the flocculation behaviour.

Generally, it can be concluded that strain softening behaviour described by the Payne effect relates to the carbon black structure complexity. The higher the structure, the higher the modulus. This is connected to the shielding, occluded rubber and strain amplification effects [4, 7, 11 and 30]

On the other hand, flocculation behaviour relates to the specific surface area of carbon black or alternatively the smallest primary particle diameter. It can be seen that N121 having the smallest particles shows the largest extent of the modulus recovery. In Table V-9, time constants for samples varying in carbon black grades are shown.

Table V-9. Time constants from bi-exponential fit for samples varying in carbon black grades.

Carbon black grade	**Mixing**	**Carbon black loading [phr]**	k_{fast} **[min]**	k_{slow} **[min]**
N121	good	50	0.53	70.10
N220	good	50	0.54	92.60
N326	good	50	0.47	102.99
N339	good	50	0.51	70.91
N550	good	50	0.36	96.70

Furthermore, in Table V-10, the example of the mean squared displacement (*msd*) of Brownian particle in three dimensions calculated according to Equation 9 is shown. This expresses the distance which the particle in matrix diffuses in time k_{fast}. At the constant matrix viscosity, the highest mean squared displacement was found for N121 grade. The mean squared displacement scales with carbon black surface area giving Pearson's correlation parameter 0.997. The mean squared displacement is calculated for single primary particle of specific carbon black here which is only hardly seen in real compounds. Thus, it is recommended to see this data only as an illustration for systems where primary carbon black particles are present.

Table V-10. The comparison of mean squared displacement calculated for k_{fast}.

	N121	**N220**	**N326**	**N339**	**N550**	**Pearson's correlation coefficient**
msd_{fast} [$x10^{-15}$ m^3]	1.01	0.93	0.63	0.72	0.23	0.99
STSA [$m^2.g^{-1}$]	107.1	101.9	73.7	86.6	39.1	

*Particle radius data was used according to literature [31].

CONCLUSIONS OF SECTION A

In this section, the influence of mixing, carbon black loading and carbon black properties on the rheology of filled rubber compounds were investigated. It was found that Payne effect and flocculation processes both depend on all the mentioned variables significantly. Insufficient mixing process show samples with higher moduli. However, the carbon black network in these samples appears to be very fragile and can be rapidly disrupted at large strains which results in steep decrease of the modulus. The decrease of the modulus scales up with higher carbon black loading then. These effects were assigned to the poor macrodispersion of carbon black as examined by Dispergrader. On the other hand, the quality of microdispersion was monitored by the flocculation tests. It was found that samples containing smaller, well distributed primary aggregates flocculate to lower extents than compounds with poor microdispersion. This was assigned to attractive interactions between particles described by the DLVO theory as well as the Stokes-Einstein relation.

B. THE INFLUENCE OF MATRIX PROPERTIES ON FILLER FLOCCULATION IN RUBBER COMPOUND MELTS

METHODOLOGY OF SECTION B

Carbon black

Three different carbon black grades (Orion Engineered Carbons GmbH, Germany) were used throughout the experiment. General characteristics of specific surface area (SSA), i.e. iodine number, statistical thickness surface area

(STSA) and nitrogen adsorption (NSA) as well as the oil absorption techniques describing the complexity of structure are presented in Table V-11.

Table V-11. Properties of carbon black grades given by the manufacturer.

Carbon black grade	Iodine adsorption [mg/g]	STSA* [m^2/g]	BET* [m^2/g]	OAN* [cm^3/100 g]	COAN* [cm^3/100 g]
N121	121	114	122	132	111
N326	82	77	78	72	68
N660	36	34.8	35	91.4	74

*STSA – statistical thickness surface area; NSA – nitrogen surface area (based on the B.E.T. theory); OAN – oil absorption number; COAN – oil absorption number of compressed sample.

Rubber matrix

Natural rubber (NR), styrene-butadiene rubber (SBR) and ethylene propylene diene rubber (EPDM) were used as matrices throughout this experiment.

Chemical formulas, rheological characteristics and molecular weights of matrices are presented in section 1 called “Rubber reinforcement by carbon black - a novel method for study of strain-softening behaviour of rubbers filled with various carbon blacks” in Chapter V.

Sample preparation

Presented carbon black grades were incorporated in to the rubber matrices according to the international standard ASTM D3192 with the addition of anti-ageing agents as shown in recipe in Table V-12. Standardised mixing process was executed using a Laboratory mixer (Everplast Machinery, Taiwan) when nine rubber compounds varying in a carbon black grades and the matrix type were prepared.

Table V-12. Samples were mixed according to the recipe in ASTM D3192.

Ingredients	Rubber compound [phr]
Matrix	100
Carbon black	50
Antioxidant	1.5
Antiozonant	2.5
Stearic acid	3
Zinc oxide	5

Sample characterisation

For the rheological characterisation of prepared samples the RPA 2000 was used. Within the test, firstly the Payne effect is measured using a dynamic shear strain sweep from 1 to 140.0 %. Subsequently, a series of single small strains (1 %) is applied to the sample in order to monitor the filler network recovery resulting in the increase of the storage modulus. Small strains are imposed every 2^n minute (where n = 1, 2, 3, …8). All rheological tests were done on uncured samples in triplicate at a constant temperature 70 °C and frequency 1.667 Hz (100 cpm).

RESULTS AND DISCUSSION OF SECTION B

As mentioned in the experimental section, the viscosity data of neat matrices as well as GPC characteristics are presented in section 1 called "Rubber reinforcement by carbon black - a novel method for study of strain-softening behaviour of rubbers filled with various carbon blacks" in Chapter V and author is referring to them in the discussion of the results.

Examination of the strain sweep data shows that matrices' structural properties as measured via GPC have only a small effect on the storage modulus at small strains as presented in the left hand side of Figure V-13. However, slightly higher storage moduli were observed for compounds based on EPDM having the highest molecular weight distribution. This effect is visible particularly in EPDM filled with N121 grade. From examination of the high strain response it is apparent that moduli of all samples are roughly equal. This can be understood in terms of hydrodynamics. The majority of the filler

structure is broken down by large strains and only the hydrodynamic reinforcing effect of the disaggregated particulates is left.

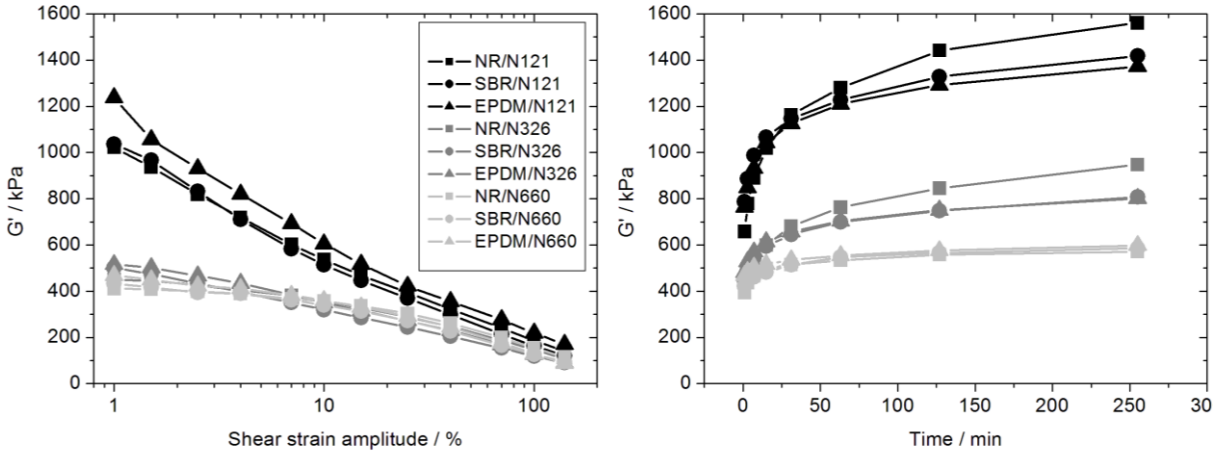

Figure V-13. The rheological of various matrices filled with different carbon black grades. In the left hand side, the Payne effect and on the right the flocculation tests are plotted (legend is valid for both pictures).

Flocculation data is presented in the right hand side of Figure V-13. The most pronounced modulus recovery is monitored in the NR matrix. This effect scales up with surface area or particle size respectively for N326 and N121 grades. The flocculation behaviour can be explained on the base of matrices viscosities when NR showed, at conditions of the flocculation test (70 °C, 1.667 Hz), the lowest viscosity – η'_{NR} = 5011 Pa.s^{-1}, and followed by η'_{SBR} = 7419 Pa.s^{-1} and η'_{EPDM} = 7657 Pa.s^{-1}. On the other hand, there is only a small influence of matrix properties on the flocculation behaviour of carbon black when compared to the influence of carbon black properties.

Calculated diffusion coefficients for samples are presented in Table V-13. It was proved that at a specific temperature, the flocculation rate of filler is driven by the matrix viscosity and the size of carbon black aggregates.

Table V-13. The calculated diffusion coefficients of different carbon black types in different rubber matrices.

Matrix type	Diffusion coefficient D_0 [x10^{-18} $m^2.s^{-1}$]		
	N121	**N326**	**N660**
NR	5.28	3.72	1.50
SBR	3.57	2.51	1.01
EPDM	3.46	2.43	0.98

*Particle radius data was used according to literature [31].

CONCLUSIONS OF SECTION B

Throughout the experiment, it was found that structure properties of matrices as measured by GPC has only a slight effect on the flocculation behaviour of carbon black in rubber melts. It can be concluded that polymer-filler interactions does not play any significant role in the modulus recovery process and filler-filler interactions predominate. This discovery seems to be in accordance with the flocculation concept based on the filler agglomeration-deagglomeration process of particulates connected to Van der Waals attraction [31, 32] rather than the polymer bridging mechanism caused by chains' adsorption on the filler surface [22] as argued in the literature.

On the other hand, diffusion coefficients calculated according to the Stokes-Einstein relation showed that carbon black flocculation behaviour in rubbers is driven by the carbon black particle size and the matrix viscosity. This was validated when the largest extent of the modulus recovery was found for NR having the lowest dynamic viscosity at the specific temperature. Moreover, the recovery extent was scaling up with surface area (or particle size) of carbon black.

Considering the Payne effect, slightly higher storage modulus at small strains was observed for EPDM having the highest molecular weight distribution as measured via GPC.

C. THE INFLUENCE OF TEMPERATURE ON FILLER FLOCCULATION IN NATURAL RUBBER MELTS AND CROSSLINKED SAMPLES

METHODOLOGY OF SECTION C

Carbon black

Three varied carbon black grades (Orion Engineered Carbons GmbH, Germany) were used throughout the experiment and their characteristics are presented in Table V-14.

Table V-14. Properties of carbon black grades given by the manufacturer.

Carbon black grade	Iodine adsorption [mg/g]	STSA* [m^2/g]	BET* [m^2/g]	OAN* [cm^3/100 g]	COAN* [cm^3/100 g]
N121	121	114	122	132	111
N339	90	88	91	120	99
N550	43	39	40	121	85

*STSA – statistical thickness surface area; NSA – nitrogen surface area (based on the B.E.T. theory); OAN – oil absorption number; COAN – oil absorption number of compressed sample.

Sample preparation

Presented carbon black grades were incorporated in to the natural rubber type SMR 10 (SMR – Standard Malaysian rubber) having the index of polydispersity 2.5, M_n = 132000 and M_w = 329000 as measured using gel permeation chromatography (PL–GPC 220, Agilent Technologies). GPC tests were carried out at 160°C and trichlorobenzene was used as the solution. The mixing process was executed using a laboratory mixer (Everplast Machinery, Taiwan) according to the international standard ASTM D3192 with the addition of anti-ageing agents as shown in recipe in Table V-15. Standardised mixing process

Table V-15. Samples were mixed according to the recipe in ASTM D3192.

Ingredients	Rubber compound [phr]
Matrix	100
Carbon black	50
Antioxidant	1.5
Antiozonant	2.5
Stearic acid	3
Zinc oxide	5

Sample characterisation

For the characterisation of prepared samples the rotorless shear rheometer RPA 2000 (Alpha Technologies) was used. Rheological tests of non-crosslinked samples were carried out at temperatures 70, 100 and 160 °C and a single frequency 1.667 Hz (100 cpm).

Firstly, the Payne effect was measured using a dynamic shear strain sweep from 0.3 to 140.0 %. After the disintegration of the filler network, a series of single small strains (0.3 %) was applied to the sample immediately for 20 minutes in order to monitor the storage modulus recovery.

In the second stage, samples were crosslinked at 160 °C in 60 minutes prior to Payne effect and flocculation behaviour examination. The investigation of shear strain behaviour of crosslinked samples was carried out at strain sweep from 0.3 to 10 %. The storage modulus recovery was monitored for 20 minutes at 160 °C and at single small strains (0.3 %).

Results and discussion of section C

Firstly, the influence of temperature on the flocculation process in non-crosslinked samples was examined.

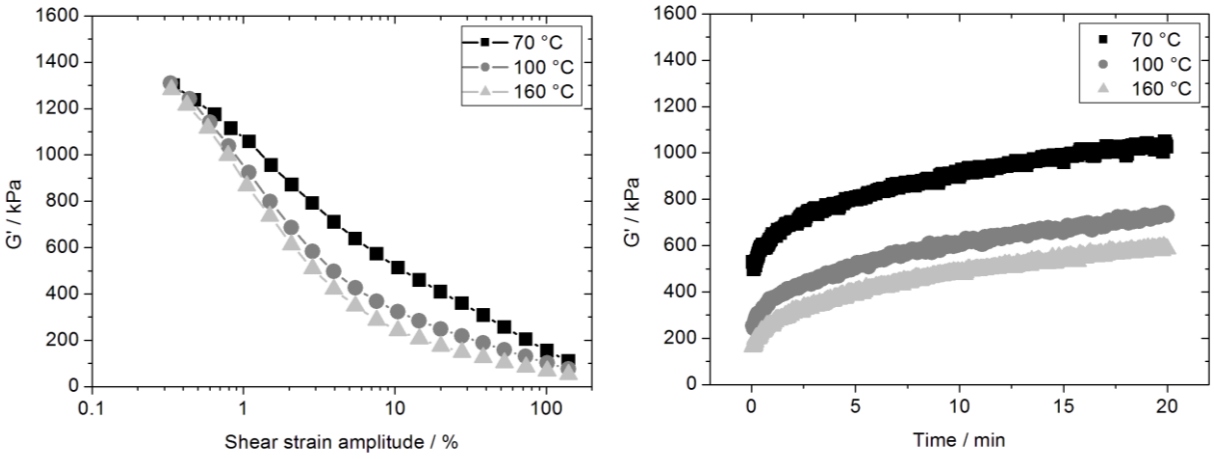

Figure V-14. The influence of temperature on the flocculation process measured for the NR/N121 compound.

In Figure V-14, the influence of temperature on the flocculation process of N121 grade in natural rubber melts was examined. Strain sweep data (in the left hand side) shows the behaviour of the natural rubber matrix at various temperatures when the viscosity of matrix changes. At small strain amplitudes, the storage modulus is at the approximately same level for all the temperatures. However, at increasing strain amplitude, the decrease of the modulus is steeper at higher temperatures. This might be due to desorption of rubber macromolecules from carbon black surface which will proceed more likely at higher temperatures (when the viscosity of matrix is lower). The moduli of compounds converge again at large strain amplitudes. There might be a critical level of the structure disintegration where the behaviour of the system is independent of polymer. Apart from the desorption mechanism the modulus decrease is explained by the breakdown of the filler network. At large strain amplitudes, the reinforcement effect is assigned to hydrodynamic effects of disintegrated particulates primarily.

The flocculation data in the right hand side of Figure V-14 show on the structure relaxation phenomena in rubber melts observed at various temperatures. The results show more pronounced flocculation effect resulting in the higher storage modulus for lower temperatures. This is due to the higher viscosity of the matrix. This behaviour might suggest the importance of macromolecular chains in the flocculation process of carbon black. The significant contribution of macromolecular chains to the modulus recovery of

filled sample was explained by Schwartz et al. by bridging flocculation and depletion forces [22].

The investigation of shear strain behaviour and flocculation of different carbon black grades in crosslinked natural rubber is presented below.

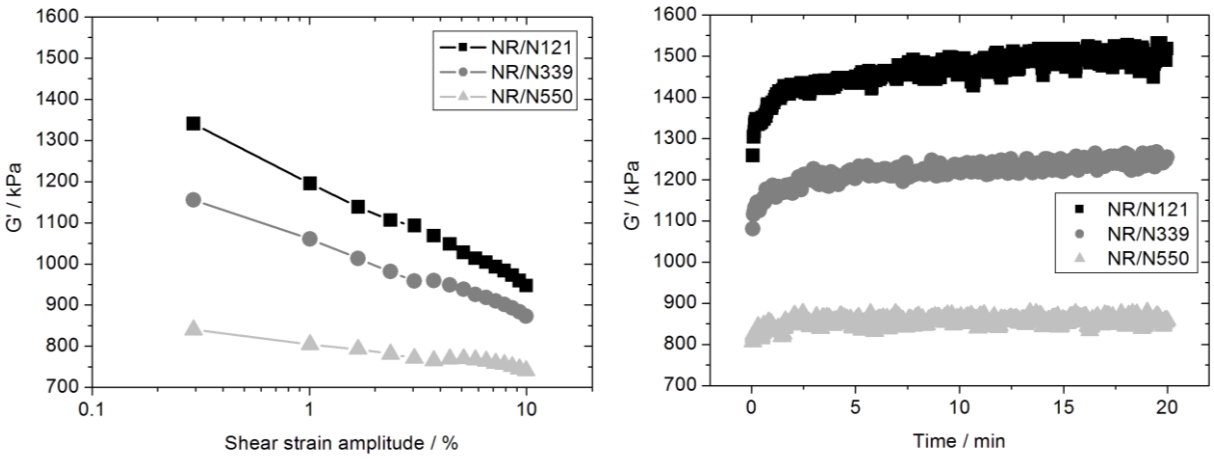

Figure V-15. Rheological data of crosslinked natural rubber samples. On the left Payne effect. On the right flocculation behaviour.

The strain sweep behaviour in the left hand side of Figure V-15 shows gradual decrease of storage modulus with increasing shear amplitude for all the samples where the highest modulus was observed for N121 filled sample. This is given by the highest structure of N121.

The modulus recovery for crosslinked samples is shown in the right hand side of Figure V-15 then. The most pronounced effect of structural relaxation can be seen for sample filled with N121. Due to the lowest particle size of N121 among other carbon black grades, this carbon black might be able to penetrate in between crosslinked macromolecular chains which can result in filler flocculation thus contribute to the recovery of the modulus. On the other hand, basically no flocculation was observed for large carbon black particles of N550.

Generally, only slight flocculation effects were monitored in crosslinked samples when compared to rubber melts.

During the experiment, the influence of temperature on filler flocculation in non-crosslinked samples was found. Considering the strain sweep data a lower modulus was found at elevated temperatures. Moreover, the Payne effect was more significant at higher temperatures. The data of flocculation process showed less pronounced flocculation at elevated temperatures which could be assigned to the effect of bridging flocculation.

In crosslinked samples the strain sweep dependence revealed differences in moduli according to various properties of used carbon black grades. Modulus recovery of crosslinked samples was pronounced the most in the case of N121 having the smallest particle diameter. Generally, only slight flocculation was monitored in crosslinked samples when compared to non-crosslinked samples.

D. COMPUTER SIMULATION OF FILLER FLOCCULATION IN RUBBER COMPOUNDS

Based on the experimental data on the flocculation process, there was an initial effort to simulate Brownian Dynamics of carbon black in rubber compounds.

For the purpose of the computer simulation an open source code LAMMPS (Large-scale Atomic/Molecular Massively Parallel Simulator) was used. LAMMPS is a classical molecular dynamics simulation code designed to run efficiently on parallel computers. LAMMPS has potentials for solid-state materials (metals, semiconductors) and soft matter (biomolecules, polymers) and coarse-grained or mesoscopic systems. It can be used to model atoms or, more broadly, as a parallel particle simulator at the atomic, meso-, or continuum scale. LAMMPS runs on single or parallel processors using message-passing techniques and a spatial-decomposition of the simulation domain. The code is designed to be easy to modify or extend with new functionality.

LAMMPS was developed at Sandia National Laboratories by Plimpton, Thompson, and Crozier [33]. It is an open-source code, distributed freely under the terms of the GNU Public License (GPL). Other significant contributions to the source code are referred as follows [34-40].

In the first step, the intention was to write a script to simulate Brownian Dynamics of rigid aggregates each formed by several point particles in continuum. The original script is attached in Appendix B. Below, example of the script and explanation of each command is presented for the simulation script and the datainput file.

The example of the LAMMPS script

```
units          lj
atom_style     atomic
pair_style     lj/cut 2.5
read_data      datainput_atomic_27agg16p_new.txt
mass           * 1
pair_coeff     * * 1 1
velocity       all create 100.0 4928459

group          clump1 id <> 1 16
group          clump2 id <> 17 32...

fix            1 all rigid group 27 clump1 clump2...

neigh_modify   exclude group clump1 clump1
neigh_modify   exclude group clump2 clump2...

dump           2 all xyz 10 dump.floc_atomic_27new.xyz

thermo         100
```

```
timestep        1e-4

run             100000
```

The description of the LAMMPS script

units lj

- *lj* sets units style
- For style *lj*, all quantities are unitless. Without loss of generality, LAMMPS sets the fundamental quantities mass, sigma, epsilon, and the Boltzmann constant = 1.
- The masses, distances, energies are multiples of these fundamental values. The formulas relating the reduced or unitless quantity (with an asterisk) to the same quantity with units is also given. Thus the mass & sigma & epsilon values can be used for a specific material and convert the results from a unitless LJ simulation into physical quantities.

- mass = mass or m
- distance = sigma, where x* = x / sigma
- time = tau, where tau = t* = t (epsilon / m / sigma^2)^1/2
- energy = epsilon, where E* = E / epsilon
- velocity = sigma/tau, where v* = v tau / sigma
- force = epsilon/sigma, where f* = f sigma / epsilon
- torque = epsilon, where t* = t / epsilon
- temperature = reduced LJ temperature, where T* = T Kb / epsilon
- pressure = reduced LJ pressure, where P* = P sigma^3 / epsilon
- dynamic viscosity = reduced LJ viscosity, where eta* = eta sigma^3 / epsilon / tau
- charge = reduced LJ charge, where q* = q / (4 pi perm0 sigma epsilon)^1/2
- dipole = reduced LJ dipole, moment where *mu = mu / (4 pi perm0 sigma^3 epsilon)^1/2
- electric field = force/charge, where E* = E (4 pi perm0 sigma epsilon)^1/2 sigma / epsilon
- density = mass/volume, where rho* = rho sigma^dim

atom_style atomic

- *atom_style atomic* sets objects as atoms. This style gives to each atom its coordinates, velocity and identification number.
- During simulations, also *atom_style sphere* was used, but for its simplicity, we focused on the *atom_style atomic.*

pair_style lj/cut 2.5

$$E = 4\epsilon \left[\left(\frac{\sigma}{r}\right)^{12} - \left(\frac{\sigma}{r}\right)^{6} \right] \quad (35)$$

- This style computes the standard 12/6 Lennard-Jones potential
- Where $r < r_c$ and r_c stands for the cutoff (distance units)
- 2.5 is the set cutoff distance for Lennard-Jones interaction

read_data datainput_atomic_27agg16p_new.txt

- Datainput file called *datainput_atomic_27agg16p_new.txt* was created parallely (shown below) and *read_data* command loads this data file for the purpose of simulation
- Datafile defines properties of atoms, its coordinates and identification numbers
- In this particular datainput file, 27 aggregates each formed by 16 particles are defined

mass * 1

- *mass* command defines the additional property of atoms
- Can overwrite the earlier information defined in the datainput file

pair_coeff * * 1 1

- *pair_coeff* command sets coefficients of the particular potential

velocity all create 100.0 4928459

- Sets initial velocity of *all* atoms in the script corresponding to the temperature T
- *create* style generates an ensemble of velocities which are not all equal using a random number generator with the specified speed as the specified temperature

group clump1 id <> 1 16

group clump2 id <> 17 32…

- Up to 30 groups can be defined
- Group command creates groups of atoms defined via datainput file where is specified which atom belongs into which group
- For example, atoms with id from 1 to 16 as defined in a datainput file, are assigned to the group called clump1

fix 1 all rigid group 27 clump1 clump2…

- *fix* defines commands that are carried at each timestep
- Command *rigid* treat one or more sets of atoms as independent rigid bodies. This means that each timestep the total force and torque on each rigid body is computed as the sum of the forces and torques on its constituent particles and the coordinates, velocities, and orientations of the atoms in each body are updated so that the body moves and rotates as a single entity.
- For bodystyle *group*, each of the listed groups is treated as a separate rigid body. Only atoms that are also in the fix group are included in each rigid body. This option is only allowed for fix rigid and its sub-styles.
- Each rigid body is acted on by other atoms which induce an external force and torque on its center of mass, causing it to translate and rotate.

- Forces between particles within a body do not contribute to the external force or torque on the body. Thus for computational efficiency, it is convenient to turn off pairwise and bond interactions between particles within each rigid body.

- The rigid performs constant NVE time integration [41] to update position and velocity for atoms in the group each timestep. N stands for moles; V is volume; E is energy. This creates a system trajectory consistent with the microcanonical ensemble.
- NVE means, that no energy is added or removed during the integration of the equations of motion as described in Chapter II – Computer modelling of filler network formation.
- The rigid style use an integration technique based on Richardson iterations [42].

neigh_modify exclude group clump1 clump1

neigh_modify exclude group clump2 clump2…

- All groups have to be defined
- This command excludes interaction between particles in created groups, i.e. clumps from 1 to 27
- This command fasten the calculation since only interaction between groups are calculated

dump 2 all xyz 10 dump.floc_atomic_27new.xyz

- Command dump exctracts information into a file
- *all* choose all the atoms in the simulation
- *xyz* coordinates are written down into the export file
- *dump.floc_atomic_27new* is the name of the exported file which subsequently can be visualised using any visualising software such as VMD.

thermo 100

- Thermo command compute and print thermodynamic info on timesteps that are a multiple of N and at the beginning and the end of a simulation
- *thermo 100* outputs thermodynamics every 100 timesteps
- A value of 0 will only print thermodynamics at the beginning and end.

timestep 1e-4

- Set the timestep size for subsequent molecular dynamics simulations in time units.

run 100000

- Runs calculation with 100000 steps.

The example of the datainput file

```
432 atoms

27 atom types


-12 12 xlo xhi

-12 12 ylo yhi

-12 12 zlo zhi


Atoms

1    1    -10  10   0.5

2    1    -9   10   0.5

3    1    -10  9    0.5

4    1    -9   9    0.5

5    1    -10  10   -0.5...
```

The description of the datainput file

432 atoms

- 432 atoms are defined in the system

27 atom types

- 27 different types of atoms

-12 12 xlo xhi
-12 12 ylo yhi
-12 12 zlo zhi

- 3-dimensional cubic system where coordinates are defined and the length of cubic side is from -12 to +12 (distance unit)

Atoms

1 1 -10 10 0.5
2 1 -9 10 0.5
3 1 -10 9 0.5
4 1 -9 9 0.5
5 1 -10 10 -0.5...

- Position 0 – identification number of atom; 1 – atom type; 2 – x coordinate in the defined cubic system; 3 – y coordinate; 4 – z coordinate.

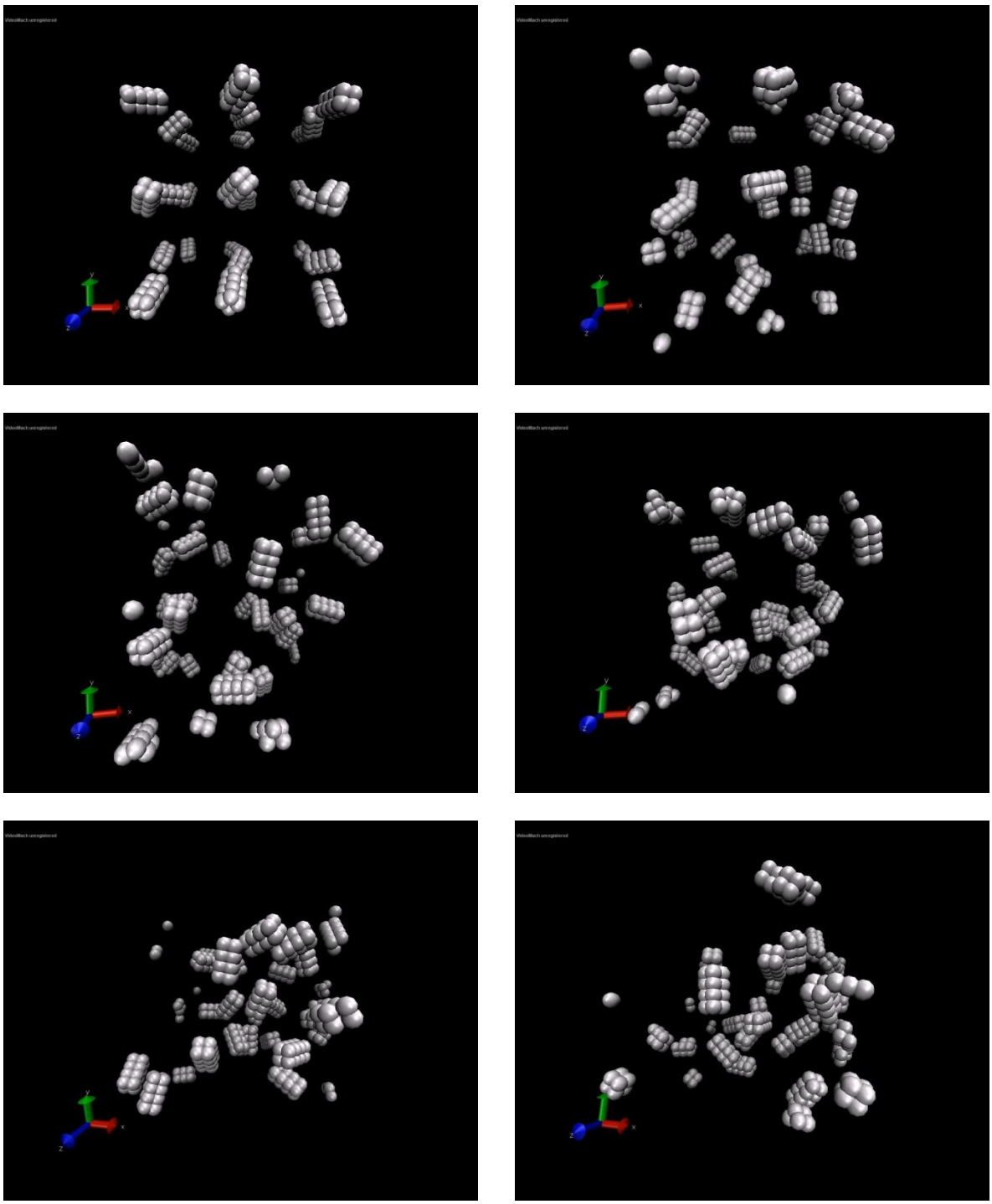

Figure V-16. Visualisation of the LAMMPS simulation; top left picture shows simulation progress in 1 s; top right – 5 s; middle left – 10 s; middle right – 20 s; bottom left – 30 s; bottom right – 40 s.

Visualisation of the simulation is shown in Figure V-16. The visualisation has been carried out via free Visual Molecular Dynamics (VMD) program [43]. Within the simulation, random Brownian movement of single model aggregates, where there are no interactions between the aggregates, can be seen. Periodic boundary conditions of the system are set which causes that separate single particles can be seen in the visualisation. However, these are only part of rigid aggregates pervading through boundaries. Periodic boundary conditions ensure that the exact amount of objects that flow away through boundaries will flow back in to the system again.

CONCLUSIONS OF SECTION D

The initial effort to use computer simulations in order to model the flocculation phenomena of filler aggregates in polymer matrix has been performed. At the moment, the Brownian dynamics of the model aggregates in continuum were simulated with no set interactions between aggregates. However, extended research in the field of simulations would be necessary to observe physically relevant data from the simulations.

In the further work, the model aggregates should be replaced by real filler (e.g. carbon black) aggregates which can be modelled using MATLAB or other software based on TEM pictures. LJ units can be replaced by SI units and experimentally observed data will be used for the purpose of the simulation. Interactions between carbon black aggregates should be set. Properties of a matrix such as viscosity should be set.

ACKNOWLEDGEMENTS

This work has been carried out with the financial support of Internal Grant Agency of Tomas Bata University in Zlín (reg. number: IGA/FT/2013/012, IGA/FT/2014/014) funded from the resource of specific university research. This contribution was written with the support of the ´Operational Program Education for Competitiveness´ co-funded by the European Social Fund (ESF) and the national budget of the Czech Republic, within the entitled project ´Advanced Theoretical and Experimental Studies of Polymer Systems´ (reg. number: CZ.1.07/2.3.00/20.0104) and with the support of the 'Research and Development for Innovations' Operational Programme co-funded by the

European Regional Development Fund (ERDF) and the national budget of the Czech Republic, within the project entitled ‘Centre of Polymer Systems’ (reg. number: CZ.1.05/2.1.00/03.0111). Authors are grateful for the help of Pavol Priekala of Alpha Technologies.

REFERENCES

1. J.W. Mani, J.G Meier, M. Klüppel. Study of Flocculation Dynamics of Carbon Black in Rubber Melts under Shear by Dielectric Spectroscopy. KGK 2006; 59(12): p. 648–652.
2. M. Gerspacher, L. Nikiel, H.H. Yang, et al. Flocculation in Carbon Black Filled Rubber Compounds. KGK 2002; 55(11): p. 596–604.
3. Ch.J. Lin, T.E. Hogan, W.L. Hergenrother. On the Filler Flocculation in Silica and Carbon Black Filled Rubbers. II. Filler Flocculation and Polymer-Filler Interactions. Rubb Chem Technol 2004; 70(1): p. 90–114.
4. J. B. Donnet, E. Custodero, Reinforcement of Elastomers by Particulate Fillers. J.E. Mark, B. Erman, F.R. Eirich, Science and Technology of Rubber. Elsevier Academic Press 2005; 8: p. 367–400. ISBN: 0-12-464786-3.
5. G. Wu, S. Asai, M. Sumita, et al. Estimation of Flocculation Structure in Filled Polymer Composites by Dynamic Rheological Measurements. Colloid Polym Sci 2000; 278(3): p. 220–228.
6. J.J.C. Busfield, A.G. Thomas, K. Yamaguchi. Electrical and Mechanical Behavior of Filled Rubber. III. Dynamic Loading and the Rate of Recovery. J Polym Sci Pol Phys 2005; 43(13): p. 1649–1661.
7. G. Kraus. Reinforcement of Elastomers by Carbon Black. Rubb Chem Technol 1978; 51(2): p. 297–321.
8. T.A. Witten, L.M. Sanders. Diffusion-Limited Aggregation, a Kinetic Critical Phenomenon. Phys Rev Lett 1981; 47(19): p.1400–1403.
9. P. Meakin. Formation of Fractal Clusters and Network by Irreversible Diffusion-Limited Aggregation. Phys Rev Lett 1983; 51(13): p.1119–1122.
10. M.J. Wang, S. Wolff, J.B. Donnet. Filler-Elastomer Interactions. III. Carbon-Black-Surface Energies and Interactions with Elastomer Analogs. Rubb Chem Technol 1991; 64(5): p. 714–736.
11. M.J. Wang. Effect of Polymer-Filler and Filler-Filler Interactions on Dynamic Properties of Filled Vulcanizates. Rubb Chem Technol 1998, 71(3): p. 520–589.
12. G.G.A. Böhm, M.N. Nguyen. Flocculation of Carbon Black in Filled Rubber Compounds. I. Flocculation Occurring in Unvulcanized

Compounds during Annealing at Elevated Temperatures. J Appl Polym Sci 1995; 55(7): p. 1041–1050.

13. E. Allen, J. Henshaw, P.A. Smith. Review of Particle Agglomeration. AEAT/R/PSEG/0398; AEA Technology Engineering Services, Inc.: Harwell, Oxford, 2001.
14. T. Wang, M.J. Wang, J. Shell, et al. The Effect of Compound Processing on Filler Flocculation. KGK 2000; 53(9): p. 497–505.
15. A.Y. Coran, J.B. Donnet. The Dispersion of Carbon Black in Rubber. III. The Effect of Dispersion Quality on the Dynamic Mechanical Properties of Filled Natural Rubber. Rubb Chem Technol 1992; 65(5): p. 1016–1041.
16. E. Kissa. Dispersions – Characterization, Testing and Measurement. Marcel Dekker, Inc. 1999; p. 708. ISBN: 0-8247-1994-8.
17. L.B. Tunnicliffe, J. Kadlcak, Y. Shi, et al. Flocculation and Viscoelastic Behaviour in Carbon Black-Filled Natural Rubber. Macromol Mater Eng 2014; DOI: 10.1002/mame.201400117.
18. J. Kadlcak, J. Lacayo, R. Cermak, et al. The Influence of Mixing on the Flocculation Time of Carbon Black Aggregates in Rubber Compounds. Plastko Conference 2012. Tomas Bata University in Zlín 2012; p. 294–295. ISBN 978-80-7454-137-7.
19. J. Kadlcak, L.B. Tunnicliffe, J.J.C. Busfield, et al. Evaluation of Carbon Black Flocculation in Rubber Melts. Plastko Conference 2014, Tomas Bata University in Zlín 2014; p. 428-438. ISBN 978-80-7454-335-7.
20. J. Kadlcak, L.B. Tunnicliffe, J.J.C. Busfield, et al. Evaluation of Carbon Black Flocculation in Natural Rubber Melts. RubberCon 2014, Manchester 2014; p. 1-9. ISBN 1-86125-176-9.
21. J.G. Meier, M. Klüppel. Carbon black networking in elastomers monitored by dynamic mechanical and dielectric spectroscopy. Macromol Mat Eng 2008; 293: p. 12–38.
22. G.A. Schwartz, S. Cerveny, A.J. Marzocca, et al. Thermal Ageing of Carbon Black Filled Rubber Compounds. I. Experimental Evidence for Bridging Flocculation. Polymer 2003; 44(23): p. 7229-7240.
23. A.R. Payne. The Dynamic Properties of Carbon Black-Loaded Natural Rubber Vulcanizates. Part I. J Appl Polym Sci 1962; 6(19): p. 57–63.

24. R. Houwink. Slipping of Molecules during the Deformation of Reinforced Rubber. Rubb Chem Technol 1956; 29(3): p. 888–893.

25. L. Mullins. Softening of Rubber by Deformation. RubbChemTechnol1969; 42(1): p. 339–362.

26. E.M. Dannenberg. Bound Rubber and Carbon Black Reinforcement. RubbChemTechnol1986; 59 (3): p. 512–524.

27. P.G. Maier, D. Goritz. Molecular Interpretation of the Payne Effect. KGK 1996; 49(1): p. 18–21.

28. M. Elimelech, J. Gregory, X. Jia, R.A. Williams. Particle Deposition and Aggregation – Measurement, Modelling and Simulation. Butterwort-Heinemann USA 1995; p. 441. ISBN 0-7506-7024-X.

29. T.A. Witten, P.A. Pincus. Structured fluids – Polymers, Colloids, Surfactants. Oxford University Press. New York 2004; p. 216. ISBN 978-0-19-958382-9.

30. L. Mullins, N.R. Tobin. Stress Softening in Rubber Vulcanizates .I. Use of a Strain Amplification Factor to Describe Elastic Behavior of Filler-Reinforced Vulcanized Rubber. J Appl Polym Sci 1965; 9(9): p. 2993–3009.

31. J.B. Donnet, R.Ch. Bansal, M.J. Wang. Carbon Black - Science and Technology. Marcel Dekker Inc. 1993; 461p. ISBN 0-8247-8975-X.

32. G. Kraus. Reinforcement of Elastomers by Carbon Black. Rubb Chem Technol 1978; 51(2): p. 297-321.

33. S. Plimpton. Fast Parallel Algorithms for Short-Range Molecular Dynamics. J Comp Phys 1995; 117(1): p. 1-19.

34. T.W. Sirk, S. Moore, E.F. Brown. Characteristics of thermal conductivity in classical water models. J Chem Phys 2013; 138(6): 064505.

35. S.J. Plimpton and A.P. Thompson. Computational Aspects of Many-body Potentials. MRS Bulletin 2012; 37(5): p. 513-521.

36. H.M. Aktulga, J.C. Fogarty, S.A. Pandit, A.Y. Grama. Parallel reactive molecular dynamics: Numerical methods and algorithmic techniques. Parallel Computing 2012; 38(4-5): p. 245-259.

37. A.P. Thompson, S.J. Plimpton, W. Mattson. General formulation of pressure and stress tensor for arbitrary many-body interaction potentials under periodic boundary conditions. J Chem Phys 2009; 131(15): 154107.

38. R.M. Mukherjee, P.S. Crozier, S.J. Plimpton, et al.. Substructured molecular dynamics using multibody dynamics algorithms. Intl J of Non-Linear Mechanics 2008; 43(10): p. 1045-1055.

39. P.J. In't Veld, S.J. Plimpton, G.S. Grest. Accurate and Efficient Methods for Modeling Colloidal Mixtures in an Explicit Solvent using Molecular Dynamics. Comp Phys Comm 2008; 179(5): p. 320-329.

40. R. Auhl, R. Everaers, G.S. Grest, et al.. Equilibration of long chain polymer melts in computer simulations. J Chem Phys 2003; 119(24): p. 12718-12728.

41. Molecular dynamics, Microcanonical ensemble (NVE) [online]. [viewed 2014-06-22]. Available from: http://en.wikipedia.org/wiki/Molecular_dynamics#Microcanonical_ensemble .28NVE.29.

42. Modified Richardson iteration [online]. [viewed 2014-06-28]. Available from: http://en.wikipedia.org/wiki/Modified_Richardson_iteration.

43. VMD Visual Molecular Dynamics [online]. [viewed 2014-04-27]. Available from: http://www.ks.uiuc.edu/Research/vmd/.

CHAPTER VI. GENERAL CONCLUSIONS AND FUTURE EFFORT

CARBON BLACK STRUCTURE – EVALUATION BY MECHANICAL COMPRESSION

In the first area, the pilot investigation of carbon black structure using mechanical compression via Void Volume Tester has been carried out. It was found that this novel method could offer an alternative method for carbon black structure evaluation beside oil absorption methods which are less favourable nowadays due to use of aromatic oils. Moreover, it was found that Void Volume Tester gives qualitatively the same results as the COAN method. Apart from being a clean, precise and quick method, it was proven that Void Volume Tester offers better insight to carbon black behaviour in rubber compounds compared to oil absorption methods when very high correlations to in-rubber properties such as Payne effect was found compared to oil absorption methods. Consequently, void volume measured by mechanical compression can be potentially used for prediction of carbon black behaviour in rubbers. Moreover, some suggestions and recommendations coming from the investigation were given to the producer of the device.

Despite the numerous measurements carried out on Void Volume Tester, its use in the rubber industry will still need more investigation, discussion and time. However, the evaluation of carbon black structure by mechanical compression has proved its potential to replace harmful oil absorption methods.

MACRODISPERSION EVALUATION – REFERENCE OBJECT FOR TOPOGRAPHY OF MATERIALS

The second area was dedicated to the evaluation of filler macrodispersion via Dispergrader. In the framework of this doctoral thesis, a tool for the calibration of devices evaluating filler macrodispersion from the surface roughness of a sample was designed. This was carried out due to the lack of any precision statement in the international standard ASTM D7723 – 11 called “Standard Test Method for Rubber Property – Macro-Dispersion of Fillers in Compounds”. The designed tool called the reference object for topography of materials offers simple and rapid method for the calibration. The patent application for this

reference object has been submitted and accepted. Moreover, the international PCT (Patent Cooperation Treaty) application has been submitted for Europe and USA. The reference object for topography of materials is discussed by ASTM committee to become an official part of the ASTM standard.

Future work is supposed to be related to the calibration of devices evaluating filler microdispersion, i.e. the dispersion of fillers having diameter less than 1 micrometre.

EVALUATION OF CARBON BLACK BEHAVIOUR IN RUBBER COMPOUNDS

The third topic presented in this doctoral thesis is related to the filler networking. This is the most extended area of the research, when the test evaluating carbon black reinforcement and flocculation in rubbers was defined, the investigation using this test has been performed and at the end an initial effort to simulate the process of flocculation has been carried out.

During the research it was found that carbon black flocculation is one of the main mechanisms of the structural relaxation phenomenon in rubber compound melts as well as in crosslinked samples. The influence of carbon black macrodispersion, carbon black particle size, structure, carbon black loading and polymer matrix on filler flocculation have been investigated. Also the influence of temperature on the flocculation of carbon black in rubber melts has been discussed. It was found that the primary particle size, the filler-filler and the filler-polymer interactions play the dominant role in the shear initiated flocculation. Also, it was found that the bridging flocculation plays an important role in the structural relaxation of filled rubbers.

Since, the flocculation phenomenon of carbon black in rubber compounds was investigated mainly by rheological measurements in this doctoral thesis, in the next step it should be focused on the investigation of this effect by dielectric spectroscopy since carbon black is a conductive material able to form a percolating filler network in matrix. Initial examinations using dielectric spectroscopy have been carried out but observed results are not satisfactory enough to be published at this stage.

The initial effort to use computer simulations in order to model the flocculation phenomena of filler aggregates in polymer matrix has been performed. However, extended research in the field of simulations would be

necessary to observe relevant data from the simulations. In the further work, the model aggregates should be replaced by real filler (e.g. carbon black) aggregates. LJ units should be replaced by SI units and experimentally observed data should be used for the purpose of the simulation. Interaction energy between carbon black aggregates and properties of the matrix such as viscosity should be set. Still, there is a lot of potential in the simulation of the carbon black aggregation process and authors would like to continue this work since not many institutions have the capacity to connect the experimental work with the theoretical investigation in order to observe compact information on this process.

LIST OF SYMBOLS AND ABBREVIATIONS

%	Percentage
Π	Osmotic pressure
Å	Angström, unit of length equal to 0.1 nanometres
°C	Degrees of Celsius
ΔG	The Gibbs free energy
μm	micrometre
γ(%)	Dynamic shear strain in percentage
ASTM	American Society for Testing and Materials
BET	Brunauer-Emmett-Teller, a technique for the evaluation of specific surface area
BR	Butadiene rubber
cca	Circa – around, about
CCA	Cluster-cluster aggregation
CDBP	Dibutyle phtalate, an oil absorption technique for the evaluation of carbon black structure of compressed sample
COAN	Oil absorption number of compressed sample, a technique for the evaluation of carbon black structure
CTAB	Cetyltrimethyl ammonium bromide, a technique for the evaluation of specific surface area
D_0	The diffusion coefficient
d_f	Fractal dimension
DBP	Dibutyle phtalate, an oil absorption technique for the evaluation of carbon black structure
DLA	Diffusion-limited aggregation

DLCA	Diffusion-limited cluster-cluster aggregation
DLVO	The theory developed independently by Derjaguin and Landau (1941) and Verwey and Overbeek (1948) describing Van der Waals attraction and electric double layer repulsion
e.g.	Exampli gratia – for example
EPDM	Ethylene-propylene diene rubber
et al.	et (“and”) and alii (“others”), and others
etc.	Etcetera
FT	Faculty of technology
g	Gram
G'	Storage modulus
G''	Loss modulus
$g.cm^{-3}$	Grams per cubic centimetre
$g.mol^{-1}$	Grams per mole
GM	Geometrical mean
H-NMR	(Hydrogen-1 NMR, or 1H NMR) is the application of nuclear magnetic resonance in NMR spectroscopy with respect to hydrogen-1nuclei within the molecules of a substance, in order to determine the structure of its molecules
hod.	Hour
Hz	Hertz
i.e.	Id est – that is
$kJ.mol^{-1}$	Kilojoules per mole
$m^2.g^{-1}$	Squared metres per gram
MBTS	Mercaptobenzothiazole

$mg.g^{-1}$	Milligrams per gram
min	Minute
min.	Minimally
ml	Millilitre
mm	Millimetre
$mm.min^{-1}$	Millimetres per minute
MPa	Megapascal
N_A	Avogadro's number, 6.022×10^{23} mol^{-1}
nm	Nanometre
NR	Natural rubber
nRM	No remix, a compound was not additionally remixed
OAN	Oil absorption number, a technique for the evaluation of carbon black structure
phr	Per hundred rubber
psi	Pounds per square inch
RLA	Reaction-limited aggregation
RLCA	Reaction-limited cluster-cluster aggregation
RM	Re-mix, a compound was additionally remixed
RPA	Rubber process analyzer
RPST	Rapid Payne Softening Test
s^{-1}	Reciprocal second
SBR	Styrene-butadiene rubber
SEM	Scanning electron microscopy

SPST	Standard Payne Softening Test
SSA	Specific surface area
STSA	Statistical thickness surface area, a technique for the evaluation of specific surface area
UTB/TBU	Univerzita Tomáše Bati ve Zlíně/Tomas Bata University in Zlín
viz	Videre licet – it may be seen, evidently, clearly
VV	Void volume

LIST OF FIGURES

LIST OF TABLES

LIST OF EQUATIONS

LIST OF PUBLICATIONS

PATENT

2014 J. Kadlcak (50%), R. Cermak. Reference Object for Topography of Materials. Czech Patent CZ 304580 B6. 2014.

PAPERS

1. L.B. Tunnicliffe, J. Kadlcak, Y. Shi, et al. Flocculation and Viscoelastic Behaviour in Carbon Black-Filled Natural Rubber. Macromol Mater Eng 2014; DOI: 10.1002/mame.201400117.

2. J. Kadlcak (50%), L.B. Tunnicliffe, J. Lacayo, et al. Rapid Payne Effect Test – A Novel Method for Study of Strain-Softening Behavior of Rubbers Filled with Various Carbon Blacks. – Manuscript number POTE-D-14-00258 (Polymer Testing). – Submitted, under review.

3. J. Kadlcak (60%), R. Cermak, P. Ponizil et al. The Evaluation of Carbon Black Structure Using Mechanical Compression. (Polymer testing). – Manuscript in preparation.

CONFERENCE CONTRIBUTIONS

1. J. Kadlcak (50%), P. Konecny, R. Cermak, et al.. The Effect of ZnO Modification on Rubber Compound Properties. Recent Research in Geography, Geology, Energy, Environment and Biomedicine, WSEAS. Greece 2011; p. 347–352. ISBN 978-1-61804-022-0.

2. J. Kadlcak (80 %), J. Lacayo, R. Cermak, et al.. The Influence of Mixing on the Flocculation Time of Carbon Black Aggregates in Rubber Compounds. Plastko Conference 2012, Tomas Bata University in Zlín. Zlín 2012; p. 294–295. ISBN 978-80-7454-137-7.

3. J. Kadlcak (60%), L.B. Tunnicliffe, J.J.C. Busfield, et al.. Evaluation of Carbon Black Flocculation in Rubber Melts. Plastko Conference 2014, Tomas Bata University in Zlín 2014; p. 428-438. ISBN 978-80-7454-335-7.

4. J. Kadlcak (60%), L.B. Tunnicliffe, J.J.C. Busfield, et al.. Evaluation of Carbon Black Flocculation in Natural Rubber Melts. RubberCon 2014, Manchester 2014; p. 1-9. ISBN 1-86125-176-9.

PROOF OF CONCEPT

2012 I. Kuritka, J. Kadlcak (45%), R. Cermak. ZnO Activator of Sulfur Vulcanization with a Prolonged Scorch Time. The proof of concept no. 28110. 2012.

THESES

1. J. Kadlcak. Ionomers. Bachelor thesis. Tomas Bata University in Zlín 2008.

2. J. Kadlcak. The Effect of ZnO Modification on the Rubber Compound Properties. Master thesis. Tomas Bata University in Zlín 2010.

CURRICULUM VITAE

Ing. Jakub Kadlcak

Pricni 729
Napajedla 763 61
The Czech Republic
kadlcak@gmail.com
+420723045903

Polymer Engineer, Tomas Bata University in Zlín

Education

2010 – 2014. Tomas Bata University in Zlín, Zlín, The Czech Republic
Study programme: Technology of Macromolecular Compounds, Ph.D.
Buddy Student System

2013 – 2014. Queen Mary University of London, London, The Great Britain
Soft Matter Group
Supervisors: Prof. James Busfield, Dr. Lorenzo Botto.
Study/research internship
Research topic: The flocculation process of carbon black in rubber compound melts

2008 – 2010. Tomas Bata University in Zlín, Zlín, The Czech Republic
Study programme: Polymer Engineering, Ing.
Buddy Student System

2008. Chalmers University of Technology in Gothenburg, Gothenburg, Sweden.
Study internship
Study programme: Material Engineering

2005 – 2008. Tomas Bata University in Zlín, Zlín, The Czech Republic
Study programme: Chemistry and Technology of Materials, Bc.

Internship **2011. Continental Reifen Deutschland GmbH, Hannover, Germany**
Chemical and Material Laboratories
Supervisor: Prof. Jorge Lacayo-Pineda
Research internship
Research topics: The characterisation of a carbon black structure using a new method called Void Volume, Rheology of rubber compounds

Language skills English course in Cambridge, England
English for Engineers course at Chalmers University of Technology in Gothenburg, Sweden
English – professional communication
Spanish – beginner
German – basics

Projects

2014 Centre of Competence, "AlterBio", Zlín, Czech Republic (Alternative environment friendly high effective polymer antimicrobial agents for industrial applications), member of research team

2013 The verification of Leonov model, Continental, Hannover, Germany, member of research team

2013 IGA/FT/2013/012, Tomas Bata University in Zlín, Czech Republic (Controlling of polymer properties by additives addition and process parameters modification), member of research team

2013 Centre of Competence, SPUR a.s., Zlín, Czech Republic (Additives increasing strength and stability of polymer melts), member of research team

2012 IGA/FT/2012/040, Tomas Bata University in Zlín, Czech Republic (Novel approaches in polymer manufacturing, structure controlling and properties evaluation), member of research team

2012 Centre of Polymer Systems (reg. number: CZ.1.05/2.1.00/03.0111), Tomas Bata University in Zlín, Czech Republic, member of research team

2012 IPIC Implementation I, Barum Continental, Otrokovice, Czech Republic (Identification of cobalt/halobutyl rubber), member of research team

2012 IPIC Implementation II, Barum Continental, Otrokovice, Czech Republic (Compound identification at tread extrusion), member of research team

2011 COBOL, Continental, Hannover, Germany (Electrical capacity of rubber compounds), member of research team

2011 INSPEC, Continental, Hannover, Germany (Void Volume Tester implementation), member of research team

LIST OF APPENDICES

APPENDIX A.

J. KADLCAK (50%), R. CERMAK. REFERENCE OBJECT FOR TOPOGRAPHY OF MATERIALS. CZECH PATENT CZ 304580 B6. 2014.

APPENDIX B.

THE LAMMPS SCRIPT FOR SIMULATION OF 27 AGGREGATES IN CONTINUUM.

APPENDIX C.

L.B. TUNNICLIFFE, J. KADLCAK, Y. SHI, ET AL. FLOCCULATION AND VISCOELASTIC BEHAVIOUR IN CARBON BLACK-FILLED NATURAL RUBBER. MACROMOL MATER ENG 2014; DOI: 10.1002/MAME.201400117.

APPENDIX A.

J. KADLCAK (50%), R. CERMAK. REFERENCE OBJECT FOR TOPOGRAPHY OF MATERIALS. CZECH PATENT CZ 304580 B6. 2014.

PATENTOVÝ SPIS

(11) Číslo dokumentu:

304 580

(13) Druh dokumentu: **B6**

(51) Int. Cl.:

G01N 21/93	(2006.01)
G01N 33/44	(2006.01)
C08J 3/20	(2006.01)
G01N 1/28	(2006.01)
G01N 15/02	(2006.01)

(19) ČESKÁ REPUBLIKA

ÚŘAD PRŮMYSLOVÉHO VLASTNICTVÍ

(21) Číslo přihlášky: **2013-314**

(22) Přihlášeno: **26.04.2013**

(40) Zveřejněno: **16.07.2014**
(Věstník č. 29/2014)

(47) Uděleno: **04.06.2014**

(24) Oznámení o udělení ve věstníku: **16.07.2014**
(Věstník č. 29/2014)

(56) Relevantní dokumenty:

JP S 57114840; CN 102936355; WO 2007/122930 A1; US 6174728 B1; US 5304324.

(73) Majitel patentu:
Univerzita Tomáše Bati ve Zlíně, Zlín, CZ

(72) Původce:
Ing. Jakub Kadlčák, Napajedla, CZ
doc. Ing. Roman Čermák, Ph.D., Zlín, CZ

(74) Zástupce:
UTB ve Zlíně, Univerzitní institut, Ing. Jan Görig, Nám. T. G. Masaryka 5555, 760 01 Zlín

(54) Název vynálezu:
Etalon k hodnocení topografie materiálů

(57) Anotace:
Řešení se týká etalonu k hodnocení topografie materiálů, který je určen ke kalibraci přístroje hodnotícího kvalitu makro-disperze plniv. Etalon je zhotoven z dvoufázového kompozitního materiálu na bázi spojité fáze a inertních částic globulárních tvarů o rozměrech od 0,5 do 500 mikrometrů a úzké distribuci velikosti částic s variačním koeficientem do hodnoty 1. Spojitou fázi může tvořit polymerní matrice na bázi elastomeru, zejména pak silikonového kaučuku, polymerní matrice na bázi termoplastu nebo polymerní matrice na bázi reaktoplastu. V jiném provedení etalonu může spojitou fázi tvořit také nízkomolekulární organický materiál jako vosk, parafínový olej nebo lepidlo. Inertními částicemi globulárních tvarů jsou s výhodou skleněné kuličky, mohou jí být ale také částice organického původu, například částice sazí, keramické kuličky nebo i kovové kuličky.

CZ 304580 B6

Etalon k hodnocení topografie materiálů

Oblast techniky

Vynález se týká etalonu k hodnocení topografie materiálů, který je určen ke kalibraci přístroje hodnotícího kvalitu makro–disperze plniv.

Dosavadní stav techniky

V současné době se za účelem hodnocení kvality disperze plniva využívá v gumárenském průmyslu řada metod. Důvodem je skutečnost, že úroveň disperze plniva výrazně ovlivňuje výkonnost a vlastnosti finálních produktů jako např. pneumatik. Kvalita zamíchání plniva se popisuje hodnotou makro–disperze plniva. Tento parametr je definován jako distribuce aglomerátů plniva menších než 100 mikrometrů, ale větších než 2 mikrometry ve směsi a reprezentuje mikro oblast aglomerace. Jednou z nejrozšířenějších metod užívaných pro hodnocení kvality makro–disperze ztužujících plniv (jako jsou silika, saze nebo jiná inertní plniva – např. vápenec a jíl) je, především z důvodu její rychlosti a relativní jednoduchosti, technika pracující na základě principu vyhodnocování povrchové nerovnosti čerstvě připraveného řezu vzorku pomocí optické mikroskopie pracující v reflexním módu. Tato standardizovaná metoda (popsaná v mezinárodní normě ASTM D7723–11 s názvem „Standard Test Method for Rubber Property – Macro–Dispersion of Fillers in Compounds“) využívá algoritmů ke kvantifikaci hrubosti povrchu čerstvě připraveného vzorku měřené za pomoci optické metody, kdy jsou velké aglomeráty, během přípravy vzorku řezáním, zatlačeny na jednu nebo druhou stranu řezu a vytváří tak profilovaný povrch. Příprava vzorku z nevulkanizované směsi je popsána v dokumentu US 6 795 172 s názvem „Metoda pro přípravu nevytvrzených kaučukových vzorků pro měření disperze plniv“. Světelný mikroskop je vybaven CCD nebo CMOS senzorem zaznamenávajícím snímky povrchu. Mikroskop pracuje v temném poli, kdy je vzorek za účelem analýzy ozařován světlem dopadajícím pod úhlem 30°. Paprsky světla dopadající na povrchové nerovnosti reprezentující nedispergované plnivo jsou odráženy směrem do senzoru, který je zaznamenává a paprsky dopadající na povrch bez nerovností – povrch hladký, jsou odráženy směrem pryč od senzoru a na snímku se jeví jako tmavá oblast. Snímek povrchu je digitalizován a jako binární obrázek analyzován softwarem k tomu určeným. Postup analýzy je standardizován a popsán v mezinárodní normě ISO 11345/B s názvem „Rubber – Assessment of Carbon Black and Carbon Black/Silica Dispersion – Rapid Comparative Methods“. Z binárního obrázku je vypočten poměr bílé plochy reprezentující nerovnosti povrchu a celkové plochy snímku podle normy ASTM D7723–11 a tento poměr v procentech udává celkovou kvalitu makro–disperze plniva ve směsi.

Zkoušky prováděné na kaučukových směsích se v gumárenské praxi provádějí z důvodu zjištění vlastností a chování materiálů. Zjištěné charakteristiky následně mohou sloužit k monitorování výrobních a zpracovatelských procesů a v neposlední řadě k řízení kvality surovin, polotovarů i finálních výrobků. Gumárenské materiály se vyznačují vysokou molekulární hmotností a jsou charakteristické velmi složitým viskoelastickým chováním, kdy jsou schopny velmi vysokých vratných deformací až 1000 % při nízké stlačitelnosti. Díky tomuto chování je poměrně komplikované jejich zpracování. Vlastnosti těchto materiálů se potom liší v závislosti na složení jednotlivých směsí a typů použitých složek ve směsi. Jednotlivé zkoušky a jejich podmínky je potom nutné vybírat s ohledem na tuto variabilitu kaučukových směsí, protože viskoelastická odezva se bude lišit podle teploty testování, frekvence namáhání, velikosti vložené deformace vzorku a dalších parametrů testů. Velmi důležitá u gumárenských zkoušek je také příprava zkušebních vzorků, jejíž důkladnost může mít vliv na výsledky zkoušek, a dále historie zkušebních těles, jako stáří a podmínky skladování. Obecně platí fakt, že zkoušení vzorků by mělo probíhat za podmínek, které maximálně kopírují podmínky při praktické aplikaci hotového výrobku.

Podstata vynálezu

Uvedené nevýhody a nedostatky dosud známých řešení do značné míry odstraňuje etalon k hodnocení topografie materiálů, určený ke kalibraci přístroje hodnotícího kvalitu makro–disperze plniv podle vynálezu. Podstata vynálezu spočívá v tom, že tento etalon je zhotoven z dvoufázového kompozitního materiálu na bázi spojité fáze a inertních částic globulárních tvarů, jako jsou skleněné kuličky, kovové kuličky nebo částice sazí o rozměrech od 0,5 do 500 mikrometrů a úzké distribuci velikosti částic s variačním koeficientem do hodnoty 1.

Preferované rozměry inertních částic globulárních tvarů jsou od 0,5 do 25 mikrometrů, jejich obsah činí s výhodou 1 až 100 hmotnostních dílů na 100 hmotnostních dílů spojité fáze.

Spojitou fázi může tvořit polymerní matrice na bázi elastomeru, zejména pak silikonového kaučuku, polymerní matrice na bázi termoplastu nebo polymerní matrice na bázi reaktoplastu. V jiném provedení etalonu může spojitou fázi tvořit také nízkomolekulární organický materiál jako vosk, parafinový olej nebo lepidlo.

Inertními částicemi globulárních tvarů jsou s výhodou skleněné kuličky, mohou jí být ale také částice organického původu, například saze, keramické kuličky nebo i kovové kuličky.

Etalon k hodnocení topografie materiálů podle vynálezu zlepšuje proces vyhodnocení kvality makro–disperze plniva na základě drsnosti čerstvě připraveného povrchu vzorku především tím, že slouží ke kalibraci přístroje měřícího makro–disperzi směsi na základě topografie povrchu.

Přehled obrázků na výkresech

K bližšímu objasnění podstaty vynálezu slouží přiložené výkresy, kde představuje

Obr. 1 – Schematické znázornění principu optického mikroskopu pracujícího v temném poli.

Obr. 2 – Grafické znázornění standardní distribuce velikostí aglomerátů sazí.

Obr. 3 – Grafické znázornění úzké distribuce velikostí skleněných kuliček (je užší než v případě sazových aglomerátů).

Příklady provedení vynálezu

Příklad 1

Etalon k hodnocení topografie materiálů je zhotoven z dvoufázového kompozitního materiálu, který obsahuje jako spojitou fázi 100 hmotnostních dílů silikonového kaučuku s 10 hmotnostními díly síťovacího činidla a 1 hmotnostní díl inertních částic globulárních tvarů – konkrétně skleněných kuliček o velikosti 0,5 až 25 mikrometrů, s úzkou distribucí velikosti částic s variačním koeficientem do hodnoty 1 (graficky znázorněnou na Obr. 3).

Při přípravě etalonu se silikonový kaučuk v kapalném stavu odměří v požadovaném množství do kádinky, kde je smíchán se síťovacím činidlem. Následně je přidáno specifikované množství skleněných kuliček. Získaná směs je míchána za pokojové teploty elektrickým míchadlem po dobu 5 minut rychlostí 300 otáček/min. Suspenze je pak přenesena do nádobky o požadované velikosti a tvaru etalonu tak, aby plocha zkoumaného řezu vzorku mohla být v souladu s normou ASTM D7723, minimálně 5 x 5 milimetrů. Následně je nádobka obsahující suspenzi vložena do vakuové sušárny na dobu minimálně půl hodiny za účelem odstranění vzduchu (alternativně je

také možné použít exikátoru). Po odstranění vzduchu se nádobka ohřívá na teplotu 40±5 °C, která se udržuje po dobu minimálně 1,5 hodiny, až do doby dokončení síťovací reakce.

Připravený etalon je určen ke kalibraci přístroje hodnotícího kvalitu makro–disperze plniv – světelného mikroskopu vybaveného CCD nebo CMOS senzorem zaznamenávajícím snímky povrchu připraveného řezu. Mikroskop (viz schéma na Obr. 1) pracuje v temném poli, kdy je vzorek 1 za účelem analýzy ozařován světlem ze světelného zdroje 4 dopadajícím pod úhlem 30°. Paprsky světla dopadající na povrchové nerovnosti reprezentující nedispergované plnivo jsou odráženy přes objektiv 2 s optikou do senzoru 3, který je zaznamenává a paprsky dopadající na povrch bez nerovností – hladký povrch, jsou odráženy směrem pryč od senzoru a na snímku se objeví jako tmavá oblast. Snímek povrchu je digitalizován a jako binární obrázek analyzován softwarem k tomu určeným.

Příklad 2

Etalon k hodnocení topografie materiálů je zhotoven z dvoufázového kompozitního materiálu, který obsahuje jako spojitou fázi polypropylenovou matrici plněnou 5 hmotnostními díly skleněných kuliček o úzké distribuci velikosti částic frakce v intervalu 25 až 75 mikrometrů.

Při přípravě etalonu je polypropylen v čase nula v podobě granulí vpraven do komory integrálního hnětače vyhřáté na 200 °C a je homogenizován po dobu 2 minuty při rychlosti 20 otáček/min. Po této době je přidáno specifikované množství kuliček a otáčky jsou v průběhu 1 minuty, za současného míchání směsi, kontinuálně zvyšovány na hodnotu 50 otáček/min. Při této rychlosti je směs míchána ještě další 4 minuty a proces míchání je ukončen vyjmutím směsi z komory. Jedná se o jednostupňové míchání. Po vychladnutí jsou ze zamíchaného materiálu připraveny zkušební vzorky.

Příklad 3

Etalon k hodnocení topografie materiálů je zhotoven z dvoufázového kompozitního materiálu, který obsahuje jako spojitou fázi reaktoplastovou matrici připravenou ze 100 hmotnostních dílů Bisfenolu A diglycidyleteru, 6 hmotnostních dílů dietylentriaminu a 10 hmotnostních dílů skleněných kuliček o úzké distribuci velikosti částic frakce v intervalu 75 až 150 mikrometrů.

Při přípravě etalonu se Bisfenol A diglycidyleter v požadovaném množství odměří do kádinky, kde je při teplotě 80 °C a rychlosti míchání 300 otáček/min smíchán se skleněnými kuličkami. Po vychladnutí je přimíchán dietylentriamin a směs je pak přenesena do nádobky o požadované velikosti a tvaru etalonu tak, aby plocha zkoumaného řezu vzorku mohla být v souladu s normou ASTM D7723, minimálně 5 x 5 milimetrů. Následně je nádobka obsahující směs vložena do vakuové sušárny na dobu minimálně půl hodiny za účelem odstranění vzduchu (to je také možné za použití exsikátoru). Po odstranění vzduchu se nádobka ohřívá na teplotu 80±5 °C, která se udržuje po dobu cca 8 hodin a po této době se teplota na 2 hodiny zvýší na 120 °C, z důvodu úplného dokončení síťovací reakce.

Příklad 4

Etalon k hodnocení topografie materiálů je zhotoven z dvoufázového kompozitního materiálu, který obsahuje spojitou fázi na bázi dvousložkového lepidla, tvořeného z 50 hmotnostních dílů polystyrenu rozpuštěného ve 100 hmotnostních dílech acetonu, naneseného na laboratorní sklíčko. V tomto dvousložkovém lepidle je ručně rozmícháno 15 hmotnostních dílů skleněných kuliček o úzké distribuci velikosti částic frakce v intervalu 150 až 300 mikrometrů.

Příklad 5

Etalon k hodnocení topografie materiálů je zhotoven z dvoufázového kompozitního materiálu, který obsahuje jako spojitou fázi 100 hmotnostních dílů silikonového kaučuku s 10 hmotnostními díly síťovacího činidla a 25 hmotnostních dílů inertních částic globulárních tvarů – konkrétně skleněných kuliček o velikosti 300 až 450 mikrometrů, s úzkou distribucí velikosti částic s variačním koeficientem do hodnoty 1 (graficky znázorněnou na Obr. 3).

Při přípravě etalonu se silikonový kaučuk v kapalném stavu odměří v požadovaném množství do kádinky, kde je smíchán se síťovacím činidlem. Následně je přidáno specifikované množství skleněných kuliček. Získaná směs je míchána za pokojové teploty elektrickým míchadlem po dobu 5 minut rychlostí 300 otáček/min. Suspenze je pak přenesena do nádobky o požadované velikosti a tvaru etalonu tak, aby plocha zkoumaného řezu vzorku mohla být v souladu s normou ASTM D7723, minimálně 5 x 5 milimetrů. Následně je nádobka obsahující suspenzi vložena do vakuové sušárny na dobu minimálně půl hodiny za účelem odstranění vzduchu (alternativně je také možné použít exsikátoru). Po odstranění vzduchu se nádobka ohřívá na teplotu 40±5 °C, která se udržuje po dobu minimálně 1,5 hodiny, až do doby dokončení síťovací reakce.

Příklad 6

Etalon k hodnocení topografie materiálů je zhotoven z dvoufázového kompozitního materiálu, který obsahuje jako spojitou fázi 100 hmotnostních dílů silikonového kaučuku s 10 hmotnostními díly síťovacího činidla a dále 1 až 100 hmotnostních dílů sazí standardně užívaných v gumárenské výrobě a definovaných dle mezinárodní normy ASTM D1765–10. Příkladná distribuce velikostí aglomerátů sazí je graficky znázorněna na Obr. 2.

Při přípravě etalonu se silikonový kaučuk v kapalném stavu se v požadovaném množství odměří do kádinky, kde je smíchán se síťovacím činidlem. Následně je přidáno specifikované množství sazí. Tato směs je míchána za pokojové teploty elektrickým míchadlem po dobu 5 minut rychlostí 300 otáček/min. Suspenze je pak přenesena do nádobky o požadované velikosti a tvaru etalonu tak, aby plocha zkoumaného řezu vzorku mohla být v souladu s normou ASTM D7723, minimálně 5 x 5 milimetrů. Následně je nádobka obsahující suspenzi vložena do vakuové sušárny na dobu minimálně půl hodiny za účelem odstranění vzduchu (také je možné použít exsikátoru). Po odstranění vzduchu se nádobka ohřívá na teplotu 40±5 °C, která se udržuje po dobu minimálně 1,5 hodiny, až do doby dokončení síťovací reakce.

Příklad 7

Etalon k hodnocení topografie materiálů je zhotoven z dvoufázového kompozitního materiálu, který obsahuje jako spojitou fázi 100 hmotnostních dílů silikonového kaučuku s 10 hmotnostními díly síťovacího činidla a 30 hmotnostních dílů inertních částic globulárních tvarů – konkrétně kovových kuliček o úzké distribuci velikosti částic frakce v intervalu 350 až 500 mikrometrů.

Při přípravě etalonu se silikonový kaučuk v kapalném stavu odměří v požadovaném množství do kádinky, kde je smíchán se síťovacím činidlem. Následně je přidáno specifikované množství kovových kuliček. Získaná směs je míchána za pokojové teploty elektrickým míchadlem po dobu 5 minut rychlostí 300 otáček/min. Suspenze je pak přenesena do nádobky o požadované velikosti a tvaru etalonu tak, aby plocha zkoumaného řezu vzorku mohla být v souladu s normou ASTM D7723, minimálně 5 x 5 milimetrů. Následně je nádobka obsahující suspenzi vložena do vakuové sušárny na dobu minimálně půl hodiny za účelem odstranění vzduchu (alternativně je také možné použít exsikátoru). Po odstranění vzduchu se nádobka ohřívá na teplotu 40±5 °C, která se udržuje po dobu minimálně 1,5 hodiny, až do doby dokončení síťovací reakce.

Průmyslová využitelnost

Vynález je možno využít pro kalibraci přístroje pro hodnocení makro–disperze sazí a/nebo dalších částic ve spojité matrici.

PATENTOVÉ NÁROKY

1. Etalon pro hodnocení topografie materiálů, určený ke kalibraci přístroje hodnotícího kvalitu makro–disperze plniv, **vyznačující se tím**, že je zhotoven z dvoufázového kompozitního materiálu na bázi spojité fáze a inertních částic globulárních tvarů, jako jsou skleněné kuličky, kovové kuličky nebo částice sazí o rozměrech od 0,5 do 500 mikrometrů a úzké distribuci velikosti částic s variačním koeficientem do hodnoty 1.

2. Etalon podle nároku 1, **vyznačující se tím**, že preferované rozměry inertních částic globulárních tvarů jsou od 0,5 do 25 mikrometrů při úzké distribuci velikosti částic s variačním koeficientem do hodnoty 1.

3. Etalon podle nároku 1, **vyznačující se tím**, že obsah inertních částic globulárních tvarů činí 1 až 100 hmotnostních dílů na 100 hmotnostních dílů spojité fáze.

4. Etalon podle nároku 1, **vyznačující se tím**, že spojitou fázi tvoří polymerní matrice na bázi elastomeru, zejména pak síťovaného silikonového kaučuku.

5. Etalon podle nároku 1, **vyznačující se tím**, že spojitou fázi tvoří polymerní matrice na bázi termoplastu.

6. Etalon podle nároku 1, **vyznačující se tím**, že spojitou fázi tvoří polymerní matrice na bázi reaktoplastu.

7. Etalon podle nároku 1, **vyznačující se tím**, že spojitou fázi tvoří nízkomolekulární organický materiál jako vosk, parafinový olej nebo lepidlo.

8. Etalon podle nároku 1, **vyznačující se tím**, že inertními částicemi globulárních tvarů jsou skleněné kuličky.

9. Etalon podle nároku 1, **vyznačující se tím**, že inertními částicemi globulárních tvarů jsou saze.

10. Etalon podle nároku 1, **vyznačující se tím**, že inertními částicemi globulárních tvarů jsou kovové kuličky.

2 výkresy

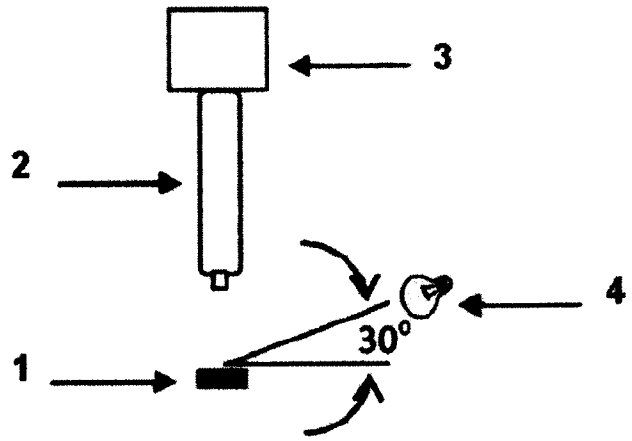
3
2
4
30°
1

Obr. 1

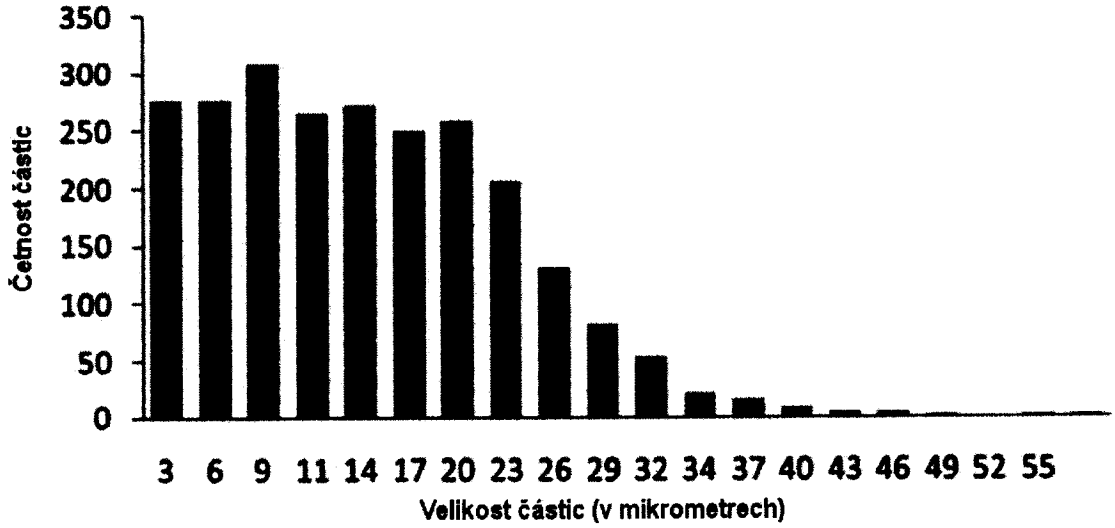
350
300
250
200
150
100
50
0
Četnost částic
3 6 9 11 14 17 20 23 26 29 32 34 37 40 43 46 49 52 55
Velikost částic (v mikrometrech)

Obr. 2

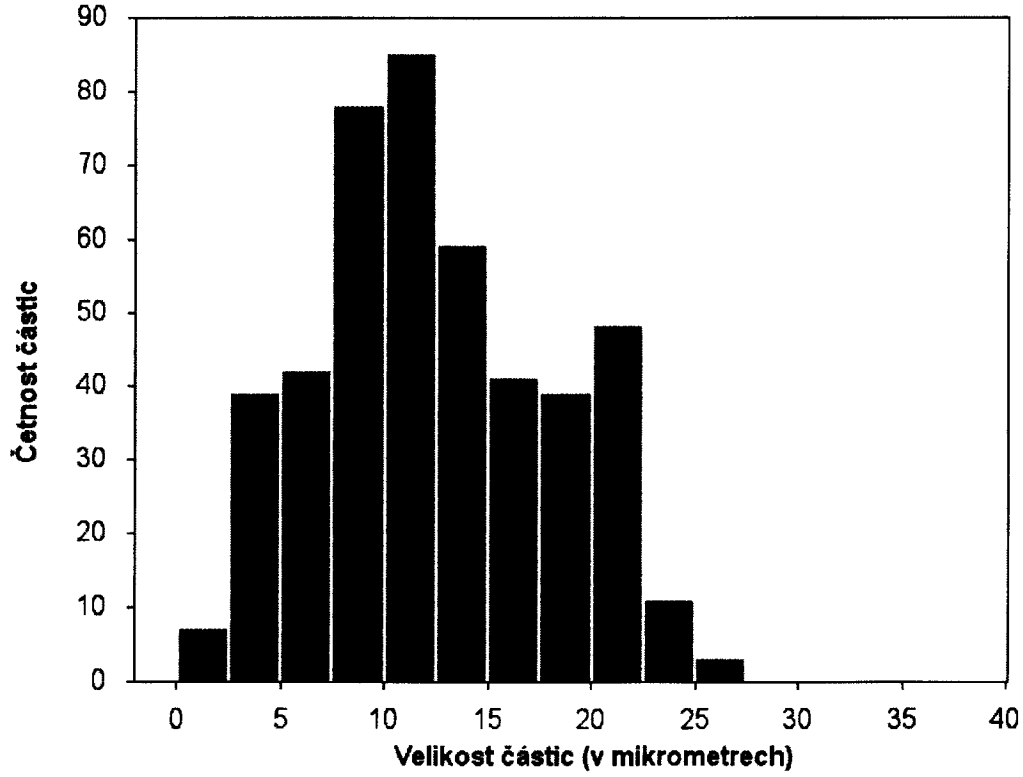

Obr. 3

Konec dokumentu

APPENDIX B.

THE LAMMPS SCRIPT FOR SIMULATION OF 27 AGGREGATES IN CONTINUUM

```
# 27 rigid aggregates composed of 16 point particles each -
Brownian dynamics

units          lj

atom_style     atomic

pair_style     lj/cut 2.5

read_data      datainput_atomic_27agg16p_new.txt

mass           * 1

pair_coeff     * * 1 1

velocity       all create 100.0 4928459


group          clump1 id <> 1 16

group          clump2 id <> 17 32

group          clump3 id <> 33 48

group          clump4 id <> 49 64

group          clump5 id <> 65 80

group          clump6 id <> 81 96

group          clump7 id <> 97 112

group          clump8 id <> 113 128

group          clump9 id <> 129 144

group          clump10 id <> 145 160

group          clump11 id <> 161 176

group          clump12 id <> 177 192

group          clump13 id <> 193 208

group          clump14 id <> 209 224

group          clump15 id <> 225 240

group          clump16 id <> 241 256

group          clump17 id <> 257 272

group          clump18 id <> 273 288
```

```
group          clump19 id <> 289 304

group          clump20 id <> 305 320

group          clump21 id <> 321 336

group          clump22 id <> 337 352

group          clump23 id <> 353 368

group          clump24 id <> 369 384

group          clump25 id <> 385 400

group          clump26 id <> 401 416

group          clump27 id <> 417 432


fix            1 all rigid group 27 clump1 clump2 clump3 clump4
               clump5  clump6  clump7  clump8  clump9  clump10
               clump11 clump12 clump13 clump14 clump15 clump16
               clump17 clump18 clump19 clump20 clump21 clump22
               clump23 clump24 clump25 clump26 clump27


neigh_modify   exclude group clump1 clump1

neigh_modify   exclude group clump2 clump2

neigh_modify   exclude group clump3 clump3

neigh_modify   exclude group clump4 clump4

neigh_modify   exclude group clump5 clump5

neigh_modify   exclude group clump6 clump6

neigh_modify   exclude group clump7 clump7

neigh_modify   exclude group clump8 clump8

neigh_modify   exclude group clump9 clump9

neigh_modify   exclude group clump10 clump10

neigh_modify   exclude group clump11 clump11

neigh_modify   exclude group clump12 clump12

neigh_modify   exclude group clump13 clump13
```

```
neigh_modify   exclude group clump14 clump14
neigh_modify   exclude group clump15 clump15
neigh_modify   exclude group clump16 clump16
neigh_modify   exclude group clump17 clump17
neigh_modify   exclude group clump18 clump18
neigh_modify   exclude group clump19 clump19
neigh_modify   exclude group clump20 clump20
neigh_modify   exclude group clump21 clump21
neigh_modify   exclude group clump22 clump22
neigh_modify   exclude group clump23 clump23
neigh_modify   exclude group clump24 clump24
neigh_modify   exclude group clump25 clump25
neigh_modify   exclude group clump26 clump26
neigh_modify   exclude group clump27 clump27

dump           2 all xyz 10 dump.floc_atomic_27new.xyz

thermo         100
timestep       1e-4
run            100000
```

APPENDIX C.

L.B. TUNNICLIFFE, J. KADLCAK, Y. SHI, ET AL. FLOCCULATION AND VISCOELASTIC BEHAVIOUR IN CARBON BLACK-FILLED NATURAL RUBBER. MACROMOL MATER ENG 2014; DOI: 10.1002/MAME.201400117.

mame.201400117

Flocculation and Viscoelastic Behaviour in Carbon Black-Filled Natural Rubber

Lewis B. Tunnicliffe, Jakub Kadlcak, Michael D. Morris, Ye Shi, Alan G. Thomas, James J. C. Busfield*

The process of particulate flocculation in natural rubber melts and subsequently crosslinked samples is investigated using carbon blacks of varying surface free energy, surface area and morphology. The surface free energies are varied via thermal treatment of the carbon blacks (graphitization). Reduction in surface free energy of the particulates accelerates the flocculation processes in the melt as measured by rheological experiments and reduces the percolation volume fraction threshold as determined by D/C conductivity measurements. The consequent effects on amplification of the small strain storage moduli of the crosslinked compounds are dramatic. Reduced polymer–filler interactions result in both an increased small strain modulus versus the unmodified carbon black-filled materials and an increased mechanical fragility of the fractal networks. Examination of the dynamic elastic moduli of carbon black samples loaded at volume fractions below the onset of network development reveal a significant temperature dependence isolated at the filler–rubber interface.

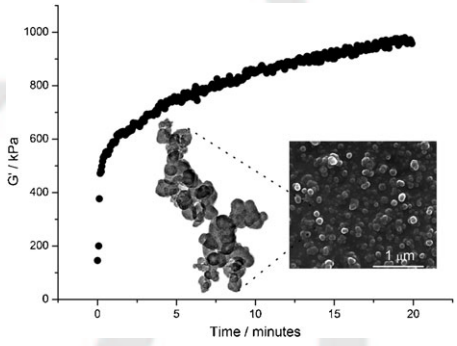

1. Introduction

The process of networking of carbon black particulates in rubber melts is of major industrial significance. What can broadly be termed the filler 'network' or 'structure' that evolves in filled rubber melts during shear and thermal processing is responsible for significant modifications of the melt rheology and processability of filled rubbers, the electrical properties of vulcanizates, the elastic stiffening and the strain-dependent viscoelasticity of filled elastomer products. Broadly, the nature of the filler network in crosslinked rubbers (elastomers) is dependent upon two key processes. Firstly the incorporation of filler into the rubber phase via mechanical mixing aims to break down agglomerated, often pelletised structures of the filler into individual rigid aggregates and then distribute these as effectively as possible throughout the rubber. Secondly, during subsequent thermal processing (vulcanization), the tendency of the filler particles to flocculate promotes the development of an agglomerated filler network. This paper focuses on the second process.

Many researchers have considered flocculation of carbon blacks and other particulate fillers in the polymer melt in terms of Brownian motion and particulate mobility via the particle diffusion coefficient given by the Stokes–Einstein equation (Equation 1 where δ is the diffusion coefficient, $\mathbf{k}$ the Boltzman constant, T the temperature, η the viscosity of the matrix, and r is the particle radius). The viscosity term, η, can be viewed as the effective viscosity experienced

Prof. J. J. C. Busfield, L. B. Tunnicliffe, Y. Shi, Prof. A. G. Thomas
Materials Research Institute, Queen Mary University of London, Mile End Road, London, E1 4NS, United Kingdom
E-mail: j.busfield@qmul.ac.uk
J. Kadlcak
Centre of Polymer Systems, University Institute, Thomas Bata University in Zlín, Nad Ovcirnou 3685, 760 01 Zlín, Czech Republic
Department of Polymer Engineering, Faculty of Technology, Thomas Bata University in Zlín, Nam. T. G. Masaryka 275, 762 72 Zlín, Czech Republic
Dr. M. D. Morris
Cabot Corporation, 157 Concord Road, Billerica, MA, USA

by the particle and can be a function of particle shape, boundary condition at the particle surface ~~and particle concentration.~~[1]

$$\delta = \frac{\mathbf{k}T}{\eta 6\pi r} \quad (1)$$

Gerspacher et al.[2] studied flocculation of carbon black in natural rubber (NR) and solution styrene butadiene rubber (S-SBR) using resistivity measurements. They highlighted the dependence of flocculation on factors such as carbon black loading, particle size and particle structure. Mihara et al.[3] examined precipitated silica flocculation processes in S-SBR. They determined an Arrhenius dependence for the kinetics of flocculation and calculated activation energies for the process of about 10 kJ · mol^{-1}. However Schwartz et al.[4] noted that carbon black flocculation may actually constitute several different physical processes. They found no evidence of filler particle mobility (Brownian motion) in the melt from TEM observations and so proposed that a contribution to the flocculation process arises from ~~time~~-dependent bridging of adjacent filler particles by polymer chains whereby a single chain becomes attached to two filler aggregates in close proximity.

The physical process of filler networking has also been described using percolation theory and diffusion-limited cluster–cluster aggregation (CCA) processes which generate flocculated structures of characteristic fractal dimensions.[5,6] It was further proposed on the basis of dielectric spectroscopy measurements of carbon black flocculation in various rubber melts that the polymer between filler aggregates plays a key role in determining the mechanical properties of the filler network. Meier and Klüppel[7] proposed that the gap size between aggregates dictates the dynamics of the entrapped polymer which effectively constitutes a filler–filler bond or a kind of viscoelastic glue between particles. They determined gap sizes experimentally through measurements of the electron tunnelling process between filler aggregates using dielectric spectroscopy.

The ~~above~~ studies note the importance of filler surface activity on the flocculation process. For carbon blacks the nature of the surface activity is dictated by the industrial production method. The spatial distribution of free energy at the surface of regular tire grade carbon blacks is highly heterogeneous. Depending on the grade of carbon black there exists to varying extents, regions of amorphous carbon interspersed with graphitic crystal layers and edges. Schröder et al.[8] identified four discrete types of energetic sites: isolated at the lateral surface of the graphitic crystals; the amorphous carbon regions between crystallites; at the crystallite edges and within slit-shaped cavities between graphitic layers present on the surfaces of a range of different carbon blacks. In addition, oxygen-containing chemical functionalities such as carboxyl, quinonic, phenol, and lactone groups have been identified on the carbon black surface. Both physical and chemical activities have been investigated in terms of physical interaction with polymer chains and also crosslinking chemistry.[9] Several investigations into rubber/elastomer reinforcement by carbon black have made use of the 'graphitization' technique to modify the physico-chemical activity of the carbon black surface and alter the nature of the filler–elastomer interfacial interaction.[10,11] During the graphitization process carbon black is exposed to high temperatures, often between 1 000 and 3 000 °C, under an inert atmosphere. This results in a reduction of the high energy sites on the particle surface by crystallization of amorphous carbon regions producing a growth of graphitic layers and results in a net reduction in the concentration of crystallite edges.

This work examines the effect of surface activity, particle size and particle morphology on the flocculation behaviour of carbon black in the natural rubber melt and in the subsequently crosslinked samples and attempts to relate the observed phenomena to underlying physical mechanisms.

2. Experimental Section

2.1. Graphitization of Carbon Blacks

Three different grades of carbon black were obtained from commercial suppliers. Physico-chemical properties of these fillers are provided in Table 1. For the graphitization process, 200 g of carbon black were placed inside a Carbolite STF tube furnace which was connected to a flushing nitrogen supply. The nitrogen was allowed to purge the samples and furnace chamber for a minimum of 6 h before the temperature was ramped to 1 250 °C at a rate of 10 K · min^{-1}. The peak temperature was held for 1 h before cooling to room temperature. Samples were removed from the furnace and stored under a nitrogen atmosphere until they were compounded with rubber.

2.2. Characterization of Carbon Black Particulates Prior to Incorporation into Rubber

A range of analyses were performed on the unmodified and graphitized carbon blacks (GCBs) to determine their physico-chemical characteristics.

2.2.1. Nitrogen Specific Surface Area

Nitrogen-specific surface areas were determined for each filler type using a Micrometrics BET-method surface area analyser.

2.2.2. Raman Spectroscopy

Crystallinity was determined by measuring the relative intensities of the D band, centred around 1 350 cm^{-1} and the G band, centred around 1 580 cm^{-1}. The percentage crystallinity of the carbon is defined as: % crystallinity $= I_G/(I_G + I_D)$, where I_G and I_D are the areas of the G and D bands. A calibration of this method of

Table 1. Physiochemical characteristics of the carbon black fillers.

Carbon black grade	Supplier	Surface area [$m^2 \cdot g^{-1}$]	L_A/Å	L_C/Å	Crystallinity [%]	Density [$g \cdot cm^{-3}$]	Surface Free Energy [$mJ \cdot m^{-2}$]
N134	Cabot	134	17.4	10.5	28.6	1.80[a)]	39.1
N134g	Modified	136	24.0	12.0	35.5	1.96	5.2
N330	Cabot	77	17.5	14.3	28.7	1.80[a)]	19.0
N330g	Modified	78	22.2	15.3	33.7	1.90	1.6
N990	Cancarb	8	20.6	16.5	32.2	1.80[a)]	17.5
N990g	Modified	8	32.3	19.4	45.6	1.95	6.9

[a)]Literature values from Donnet.[8]

crystallinity determination with X-ray diffraction (XRD) measurements has shown a correlation coefficient of 0.98. The in-plane crystallite dimension, L_A, was calculated using the formula, $L_A = 43.5(I_D/I_G)^{-1}$.

2.2.3. X-ray Diffraction

Powder XRD patterns were obtained for each carbon black sample between 10° and 40° 2θ on a Bruker D8 Advance diffractometer. Values of graphitic crystallite dimensions in the crystallographic *c*-axis were extracted from the basal reflection using the Scherrer equation (Equation 2 where L_C *is* the crystallite dimension along the *c*-axis, K is a shape factor taken as 0.9, β the line broadening of the basal peak at half maximum, λ the radiation wavelength and θ is the Bragg angle)).

$$L_C = \frac{K\lambda}{\beta \cos\theta} \quad (2)$$

2.2.4. Transmission Electron Microscopy (TEM)

Morphology of the carbon black filler particles was qualitatively determined by (TEM). Dilute particle dispersions were made by ultrasonicating small quantities of the particulates in ethanol for 10 min. A TEM grid was then dipped into the dispersion and the ethanol was evaporated prior to examination. A JEOL 2010 TEM was used to obtain the images.

2.2.5. Surface Free Energy (SFE) Determination

SFE is defined as the spreading pressure of water, π_e, in Equation (3) where R is the gas constant, T absolute temperature, A the specific surface area of the test sample, Γ the amount of adsorbed water in moles/g, P the partial pressure of water and P_0 is the saturation vapour pressure. Adsorption was measured using a Dynamic Vapor Sorption Instrument, manufactured by SMS instruments. 11 partial pressures were used, between 5 and 92% relative humidity, with 20 min equilibration at each level. Results are the average of duplicate samples.

$$\pi_e = \frac{RT}{A}\int_0^{P_0} \Gamma d \ln P \quad (3)$$

2.2.6. Helium Displacement Pyconometry

Densities of the graphitized fillers were determined by helium displacement using a Micrometrics AcuPyc 1330 Pycnometer. Graphitized fillers were rapidly transferred from the nitrogen storage atmosphere to the helium displacement cylinder and 10 sequential density determinations were performed. There was no significant drift in the sequential density values obtained indicating that little adsorption of atmospheric moisture onto the filler surfaces had occurred. For the unmodified carbon black samples, a literature value of 1.8 $g \cdot cm^{-3}$ obtained by Donnet[9] from XRD measurements was used.

2.3. Sample Preparation

The carbon blacks were compounded with SMR CV60 grade natural rubber supplied by the Tun Abdul Razak Research Centre (TARRC), Hertfordshire, UK. Masterbatch material was prepared using a Banbury-type Brabender laboratory internal mixer (tangential rotors) with a mixing chamber volume of 390 ml and a fill factor of 0.7. A warm-up mix was performed prior to the compounding. NR was added to the mixing chamber with a rotor speed of 70 rpm then the filler was added and mixed for 2 min. Rotors were stopped and filler caught on the chute was then swept down into the chamber and mixed for a further 5 min before dumping. Dump temperatures were around 150 °C. Density values determined from pyconometry were used to ensure a consistent volume fraction for each grade of filler equal to 0.20. This is equivalent to 50 parts per hundred (phr) mass loading of unmodified carbon black. A second mixing step was performed on a laboratory 2-roll mill to ensure effective dispersion of the particles. At this point samples were taken for the rheological investigations detailed below prior to addition of curatives. To prepare cured samples, 2 phr of dicumyl peroxide curative was added to the filled rubbers on the 2-roll mill. 2 mm thick cured sheets were prepared by compression moulding in a hot press. The cure time was 100 min at 150 °C. This was determined using an Alpha Technologies MDR2000 rheometer as the cure time required to achieve near total decomposition and reaction of the peroxide curative. Samples requiring lower filler loadings were prepared via back-addition of NR to the masterbatch on a two-roll mill.

2.4. Scanning Electron Microscopy (SEM)

Fracture surface morphology was evaluated for all the filled, crosslinked elastomers. Strips of sample were immersed in liquid nitrogen for 60 s and then fractured. Samples were mounted on an SEM stub with the fracture surface facing upwards. Samples were coated in gold and secondary electron images of the fracture surfaces were taken using an FEI Inspect SEM at various levels of magnification.

2.5. Rheological Testing

Rheological properties of the filled NR melts prior to the incorporation of curing chemicals were examined using a Rubber Process Analyser (RPA) from Alpha Technologies. The plate temperature was set to 150 °C and samples were loaded at room temperature. In an attempt to ameliorate strain and thermal histories of the samples, a rest period of 10 min was incorporated into the test procedure prior to the initiation of dynamic testing. Subsequently a dynamic shear strain sweep was performed between 0.067 and 10% strain. Then the shear strain was immediately dropped to 0.1% and dynamic properties were monitored for 20 min. The frequency for all testing was fixed at 1 Hz.

2.6. D/C Conductivity Testing

Strips of crosslinked samples were tested on a D/C electrical testing stage constructed according to ASTM D991-89 standard to determine their static volume resistivity values. The testing stage measured 4 point contact resistance. From Ohmic current–voltage plots the resistance was calculated and transformed to sample volume resistivity according to Equation (4) (where ρ is the volume resistivity, R the measured resistance and A and L are the cross sectional area and sample length, respectively).

$$\rho = \frac{RA}{L} \tag{4}$$

2.7. Dynamic Mechanical Properties

Temperature dependent dynamic mechanical properties of the filled elastomers were measured using a TA Instruments Q800 DMA with a double shear clamp geometry. Square samples were cut from sheets of elastomer and mounted into the clamp using a 5% compressive strain. A temperature sweep was performed from +50 to −100 °C at a ramp rate of $-5\ \mathrm{K \cdot min^{-1}}$ with a dynamic shear strain of 0.1% at a frequency of 1 Hz.

3. Results and Discussion

3.1. Morphology and Surface Properties of Carbon Blacks

Characterization data for the various types of carbon blacks are presented in Table 1. It is clear from the BET data that thermal processing of the fillers did not affect their surface areas significantly. Values of total crystallinity and lateral graphitic crystallite size (L_A) from Raman spectroscopy and orthogonal crystallite size (L_C) from XRD indicate a preferential lateral growth of crystalline regions within the carbon blacks during the thermal treatment. Densification of the carbon blacks upon graphitization was also observed. The effect of graphitization on the SFE of the particles is marked; with a significant drop in SFE seen for all graphitized fillers. Representative TEM images for the N134 series of carbon black are given in Figure 1. The micrographs show, in a qualitative sense, that the branched microstructure and primary particle size of the carbon black is retained after the graphitization process. This is also the case for the other carbon black grades investigated. It is apparent therefore that the process of graphitization has no significant effect on the filler morphologies or surface areas but fundamentally alters the surface energetics of the carbon blacks.

3.1.1. SEM Microstructure of Compounded Fillers

SEM observation of the filler dispersion at the fracture surface was used to qualitatively asses the efficacy of the compounding process. Figure 2 shows a series of SEM micrographs

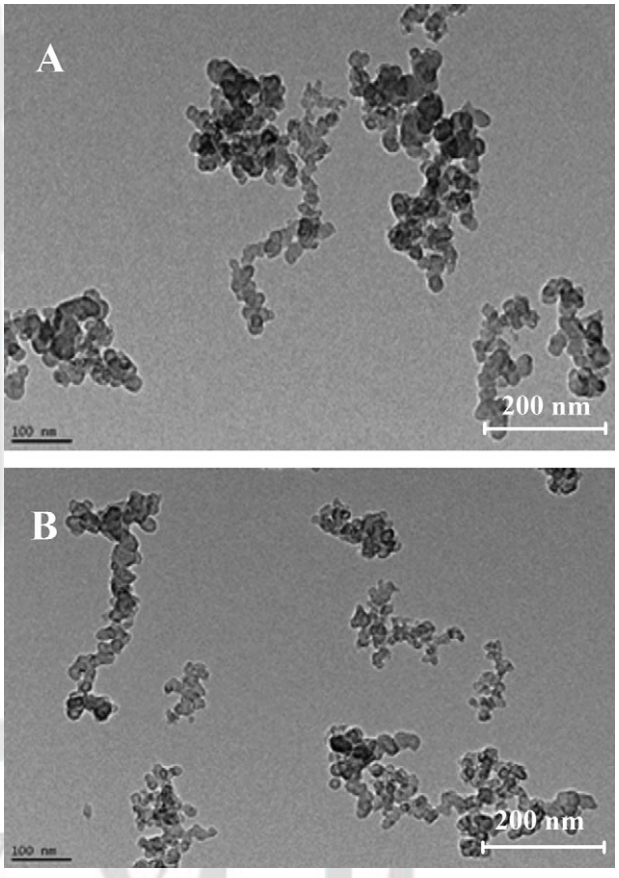

Figure 1. TEM images of (A) unmodified and (B) graphitised carbon black.

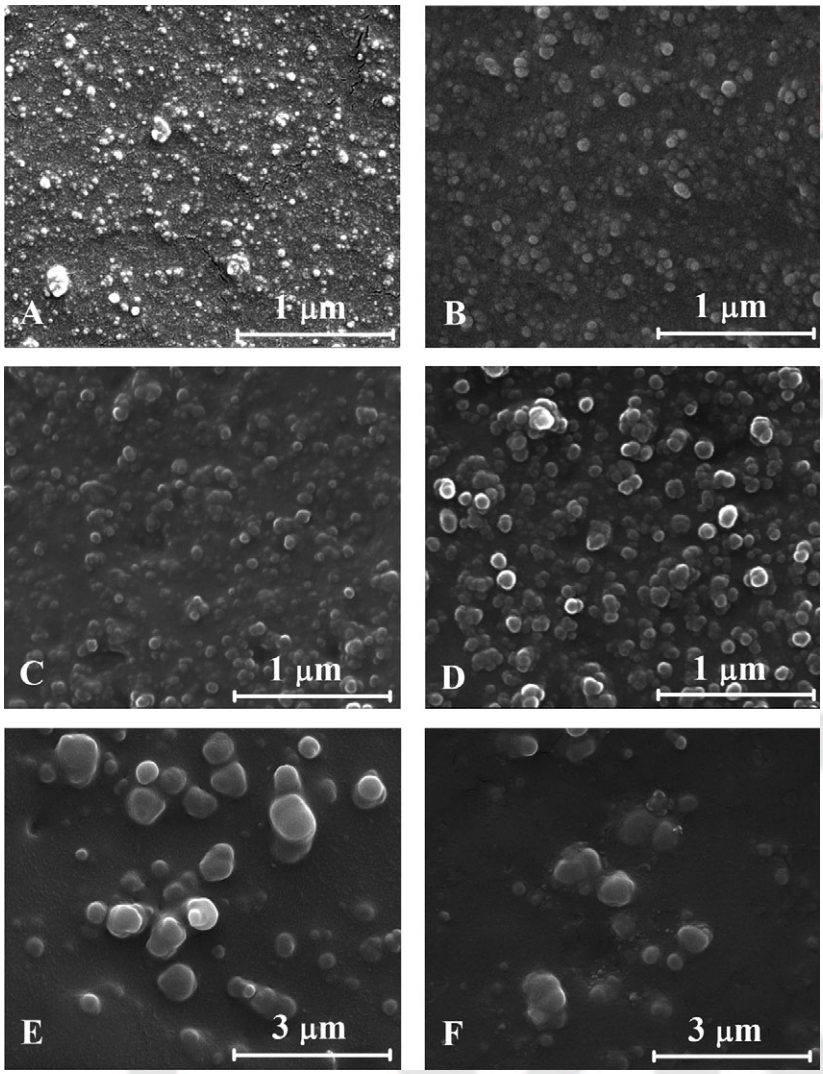

Figure 2. SEM micrographs of filler dispersions in crosslinked compounds. (A) N134, (B) N134g, (C) N330, (D) N330g, (E) N990, (F) N990g.

representative of fracture surface morphologies of the crosslinked compounds. Examination of the micrographs reveals that the dispersion states of unmodified and graphitised carbon blacks are qualitatively similar. There is no evidence of substantial quantities of poorly dispersed particles within the samples and the observed particles appear to be comparable in size. Therefore we conclude that, at least on the micrometer length scale (macrodispersion), all the compounded samples studied exhibited ~~good~~ levels of particulate dispersion. Differences in rheology are therefore rooted in the microdispersion of the ~~carbon blacks.~~

3.2. Shear-Induced Flocculation Behaviour of Carbon Black Networks in the Melt

Rheological data is presented in Figure 3. The ordinate scales are equivalent for ease of comparison. It is immediately clear that a change in surface free energy (SFE) has a dramatic effect on the rheological properties of the filled rubbers. Examination of the strain sweep data shows that graphitization of the filler results in an approximate trebling of the modulus at small strain. These effects seem to scale with surface area and particle size for N330- and N134-based grades. It is noteworthy that linear viscoelastic behaviour is not particularly pronounced especially for the GCBs; indicating that the filler structures in the melt are fragile when compared to their crosslinked analogues. For a more quantitative analysis, the data collected from the strain yielding process were fitted with the Kraus Equation[12] (Equation (5) where $G'(\gamma)$ is the storage modulus, G''_{∞} the storage modulus at high strain, γ the applied dynamic strain, γ_C the critical strain and m is the power law exponent) which is based upon a physical concept of agglomeration and de-agglomeration of particulates connected via van der Waals forces.

$$\frac{G'(\gamma) - G'_{\infty}}{\Delta G'} = \frac{1}{1 + \left(\frac{\gamma}{\gamma_C}\right)^{2m}} \quad (5)$$

The fits to the data are presented in Figure 3 as dashed lines. The Kraus Equation contains two fitting parameters including a value, γ_C, which corresponds to the strain at which half the filler–filler contacts have been ruptured and a term, m, which describes the shear sensitivity of the yielding process. These fitting parameters are reported in Table 2. From examination of these parameters is clear that a reduction in SFE of carbon black results in an increased shear sensitivity of the filler structure and a more rapid yielding of the filler structure under the application of strain. From examination of the high strain response of these filled rubbers it is also apparent that at the highest strain (10%) the moduli of the graphitised carbon black-filled rubbers ~~is~~ roughly equal to that of the unmodified carbon black-filled rubbers. This can be understood in terms of hydrodynamics; as the filler morphologies and surface areas are essentially unchanged by the graphitization process, their potential for hydrodynamic, rigid body reinforcement should remain equivalent to their unmodified counterparts. The majority of structure is broken down at large strains leaving only the hydrodynamic reinforcing effect of the disaggregated particulates. The dramatic

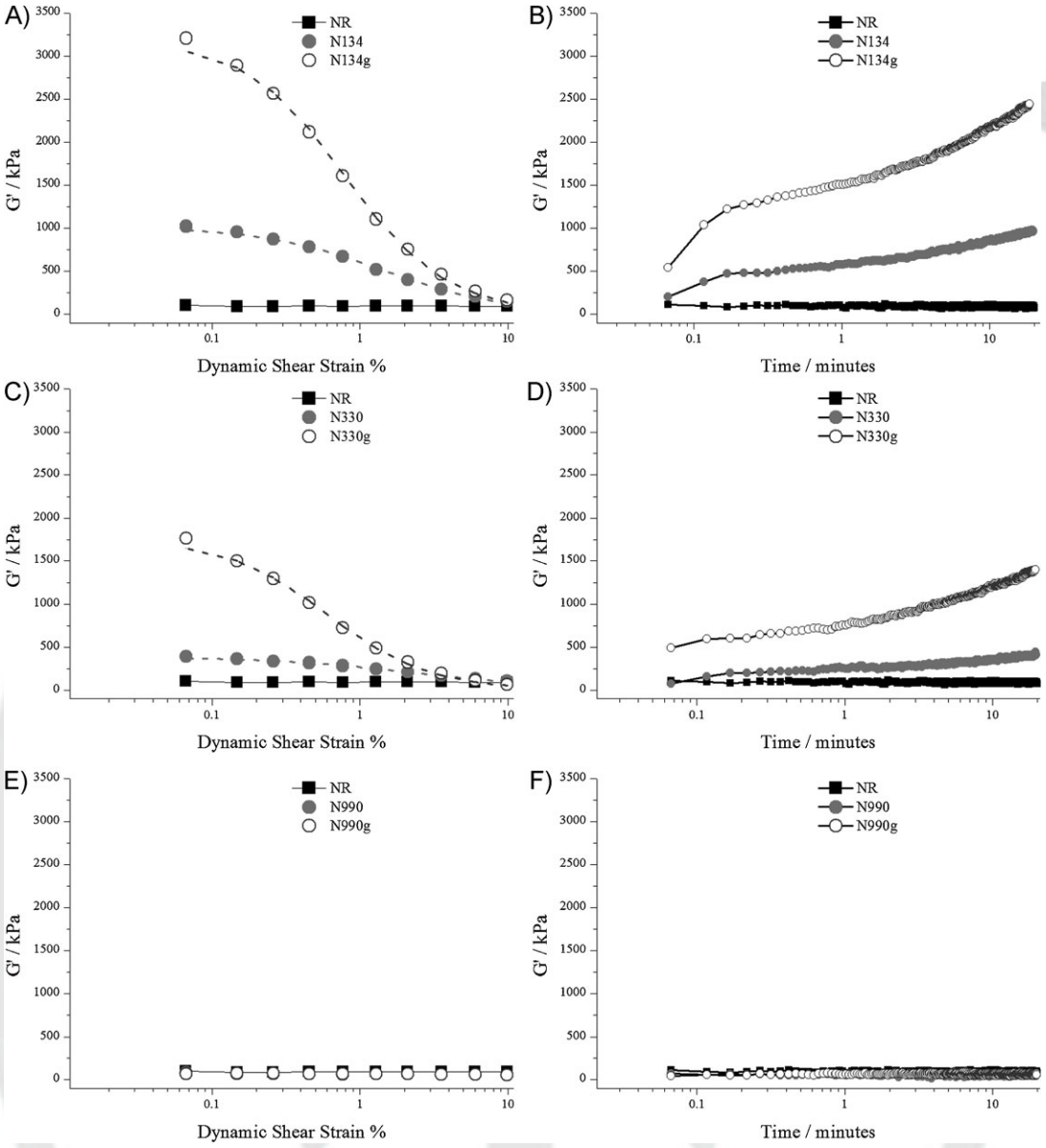

Figure 3. Rheological data for filled and unfilled rubbers. Left: Strain sweeps (dashed lines are fits to Equation 5), right: modulus recovery (solid lines are guides for the eye).

differences observed at smaller strains are therefore the result of strain and temperature-induced flocculation effects only. The N990-based fillers display no strain or time dependent rheology. This is not surprising considering the size of the particles—approximately 280 nm in diameter—and the theoretical percolation threshold for N990 which is equivalent to a mass loading of around 200 phr. For N990 no filler networking occurs either through percolation or flocculation processes.

Considering the time dependence of the recovery of the dynamic modulus, G', after the applied strain sweep (Figure 3 b, e and f) it is clear that for the N330 and N134-based fillers there exist significant strain-induced flocculation effects. From these data it is apparent that the flocculation process operates across a broad range of timescales. The time axis is plotted logarithmically to highlight this. Within the initial minute of the experiment a substantial amount of structure (modulus) is recovered (note that data is lost in the initial few seconds of the experiment ~~run~~ due to the equipment response time). Over longer timescales a much slower contribution to the total recovery process is observed. Meier and Klüppel[7] have observed similar effects induced by thermal annealing of carbon black-filled S-SBR using a

Table 2. Kraus Equation fitting parameters and rate constants from bi-exponential fitting.

Carbon Black	$\gamma_{C\ \%}$	m	k_{fast} [s]	$k_{slow}/\times 10^{-3}$ [s]
N134	1.439	0.514	0.14	1.6
N134g	0.783	0.616	0.16	1.7
N330	2.644	0.414	0.13	1.2
N330g	0.594	0.621	0.24	1.9

bi-exponential deconvolution (Equation (6) where t is the experimental time, k_{fast} is the rate constant corresponding to the initial rapid contribution and k_{slow} is the rate constant for the slower contribution).

$$G' = G'_1(1 - e^{-k_{fast}t}) + G'_2(1 - e^{-k_{slow}t}) \quad (6)$$

Such a fitting process is also able to reasonably describe the data reported here (Figure 4) indicating that there is a microstructural equivalence between flocculation effects induced by a step change in temperature (annealing) and those induced by pre-shearing. Rate constants corresponding to the fast and slow flocculation processes extracted from the fitting de-convolution are given in Table 2. The rate constants for both processes increase upon graphitization of the carbon black filler—particularly for the case of N330 carbon black.

3.3. Electrical Percolation of Filler Networks in Crosslinked Rubbers

Figure 5 shows a plot of log resistivity versus volume fraction of filler for the various types of carbon blacks studied. Note that data for N990-based fillers are not shown as the maximum volume loading considered in this paper falls substantially below the filler's percolation volume fraction. The electrical behaviour of N990-filled elastomers at $\varphi = 0.20$ was found to be identical to that of the insulating unfilled material. Data was fitted to Equation (7), which is derived from percolation theory,[13] to give the quantitative values of the percolation thresholds reported in Figure 5. (In Equation 7 σ_{dc} is the D/C conductivity, σ_0 is the D/C conductivity above the percolation threshold, φ is the volume fraction of filler loading, φ_C is the percolation volume fraction and μ is the power law exponent). As can be seen in Figure 5 both larger particle surface areas and reductions in SFE significantly reduce the percolation thresholds of the carbon blacks in the crosslinked samples. This is as a direct result of flocculation during the early stages of the crosslinking process.

$$\sigma_{dc} = \sigma_0 \left(\frac{\varphi - \varphi_C}{1 - \varphi_C}\right)^{\mu} \quad (7)$$

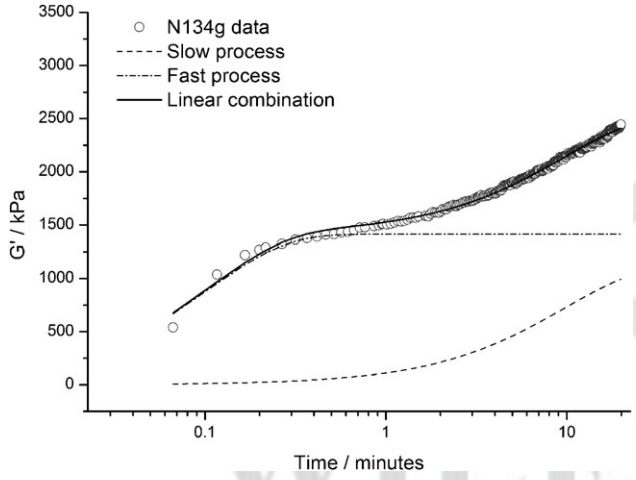

Figure 4. Bi-exponential fitting of flocculation data.

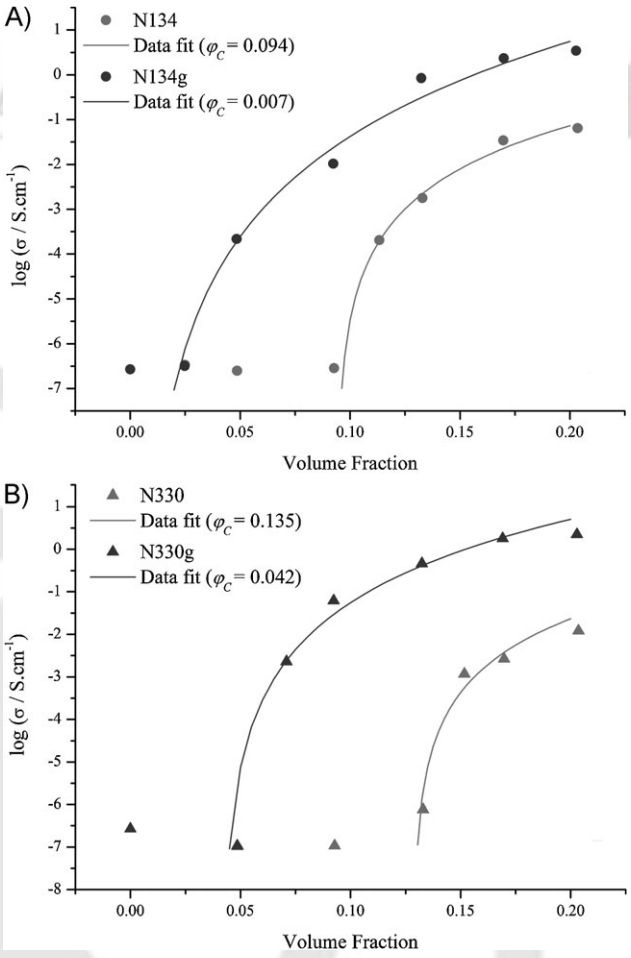

Figure 5. D/C percolation behaviour of carbon black-filled elastomers. A) N134-based fillers, B) N330-based fillers.

3.4. Flocculation and Reinforcement in Filled, Crosslinked Rubbers

Figure 6 shows the small strain, dynamic mechanical storage moduli of the filled and unfilled crosslinked compounds as a function of temperature. Figure 7 shows the moduli of the filled compounds normalized to that of the unfilled compound as a function of temperature; defined by Berriot et al.[14] as the small strain reinforcement. In the glassy region (<≈210 K) there is very little difference in dynamic properties of the filled and unfilled compounds. However above the T_g the dramatic amplification of the storage moduli due to the presence of the filler is apparent as is the clear non-entropic temperature dependence. The magnitude of the amplification reflects the flocculation behaviour observed in the rubber melts. GCBs display

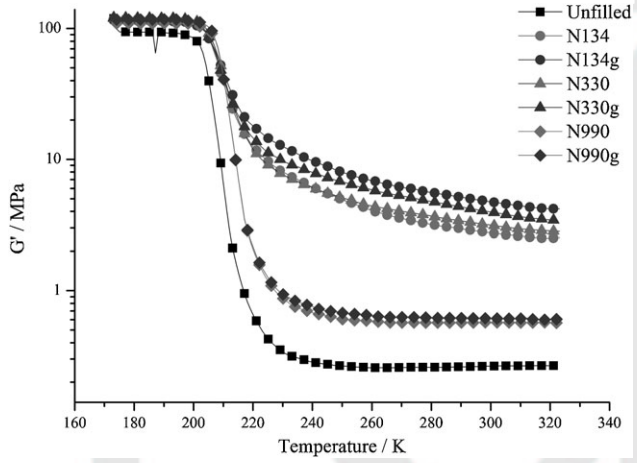

Figure 6. Small strain storage moduli of filled and unfilled samples.

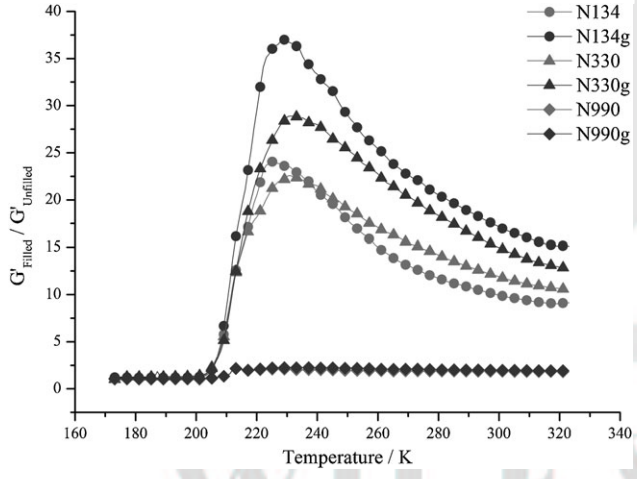

Figure 7. Small strain storage moduli of filled samples normalized to the unfilled sample.

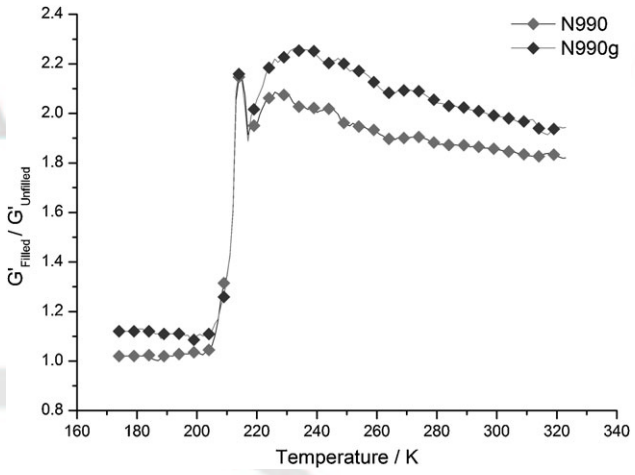

Figure 8. Normalized moduli for N990 samples.

significantly increased small strain moduli versus their unmodified counterparts. This is apparent in the plots of normalised moduli which also highlights the contrasting temperature dependencies of the modulus reinforcement. Data for N990-based carbon black filled samples is also plotted in Figure 8. The degree of modulus amplification between N330 and N134 filled samples does not fit the convention whereby modulus enhancement scales with surface area of the carbon black. This indicates that small strain mechanical properties are not solely dictated by particulate flocculation. This issue is addressed in more detail in forthcoming papers.[15,16]

3.5. Discussion

The phenomenology of the flocculation process documented in this paper is summarised as follows:

- Flocculation of carbon black in the NR melt proceeds via a physical process (or processes) operating across a range of timescales.
- Graphitization of carbon black accelerates flocculation.
- Flocculated GCB networks in the melt display increased fragility versus their unmodified counterparts.
- Reduction in particle surface activity results in a significant drop in the D/C percolation thresholds for crosslinked compounds.
- For the GCB-filled crosslinked compounds, small strain moduli are significantly larger than for their corresponding unmodified counterparts.

Due to the relatively high volume fraction of the networked carbon blacks in the melt it is likely that the application of shear significantly disrupts the established filler network by overcoming attractive forces between particles. Such forces have been proposed to result from

van de Waals attractions,[9,12] bridging polymer chains adsorbed onto adjacent particulates[4] or immobilised polymer in gaps between aggregates.[7] In a previous investigation some of the authors investigated the effect of these carbon blacks and other types of filler particles on the glass transition of NR. Little evidence was found to indicate any effect of the fillers on the T_g—seemingly precluding the formation of significant amounts of immobilized polymer between aggregates.[17] Whatever the physical origin of the binding force between particles, they must be overcome to some extent by mechanical deformation. Due to the crowded nature of the particulate filled system such attractive connections are rapidly re-established between particles in close proximity upon secession of deformation. Longer timescale effects correspond to agglomeration or reorientation of structures with a larger length scale than that of the individual filler aggregates. Deactivation of the surface of carbon black via graphitization increases the rate of flocculation potentially by lowering the (effective) viscosity term in Equation (1) due to an easier detachment and slippage of polymer at the filler surface. The increased fragility of the filler networks upon graphitization suggests that the strength of filler–filler bonding is also reduced.

It is of interest to compare the magnitudes of melt reinforcement during the flocculation process associated with unmodified and GCBs (Figure 3). Up to three times the small strain modulus is obtained for carbon blacks with weaker rubber–filler interactions. The exact mechanism by which a filler network reinforces the rubber melt (and subsequently crosslinked elastomer) at small strain is still open to some debate. Besides the basic hydrodynamic effects of incorporating rigid particles, a number of additional contributory mechanisms have been proposed. In the absence of significant immobilization of polymer in proximity to the filler particles—as is the case for these samples, both the fractal geometry of the percolating network and its relative flexibility become increasingly significant for reinforcement.

If, during small deformations, the filler network is essentially rigid when compared to the rubber phase, then strain energy is stored entirely within the rubber component of the compound (as in the hyperelastic models of Ahmadi and Muhr[18] and Bergström and Boyce.[19]) Here strain amplification[20] and occlusion of rubber (which increases the effective volume fraction of the solid phase as outlined by Medalia,[21]) are responsible for the observed levels of reinforcement. Using finite element simulations Bergstrom and Boyce,[19] Jha et al.,[22] and Busfield et al.[23] have demonstrated that random dispersions of fillers at realistic volume fraction can accurately match, and in some cases exceed, the small strain stiffening effect observed in experimental data. Both occlusion of elastomer phase and strain amplification mechanisms are apparent in their simulation results. Furthermore Akutagawa et al. finite element analyses of three-dimensional representations of real filler dispersions (determined experimentally using a microtomography technique) embedded in an hyperelastic continuum have demonstrated that such mechanisms in fact significantly over estimate the magnitude of stiffening observed experimentally.[24]

Alternatively, if the filler network is flexible and of comparable stiffness compared to that of the elastomer phase, as suggested by Meier and Klüppel,[7] then strain energy is preferentially stored within the filler network through tension and torsion of aggregate–aggregate bonds. In this case, the level of reinforcement is associated with the specific dynamics and mechanics of the particulate network—in particular the (visco)elastic bonds between filler aggregates.

Therefore in the context of these mechanisms the underlying reason behind the differences in flocculation magnitude between unmodified and GCBs (in both melt and crosslinked situations) lies in the physical nature of the filler network. Filler networks can be described by their fractal dimensions. Two pertinent questions arising from this are: 1. what is the relationship between particle surface activity and the resulting fractal dimension of the flocculated network and 2. what is the effect of filler networks with differing fractal dimensions on the degree of rubber occlusion and distribution of local strains in the rubber phase under small deformations. Some of the authors are currently developing a mesoscale simulation to further explore these issues.

Considering the reinforcement apparent for the crosslinked samples in this paper (Figure 7) it is clear that the stiffening imparted by the fillers scales with their tendency to flocculate in the melt. It has been suggested that the observed non-hydrodynamic temperature dependence of the reinforcement may be due to temperature-dependent slippage of polymer at the filler interface[25–27] or a temperature dependence inherent to the mechanics of the percolating filler network.[7,12,18] The N990 series of fillers are effectively isolated spherical particles within an elastomer matrix and display no tendency for particle networking as illustrated by the SEM fracture surface image inset in Figure 7. Closer examination of the reinforcement of the N990 series (Figure 8) reveals that a marked temperature dependence is apparent even in samples without a networked, percolated filler structure. Therefore the physical mechanism underlying this temperature dependence in both high and low surface area carbon blacks is, at least partially, if not wholly isolated at the filler interface rather than being related to the specific temperature-dependent mechanics of the filler network. In fact previously Jha et al.[22] and Busfield et al.[23] noted that their mesoscale FEA simulations of N990 reinforced carbon black actually overestimated the level of small strain

modulus reinforcement observed in room temperature experiments. They subsequently introduced a slippage boundary condition into their simulations to account for this. Maier and Göritz's molecular-based model for the Payne effect describes the small strain modulus temperature dependence by defining the number of unstable bonded chains attached to the filler particles as subject to an Arrhenius temperature dependence and suggests that the activation energies for such desorption processes are in the range of van der Waals bonding energies.[27] These concepts will be explored in more detail in a forthcoming paper.

4. Conclusion

The role of surface activity, surface area and morphology of carbon black particles on the flocculation process and viscoelasticity was explored experimentally. N990 filled melts exhibited no filler networking behaviour due to the particle size and loading of the carbon black. N330 and N134-based samples all displayed time and strain dependent rheology characteristic of flocculation. Reduction in surface free energy of the networking carbon blacks resulted in an increase in flocculation rates and magnitude. This was observed in the crosslinked samples as a significant reduction in the D/C percolation thresholds of the graphitised carbon blacks versus their unmodified counterparts. Reinforcement was discussed in terms of filler network structures and the potential for exploring these effects in more detail using appropriate simulations was outlined. Reinforcement in the crosslinked samples was found to be strongly temperature dependent even for the N990 samples; which display no evidence of filler networking. As such the temperature dependence—potentially a polymer slippage mechanism—could be isolated at the filler–rubber interface.

Acknowledgements: L.B.T. thanks EPSRC (UK) and Sibelco for doctoral funding and Dr Lorenzo Botto of QMUL for helpful discussions. J.K. thanks the support of 'Operational Program Education for Competitiveness' co-funded by the European Social Fund (ESF) and the national budget of Czech Republic within the project 'Advanced Theoretical and Experimental Studies of Polymer Systems' (reg. number CZ.1.07/2.3.00/20.0104) and with the support of the 'Research and Development for Innovations' operational program co-funded by the European Regional Development Fund (ERDF) and the national budget of the Czech Republic within the project entitled 'Centre of Polymer Systems' (reg. number CZ.1.05/2.1.00/03.0111). The thank TARRC for assistance with ~~internal~~ mixing of compounds and Christine Martin of Alpha Technologies for kindly allowing access to the RPA.

Received: April 11, 2014; Revised: May 23, 2014; Published online:
DOI: 10.1002/mame.201400117

Keywords: carbon black; elastomer; flocculation; reinforcement; rubber

[1] F. Brochard Wyart, P. G. de Gennes, *Eur. Phys. J. E* **2000**, *1*, 93.
[2] M. Gerspacher, L. Nikiel, H. H. Yang, C. P. O'Farrell, G. A. Schwartz, *Kaut. Gummi Kunstst.* **2002**, *55*, 596.
[3] S. Mihara, R. N. Datta, J. W. M. Noordermeer, *Rubber Chem. Technol.* **2009**, *82*, 524.
[4] G. A. Schwartz, S. Cerveny, A. J. Marzocca, M. Gerspacher, L. Nikiel, *Polymer* **2003**, *44*, 7229.
[5] M. Klüppel, *Adv. Polym. Sci.* **2003**, *164*, 1.
[6] G. Heinrich, M. Klüppel, *Adv. Polym. Sci.* **2002**, *160*, 1.
[7] J. G. Meier, M. Klüppel, *Macromol. Mater. Eng.* **2008**, *293*, 12.
[8] A. Schroeder, M. Klüppel, R. H. Schuster, *Macromol. Mater. Eng.* **2007**, *292*, 885.
[9] J. B. Donnet, R. C. Bansal, M. J. Wang, "*Carbon Black*", 2nd edition, Marcel Dekker Inc, New York **1993**.
[10] E. M. Dannenberg, *Rubber Chem. Technol.* **1975**, *48*(3), 410.
[11] E. Geberth, M. Klüppel, *Maromol. Mater. Eng.* **2012**, *297*, 914.
[12] G. Kraus, *J. Poly. SC.* **1984**, *39*, 75.
[13] G. Heinrich, R. H. Schuster, M. Klüppel, *Rubber Chem. Technol.* **1997**, *70*, 243.
[14] J. Berriot, H. Montes, F. Lequeux, D. Long, P. Sotta, *Macromolecules* **2002**, *35*, 9756.
[15] L. B. Tunnicliffe, J. L. Valentín, A. Gonzalez, A. G. Thomas, J. J. C. Busfield, unpublished. **Please provide update if available.**
[16] L. B. Tunnicliffe, J. L. Valentín, A. Gonzalez, A. G. Thomas, J. J. C. Busfield, unpublished. **Please provide update if available.**
[17] M. Huang, L. B. Tunnicliffe, A. G. Thomas, J. J. C. Busfield, unpublished. **Please provide update if available.**
[18] H. R. Ahmadi, A. H. Muhr, *Rubber Chem. Technol.* **2011**, *84:1*, 24.
[19] J. S. Bergström, M. C. Boyce, *Rubber Chem. Technol.* **1999**, *72*, 633.
[20] L. Mullins, N. R. Tobin, *J. Appl. Polym. Sci.* **1965**, *9*, 2993.
[21] A. I. Medalia, *J. Colloid Interf. Sci.* **1970**, *32*, 115.
[22] V. Jha, A. A. Hon, A. G. Thomas, J. J. C. Busfield, *J. Polym. Sci. A2* **2008**, *107*, 2572.
[23] J. J. C. Busfield, A. G. Thomas, K. Yamaguchi, *J. Polym. Sci. A2* **2004**, *42*, 2161.
[24] K. Akutagawa, K. Yamaguchi, A. Yamamoto, H. Heguri, H. Jinnai, Y. Shinbori, *Rubber Chem. Technol.* **2008**, *81*, 182.
[25] S. S. Sternstein, S. Amanuel, M. L. Shofner, *Rubber Chem. Technol.* **2007**, *83*, 181.
[26] S. S. Sternstein, A. J. Zhu, *Macromolecules* **2002**, *35*, 7268.
[27] P. G. Maier, D. Göritz, *Kaut. Gummi Kunstst.* **1996**, *49*, 1.